The author of the Ph.D. dissertation: Sarath Pampayil Sasikumar

Scientific discipline: Chemical Sciences

DOCTORAL DISSERTATION

Title of Ph.D. dissertation: **Graphene-based Silicone rubber Nanocomposites: Preparation, Characterization, and Properties**

Scientific discipline: Chemical Sciences

Title	Supervisor	Auxiliary supervisor
Name	Prof. dr hab. inż. Józef T. Haponiuk	Dr.Soney C George
Signature		

STATEMENT

The author of the Ph.D. dissertation: Sarath Pampayil Sasikumar

I, the undersigned, agree/do not agree* that my Ph.D. dissertation entitled: **Graphene-based Silicone rubber Nanocomposites: Preparation, Characterization, and Properties** may be used for scientific or didactic purposes.

11 Gdańsk,23-08-2022.....

Signature of the Ph.D. student

Aware of criminal liability for violations of the Act of 4th February 1994 on Copyright and Related Rights (Journal of Laws 2006, No. 90, item 631) and disciplinary actions set out in the Law on Higher Education (Journal of Laws 2012, item 572 with later amendments),22as well as civil liability, I declare, that the submitted Ph.D. dissertation is my work.

I declare that the submitted Ph.D. dissertation is my own work performed under and in cooperation with the supervision of Prof. dr hab inż. Józef Tadeusz Haponiuk, and the auxiliary supervisor Dr.Soney C George.

This submitted Ph.D. dissertation has never been the basis of an official procedure associated with awarding a Ph.D. degree.

All the information in the above thesis derived from written and electronic sources is documented in a list of relevant literature in accordance with art. 34 of the Copyright and Related Rights Act.

I confirm that this Ph.D. dissertation is identical to the attached electronic version.

Gdańsk, 23-08-2022....

Signature of the Ph.D. student

I, the undersigned, agree/do not agree* include an electronic version of the above Ph.D. dissertation in the open, institutional, digital repository of Gdańsk University of Technology, Pomeranian Digital Library, and for it to be submitted to the processes of verification and protection against misappropriation of authorship.

Gdańsk,.. 23-08-2022.

Signature of the Ph.D. student *)

1 Decree of Rector of Gdansk University of Technology No. 34/2009 of 9th November 2009, TUG archive instruction addendum No. 8.

2 Act of 27th July 2005, Law on Higher Education: Chapter 7, Criminal responsibility of Ph.D. students, Article 226

MOST WIEDZY Downloaded from mostwiedzy.pl

DESCRIPTION OF DOCTORAL DISSERTATION

The author of the Ph.D. dissertation: Sarath Pampayil Sasikumar

Title of Ph.D. dissertation: Graphene-based Silicone rubber Nanocomposites: Preparation, Characterization, and Properties

Title of Ph.D. dissertation in Polish: Nanokompozyty kauczuku silikonowego na bazie grafenu. Otrzymywanie, charakterystyka I właściwości.

Language of Ph.D. dissertation: English

Supervision: Prof. dr hab inż. Józef Tadeusz Haponiuk and Auxiliary supervision* Dr. Soney C. George

Keywords of Ph.D. dissertation in Polish: Kauczuk silikonowy, nanokompozyty, pochodne grafenu, tribologia, właściwości mechaniczne i termiczne

Keywords of Ph.D. dissertation in English: Silicone rubber, Nanocomposites, Graphene Derivatives Tribology, Mechanical and Thermal Properties,

Summary of Ph.D. dissertation in polish

Summary of Ph.D. dissertation in English

Streszczenie

Celem pracy było lepsze poznanie mechanicznego, termicznego i trybologicznego zachowania nanokompozytów kauczuku silikonowego w odniesieniu do rodzaju i zawartości nanonapełniacza na bazie grafenu. W badaniach zastosowano grafit, eksfoliowany grafit, zredukowany tlenek grafenu, tlenek grafenu modyfikowany cieczą jonową, tlenek grafenu modyfikowany silanem, krzemionkę koloidalną i inne wypełniacze. Dodatek nanonapełniacza na bazie grafenu do matrycy z gumy silikonowej znacznie poprawia właściwości mechaniczne, termiczne i trybologiczne nanokompozytu. Analizy DMA i DSC potwierdziły poprawę oddziaływań pomiędzy matrycą polimerowa a nanonapełniaczem w badanych

MOST WIEDZY Downloaded from mostwiedzy.pl

nanokompozytach. W porównaniu do czystej gumy silikonowej, dodanie grafitu (20 części) znacznie zmniejsza współczynnik tarcia (o 40%) i szybkość zużycia tribologicznego QM (o 50%). Zmodyfikowany proces Hummersa został wykorzystany do syntezy tlenku grafenu (GO), a badania FT-IR, XRD, Ramana i XPS zostały przeprowadzone w celu potwierdzenia redukcji GO. Badania XRD, AFM, SEM i TEM zostały wykorzystane do zbadania dyspersji i interakcji nanonapełniacza w matrycy polimerowej. Testy trybologiczne przeprowadzono przy użyciu trybometru typu pin-on-disc ASTM G99-05 w celu zbadania wpływu zmiennych roboczych, takich jak przyłożone obciążenie, prędkość poślizgu i temperatura. Jednowarstwowa powłoka grafenowa funkcjonalizuje powierzchnię kompozytu polimerowego w mikrostrukturze kompozytów grafenowych. Według skaningowej mikroskopii elektronowej (SEM), mikroskopii transmisyjnej (TEM) i analizy rentgenowskiej z dyspersją energii (EDX) nanokompozyty mają lepszy rozkład wypełniaczy. Właściwości mechaniczne nanokompozytów, takie jak wytrzymałość na rozciąganie i twardość, a także właściwości elektryczne i termiczne, takie jak przewodność cieplna, degradacja termiczna i właściwości dielektryczne, są lepsze w porównaniu z konwencjonalnymi nanokompozytami, co można przypisać lepszej dystrybucji nanonapełniaczy. Morfologia powierzchni kompozytu wykazuje gładką powierzchnię, co wskazuje, że obecność nanonapełniaczy znacznie ograniczyła kontakt z metalem. Mechanizm zużycia polega na tworzeniu filmu smarnego na powierzchni współpracującej, który zapobiega stykaniu się nierówności z powierzchnią kompozytu. W rezultacie współczynnik tarcia i właściwa szybkość zużycia ulegają zmniejszeniu. Oprócz wysokiej przepuszczalności i wysokiej odporności na temperaturę, guma silikonowa ma również wyjątkową odporność na starzenie i izolację elektryczną. W rezultacie jest często wykorzystywany w różnych gałęziach przemysłu, w tym w motoryzacji, tekstyliach, elektronice, medycynie, uszczelniaczach, sprzęcie i magazynowaniu żywności itp.

MOST WIEDZY Downloaded from mostwiedzy.pl

Summary

This study aims to understand better the mechanical, thermal, and tribological behavior of silicone rubber nanocomposites. Graphite, exfoliated graphite, reduced graphene oxide, ionic liquid modified graphene oxide, silane-modified graphene oxide, fumed silica, and other fillers were used in this study. Adding graphene-based fillers to the silicone rubber matrix substantially improves the nanocomposite's mechanical, thermal, and tribological properties. The DMA and DSC analyses confirmed the improved polymer filler contact in the composite. When compared to the neat silicone rubber, the inclusion of graphite (20 phr) reduces the friction coefficient (40%) and the specific wear rate of QM significantly (50 percent). The modified Hummers process synthesized graphene oxide, and FT-IR, XRD, Raman, and XPS studies were performed to validate GO reduction. XRD, AFM, SEM, and TEM studies were used to investigate the dispersion and interaction of the filler in the polymer matrix. The tribological tests were conducted utilizing an ASTM G99-05 pin-on-disc tribometer to examine the effect of operating variables such as applied load, sliding velocity, and temperature. A single-layer graphene film functionalizes the polymer composite surface in the microstructure of graphene composites. Nanocomposites have a better filler distribution, according to scanning electron microscopy (SEM), transmission microscopy (TEM), and energy dispersive X-ray analysis (EDX). The mechanical properties of the nanocomposites, such as tensile strength and hardness, as well as the electrical and thermal properties, such as thermal conductivity, thermal degradation, and dielectric properties, are improved when compared to pure silicone rubber, which can be attributed to the improved distribution of the nanofillers. The composite's worn surface morphology exhibits a smooth surface, indicating that the presence of fillers significantly reduced metal contact. The wear mechanism involves the formation of a lubricant film on the counter surface, which prevents the asperities from touching the composite surface. As a result, the friction coefficient and specific wear rate are reduced. In addition to having high permeability and strong temperature resistance, silicone rubber also has outstanding age resistance and electrical insulation. As a result, it is frequently utilised in a variety of industries, including automotive, textiles, electronics, medical field, sealants, hard ware and food storage etc.

MOST WIEDZY Downloaded from mostwiedzy.pl

Contents

1. Introduction ----------1
2. Composites ---------- 3
2.1 Nanocomposites ----------4
2.2 Types of Polymer Matrix Nanocomposites ----------6
2.2.1 Thermoplastics-based polymer composites ----------7
2.2.2 Thermosets-based polymer composites ----------8
2.2.3 Elastomers-based polymer composites ----------9
2.3 Silicone rubber ----------9
2.3.1 Curing agents ---------- 11
2.4 Nanofillers ----------14
2.5 Carbon nanofillers----------14
2.5.1 Graphite ----------14
2.5.2 Exfoliated graphite----------15
2.5.3 Graphene ----------15
2.6 Surface modification of Graphene oxide ----------17
2.6.1 Ionic liquid----------18
2.6.2 Silane modification----------18
2.6.3 Hybrid nanofillers----------19
2.7 Tribology ----------21
2.7.1 Tribology of polymers reinforced with nanofillers----------23
2.7.2 Tribology of rubber nanocomposites ----------24
2.8 Research Gap----------29
2.9 Aim of the research work----------30

MOST WIEDZY Downloaded from mostwiedzy.pl

3. **Publication -1 -** An investigation on the tribological and mechanical properties of silicone rubber/graphite composites---------- 32

Publication -2 - Fabrication of exfoliated graphite reinforced silicone rubber composites-Mechanical, tribological and dielectric properties------ 45

Publication -3 A study on the influence of reduced graphene oxide on the mechanical, dynamic mechanical and tribological properties of silicone rubber nanocomposites ----------**58**

Publication -4 study the characteristics of novel ionic liquid functionalized graphene oxide on the mechanical and thermal properties of silicone rubber nanocomposites. ----------**73**

Publication -5 Study the effect of fumed silica on the mechanical, thermal and tribological properties of silicone rubber nanocomposites ----**84**

Publication -6 Tribological performance of ionic liquid modified graphene oxide/silicone rubber composite and the correlation of properties using machine learning ----------**98**

Publication -7 Fabrication, characterization and properties of silane functionalized graphene oxide/silicone rubber nanocomposites ----------**111**

Publication -8 Study the synergistic effect of fumed silica and reduced graphene oxide insertion on the thermal, mechanical, tribological, and solvent transport properties of silicone rubber nanocomposites----------**126**

4. **Conclusions** ----------**144**

Future Scope for research ----------**146**

Research achievements ----------**147**

List of publications----------**147**

Funding----------**149**

Acknowledgment ----------**150**

References ----------**151**

MOST WIEDZY Downloaded from mostwiedzy.pl

"Dedicated to my beloved Parents,

Family, and My Guides"

For their love, endless support

& encouragement

MOST WIEDZY Downloaded from mostwiedzy.pl

1. Introduction

The study of surfaces in relative motion is known as tribology and is derived from the Greek word tribos, which means to rub. The science of two interacting solid surfaces in relative motion causes friction and wear while considering the impact of lubrication between them. It is also a genuinely interdisciplinary interfacial phenomenon, incorporating the two interacting substances' physics, chemistry, mechanics, thermodynamics, and materials science[1], [2]

The tribology of polymers, however, differs significantly from that of metals for various reasons. Polymers are visco-elastic and have time-dependent characteristics, in contrast to metals. Due to their elasticity, ability to accommodate stress loading, minimal friction, and resistance to wear, polymers are being employed more frequently in tribological applications[3].

A polymer composite is a multi-phase material in which reinforcing fillers are integrated with a polymer matrix, resulting in synergistic mechanical properties that cannot be achieved from either component alone. Polymeric materials are increasingly used to construct mechanical systems with rubbing contacts[4].

Polymeric contacts are replacing traditional technical materials in rolling and sliding contacts. The extent of mechanical lubrication can be lowered by substituting traditional metallic or ceramic materials with polymeric systems. This replacement allows for more control over the coefficient of friction. Polymers' wear mechanism differs significantly in surface topography and bulk mechanical characteristics when comparing engineered metals and ceramics. Polymers are commonly used in tribo-systems due to their viscoelastic properties and low surface energy[5].

Silicone rubber (QM) and its nanocomposites are commonly used industrial materials because of their excellent physical properties, chemical inertness, wide operating temperature range, and resistance to ultraviolet, ozone, and aging[6]. Therefore, these materials are used are appropriate for environmental applications. Traditionally, the QM has been used in applications requiring high thermal stability, dielectric strength, or fire resistance. However, researchers are currently working on developing silicone materials with multifunctional features. As a result of the evolution of current technologies, there is a growing demand for high thermal conductivity rubber materials with good mechanical properties that can be used in extreme conditions.

MOST WIEDZY Downloaded from mostwiedzy.pl

Graphene is a two-dimensional, one-atom-thick nanomaterial composed of sp^2 -hybridized carbon atoms first isolated in 2004 [7], [8]. Graphene, the most promising material of the decade, has sparked widespread interest in various applications. It has tremendous potential as a reinforcement in polymer composites because of its remarkable mechanical, thermal, and electric properties [9], [10]. Zheng et al. used solution and co-coagulation methods to develop graphene-silicone rubber nanocomposites. Silicone rubber-graphene composites, a vast strain sensing range, and high strain sensitivity properties have been greatly enhanced [11]. XU et al. studied the influence of different processing conditions on graphene-filled-silicone rubber composites' electrical and mechanical properties [12]. Kumar et al. also demonstrated that using carbon nanotubes (CNTs) as a nanofiller in a silicone rubber matrix improves the mechanical and electrical properties[13]. In recent years, the chemical modification of graphene oxide has been an essential topic in academia. This is mainly accomplished by selecting proper reagents due to the active oxygen functionalities associated to graphene oxide (GO). Such modifications improve the compatibility of GO in various systems, and this modified graphene offers prospective uses in polymer composites, energy-related materials, field-effect transistors, and lubricant coatings, among others [7], [14], [15]. Ge et al. synthesized diisocyanate functionalized graphene oxide (FGO), and as the amount of FGO filler increased, the thermal conductivity of the silicone rubber was continuously enhanced [16]. Bai et al. studied the effect of rGO (reduced graphene oxide) reduction degree on the reinforcement in silicone rubber. It was observed that rGO reinforcement increased with the degree of reduction of graphene oxide. The oxidation of the side group of silicone rubber chains was slowed by rGO, which has a good barrier effect[17]. Ren et al. studied the thermal conductivity of silane-functionalized graphene nanoplatelets (GNPs) reinforced silicone rubber. It was found by Raman mapping that the silane-functionalized GNPs could be dispersed uniformly into the silicone rubber matrix, leading to an increase of Young's modulus and a considerable enhancement in the thermal conductivity [18]. Gan et al. studied the effect of silicone rubber's vinyl concentration on the mechanical properties of the composites they produced. The GO sheets were distributed throughout the QM matrix, improving the composites' thermal and mechanical properties tremendously [19].

MOST WIEDZY Downloaded from mostwiedzy.pl

2. Composites

A composite is a material made from two or more different materials that, when combined, are more robust than those individual materials by themselves. Composite materials are the only material that meets industry needs [20]. These materials are created with the desired qualities in consideration[21]. Composites are metal, ceramic, and polymer matrix composites based on the matrix materials used[22]. Among other composite materials, polymer composite materials play a significant part in current technology due to their exceptional physical, mechanical, and thermal qualities. The composites consist of the discontinuous phase (filler/fiber) and the continuous phase (matrix)[23]. Based on matrix material, the composites were classed into three, polymer-based, metal-based, and ceramic-based [24]. Among the various composites, polymer-based composites have many advantages: lightweight, high strength, easy processing, good thermal properties, and low cost[25]. The development of lightweight polymer composites has revolutionized the 21st-century composite-related industries. By incorporating various reinforcing fillers/fibers/fabrics, the polymer's physical, thermal, mechanical, and other functional characteristics can be enhanced[26], [27].formulation of the composite as shown in figure 1.

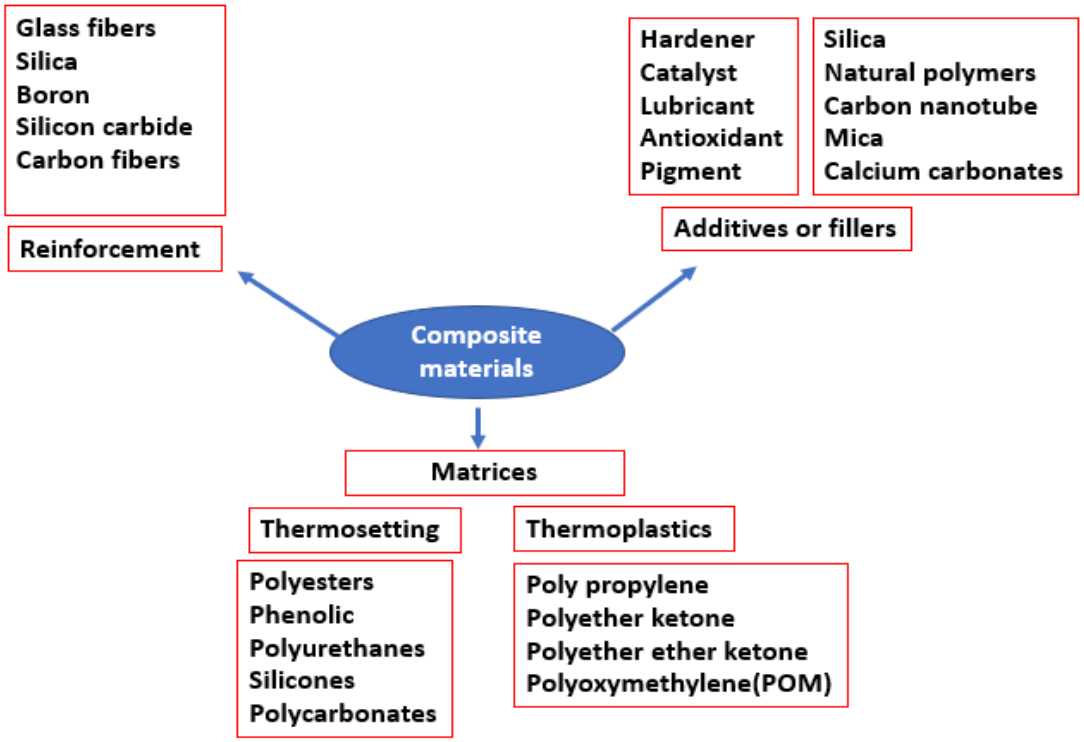

Fig.1 Composite material formulation

MOST WIEDZY Downloaded from mostwiedzy.pl

A composite material is a system made up of several various constituents. The nature of the matrix, the types of reinforcements, the additives, and the relative amounts of these elements entering the formulation and the implementation technique significantly impact the end product's properties. As a result, the number of possible implementations from this set of fundamental constituents is nearly limitless.

2.1 Nanocomposites

A nanocomposite is a multi-phase material. In contrast to micro composites, one of the phases has one, two, or three dimensions of less than 100 nm, or the composite phases have nanoscale distances between them. The fascinating properties of the nanocomposites are dictated by the complex interactions between the polymeric matrices and the nanoparticles in their interface regions. Schematic representation of types of nanocomposites as shown in figure-2.

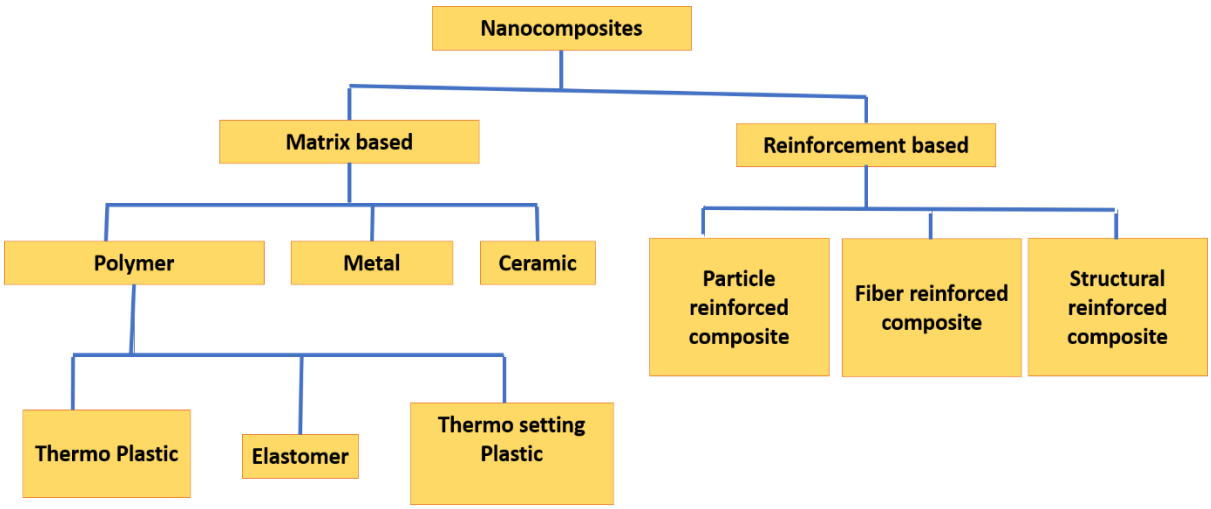

Fig -2 Schematic representation of types of nanocomposites

According to the matrix materials, nanocomposites are classified as Ceramic Matrix Nanocomposites (CMNC), Metal Matrix Nanocomposites (MMNC), Polymer Matrix Nanocomposites (PMNC)

- Ceramic matrix nanocomposites mainly have Al_2O_3 or SiC systems. Most studies have confirmed the noticeable strengthening of the $Al2O3$ matrix after additive on a low (i.e., appro: 10%) volume fraction of SiC particles of suitable size and hot pressing of the resulting mixture.

MOST WIEDZY Downloaded from mostwiedzy.pl

- Metal matrix nanocomposites (MMNC) refer to materials consisting of a ductile metal or alloy matrix in which some nanosized reinforcement material is implanted. These materials combine metal and ceramic features.
- Polymer matrix nanocomposites are widely used in industry due to their ease of production, lightweight, and ductile nature. They have some disadvantages, such as low modulus and strength compared to metals and ceramics. The schematic representation of the formation of polymer nanocomposites are their properties are displayed in figure 3, and the classification of composites with examples is shown in table 1

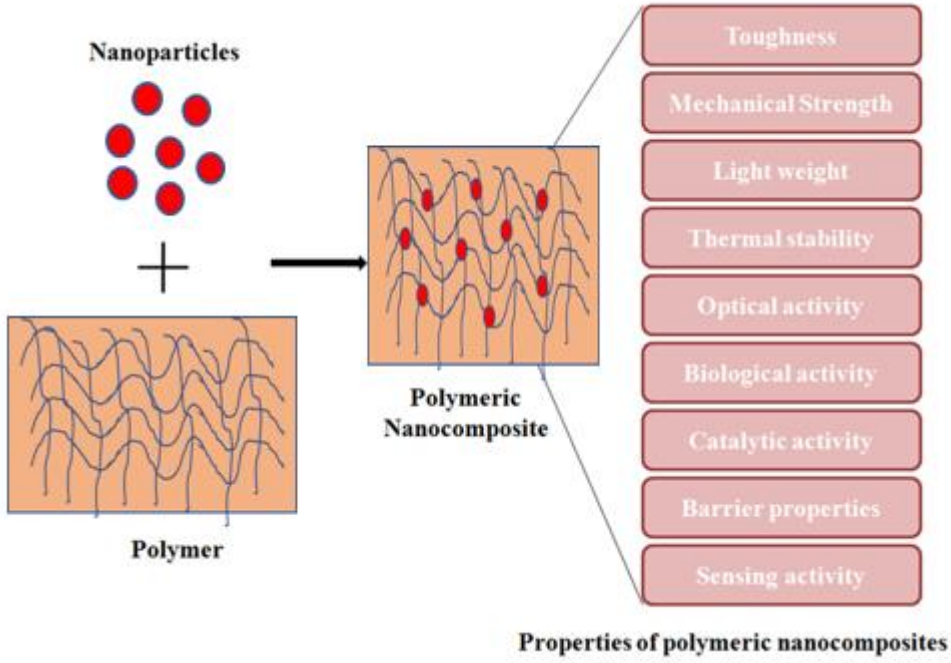

Fig.3 - Properties of polymeric nanocomposites

Table-1 classification of composites

Type of Matrices	Examples
Ceramic	Al_2O_3/SiO_2, SiO_2/Ni, Al_2O_3/TiO_2, Al_2O_3/SiC
Metal	Fe-Cr/Al_2O_3,Co/Cr, Fe/MgO, Mg/CNT
Polymer	Thermoplastic/thermoset polymer/layered silicates, polyester/TiO_2, polymer/CNT, polymer/layered double hydroxides

MOST WIEDZY Downloaded from mostwiedzy.pl

The size of a particle is an important determining factor of the wear resistance. Thus, reducing the particle size to the nanoscale significantly influences and improves the efficiency of the nanocomposites. It has been known for a long time that nanoparticles can help improve and enhance polymers' tribological and mechanical properties. Thus, this area has remained a focus of interest for many researchers. This knowledge and nanotechnology have given rise to polymers modified by incorporating inorganic and organic nanoparticles into their matrix, known as polymer nanocomposites (PNCs). These are an amazing group of materials for various applications in different fields due to their unique three-dimensional interphase physical network topology achieved due to the increased surface area of the nanofillers (Karger-Kocsis, 2005). The fascinating properties of the nanocomposites are dictated by the complex interactions between the polymeric matrices and the nanoparticles in their interface regions. The size of a particle is an important determining factor of the wear resistance. Thus, reducing the particle size to the nanoscale significantly influences and improves the efficiency of the nanocomposites[28].

2.2 Types of Polymer Matrix Nanocomposites

The significant component in polymer matrix nanocomposite is the polymer itself. Wide varieties of polymers are used in the preparation of polymer matrix nanocomposites. These polymers are listed below:

1. Thermoplastics
2. Thermosets
3. Elastomers

The choice of polymer matrix material for preparing polymer matrix nanocomposites for a specific application is generally guided by their mechanical, electrical, magnetic, optical, biocompatibility, chemical stability, and functionalization. Thermoset-based nanocomposites are usually the most common nanocomposites. They are used in many applications, but recently thermoplastic-based nanocomposites have attracted much research interest in industry and academia. The properties of polymers mainly depend on the polymer structure, which depends on the chemical composition, surface morphology, and processing parameters. The difference between thermoplastic and thermosets polymer is that they respond entirely differently to heat, mainly due to the difference in their molecular structure.

MOST WIEDZY Downloaded from mostwiedzy.pl

2.2.1 Thermoplastics-based polymer composites

Thermoplastic materials have relatively low melting temperatures and, more significantly, soften to a flexible or liquid condition when heated. This feature enables them to be formed into almost any mold or pattern. Furthermore, even great heat has little effect on the material's makeup; hence, when a thermoplastic material has been formed and cured, it may be reheated and melted or molded into another design, and the qualities will not be dramatically affected. Thermoplastics are mainly produced from long-chain molecules held by van der Waals forces. Some examples of thermoplastics are polyvinyl chloride (PVC), poly trimethylene terephthalate (PTT), polystyrene (PS), polypropylene (PP), polyethersulfone (PES), polyamide (PA), polyamide-imide (PAI), polyacrylonitrile (PAN), ethylene vinyl alcohol (EVOH), acrylic (PMMA) and acrylonitrile butadiene styrene (ABS)[29]. Thermoplastic has several tribological applications when mixed with nanofillers due to its unique character. Thermoplastic materials soften to a flexible or liquid state when heated, owing to their comparatively low melting temperatures. This characteristic may shape them into practically any mold or design.

Furthermore, even high temperatures have minimal influence on the material's constitution; hence, when a thermoplastic material has been produced and cured, it may be reheated and melted or molded into a different design without significantly altering the properties. The increasing use of polymer nanocomposites is also a consequence of the demands of modern precision machines and intensive tribological research. The thermoplastic material choice depends on the tribological end-user requirement, such as low weight, thermal resistance, or flammability, and the choice of specific nanomaterial needed for the nanocomposites. Thermoplastic polymer nanocomposites for tribological applications are produced via conventional production techniques such as nano infusion, in-situ polymerization, coating, solution mixing, and melt blending[30].

2.2.2 Thermoset-based polymer composites

Thermoset plastics and thermoset composites are synthetic materials that become strengthened when heated but cannot be adequately remolded or warmed once they have been heat-formed or molded. Thermosets have virtually all of their molecules linked with strong, permanent, physical connections that do not heat reversible after shaping. Molded thermosets resist high working temperatures, corrosion, and chemical attack. These material property

MOST WIEDZY Downloaded from mostwiedzy.pl

advantages enable molded thermoset parts in various aggressive and demanding end-use settings, from electrical applications to automobile engine and transmission components to outdoor element exposed items. Thermoset molding ensures that finished components and assemblies are dimensionally and chemically stable. Examples of thermoset materials include Bulk Molding Compounds (BMCs), Phenolic or Phenolic Molding compounds, Epoxy, Diallyl Phthalate (DAP). The BMCs are also known as unsaturated polyesters and vinyl esters. When thermosets are mixed with nanostructured particles like polyhedral oligomeric silsesquioxane (POSS), graphene, MXene, silica, and clay[31]–[34], thermoset nanocomposites exhibit superior thermal, electrical, and mechanical properties that are well-balanced for several tribological applications[35]. Their exceptional strength lends itself to tribological applications in the marine, aerospace, and automotive sectors. Other features, such as working at higher temperatures, creep and solvent resistance, an affinity for heterogeneous materials, and simplicity of processing, expand their usage in various other technical applications[36].

2.2.3 **Elastomer-based polymer composites**: Rubbers (elastomers) are soft polymeric materials with sub-ambient glass-rubber transition temperature, excellent elastic properties, and flexibility. They have found important applications in different fields, such as automobile, aerospace, biomedical, etc. Incorporating rigid fillers in elastomer compounds has been a common practice for improving mechanical properties (reinforcement) and thermal, dynamic-mechanical, electrical, and magnetic properties, among others. The reinforcement effect of the rigid fillers may be attributed to the filler matrix interactions, which depend on the structure of both filler and matrix components[37].

The preparation of graphene elastomer composites has been accomplished using various synthetic techniques, each of which has a unique impact on the properties of the finished composites. Multiple factors, such as filler-filler interactions, filler-matrix interactions, filler dispersion in the matrix, impurity concentration, and consistency of the formula's composition, might change as the mixture is mixed. Each of the abovementioned factors results in a composite with unique defining characteristics.

MOST WIEDZY Downloaded from mostwiedzy.pl

2.3 Silicone rubber

The first-time silicon was successfully isolated on its own using potassium was in 1824 by the Swedish chemist Jöns Jackob Berzelius. He then heated silicon in chlorine, creating intense combustion in the process. The outcome was silicon tetrachloride, used to make silicones today. Silicon was created, in our opinion, by Berzelius. It took Henry Sainte-Claire Deville another 31 years to develop silicon in its more widely used crystalline form. Deville used an electrolytic smelting procedure to acquire pure silicon in 1854. Throughout the 19th century, numerous chemists continued their investigation into silicon chemistry and current silicone elastomers market report shown in table-2.

Table-2 Silicone Elastomers Market Report Coverage[38]

Report Attribute	Details
Historical Years	2017-2021
Forecast Years	2022-2030
Market Size in 2021	$8,344.8 Million
Revenue Forecast in 2030	$16,425.2 Million
Growth Rate	7.8% CAGR
Report Scope	Market Trends, Drivers, and Restraints; Revenue Estimation and Forecast; Segmentation Analysis; Impact of COVID-19; Companies' Strategic Developments; Market Share Analysis of Key Players; Company Profiling

Silicone rubber is an elastomer of silicon and other carbon, hydrogen, and oxygen elements. Its structure always comprises a siloxane backbone (silicon-oxygen chain) and an organic moiety bound to the silicone. Silicone rubber is nonreactive, stable, and resistant to harsh conditions and temperatures ranging from 55°C to 300°C (67°F to 572°F) while retaining its valuable properties[39]–[41]. Silicone rubber is used in a wide range of products, including automotive applications, cooking, baking, electronics, medical equipment, and implants, due to its characteristics and convenience of manufacturing and shape. Hence, the properties of silicone rubber can vary greatly depending on the following:

MOST WIEDZY Downloaded from mostwiedzy.pl

Organic groups (methyl, vinyl, phenyl, trifluoropropyl, or other groups)

Different Types & Methods Used to Synthesize Silicone Rubbers

The organic groups in silicone rubbers may be methyl, vinyl, phenyl, or others. According to ASTM D1418 standard, which covers a system of general classification or nomenclature for rubber and rubber lattices, silicone rubbers are classified as shown in table-3:

Table-3 – Classification of silicone rubber based on the structure

Dimethyl silicone	Methyl- Vinyl silicone	Phenyl- Methyl silicone
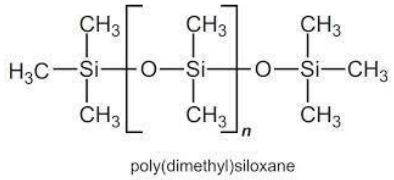 poly(dimethyl)siloxane	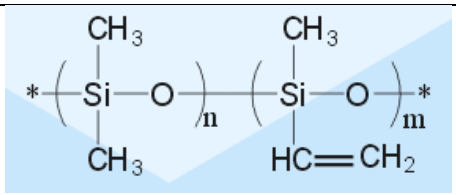	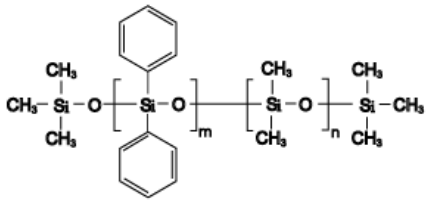

Silicone rubbers can be represented by,

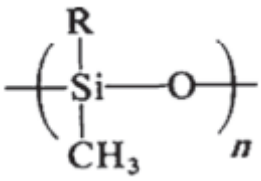

R can be any of the following: methyl, phenyl, vinyl, trifluoropropyl, or 2-cyanoethyl. Silicone rubbers with vinyl groups can be cured with dialkyl peroxides like di cumyl peroxide. Crosslinking in saturated siloxane rubbers involves hydrogen atom abstraction followed by polymeric radical coupling. The interaction of polymeric radicals with lower-molecular-weight free radicals created by the disintegration of the peroxide curative leads to the non-productive use of peroxide. The addition of vinyl groups improves the effectiveness of crosslinking. Silicone rubber is a family of thermoset elastomers that have a backbone of alternating silicone and oxygen atoms and methyl or vinyl side groups. According to the polymer employed and the vulcanization process adopted for their production, they can be classified as low-temperature vulcanizable rubbers (low-temperature vulcanizate rubber, LTV, and room temperature vulcanizate rubber, RTV) and high-temperature vulcanizable rubbers (HTV). Silicone rubber maintains its mechanical and electrical properties over a wide range of temperatures and therefore is a choice for every application, from aerospace to medical devices.

MOST WIEDZY Downloaded from mostwiedzy.pl

They are used to produce seals in the automotive industry, aerospace industry, connectors, cables for appliances and telecommunications, implants and devices for medical purposes, and packaging and baking pans for the food industry.

2.3.1 Curing Agents

Silicone rubbers are typically cured using peroxides such as benzoyl peroxide, 2,4-dichlorobenzoyl peroxide, t-butyl perbenzoate, and dicumyl peroxide, except for RTV and liquid curing methods. Vinyl containing silicones has also been effectively treated using alkyl hydroperoxides and dialkyl peroxides. The alternative curing process known as hydrosilylation or hydrosilation uses hydrosilane materials as catalysts and platinum-containing chemicals to cure silicones that contain vinyl. A free radical reaction started by peroxide results in a peroxide cure. The peroxides break down when heated, creating highly reactive radicals. The silicone liquid will react with these radicals, crosslinking the polymer to create a three-dimensional network. Solid silicone rubber can be processed with this method. Different vulcanizing agents used for curing silicone rubber shown in table-4.

Table-4 Different vulcanizing agents used for curing silicone rubber

Polymer	Applications	Appearance	Main vulcanizing ingredient
Polydimethylsiloxane	General molding, thin sections	White paste	Benzoyl peroxide Approx. 50% content
Silicone rubber (SH5060U)	General molding, steam curing, flame retardance	White putty	Dicumyl peroxide Approx. 20% content
Fluorosilicone rubber	General molding	Grayish white paste	Ditertiarybutyl peroxide Approx. 20% content
Sillicone rubber , LDPE, HDPE and fluoroelastomers	General molding, thick sections	Grayish white paste (C-8) Translucent paste (C-8A, C-8B)	2.5 dimethyl-2.5 bis (tertiarybutylperoxy) hexane Approx. 25% content (C-8), approx. 80% content (C-8A), approx. 40% content (C-8B)

MOST WIEDZY Downloaded from mostwiedzy.pl

2.3.2 Liquid Silicone Rubbers

These were two-part systems frequently delivered in pre-metered equipment deaerated and ready for use. Low-pressure forming techniques and low-pressure injection pressures were adequate. After combining the two distinct parts, they cure using procedures like hydrosilylation. At temperatures of roughly 200 C, curing frequently finished in just a few seconds, and post-curing was typically not necessary. Liquid silicone rubbers (LSRs) can compete with traditional silicones and organic rubbers due to the cheap capital expenditure needed for manufacture. Comparable to general-purpose grades and high-strength peroxide-cured elastomers in terms of physical characteristics. Silicone resin is a type of silicone utilized extensively in aerospace, automotive, electronics, electrical, and other industries due to its high dielectric qualities, good thermal stability, weather resistance, chemical reactivity resistance, and other advantages[42]–[45].

2.3.3 Room Temperature Vulcanizing (RTV) Rubbers

In general, RTV silicone rubber is always a liquid that cures to become a solid elastomer. Another way to separate RTV silicone rubber is into one-part (RTV-1) and two-part (RTV-2) silicone rubber (RTV-2)[46], [47]. The moisture can start the vulcanization reaction in the air for one-part condensation curing silicone rubber, eliminating the need for additional initiators. The air's moisture cannot begin the crosslinking process for two-part silicone rubber; instead, different catalysts are required.

2.3.4 High temperature vulcanized (HTV) Rubbers

High-temperature vulcanization (110–170°C) creates high-temperature vulcanized silicone rubbers (HTV). They combine curing agents, fillers, and a linear high molecular weight polysiloxane as the basis silicone. HTV silicone rubbers are distinguished by their high-temperature stability. Although HTV silicone rubbers are only half as strong as certain other synthetic rubbers at room temperature, they can maintain their flexibility, elastic resilience, and surface hardness when exposed to temperatures of more than 200°C.

MOST WIEDZY Downloaded from mostwiedzy.pl

Fundamental Properties and applications of Silicone Rubbers

The strong Si-O chemical structure and high bond energy give Si Elastomers unique performance properties. Several benefits of silicone rubbers include:

Wide service temperature range – excellent thermal and thermoxidative resistance (-Si-O-Si- binding energy is higher than C-C bonds)

Excellent resistance to attack by oxygen, ozone, and sunlight

- Readily resistant to electromagnetic and particle radiation (UV, alpha, beta, and gamma rays)
- Excellent non-stick and non-adhesive properties
- Low toxicity
- Flexible at low temperatures
- Optical transparency
- Good excellent insulation properties
- Low chemical reactivity
- High bio-compatibility
- Excellent mechanical properties (high tear strength, high elongation)

Among the several artificial rubbers, silicone rubber has the best attributes. It possesses various properties, including excellent temperature resistance, lower toxicity, and little odour. Silicone rubber can keep its hardness and elasticity in temperatures as low as -90°C or as high as 300°C. Additionally, silicone rubber has excellent chemical stability, oxygen resistance, and electrical insulation[48]. Due to these remarkable characteristics, silicone rubber plays a significant part in contemporary society.

Products made of silicone rubber are used in various industries, including automotive, textiles, electronics, metalwork, and food storage. Furthermore, silicone rubber finds extensive use in medical fields[49]. Many silicone medical items, including artificial blood vessels, artificial tracheas, artificial lungs, and noise-canceling earplugs, have been produced successfully. The automotive industry uses silicone rubber in practically every area[50]. Among silicone rubber's many beneficial qualities are its excellent insulation, heat and chemical resistance, adhesion, and tear strength. Silicone rubber is hence particularly well suited for the production of automobiles and the supply of automotive components.

MOST WIEDZY Downloaded from mostwiedzy.pl

The sealed self-lubricating silicone rubber can offer a reliable and robust seal for many devices, including the headlamp and the oil filter. The gasket's silicone rubber seal prevents leaks and is long-lasting[51]. Under conditions of high pressure and temperature, it won't break or crack. Low rolling resistance tyres made of silicone rubber have excellent grip, outstanding durability, and improved mileage.

Numerous qualities of silicone rubber include its ability to tolerate high temperatures and pressure, strong biocompatibility, consistent performance, and low blood coagulation. And it may be formed into many different shapes, such as thin-film, sponge, airbag, etc.

Silicone rubber sealant has another important use. This is the same silicone rubber used in the study. Glass curtain walls are one of the common uses for silicone sealant. The silicone structural glue is used to attach the glass and aluminium alloy frames that make up the exterior walls. In contrast, silicone weatherproof adhesive waterproofing seals the expansion joints.

2.4 Nanofillers

Polymer nanocomposites have attracted much scientific and industrial attention in recent years, owing to many advancements in these materials due to combining a polymeric matrix with organic and an inorganic nanomaterial. Nanocomposites can also exhibit one-of-a-kind design possibilities, which provide significant advantages in creating functional materials with desired qualities for specific applications [29]–[35]. Nanocomposites have the potential to expand the variety of applications for polymers due to their superior features, such as high temperature resistance, dimensional stability, better barrier property, flame retardancy, and enhanced thermomechanical property.

2.5 Carbon nanofillers

2.5.1 Graphite

Graphite is a naturally occurring form of crystalline carbon. It is a native element mineral found in metamorphic and igneous rocks. Graphite is a crystalline form of carbon with the sp^2 hybridization structure[59]. Carbon allotropes such as graphite are well-known. Graphite is anisotropic and behaves as an excellent thermal and electrical conductor due to its in-plane metallic bonding. The electrical conductivity of graphite makes it ideal for electrochemical electrodes and electric brushes. Graphite's anisotropic structure allows it to conduct chemical reactions by allowing the reactant molecule to intercalate between graphene layers. Charge

MOST WIEDZY Downloaded from mostwiedzy.pl

transfer occurs between the intercalate and the graphite in graphite intercalation compounds, resulting in electrically conductive material. Graphite acts as a starting material for several graphene-based nanofillers.

2.5.2 Exfoliated *graphite*

Exfoliated graphite (EG) refers to a degree of separation of a substantial portion of the carbon layers in the graphite, which can involve chemical, mechanical, and thermal methods. The separation occurs between adjacent carbon layers, but not all the carbon layers are separated. The separation may or may not occur throughout the plane between the adjacent carbon layers. Exfoliated graphite is made by rapidly heating (or flash heating) graphite intercalation compounds such as graphite hydrogen sulphate with a high particle diameter (flakes). The graphite layers are forced apart by the vaporizing intercalated substances. The exfoliated graphite takes on an accordion-like shape with hundreds of times the volume of the original graphite flakes. Because of its unusual structure, EG exhibits properties (mechanical, thermal, electrical, dielectric, and other properties) that differ from conventional graphite and have numerous applications beyond traditional graphite[60].

2.5.3 Graphene

Graphene was discovered in 2004 by Andre. K. Geim and Konstantin S. Novoselov have since transformed the scientific frontiers in nanoscience and condensed matter physics due to their extraordinary electrical, physical, and chemical capabilities[8]. Graphene is the name given to a flat monolayer of carbon atoms tightly packed into a two-dimensional (2D) honeycomb lattice. It is a fundamental building block for graphitic materials of all other dimensionalities. Exfoliation of bulk graphite into individual sheets is required to use graphene successfully. Several chemical-mechanical techniques have been devised to manufacture individual exfoliated graphene sheets, such as mechanical, chemical, and chemical vapor deposition, as shown in figure-4. Due to the enormous surface area of graphene and the strong intrinsic interaction of π- bonds between graphene sheets, graphene is difficult to disperse in polymers. The graphene dispersion in the polymer matrix significantly impacts the composites' characteristics. It's a single-atom-thick sheet of hexagonally organized sp^2-bonded carbon atoms suspended or attached to a foreign substrate. Its lateral diameters can range from a few nanometers to micrometers.

MOST WIEDZY Downloaded from mostwiedzy.pl

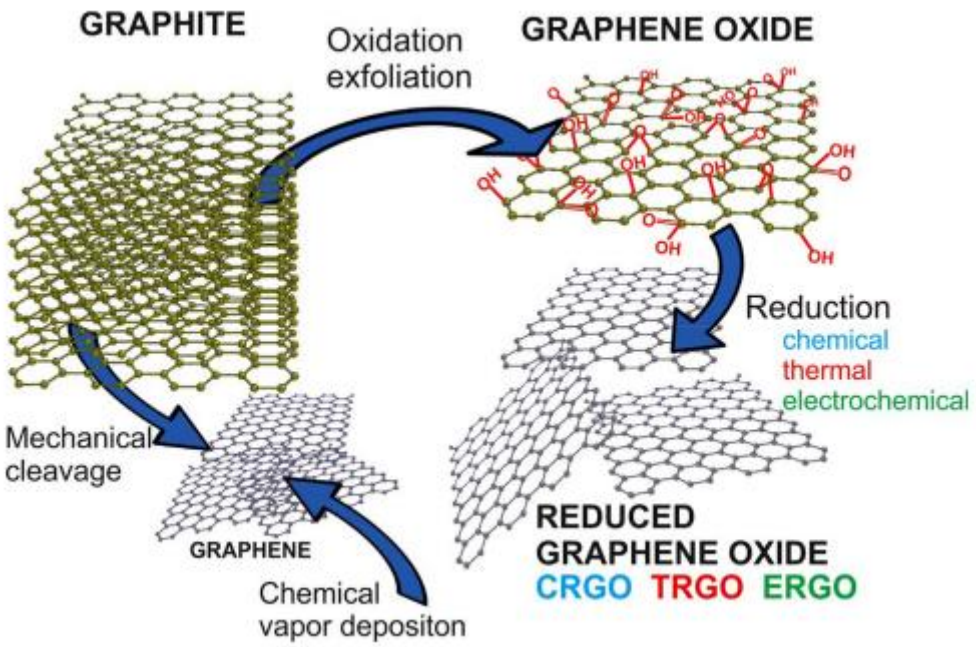

Fig.4 schematic representation of the preparation of graphene[61]

Due to its high surface area and the solid intrinsic interaction of its π- bonds, graphene can aggregate easily, making it challenging to disperse in polymers. The graphene's distribution significantly influences the characteristics of the composites in the polymer matrix[62]. Graphene oxide nanosheets possess abundant oxygen functional groups, such as carboxyl, hydroxyl, and epoxy. GO's polar groups make it disperse poorly in several organic solvents. This implies that GO will not disperse nicely within the polymer matrix. To solve this issue, graphene can be modified using different functionalizing agents to increase its dispersion in the polymer matrix. Surface modifying agents can be used to modify graphene to improve its dispersion in the polymer matrix. Song et al. developed graphene nanoplatelets (GNPs) and silicone rubber composites with improved thermal conductivity and electrical and mechanical properties. The tensile strength varies from 0.240 to 0.608 MPa with the addition of a low content (0–8%) of GNPs[10].

Graphite oxide has a layered structure similar to that of graphite. Still, the plane of carbon atoms in graphite oxide is heavily decorated by oxygen-containing groups, which expand the interlayer distance and make the atomic-thick layers hydrophilic. These oxidized layers could exfoliate in water under ultrasonication. If the exfoliated sheets contain only one or a few layers of carbon atoms like graphene, then these sheets are named graphene oxide (GO). GO can be

MOST WIEDZY Downloaded from mostwiedzy.pl

(partly) reduced to graphene-like sheets by removing the oxygen-containing groups and recovering a conjugated structure. The reduced GO (rGO) sheets are usually considered one chemically derived graphene and are known as rGO. Some other names have also been given to rGO, such as functionalized graphene, chemically modified, or reduced graphene.

2.6 Surface modification of Graphene oxide

The functionalization of GO plays an essential role in controlling the exfoliation behavior of GO and rGO but also holds the key to various applications. Once rGO has been produced, there are ways that one can functionalize it for use in different applications. Covalent functionalization and noncovalent functionalization are two approaches that are used. In covalent functionalization, oxygen functional groups on GO surfaces, including carboxylic acid groups at the edge and epoxy/hydroxyl groups on the basal plane, can be utilized to change the surface functionality of GO. By treating rGO with other chemicals or creating new compounds by combining rGO with other 2D materials, one can enhance the properties of the mixture to suit commercial applications.

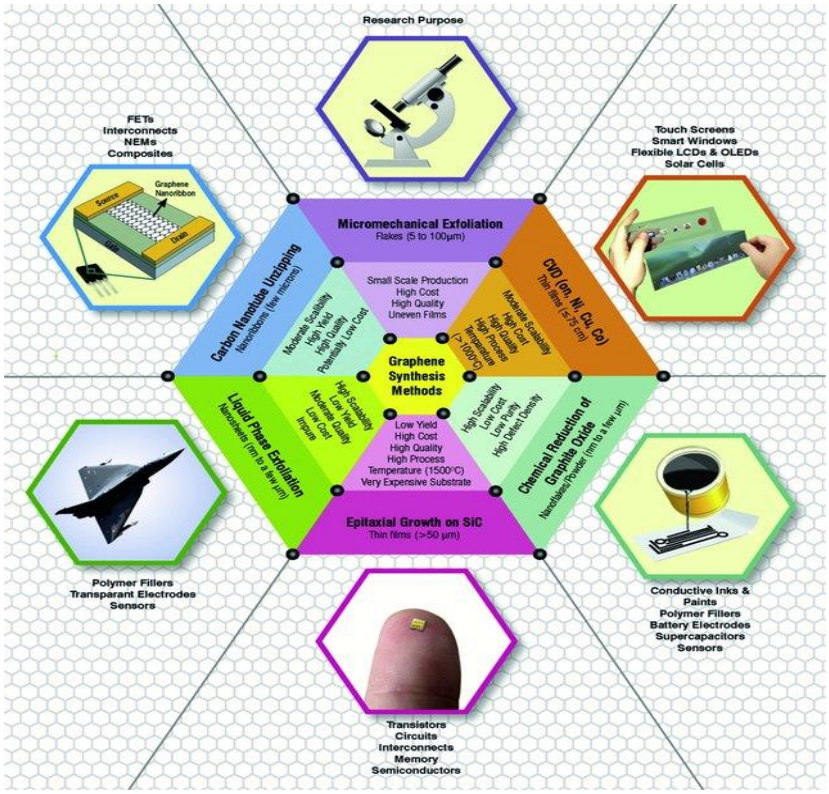

Fig.5 Schematic of some popular graphene synthesis techniques along with their respective features and their potential applications[63]

MOST WIEDZY Downloaded from mostwiedzy.pl

2.6.1 Ionic liquid

Ionic liquids (ILs) are molten salts from the association of organic cations and organic/inorganic anions with a melting point below 100 °C. Paul Walden reported the first IL (ethylammonium nitrate) in 1914. ILs are the subject of a multidisciplinary study involving chemistry, materials science, chemical engineering, and environmental science. As more information about the nature of ILs becomes available, specific key fundamental ideas diverge from the initial concepts. Ionic liquids (ILs) emerged as a greener alternative to conventional organic solvents. ILs are tunable and can be adapted to extract a given analyte by properly selecting constituent ions. IL's physicochemical features are now extensively recognized. "Non-volatile, non-flammable, air and water" is a term that is frequently used. Flammable, unstable, and volatile. This is owing to the vast number of Cation and anion combinations. In many physical and chemical processes, this occurs frequently. This method is preferred rather than using traditional volatile solvents and catalysts within a suitable spectrum of "green" and "designer" characteristics[64]. Moni et al. functionalized reduced graphene oxide (rGO) with varying amounts of IL to improve the dispersibility and interaction with the fluoroelastomer (FKM) matrix. A schematic diagram of surface modification of reduced graphene oxide with IL illustrated in figure-6.

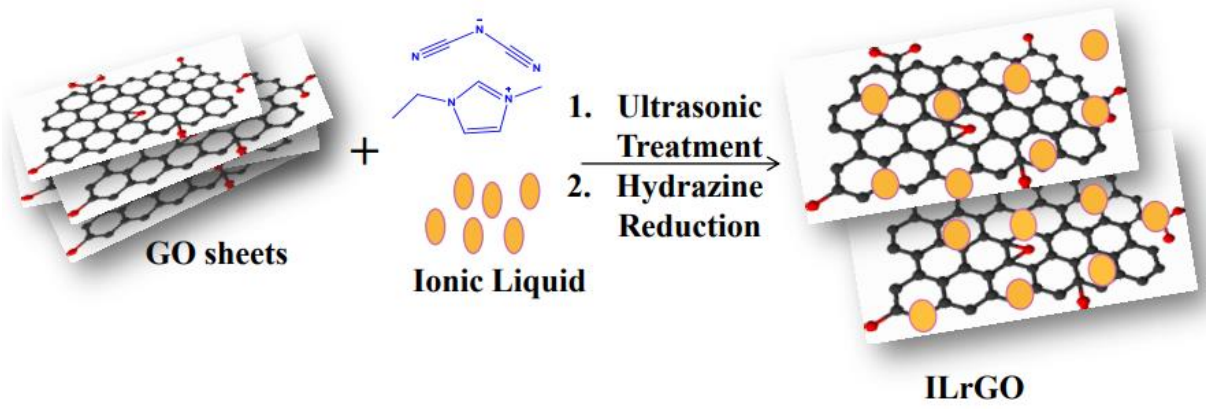

Fig-6 Preparation of Ionic Liquid Modified Reduced Graphene Oxide[65]

2.6.2 Silane modification

Silane organic compounds as a modifier of carbon-based materials could produce nanomaterial with new chemical and physical properties. Yang and coworkers prepared modified graphene via facile covalent functionalization of GO with 3-aminopropyltriethoxysilane and employed

MOST WIEDZY Downloaded from mostwiedzy.pl

it as reinforcing components in silica monoliths shown in figure-7.[66]. The resulting functionalized graphene sheets showed high dispersibility into water, polar solvents such as ethanol, dimethylformamide (DMF), and dimethyl sulfoxide (DMSO). Chemonne et al. linked chelating groups via a silanization reaction between N-(trimethoxysilylpropyl) ethylenediamine tri acetic acid (EDTA-silane) and hydroxyl groups on GO sheets. The modified GO showed high adsorption behavior for Pb (II) removal[67].

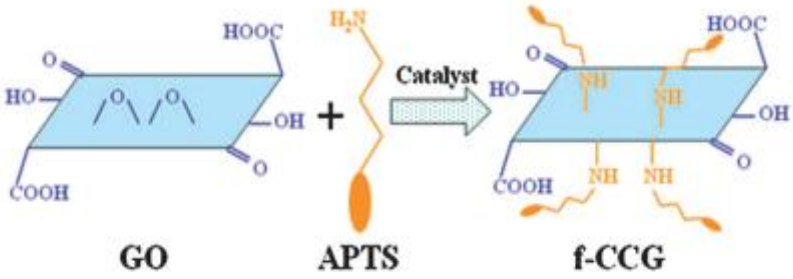

Fig.7 - Illustration of the reaction between GO and 3-amino- propyltriethoxysilane (APTS)[66]

2.6.3 Hybrid nanofillers

Hybrid multiscale fillers in polymer matrices could exploit the individual properties of nano or microscale fillers and contribute to enhanced mechanical and thermal properties[68]. Numerous studies reported that friction and wear behavior could be improved by lowering adhesion and higher stiffness and strength. This could be achieved by incorporating specific fillers individually or in combination in polymer matrices. The wear performance of hybrid nano fillers (nano-aluminium oxide, Al_2O_3, and nano-silicon carbide, SiC) infused epoxy resin composite system was discussed by Alhazmi et al.[69]They reported that Al2O3 reinforced epoxy composites during wear tests showed better wear resistance than SiC (silicon carbide) reinforced epoxy composite systems. Typically, hybrid nanocomposites consist of materials produced from several nanofillers combined through multiphase or single-phase approaches to enhance the properties of materials. The three most important principles in the design of hybrid nanofiller polymer nanocomposites, particularly for tribological applications, are "(1) economic consideration by which expensive nanofiller can be combined with less expensive ones, (2) combined functional and property enhancement, and (3) efficient preparation method hybrid effect"[70]. Tribological hybrid polymer nanocomposites are created by adding two or more nanofillers capable of synergistic impact on polymeric materials[71].

MOST WIEDZY Downloaded from mostwiedzy.pl

Table-5 Composite system of hybrid nanofiller and multiscale filler reinforced composites for tribo applications.

Matrix	Hybrid fillers	Test methods	References
Hybrid nanofiller reinforced polymer composites			
Epoxy	Aluminum oxide(Al_2O_3) and silicon carbide (SiC)	Pin –on-disc apparatus; load 5N;velocity 20rpm	[69]
Polyphenylene sulphide(PPS)	Short/micro Carbon fiber/polytetrafluroethylene	Ring on block test rig, linear velocity of 0.42m/s, load 200N, duration 120min, dry sliding	[72]
Nomex/PTFE fabric	Boron nitride nanosheets/carbon nanotubes	Sliding velocity 0.26m/s,120 min	[73]
Multiscale filler reinforced hybrid composites			
Epoxy	Glassfiber/nanoclay	Pin –on-disc apparatus	[74]
Polyphyneylene sulphide(PPS)	Nano CuO/Aramid/Kevlar fiber	Pin-on-disc sliding configuration, sliding speed 1m/s, 6h duration	[75]
Polyphyneylene sulphide (PPS)	Short carbon fiber/sub micro scale TiO_2	Pin on disc wear tests, Room temperature, sliding speed 1 to 3m/s, 20h duration	[76]
Polyetheretherketone (PEEK)	Short carbon fiber/ nano SiO_2	Block on ring tests, room temp: 21^oC; dry sliding, sliding velocity 0.5 to 2 m/s, 20 hr duration	[77]

Studies that record the inclusion of two separate carbon-based nanofillers to generate hybrid polymer nanocomposites for tribological applications are of commercial interest since such secondary hybrid nanocomposites offer better tribological capabilities than single filler-filled nanocomposites. The composite system of hybrid nanofiller and multiscale filler reinforced composites is shown in table-5. In a study of graphene/short carbon fiber/polytetrafluoroethylene/polyether ether ketone (G/SCF/PTFE/PEEK) hybrid nanocomposites, researchers discovered that graphene does not only improve the load-bearing capacity of the system but also stimulates the formation of a uniform transfer film with superior strength and contributes to better tribological performance than pristine graphite[78]. Likewise, in a ternary hybrid epoxy nanocomposite system, multi-walled carbon nanotubes (MWCNT)

MOST WIEDZY Downloaded from mostwiedzy.pl

and graphite nanopowder were mixed with carbon fiber (CF) to provide superior component interaction[79]. A more coiled and robust structure was discovered, which improved heat absorption, tensile stability, and overall toughness of the ternary nanocomposite system, resulting in greater wear-resistant capacity and lubrication effect—this improved nanocomposites' adherence to the counter-surface. The impact of hybrid fillers on the tribological performance of nanocomposites was investigated under various sliding temperatures, speeds, and loads. It was observed that as the sliding temperature rises, the coefficient of friction falls while wearing resistance increases[80]. The polymer matrix softens, and the shear force decreases when exposed to high temperatures, decreasing the coefficient of friction and simplifying material removal. Because of the improved thermal conductivity of graphene composites, it provides more excellent wear resistance at high temperatures

2.7 Tribology

Tribology is an interdisciplinary science of interacting surfaces in relative motion. The critical issues addressed in this section are friction, wear, and lubrication. For the last few decades, conventional engineering materials have been replaced by polymeric materials for most tribological applications. The self-lubricating property of polymers and scope for improving surface and bulk properties by adding suitable fillers makes it a potential candidate for replacing the conventional materials for the tribological application. Today there is a rapid increase in the application of polymeric materials for developing mechanical systems where rubbing contacts are present. These contacts can roll and slide in nature, and polymeric contacts replace conventional engineering materials. When we return the traditional metallic or ceramic materials with a polymeric system, mechanical lubrication can be reduced. By adopting this replacement, greater control over the coefficient of friction can be achieved. Compared with engineering metals and ceramic, the mechanism behind the wear in polymers significantly differs in surface topography and its bulk mechanical properties. Polymers in the tribo are their viscoelastic behavior and low surface energy. Polymer tribology is a science that deals with the analysis of abrasion, adhesion, and fatigue of polymer materials in a friction contact. Friction generally means a resistive force experienced by the bodies undergoing relative motion, and it may be due to the electromagnetic interactions on charged particles on the rubbing surfaces. Various parameters, surface roughness, surface tension, surface wettability and interaction with lubricants, etc., significantly affect the tribological performance of the

MOST WIEDZY Downloaded from mostwiedzy.pl

polymer composites. For the last few decades, greater attention has been given to developing polymer-based composites for tribological applications. The self-lubricating property of the polymer matrix is the main reason for this, and the usage of additional lubricants can be avoided to a greater extent. After adding functional fillers and reinforcements to polymer composites, it was discovered that they exhibit outstanding friction and wear properties. Because of this, they are adaptable to a variety of industrial applications.

Table -6 : Dynamic Coefficient of friction for commonly used polymer groups[81]

Polymer	COF	Polymer	COF
PTFE	0.10	PVC	0.30
UHMWPE	0.12	HDPE	0.28
Nylon6 Cast	0.26	LDPE	0.60
Nylon 6 Cast, Oil filled	0.14	Polypropylene Homo Polymer	0.26
		Nylon66	0.25
Acetal, Homopolymer	0.20	Nylon66" Super Tough"	0.28
PEEK Unfilled	0.18	Nylon 66 Extruded	0.26
PEEK 30% GF	0.31	Acetal Co polymer	0.18
Polysulphone	0.37	PEEK 30% Gr	0.30
		PEEK 30% carbon filled	0.22
		PPO/PS	0.39

The main consequence of friction is wearing. Wear leads to degradation of material performance, leading to wastage of materials. Dynamic Coefficient of friction for commonly used polymer groups is shown in table-6. Different wear mechanisms include adhesive wear, abrasive wear, corrosive wear, erosive wear, and fatigue wear. Excessive wear may lead to catastrophic failure of the system and affect productivity badly. Proper control over the coefficient of friction wear rate can be optimized. So much energy is lost in friction in mechanical components. To minimize energy loss, energy wastage in friction has to be minimized. By adequately addressing the issues in tribology, we are conserving energy. Therefore, finding new materials and technologies in tribology is critical for developing a greener and more sustainable world.

Polymer tribological properties are not inherent in the material but are specific to the sliding system[82]. Because of their viscoelastic properties, polymers' tribological behavior is primarily influenced by the nature of the material and its counter-face, sliding surface roughness, contact pressure, velocity, and temperature. These factors affect the total contact area and the transfer film generation, resulting in various friction coefficients and wear patterns.

MOST WIEDZY Downloaded from mostwiedzy.pl

The polymeric transfer layer, which occurs during polymer-metal or polymer-polymer sliding, is an essential component of polymer tribology because it modifies the contact surface [80]

2.7.1 Tribology of polymers reinforced with nanofillers

Polymer nanocomposites are widely used for tribological applications due to their ability to withstand abrasion and wear resistance and are mechanically rigid when reinforced appropriately with the suitable fillers. In the design of tribological polymer/nanocomposites, the choice of matrix, the reinforcement materials, and the mechanism to control the internal lubricants are significant. Wang et al.[83] reported studies on (PEEK) polymer with different types of nanofillers (ZrO_2, Si_3N_4, SiO_2,SiC) and found that nanofiller content below 10 wt% could lead to enhancement in wear resistance and reduced CoF[84]. The mechanisms that enhanced the tribological performance are the occurrence of transfer film and smoothened steel counterface. Schwartz et al.[85] Studied the wear resistance exhibited by PPS/nano alumina composite and revealed maximum wear resistance at nanofiller content below 10 wt%. The enhanced filler dispersion in the matrix could be observed below 10 wt% and the composite exhibited a higher wear rate. Li et al. [86] reinforced PTFE with ZnO nanoparticles, and appreciable wear resistance was observed at 15 vol% of filler, but PTFE/ZnO nanocomposite exhibited a higher friction coefficient concerning virgin PTFE. Polymethylmethacrylate (PMMA) incorporated with nanosized $CaCO_3$ particles disclosed enhanced abrasion resistance, and a noticeable increment in wear resistance was observed at 3 wt% of $CaCO_3$[87].

Table-7 The lowest wear rate reported for selected composites widely used in tribo applications.

Matrix	Nanofiller	Vol% of nano filler	Least wear rate reported, k($x10^{-6}$ mm^3/Nm)	Reference
PTFE	Al_2O_3	12(<40 nm size)	1.2	[88]
PEEK	Si_3N_4	2.8(<50 nm size)	1.3	[89]
Epoxy	Si_3N_4	0.8(<20nm size)	2	[90]
Epoxy	Al_2O_3	2(13 nm size)	3.9	[91]
PEEK	SiO_2	3.4 (<100 nm size)	1.4	[83]
PTFE	ZnO	15(50 nm)	13	[86]

MOST WIEDZY Downloaded from mostwiedzy.pl

PPS	TiO_2	2(30-50 nm)	8	[92]

The wear rate for some of the most wear-resistant nanocomposites is given in Table 7. New nanofillers have generated significant interest over the past two decades because they can provide rubbers with new functionalities like electrical conductivity, wear resistance, low gas permeability, and low heat buildup, in addition to improving the mechanical properties of the rubbers at very low loading[93]. For instance, layered silicates were added to rubbers to give them a better gas barrier property and outstanding tensile strength[94]. Rubber nanocomposites' electrical conductivity was increased by the addition of carbon nanotubes[95]. The introduction of graphite nanosheets improved rubber nanocomposites' abrasion resistance [96]. The incorporation of boron carbide into natural rubber resulted in low heat generation[50].

2.7.1 Tribology of rubber nanocomposites

Beginning in 1942, many rubber scientists studied the variation of the COF with load and found that the COF for rubber compounds used in tires decreases with increasing load[97]. Nanostructured elastomeric materials, one of the fastest-growing materials, are increasingly used in applications that include friction and wear. As a result, the practical importance of wearing such rubbery nanocomposites cannot be overstated. Thorough scientific research on the abrasion of such nanocomposites has yet to be conducted. Because of the surrounding wear's complexity and mechanism, much of the knowledge on the tribological behavior of rubbery macro composite materials is empirical. Schallamach[98] found that the COF of rubber increased as sliding velocity over a wide velocity range in a minimal range and found that the phenomenon was related to a change in temperature. Wear resistance is an essential piece of technical information directly influencing rubber products' working life, such as tires, conveyor belts, shoes, and seals. The wear resistance of pure rubbers is minimal, so wear-resistant fillers must be added to the rubber matrix. Solid lubricant is one of the most widely used wear-resistant fillers. Thavamani and Bhowmick [99] reported abrasion of carbon black filled natural rubber (NR), styrene-butadiene rubber (SBR), and hydrogenated nitrile rubber (HNBR). They confirmed the abrasive wear by slight tearing was not solely due to crack growth between wear and frictional work using an entirely different apparatus.

When a hard surface slides on a soft surface, there are possibilities for removing material from both surfaces that could lead to the formation of a groove. This is like forming a

MOST WIEDZY Downloaded from mostwiedzy.pl

ridge which leads to wedging, plowing, and cutting of materials and could be categorized as abrasive wear. The experimental evidence revealed in various articles explains that wear rate is proportional to the average load, abrasive particle size, and inversely proportional to the hardness of the material. Single-body and two-body abrasive wear are two modes of wear transfer [37]. Abrasive marks formed on one surface are called single-body abrasive wear, and abrasive wear developed on both surfaces is grouped under two-body abrasive wear [38].

Nanostructured elastomeric materials, one of the fastest-growing materials, are increasingly used in many applications to reduce friction and wear. Because of the complexity surrounding wear and its mechanism, which depends on many parameters such as the physical and mechanical properties of interacting surfaces, temperature, pressure, and the velocity at which the wear occurs, much of the knowledge on the tribological behavior of rubbery macro composite materials is empirical. As a result, the practical importance of wearing such rubbery nanocomposites cannot be overstated. Thorough scientific research on the abrasion of such nanocomposites has yet to be conducted. Ionic liquid-modified graphene (TrGO-IL) was created through an amidation reaction and thermal reduction. After that, it was blended with fluoroether rubber to create rubber composites. The ionic liquid was used as a self-lubricating layer on graphene to provide an adequate interface bonding of TrGO-IL with rubber matrix to increase FM's friction and wear resistance [96]. The composite's friction coefficient and wear rate dropped by 13.1% and 59.8%, respectively.

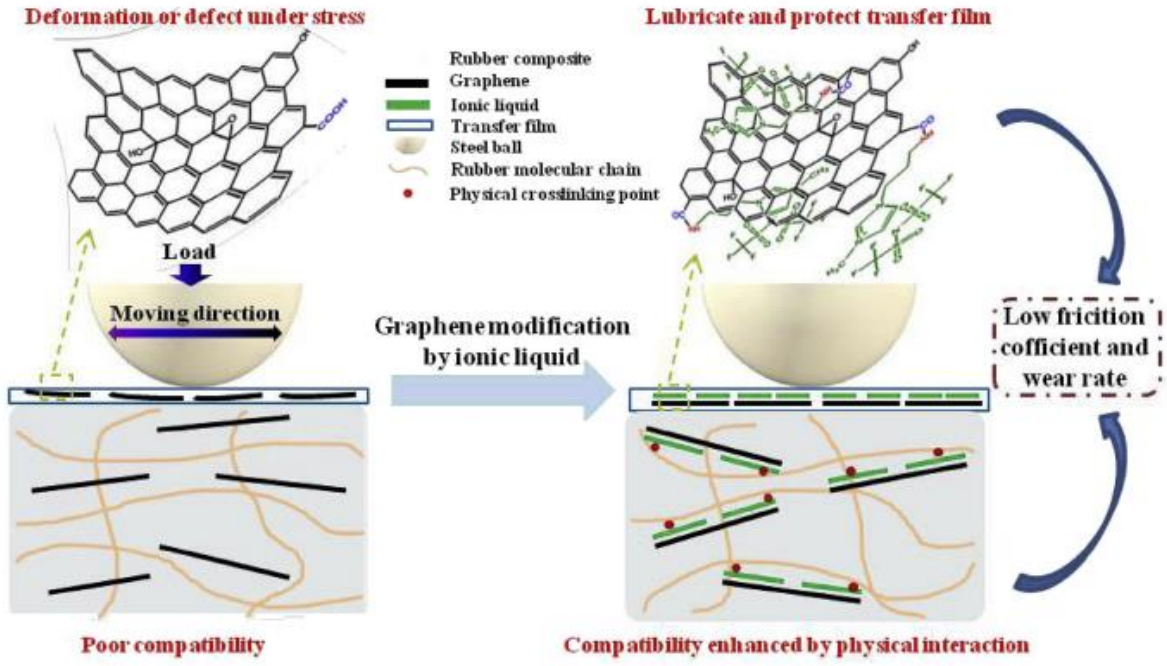

MOST WIEDZY Downloaded from mostwiedzy.pl

Fig.7 - Schematic diagram of tribological properties improvement mechanism of the graphene/fluoroether rubber composite introduced by IL[100].

Xing et al. used a modified latex compounding approach to create scalable and facile GE/SBR nanocomposites with high molecular-level interfacial contact between GE and SBR. Compared to the composite containing unmodified graphene, the compatibility of rubber withionic liquid modified reduced graphene oxide (TrGO-IL) and the crosslinking density increased. More significantly, FM-TrGO-friction IL-1's coefficient and wear rate dropped by 13.1% and 59.8%, respectively[100]. The GE/SBR nanocomposites exhibit exceptional electrical conductivity, gas impermeability, low heat buildup, enhanced wear resistance, and thermal stability[95.

2.7.2. Tribological tests

To understand the tribological features of the developed composites, two types of wear tests were carried out on the filler reinforced elastomeric specimens to study their friction and wear properties – two-body and three-body wear tests. Two body wear studies were conducted on a pin-on-disc machine as per ASTM G99 standards, as shown in figure 8. The pin gets rubbed against a rotating steel disc (EN -32) of hardness HRC 65 with a track diameter of 100 mm under loaded conditions. After noting the pin-shaped specimens' initial weight, they are subjected to an initial run-in period so that the specimen surface comes in complete contact with the disc surface. The coefficient of friction between the pin and the disc is measured by the deflection occurring in the calibrated load cell. The experiment is conducted for different loads, sliding distances, and temperatures, and the detailed experimental operating condition is listed in table-8.

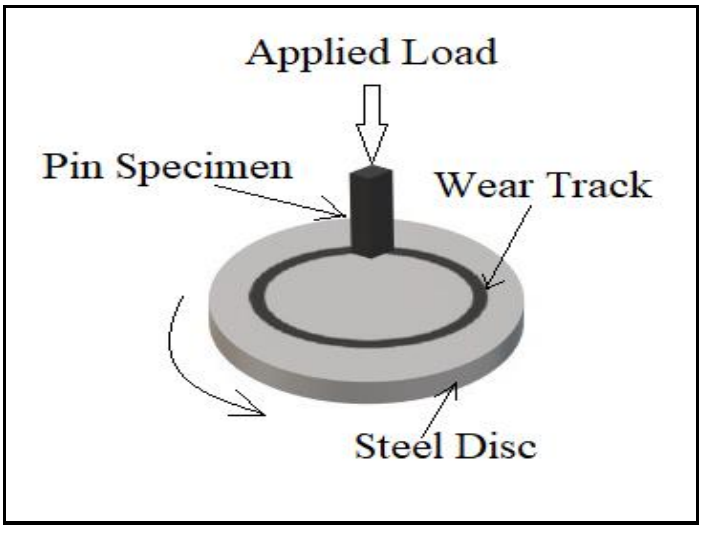

Fig.8 Schematic representation of pin-on-disc test

MOST WIEDZY Downloaded from mostwiedzy.pl

Table 8. Detailed Experimental Operating Conditions

Parameters	Operating Conditions
Temperature	Ambient conditions (temperature: 29 ° C)
Relative humidity	55(±5) %
Test disc	Hardened ground steel (EN 31, hardness 60 HRC)
Roughness of EN-31	1.6 m Ra
Rubbing duration	1800s
Load	10N,20N and30N
Sliding speed	1m/s,2m/s,3m/s and 5m/s
Sliding distance	1800mm and 3600mm
Pin size (ASTM G99 Std.)	30 mm × 10 mm × 10 mm

After completion of the tests, the specimen pins are cleaned with acetone and dried. Their final weights are noted for determining the weight loss from which the wear rates are calculated. The equipment monitor displays the generated tangential frictional force when the specimen starts to rub the counter face, and this force is recorded to calculate the coefficient of friction (μ) as follows:

$$\mu = F_f / F_n \text{----------(1)}$$

Where F_f (frictional force) and F_n(normal load which is applied). The specific wear rate (W_S) is calculated by:

$$W_S = \Delta m / \rho F_n L \text{----------(2)}$$

Here Δm is the weight loss, ρ is the composites' density, F_n is the applied load and L is the sliding distance (meters).

2.7.3 Three-body wear tests:

A dry rubber wheel abrasive wear test rig is used to conduct three-body wear studies according to ASTM G65, as shown in figure 9. The test specimen of size 76mm x 25mm x 2 mm, gets abraded by using dry sand as the abrasive particle, which is introduced in between the test specimen and the rotating wheel (rotated at a speed of 2 m/s) with a chlorobutyl rubber tire in a controlled flow rate. The wheel rotates so that its contact face moves toward sand flow. The wear tests are carried out for different load conditions. The abrasive particles used are silica

MOST WIEDZY Downloaded from mostwiedzy.pl

sand (AFS 50/70) of size 150-300 Mm, and the sand flow rate between the rubber wheel and specimen is 375 ± 5 g/min. The wear rate, determined from the measured weight loss values of the specimens, is further converted to wear volume. The equation calculates the specific wear rate (Ks);

$$K_s = \frac{V}{\mathrm{Fn} \times L} - - - - - - - - (3)$$

Where V- Volume loss (wear)

F_n- AppliedLoad

L - Sliding distance (meter)

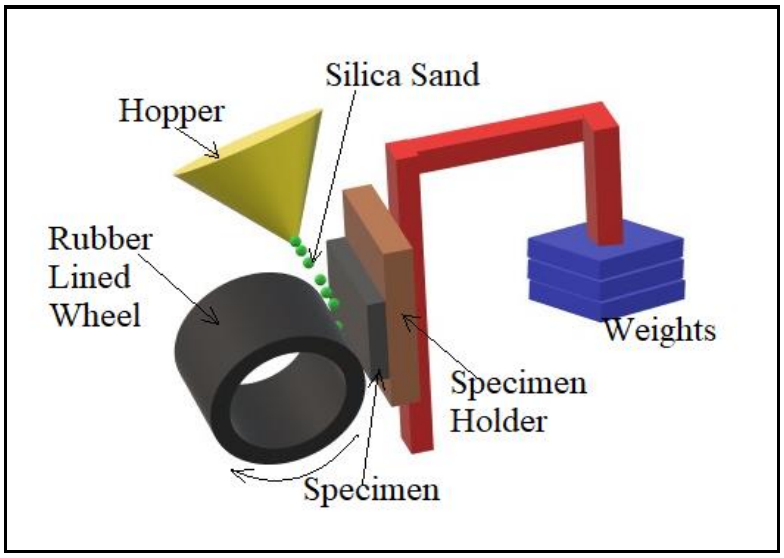

Fig. 9 -Schematic diagram of dry sand/rubber wheel abrasive wear test rig

The main techniques for reducing polymer friction are:

- Inclusion of solid (soft) fillers,
- External lubrication,
- Intrinsic (internal) lubrication.

The inclusion of solid soft fillers into a harder polymer reduces friction coefficients by using the harder polymer as a matrix and the softer filler/polymer as a lubricant, forming a transfer film at the interface between the filled polymer and a steel surface.

MOST WIEDZY Downloaded from mostwiedzy.pl

Research gap

Silicone rubber is a unique type of polymer with many applications, including seals, shock absorbers, adhesives, and the aviation sector. The lack of wear resistance and mechanical properties is a fundamental drawback of silicone rubber that restricts its continued use in particular unique situations. Graphene is a two-dimensional layered-structured material that attracted considerable interest as solid lubricants and lubrication nano-additives during the last decade due to their outstanding tribological performance stemming from their unique chemical and physical features. The excellent friction and wear-resistant properties of graphene make it a new and emerging lubricant in many applications. To our knowledge, no published work has yet examined the friction properties of graphene-silicone rubber composites.

Nanostructured fillers have recently been investigated for usage in elastomers. Even though using these filler compounds in elastomers is still challenging, they greatly enhance thermoplastic properties. In elastomers, the mixing process is still a challenging and complex task. This makes it difficult to manage filler particle agglomeration, dispersion, and interactions with the matrix. These issues are now being solved using various techniques, such as surface modification, grafting, and different compatibilizing agents. Graphene elastomer nanocomposites, also known as next-generation materials, have drawn much attention because of their excellent electrical, mechanical, and thermal capabilities. The synthesis of elastomer nanocomposites now has a promising pathway because of the discovery of graphene.

Examining the available literature and papers and publishing trends revealed the latest advancements in polymer nanocomposites in tribology. The main techniques for reducing polymer friction include solid (soft) fillers, external lubrication, and intrinsic (internal) lubrication. The effect of different forms of nanofiller on the tribological performance of polymer nanocomposites is explored, including carbon-based nanofiller, silicon-based nanofiller, and hybrid nanofiller. Polymer tribology and its friction and wear mechanisms are far more complicated but harder to understand than metal tribology.

There has been limited research on nanoparticle-filled polymer composites for tribological purposes. They prove that, despite intensive work on improving the tribological, mechanical, and thermal properties of polymers, there are still many inaccuracies in the subject, and effective management of the tribological, mechanical, and thermal properties of polymers, particularly elastomeric materials, still requires a lot of work.

MOST WIEDZY Downloaded from mostwiedzy.pl

3. Aim of the research work

This study outlines an innovative way to improve silicone rubber's tribological, mechanical, and thermal properties, unique to my work. Compared to other elastomers forms, very few results have been reported with QM reinforced graphene-based fillers in the literature, especially in tribology. Objectives of the research work, conducted during the doctoral studies, including

- To develop graphene-based Silicone rubber nanocomposites and study it is the properties of mechanical, thermal, and tribological properties
- To functionalize the surface of graphene using silane and ionic liquids and prepare modified .graphene/silicone rubber composites and thereby its properties
- To characterize the graphene-based materials and composites using XRD, FTIR, SEM, TEM, TGA, DMA, etc
- Study the synergistic effect of fumed silica and reduced graphene oxide on the mechanical, thermal, and tribological properties of silicone rubber nanocomposites
- Using Pin on Disk and Dry abrasion apparatus, examine the tribological properties of composites and the influence of different parameters on the materials' properties.
- The experimental data were utilized for training artificial neural networks (ANNs), which were then used to predict the COF of the nanocomposites for values for which the experiment was not performed

Later, the research was expanded to include tribological parameters such as coefficient of friction and composite wear rate, which were associated with the morphological examination of the worn surface. Due to the broad spectrum of research work, the following section presents published works on the abovementioned issues. The following is a list of publications that were relevant to the dissertation. The contributions of specific authors are shown in each of the included publications

MOST WIEDZY Downloaded from mostwiedzy.pl

- **P1** - Sarath, P.S., Reghunath, R., Thomas, S., Haponiuk, J.T. and George, S.C., 2021. An investigation on the tribological and mechanical properties of silicone rubber/graphite composites. *Journal of Composite Materials*, *55*(26), pp.3827-3838. https://doi.org/10.1177/00219983211031634

- **P2-** Sarath, P.S., Samson, S.V., Reghunath, R., Pandey, M.K., Haponiuk, J.T., Thomas, S. and George, S.C., 2020. Fabrication of exfoliated graphite reinforced silicone rubber composites-Mechanical, tribological and dielectric properties. *Polymer Testing*, *89*, p.106601. https://doi.org/10.1016/j.polymertesting.2020.106601

- **P3** - Sarath, P.S., Moni, G., George, J.J., Haponiuk, J.T., Thomas, S. and George, S.C., 2021. A study on the influence of reduced graphene oxide on the mechanical, dynamic mechanical and tribological properties of silicone rubber nanocomposites. *Journal of Composite Materials*, *55*(15), pp.2011-2024. https://doi.org/10.1177/0021998320981608

- **P4** - Sarath, P.S., Pahovnik, D., Utroša, P. *et al.* study the characteristics of novel ionic liquid functionalized graphene oxide on the mechanical and thermal properties of silicone rubber nanocomposites. *J Polym Res* **28,** 446 (2021). https://doi.org/10.1007/s10965-021-02806-5

- **P5** - P.S, Sarath., Prasad, V., Pahovnik, D. *et al.* Study the effect of fumed silica on the mechanical, thermal and tribological properties of silicone rubber nanocomposites. *J Polym Res* **29,** 53 (2022). https://doi.org/10.1007/s10965-022-02905-x

- **P6** - Sarath, P.S., T.Y.Mahesh, Haponiuk, J.T., Thomas, S. and George Tribological performance of ionic liquid modified graphene oxide/silicone rubber composite and the correlation of properties using machine learning. *Polymer Engineering & Science*, https://doi.org/10.1002/pen.25936

- **P7** - Sarath, P.S., Thomas, S., Haponiuk, J.T. and George, S.C., Fabrication, characterization and properties of silane functionalized graphene oxide/silicone rubber nanocomposites. *Journal of Applied Polymer Science*, p.52299. https://doi.org/10.1002/app.52299

P8 - Sarath, P.S., Pahovnik, D., Utroša, P. *et al.* Study the synergistic effect of fumed silica and reduced graphene oxide insertion on the thermal, mechanical, tribological, and solvent transport properties of silicone rubber nanocomposites. *Journal of Applied Polymer Science (Accepted -2022)*

MOST WIEDZY Downloaded from mostwiedzy.pl

Publication -1:

An investigation on the tribological and mechanical properties of silicone rubber/graphite composites

Article summary

This study discusses a novel approach to improving silicone rubber's tribological properties (QM). In this study, tribological properties and surface characteristics of silicone rubber/graphite (QMG) composites were investigated as a function of applied load, sliding velocity (1–5 m/s), and temperature). The inclusion of graphite significantly reduces the friction coefficient (40%) and the specific wear rate of QM (50%). The wear mechanism involves the formation of transfer film at the interphase between composite and steel counter surface. The tribological performance of QMG composites was found to agree with their morphological, mechanical, and dielectric properties.

Methodology

- Cure characteristics
- Mechanical properties
- Tribology
- Dielectric studies
- Thermal conductivity studies

MOST WIEDZY Downloaded from mostwiedzy.pl

Check for updates

Article

JOURNAL OF COMPOSITE MATERIALS

Journal of Composite Materials
0(0) 1–12
© The Author(s) 2021
Article reuse guidelines:
sagepub.com/journals-permissions
DOI: 10.1177/00219983211031634
journals.sagepub.com/home/jcm
SAGE

An investigation on the tribological and mechanical properties of silicone rubber/graphite composites

PS Sarath[1], Rakesh Reghunath[2], Sabu Thomas[3], Józef T Haponiuk[4] and Soney C George[1]

Abstract

In this study, tribological properties and surface characteristics of silicone rubber/graphite (QMG) composites were investigated as a function of applied load, sliding velocity (1–5 m/s) and temperature. This study discusses a novel approach to improve the tribological properties of silicone rubber (QM). Inclusion of graphite significantly reduces the friction coefficient (40%) and specific wear rate of QM (50%). Wear mechanism involves formation of transfer film at the interphase between composite and steel counter surface. Tribological performance of QMG composites were found to be in agreement with its morphological, mechanical and dielectric properties.

Keywords

Silicone rubber, Graphite, Adhesion, Tribology

Introduction

Silicone rubber (QM) finds potential applications in diverse areas of medical,[1–3] engineering, outdoor insulation,[4] electron industry[5] and so on, due to its excellent thermal, elastic and chemical resistance. However, when elastomeric material sliding against a hard material surface they exhibit high friction and wear rate. In order to overcome this limitation, it is important to investigate the mechanism involved in the contact region. Therefore, study the mechanism involves in tribological phenomena are great important.[6] In the case of dry sliding conditions, the wear nature of elastomer is more complex than that of metallic materials, it is related to various operating parameters as well as physical and mechanical properties of the polymer composites.[7]

The factors which influence rubber adhesion are contact area, surface roughness, sliding velocity, surface free energy and viscoelastic properties.[8] The substrate and rubber interaction can be minimized by reducing the actual contact area or by the addition of lubricating filler on the rubber. Carbonaceous materials like carbon nanotube (CNT), graphite, graphene are the common fillers exhibiting desirable thermal, electrical and mechanical properties with high surface area gained worldwide interest for reinforcing polymeric matrices. So it is interesting to explore the reinforcing potential of graphite and overall performance of the polymer based composites.

He et al.[9] compared the influence of fumed silica and precipitated silica on the tribological performance of silicone rubber. Their study shows that both mechanical and wear resistance properties of silicone rubber enhanced with the addition of fumed and precipitated silica. Fumed silica modified material shows better wear resistance compared to precipitated silica. It is due to the better reinforcement effect revealed from the high surface area of fumed silica. Hashmi et al.[10]

[1]Centre for Nanoscience and Technology, Department of Basic Sciences, Amal Jyothi College of Engineering, India
[2]Department of Mechanical Engineering, NSS College of Engineering, India
[3]International and Inter University Centre for Nanoscience and Nanotechnology, Mahatma Gandhi University, India
[4]Department of Polymer Technology, Chemical Faculty, Gdansk University of Technology, Poland

Corresponding author:
Soney C. George, Centre for Nanoscience and Technology, Department of Basic Sciences, Amal Jyothi College of Engineering, Kanjirappally, Kottayam, Kerala, India.
Email: soneygeo@gmail.com

MOST WIEDZY Downloaded from mostwiedzy.pl

synthesized graphite modified polyester cotton composites. They investigated the friction and sliding wear behaviour of composite at different applied loads and graphite concentrations. The reinforcement of cotton results in reduced specific wear rate and increased coefficient of friction but further addition of graphite decreased both specific wear rate and friction coefficient.

Wang et al. investigated the frictional properties of composites by varying sliding velocity and it was found to be a cause for improving mechanical and wear related properties in nitrile rubber.[11] Valentini et al.[12] explored the possibility of graphene nanoplatelets (GNPs) for improving the thermal and electrical properties of QM. Ke et al. developed fabric rubber composite to analyse its mechanism of friction, resilience and sealing properties.[13–14] Thus several articles described the benefits of carbon nanomaterials for the tribological properties of various composite materials. But there is no research work has been reported in the field of tribological aspects of QM/graphite composites so far.

The objective of this paper is to fabricate graphite-silicone rubber composites and investigate the effects of graphite loading on mechanical and tribological properties. Particular attention is paid to the frictional properties of elastomer–metal interaction, characterized by a friction coefficient (COF) and wear rate as a function of sliding speed, applied load and temperature. It is also aimed to study the effect of graphite filler on the dielectric and conductive properties of QMG composites.

Table 1. Formulation of mixes (Phr).

Ingredients	QM	QMG5	QMG10	QMG15	QMG20	QMG30
QM	100	100	100	100	100	100
Graphite	0	5	10	15	20	30
DCP	1.5	1.5	1.5	1.5	1.5	1.5

Phr*: parts per hundred rubber.

Experimental

Materials

Silicone rubber (QM) was procured from KCC Corporation, Korea (SH0060-U). Graphite (Synthetic powder, particle size <20 µm, purity - 99%) and Dicumyl peroxide (DCP) were procured by Sigma Aldrich, Banglore, India.

Preparation of silicone rubber composites

The QM, graphite, and DCP were thoroughly mixed in a two-roll mill according to the formulations given in Table 1. The total mixing of each sample took about 20 minutes. ASTM D-1646 standard was used for the cure time analysis. The graphite –silicone rubber samples were hot- pressed at 150 °C and post cured at 200 °C for 4 hours (Figure 1).

Characterization

Cure time of the rubber vulcanisates was determined using ASTM D1646. Mechanical properties of the composites were studied using INSTRON-4411 instrument at cross head speed of about 500 mm/min according to ASTM D 412 and tear strength of the composites were also determined according to ASTM D 1424. Shore–D hardness tester was used to study the

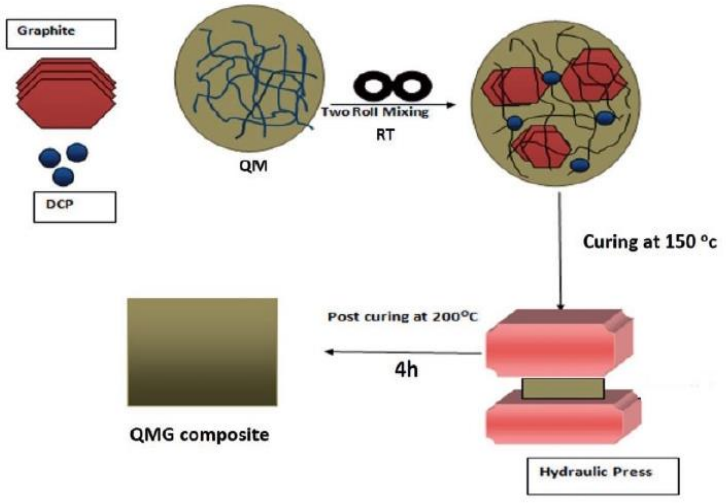

Figure 1. Pictorial representation of QMG composite synthesis.

MOST WIEDZY Downloaded from mostwiedzy.pl

hardness of the composite at ASTM D2240. Compression set was determined as per ASTM D39.

The compression set (%) was calculated as in equation (1)

$$\text{Compression set } (\%) = (t_0 - t_1)/(t_0 - t_s) \times 100 \quad (1)$$

Where t_0 and t_1 are the initial and final thickness of the specimen and t_s is the thickness of the space bar used.

The tribological studies with COF and specific wear rate were measured using a pin-on-disc tribometer as per ASTM G99-05 standards. Composite sample was allowed to contact with rotating steel disc under loaded condition. The detailed experimental conditions are placed in Table 2 and the experimental setup is displayed in Figure 2(a). The wear rates are calculated from the weight loss measurements. After the test, specimen pin was cleaned. dried and its weight loss was measured. The value of friction force was recorded directly from the instrument and the COF and the specific wear rate were determined from the reference weight loss measurements.[15]

Table 2. Experimental conditions.

Variables	Working conditions
Temperature (°c)	Room temperature, 50,100
Humidity	55(±5)%
Test disc	Hardened ground steel (EN 31, hardness 60 HRC)
Roughness of EN-31	1.6 m Ra
Rubbing time	1800 s
Load	10N, 20N and 30N
Sliding speed	1m/s, 2m/s, 3 m/s and 5 m/s
Sliding distance	3600 m
Specimen size (ASTM G99 Std.)	30 mm × 10 mm × 10 mm

$$\text{Coefficient of friction } (\mu) = F_f/F_n \quad (2)$$

Where F_f is the friction force and F_n is the normal load.

The specific wear rate (W_s) of the specimen was calculated using the following relation:

$$Ws = \Delta m/\rho FnL \quad (3)$$

In equation (3), Δm is the weight loss; ρ is the density of the composites; Fn is the applied load; L is the sliding distance.[16]

Dry abrasion technique was used to study abrasive wear pattern of composites as per ASTM G65 and the schematic representation of the experimental set up is displayed in Figure 2(b). The abrasive silica sand (AFS 50/70) of size 150–300 Mm are poured into the composite sample and the rotating wheel under varying load. The sand flow rate between rubber wheel and the specimen was 375 ± 5 g/min and the size of the specimen was 76 mm × 25 mm × 2 mm. Weight loss

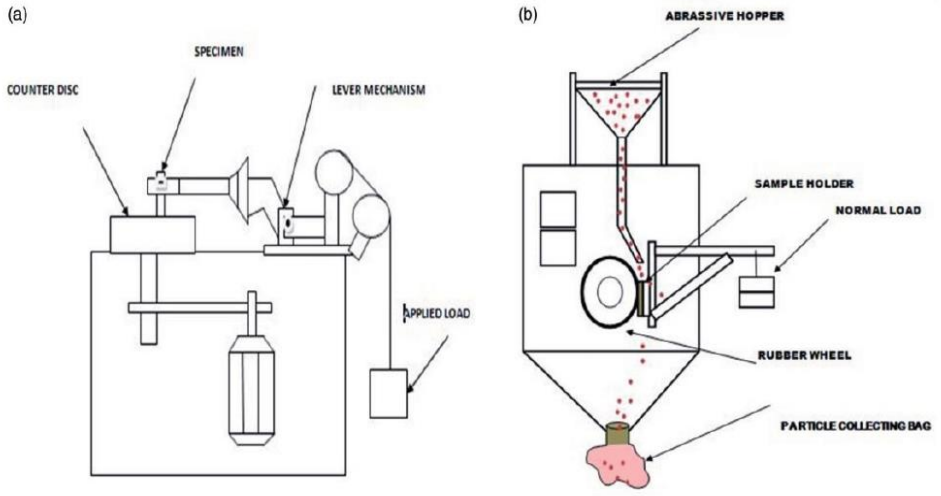

Figure 2. Instrumentation set up of (a) pin on disk and (b) dry abrasion testing machine.

MOST WIEDZY Downloaded from mostwiedzy.pl

was measured after the test and wear volume was determined as per equation (4).

$$\text{Wear volume Ks} = V/L \times D \quad (4)$$

Where, "V" is the volume loss, "L" load and "D" sliding distance.

Dielectric properties of the compression moulded samples of 10 mm diameter were measured in the frequency range (100 Hz to 2 MHz) using an impedance analyzer (Agilent E4980A). Lee disc apparatus was used to study the thermal conductivities of the composites using ASTM D5470.

Results and discussion

Cure characteristics of silicone rubber graphite composites

The cure behaviour of QM/graphite is placed in Table 3. Loading of graphite in QM matrix influences the cure kinetics of the composites. M_H (max. torque) values rise gradually with an increase in graphite loading. This is because of the enhanced curing and improved QM-graphite interaction in the composites.

The M_L (Min Torque) and M_H values increase with the concentration of graphite. M_H represents the extent of crosslinking reactions, shear modulus of the vulcanizate in addition to the filler – polymer interactions. In this case M_H increases with increase of graphite content. Moreover, the differential torque (ΔS) which denotes the degree of crosslinking is also increased with an increase of graphite content. The filler polymer interaction is attributed to chemical crosslinks as well as physical crosslinks (van der Waals).[17] Both from M_H and ΔS values, it is clear that the filled system exhibit higher values compared to the gum vulcanizates. During vulcanization of silicone rubber, peroxide crosslinks creates carbon-carbon bonds between silicone rubber chains. But physical crosslinks are also formed between silicone rubber chains and graphite filler. The extent and degree of physical crosslinks are increasing with dosage of graphite filler. During mill mixing the graphite layers are dispersed between silicone rubber and this leads to the formation of physical crosslinks. In short the improvement in M_H values is due to the sum of physical as well as chemical crosslinks.

Reinforcing effect

The reinforcing action of graphite filler in QM matrix was investigated by studying the tensile and tear properties of the composites. Figure 3 illustrates stress versus strain curves of QMG composites and there is a significant improvement in the stress and the strain values of silicone rubber with graphite loading. Silicone rubber has a weak intermolecular force of attraction which results in lower mechanical strength. It is clear from Table 4 that the addition of graphite improves the mechanical properties of the composite. Tensile stress rises with concentration of filler and reaches a maximum value of 6.36 MPa for the composite with 20 phr of graphite and then it decreases. QMG20 shows 30% improvement in tensile strength compared to the pristine sample. Elongation at break also shows an

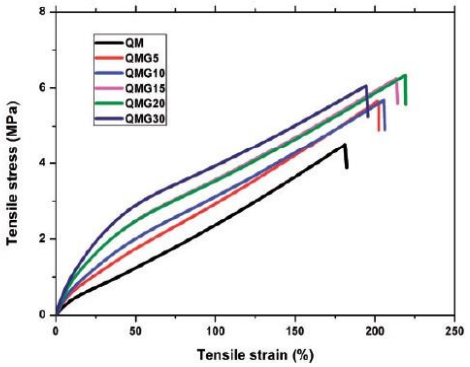

Figure 3. Stress – strain curve of QM/Graphite composites.

Table 3. Cure behavior of the QM-Graphite composites.

Sample	M_L Min Torque (dNm)	M_H Max Torque (dNm)	ΔS (dNm)	Scorch Time(ts_2) (min)	Optimum cure time t_{90} (min)	Cure rate index (min^{-1})
QM	0.65	12.90	12.25	0.86	5.76	20.40
QMG5	0.70	13.51	12.81	0.93	5.94	19.96
QMG10	0.75	14.06	13.29	0.96	6.28	18.79
QMG15	0.77	14.16	13.41	1.00	6.73	17.45
QMG20	0.86	15.08	14.21	1.03	8.84	12.80
QMG30	0.87	15.58	14.72	1.25	10.40	10.92

MOST WIEDZY Downloaded from mostwiedzy.pl

Table 4. Mechanical properties of QM-Graphite composites.

Sample	Tensile strength (MPa)	Elongation at break (%)	Modulus at 100%	Tear strength (N/mm)	Hardness (Shore A)	Compression set (%)
QM	4.74 ± 0.35	185 ± 3	2.36	20.45 ± 1.13	51	21
QMG5	5.64 ± 0.42	203 ± 2	2.92	22.75 ± 0.74	61	15
QMG10	5.81 ± 0.19	212 ± 2	3.18	23.21 ± 1.40	64	9
QMG15	6.27 ± 0.05	218 ± 3	3.56	26.43 ± 1.12	67	7
QMG20	6.36 ± 0.17	225 ± 3	3.87	27.50 ± 0.95	71	6
QMG30	6.01 ± 0.25	192 ± 4	3.97	25.12 ± 0.67	74	5

increased trend up to QMG 20 and before then it decreases with further filler loading".

The maximum value of tear strength is found to be 27.50 N/mm for QMG20 sample. Thus the graphite loading up to 20 phr is homogeneously dispersed among polymer matrix which facilitates the transfer of stress uniformly throughout the matrix material. Compression set results illustrates that, when graphite content increases there is a sharp decrease in compression set values. This indicates materials resist permanent deformation under a given deflection and the significant difference was attributed to the superior dispersion of the graphite which results in an augmented interaction at the interface between graphite and QM. The improvement in mechanical properties with filler loading is due to the better reinforcing effect of graphite in the QM matrix. As the reinforcement increases, the degree of stress transfer of polymer matrix to the filler will increase. Figure 4 represent the schematic diagram of interaction between QM and graphite. There is a weak van der Waals force of interaction between graphite layers and CH-π interaction between graphite and QM matrix.

Figure 4 shows the fracture surface morphology of tensile tested QM/Graphite composites. The dispersed phase of graphite distributes widely in the matrix and outline of the dispersed phase is clearly shown on tensile fracture with some holes left. This resulted from the pull-out of graphite agglomerates, which indicates the good interface adhesion. Figure 5(a) shows the morphology of the fracture surface of neat QM with very smooth surface. The morphology of the tensile fracture surface of QMG10 composite is given in Figure 5(b). Some voids can be noticed from QMG10 composites which indicate the de-bonding of graphite from QM matrix. In Figure 5(c) SEM image of QMG20 shows a smooth surface. Here the graphite is difficult to be pulled out during the tensile process, and exhibit a layered structure. This indicates the good interfacial adhesion between graphite and QM matrix at 20 Phr of graphite concentration. The dispersed graphite plates act as stress accumulation points and thus it prevents the crack growth in QM matrix. Figure 5(d) shows the SEM image of QMG30 in which large voids and agglomeration can be noticed from the composites. The interaction between graphite and QM matrix is very weak due to debonding and lack of cohesion.

Tribological properties

Friction and wear test. In elastomers, the frictional properties are complicated because of their special surface chemistry and low elastic modulus. The wear rate of the QMG samples was calculated by the division of the wear volume by the applied load and sliding distance. The variation of sliding time with friction coefficient is shown in Figure 6(a). It was found that the frictional coefficient for all the composites increased rapidly during the initial stages and then a gradual decrease was observed followed by achieving stable values. It is also understood that the coefficient of friction of the composites was much lower than that of pure silicone rubber. The lower COF obtained was for QMG20 composite sample.

Figure 6(b) illustrates that graphite reinforcement enhances the wear resistance of the composites. During testing, graphite forms a transfer film on the counterpart surface and prevents the asperities in contact with material and reduces the specific wear rate.[16] Addition of filler concentration up to 20phr decreases the friction coefficient and specific wear rate. Further addition of filler increases the COF and specific wear rate. Since graphite layer in composite became rougher, and this imparts more asperities comes in contact with counter metal surface.

The effect of load. The variation of applied load on the tribological performance of composites are graphically presented in Figure.7 As applied load increases, the frictional heat produced during sliding in the contact area also increases. Figure 7(a) represents that COF of the composites decreased with increased load and among them 30 N load exhibited the lowest friction coefficient as a result of formation of the film on the counter surface. At high applied load, the temperature between composite and counter surface may increase, which cause softening of the matrix and the reduction

MOST WIEDZY Downloaded from mostwiedzy.pl

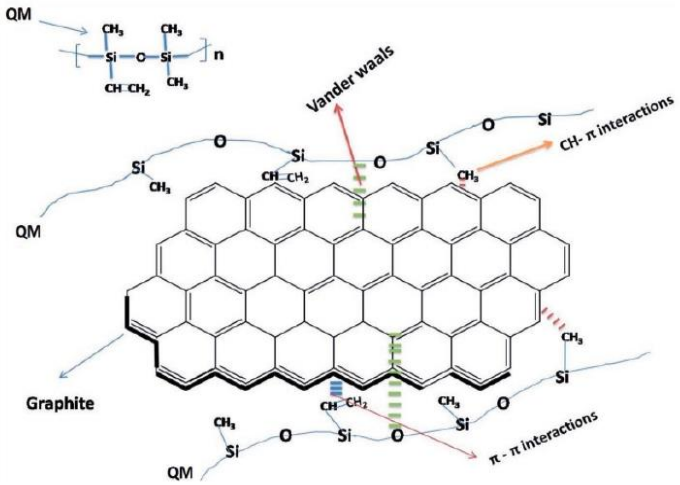

Figure 4. Schematic representation showing the QM-Graphite interaction.

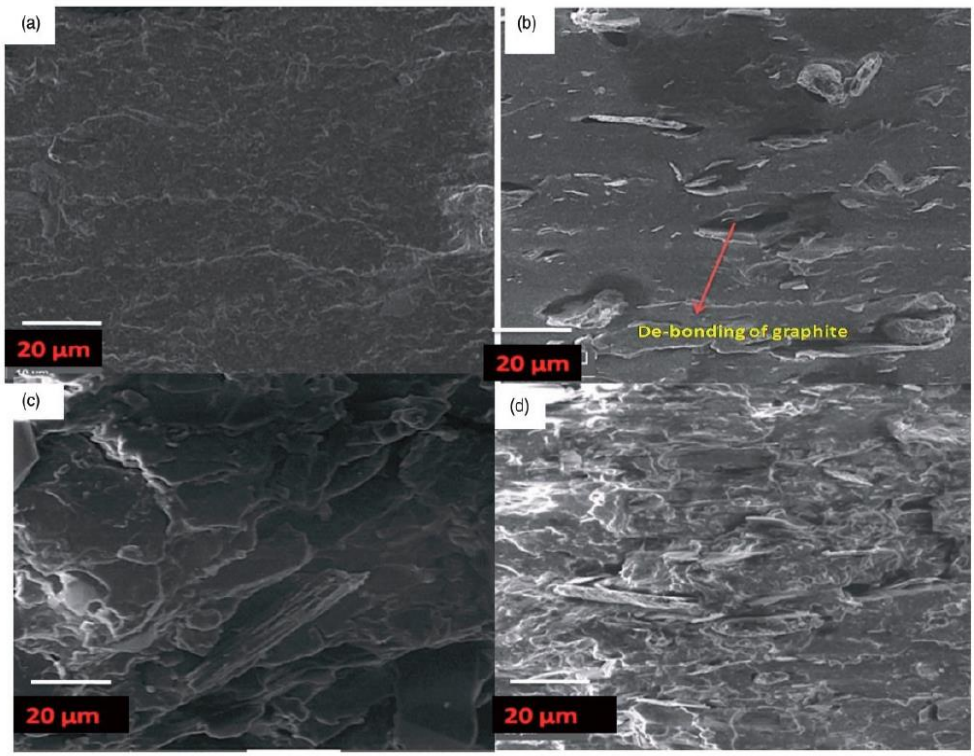

Figure 5. SEM images of fracture surfaces (a) pure QM (b), QMG10 (c), QMG20 and (d), QMG30.

MOST WIEDZY Downloaded from mostwiedzy.pl

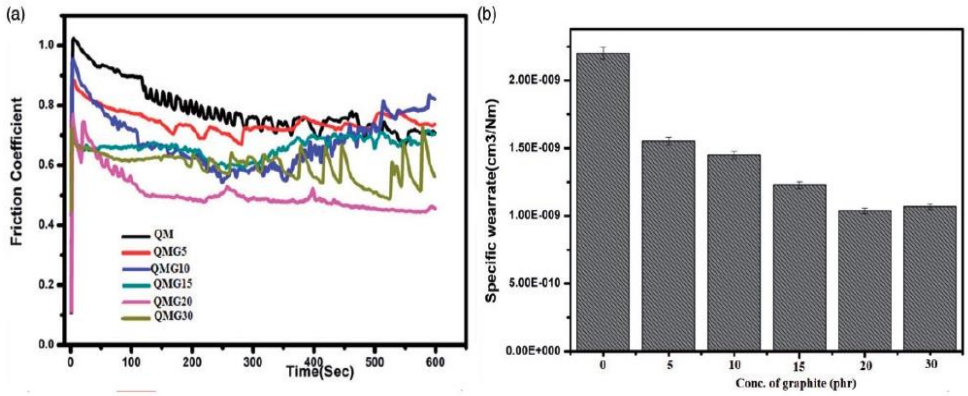

Figure 6. (a) Variation of friction coefficient with sliding time and (b) specific wear rate with graphite loading (30 N,2 m/s).

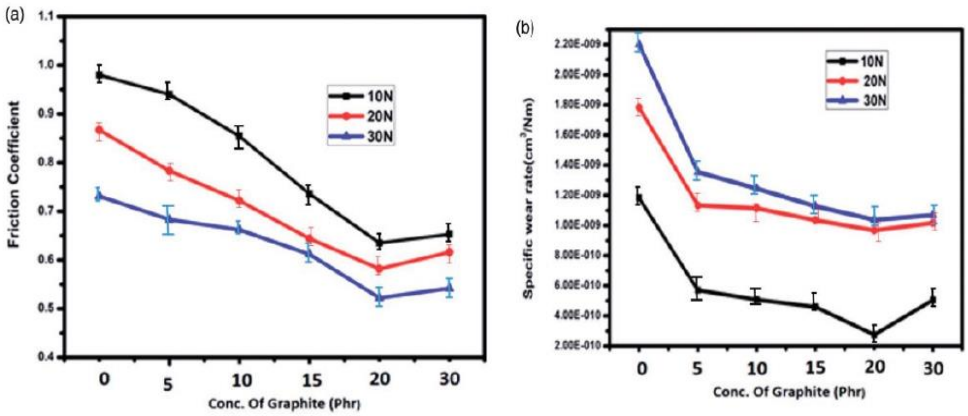

Figure 7. (a) Influence of graphite loading on COF of composite and (b) effect of graphite loading on the specific wear rate of composite (1800 m, RT, 2 m/s).

of COF and specific wear rate.[16] Specific wear rate was found to be rapidly increased with applied load as shown in Figure 6(b) due to high deformation at the surface of the composite.

The effect of sliding speed. Figure 8 shows the influence of sliding velocity on the tribological properties of QMG composites which was investigated under relatively high load (30 N), at 25°C. Figure 8(a) shows the variation of friction coefficient concerning the graphite loading for different sliding speed. When sliding speed was increased from 1 m/s to 5 m/s, it is observed that, COF and specific wear rate of the composite decreased with an increase in sliding speed. This is attributed to the fact that, as the sliding speed increases the number of adhesive point reduces and thereby transfer film will be easily formed on the frictional surface. This leads to considerable decrease in friction and wear rate.[17]

Increase in sliding speed augments thermal softening of the QM. "High frictional heat results in wear debris at the interface which get collapsed into the matrix and form a protective layer by deformation.[18] This reduces the adhesive contact region between the composite and hard material. Therefore, the coefficient of friction and specific wear rate of the composite material decrease with an increase in sliding velocity.

Worn surface morphologies. Figure 9 shows the worn surface morphologies of the composites with different amount of graphite. Worn surface morphologies analyse the wear, scars and grooves formed during the tribological process and it also offers an insight into how a material behaves in the process of wear. It can be seen

MOST WIEDZY Downloaded from mostwiedzy.pl

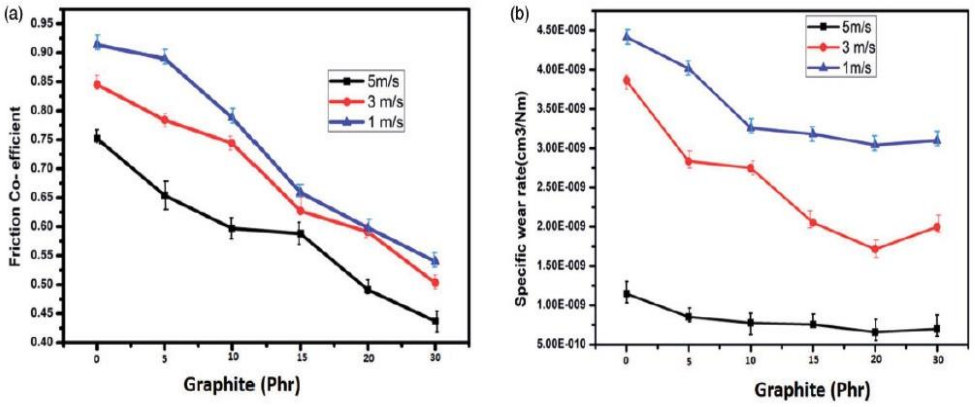

Figure 8. (a) The friction coefficient and (b) specific wear rate of QM-Graphite composites with various contents of graphite as a function of sliding velocity (30 N, RT, 1800 m).

that there are a series of parallel ridges lying perpendicular to the sliding direction on the surface of abraded rubber. Figure 9(a) shows that ridges formed on the contact surface of QM more rapidly than those in the graphite filled condition. Figure 9(b) shows that localized material removal and groove damage occurs on the worn region of the composite.

In Figure 9(c) and (d), the addition of graphite induced a decrease in the size of the ridges that led to a more uniform surface and localised removal of material. Study of worn surfaces of composite indicate that in a high shear condition, composites come in contact with metal surface and lubricating film formation occur much faster, and good interfacial interaction between graphite and QM matrix results in lower wear rate. Addition of 20 phr graphite induced a decrease in localized material removal and size of the ridges that led to a more uniform surface. The lubricating film formed on the metallic surface, protects the material from further wear loss by decreasing the area of contact. Lower COF and specific wear rate occurred as a result of the uniform distribution of shearing stress throughout the surface.

Figure 10 shows the depth wear rate and PV factor of composites with different graphite loadings. QMG20 obtained lower depth wear rate compared to other samples. When PV increases the depth wear rate starts to decrease and reaches a minimum of around 0.6 µg/h (60% decrease) and then it starts to increase. 10 N load shows higher depth wear rate and 30 N obtained in the mid - region. The falling off in depth wear rate mainly owing to the formation of lubricant film. Thus lubricant film protects the material from further wear loss. Wear depth study also gives an insight into the reinforcement effect of the filler material. QMG20 material obtained improved mechanical property and better dispersion of graphitic material into the QM matrix. Slope of the curve decreases up to the limiting PV -levels and then it starts to rise at higher values.

Dry abrasion test. The three-body abrasive wear behaviour of QMG20 composite with different loads were carried out and depicted in Figure 11.

Figure 11 shows that wear volume of QMG20 composite increased with applied load. There is a dramatic rise in wear volume observed with high loading. This is due to the fact that, sand particles slide on a composite surface and it might disrupt the interface by plastic deformation.

Dielectric properties

The variation of dielectric loss and dielectric permittivity of the composites with different graphite loading as a function of frequency as shown in Figure 12(a) and (b). The polymer composites show a percolation threshold at 20 phr loading and an abrupt rise in dielectric constant observed at low frequencies. The dielectric permittivity values of the composite up to 15 phr have not observed any noticeable changes. Composite with 30 phr filler loading shows higher dielectric permittivity among other samples. This confirms that, energy storage capacity of the composite increased with graphite loading. However, the dissipation energy of QM composites is negligibly small at 1 MHz frequency. The dielectric permittivity improved with graphite loading and decreases with increase in frequency because permittivity relay on the number of orientable dipoles within the system.

At low frequency, the dipoles align under applied electric field but at higher frequencies polymer

MOST WIEDZY Downloaded from mostwiedzy.pl

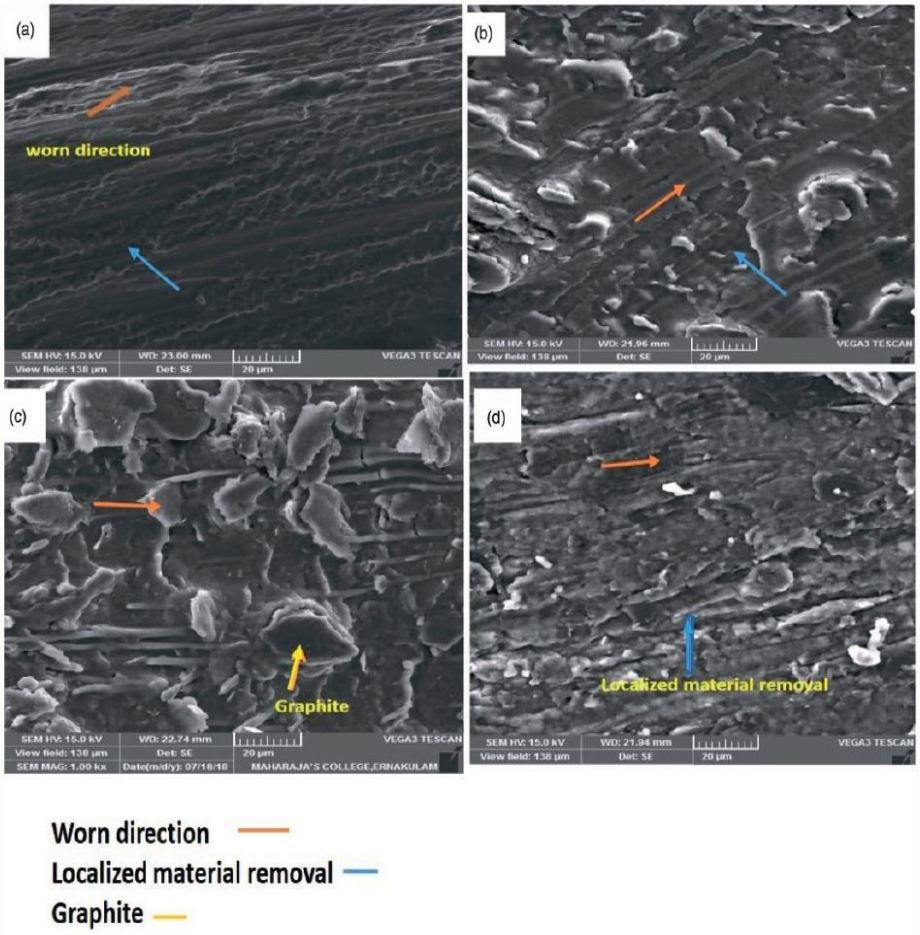

Figure 9. Surface texture of worn surface morphologies (a) silicone rubber, (b) 10 phr graphite- silicone composite, (c) 20 phr graphite- silicone composite, (d) 30 phr silicone graphite.

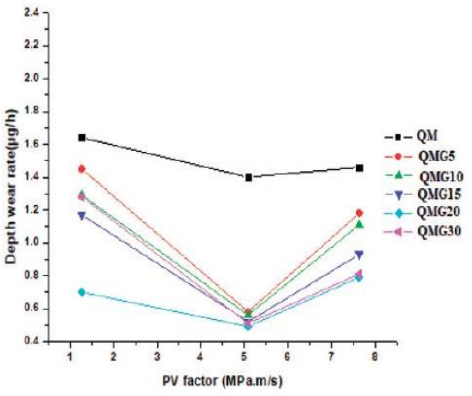

Figure 10. Variation of depth wear rate and PV factor of QMG composites.

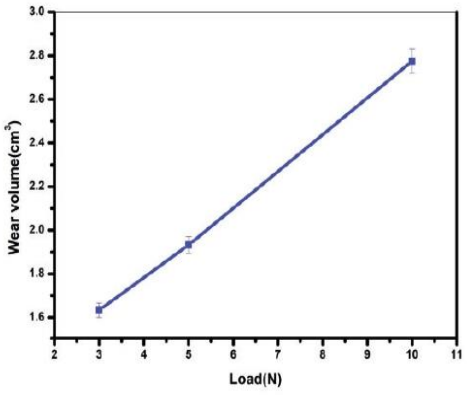

Figure 11. Wear volume and specific wear rate of QMG20 composite with different loads.

MOST WIEDZY Downloaded from mostwiedzy.pl

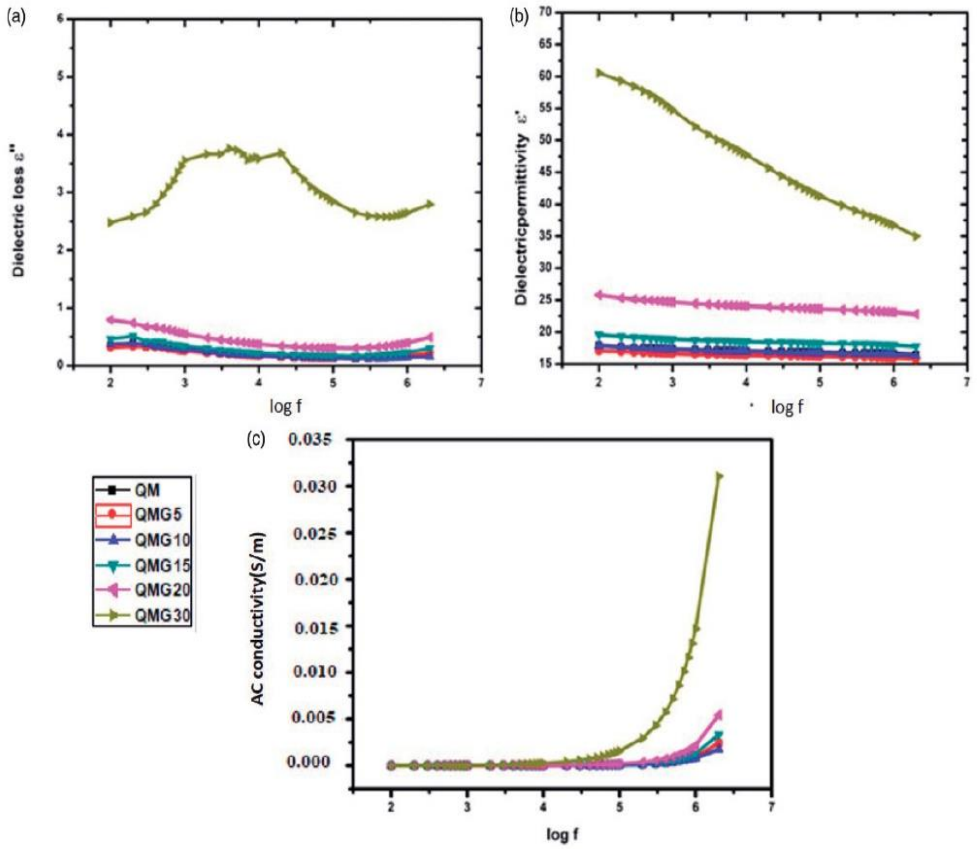

Figure 12. (a) Dielectric loss, (b) Dielectric permittivity, (c) AC conductivity of the QMG composites.

chains not able to align themselves. It is vivid from Figure 12(c) that graphite loading enhanced the AC conductivity of the composite. The addition of conductive filler resulted in enhanced filler-filler interaction and thereby a smooth continuous conducting network formed as shown in Figure 13. The mechanism involves ohmic conductance and non - ohmic conductance.[19]

The ohmic conductance mechanism involves direct contact with conductive fillers and it forms a conductive network in the system but non - ohmic conductance involves a thin polymer layer separated by conductive fillers. The polymer layer acts as a barrier for the conductive network and the mechanism involves barrier tunnelling effect. At threshold, transition occurred for composite from non ohmic conductance to ohmic conductance.[20] The dielectric permittivity of composites at ambient conditions apparently increases with graphite particle size. Such a conclusion is explained by the decrease of the percolation threshold with microsized graphite particle size, which is proved theoretically[19–21] Silicone rubber is an insulator, it doesn't contain mobile ions but the diffusion of graphite constitutes another means of charge transport, the ionic conductivity. The latter comes from the fact that ion mobility is coupled to the polymer segmental dynamics, as motion of the repeat units opens pathways for ion diffusion. Therefore diffusion of graphite into an insulative rubber matrix resulted in a conductive composite.[22] Maximum AC conductivity was achieved at 30 phr filler loading

Thermal conductivity studies

The variation of friction coefficient and thermal conductivity of the composites are shown in Figure 14. The thermal conductivity results show that addition of graphite remarkably improved the conductivity of the composites. In addition, QMG20 composite showed higher thermal conductivity and almost 52% enhancement in thermal conductivity is observed compared with the neat sample. The improvement in thermal conductivity is associated with good interaction between filler and matrix. This results in good phonon

MOST WIEDZY Downloaded from mostwiedzy.pl

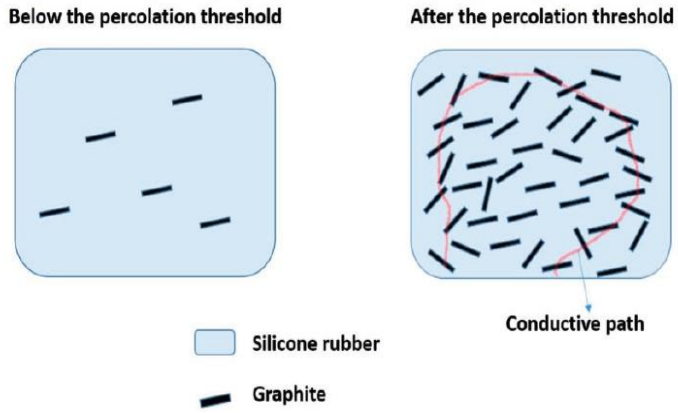

Figure 13. Schematic diagram for the conductive path of composite.

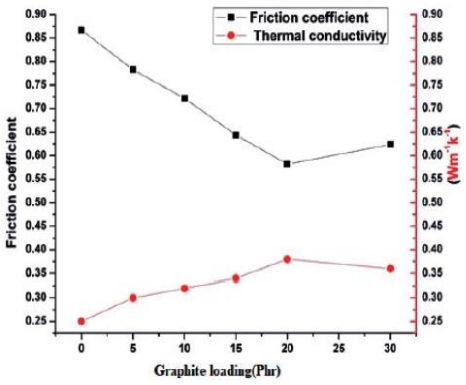

Figure 14. Dependence of COF and thermal conductivity on graphite loading.

transmission with a longer mean free path. SEM studies confirmed better dispersion of graphite in the matrix. Graphite forms a continuous conducting network inside the matrix, which helps in effective transfer of heat from one region to another. The friction coefficient of material also decreases with increase in filler concentration. 20 phr filler loading show lower friction coefficient value and on further addition, it starts to increase.

Silicone rubber surface comes in contact with heat and it diffuses slowly. Heat transfer in polymer occurs with random molecular motion which affects the thermal conductivity of QM.[23] Due to the presence of graphite, it forms a conducting network within the system. In such cases heat diffuses into the composite and reaches the first atom, it transfers to the nearest and hence the composite exhibit improved thermal conductivity compared to the neat. This helps in the transfer of frictional heat from a particular area to another region and prevent material damage.

Conclusions

Tribological properties of QM composites filled with graphite were studied at different loads, sliding velocity and temperature conditions. Specific wear rate and friction coefficient of the composites decreased with increasing graphite loading. The lowest friction coefficient and wear resistance was observed at 20 phr of graphite. The results showed that the addition of graphite improved the tribological performance of QMG composites. In this work, the wear rate of the composite decreased upto 20 phr graphite loading and further it increased. The worn surface morphology of composite shows a smooth surface and it indicates that the presence of graphite significantly reduced the metal contact. Lubricant film formed on the counter surface prevents the asperities in contact with the composite surface. This results in decreased COF and specific wear rate. Comparing to all the silicone rubber graphite composites, the QMG20 exhibit enhanced mechanical, tribological and thermal conductivity.

Declaration of Conflicting Interests

The author(s) declared no potential conflicts of interest with respect to the research, authorship, and/or publication of this article.

Funding

The author(s) disclosed receipt of the following financial support for the research, authorship, and/or publication of this article: DRDO (Order No: ERIP/ER/1504758/M/01/1667), New Delhi, India is greatly acknowledged for the financial support.

MOST WIEDZY Downloaded from mostwiedzy.pl

ORCID iD

Soney C George https://orcid.org/0000-0001-9590-3971

References

1. Chen YS, Hsieh CL, Tsai CC, et al. Peripheral nerve regeneration using silicone rubber chambers filled with collagen, laminin and fibronectin. *Biomaterials* 2000; 21: 1541–1547.
2. Hron P. Hydrophilisation of silicone rubber for medical applications. *Polym Int* 2003; 52: 1531–1539.
3. Ferraz CC, Varca GH, Ruiz JC, et al. Radiation-grafting of thermo-and pH-responsive poly (N-vinylcaprolactam-co-acrylic acid) onto silicone rubber and polypropylene films for biomedical purposes. *Radiat Physics Chem* 2014; 97: 298–303.
4. Song W, Shen WW, Zhang GJ, et al. Aging characterization of high temperature vulcanized silicone rubber housing material used for outdoor insulation. *IEEE Trans Dielect Electr Insul* 2015; 22: 961–969.
5. Lee SE, Jee SS, Park H, et al. Large reduction in electrical contact resistance of flexible carbon nanotube/silicone rubber composites by trifluoroacetic acid treatment. *Compos Sci Technol* 2017; 143: 98–105.
6. Wu YP, Zhou Y, Li JL, et al. A comparative study on wear behavior and mechanism of styrene butadiene rubber under dry and wet conditions. *Wear* 2016; 356–357: 1–8.
7. Hakami F, Pramanik A, Basak AK, et al. Elastomers' wear: comparison of theory with experiment. *Tribol Int* 2019; 135: 46–54.
8. Bragaglia M, Cacciotti I, Cherubini V, et al. Influence of organic modified silica coatings on the tribological properties of elastomeric compounds. *Wear* 2019; 434–435: 202987.
9. He Q, Li A, Zhang Y, et al. A study on mechanical and tribological properties of silicone rubber reinforced with white carbon 5black. *Tribol – Mater, Surf Interf* 2018; 12: 9–16.
10. Hashmi SAR, Dwivedi UK and Chand N. Graphite modified cotton fibre reinforced polyester composites under sliding wear conditions. *Wear* 2007; 262: 1426–1432.
11. Wang L, Zhang L and Tian M. Effect of expanded graphite (EG) dispersion on the mechanical and tribological properties of nitrile rubber/EG composites. *Wear* 2012; 276–277: 85–93.
12. Valentini L, Bon SB and Pugno NM. Severe graphene nanoplatelets aggregation as building block for the preparation of negative temperature coefficient and healable silicone rubber composites. *Compos Sci Technol* 2016; 134: 125–131.
13. Ke Y, Yao X, Yang H, et al. The compression and friction of tubular rubber seal under the curved surface loading. *Proc Inst Mech Eng, Part J: J Engineering Tribology* 2017; 231: 14–22.
14. Ke Y, Yao X, Yang H, et al. A measuring method of gas leakage along the contact interface of the stripped rubber seals. *Measurement* 2015; 61: 299–304.
15. Ozsoy I, Ozsoy N, Unal H, et al. Evaluation of the influences of wax content on the tribological and mechanical performance of polytetrafluoroethylene-blended polyamide. *Proc Inst Mech Eng, Part J: J Engineering Tribology* 2013; 227: 1399–1405.
16. Liu L, Yan F, Gai F, et al. Enhanced tribological performance of PEEK/SCF/PTFE hybrid composites by graphene. *RSC Adv* 2017; 7: 33450–33458.
17. Fröhlich J, Niedermeier W and Luginsland HD. The effect of filler–filler and filler–elastomer interaction on rubber reinforcement. *Compos Part A: Appl Sci Manuf* 2005; 36: 449–460.
18. Bahadur S. The development of transfer layers and their role in polymer tribology. *Wear* 2000; 245: 92–99. 21
19. Zhao H, Xia YJ, Dang ZM, et al. Composition dependence of dielectric properties, elastic modulus, and electroactivity in (carbon black-BaTiO3)/silicone rubber nanocomposites. *J Appl Polym Sci* 2013; 127: 4440–4445.
20. Abraham J, Kailas L, Kalarikkal, N, et al. Developing highly conducting and mechanically durable styrene butadiene rubber composites with tailored microstructural properties by a green approach using ionic liquid modified MWCNTs. *RSC Adv* 2016; 6: 32493–32504.
21. Kranauskaite I, Macutkevic J, Kuzhir P, et al. Dielectric properties of graphite-based epoxy composites. *Phys Status Solidi A* 2014; 211: 1623–1633.
22. Roland CM. Electrical and dielectric properties of rubber. *Rubber Chem Technol* 2016; 89: 32–53.
23. Li A, Zhang C and Zhang YF. Thermal conductivity of graphene-polymer composites: mechanisms, properties, and applications. *Polymers* 2017; 9: 437.

MOST WIEDZY Downloaded from mostwiedzy.pl

Publication -2:

Fabrication of exfoliated graphite reinforced silicone rubber composites - Mechanical, tribological, and dielectric properties

Article summary

The effect of exfoliated graphite (EG) on the mechanical, tribological, and dielectric properties of the silicone rubber (QM) composites have been systematically investigated and analyzed. Morphological analysis of the composites helps understand the interfacial interaction between the filler and the rubber matrix and the wear mechanism. An enhancement in the mechanical, tribological, and dielectric properties was observed with increased filler loading, and better performance was observed at 7 phr of filler loading. The AFM and TEM analysis show that the performance improvement is attributed to the better interaction between the QM chains and the EG layers. It is also apparent from the Kraus plot, which supports the reinforcing effect of EG in the QM matrix.

Methodology

- Cure characteristics
- Mechanical properties
- Tribology
- Dielectric studies
- Thermal conductivity studies

MOST WIEDZY Downloaded from mostwiedzy.pl

Polymer Testing 89 (2020) 106601

Contents lists available at ScienceDirect

Polymer Testing

journal homepage: http://www.elsevier.com/locate/polytest

Material Properties

Fabrication of exfoliated graphite reinforced silicone rubber composites - Mechanical, tribological and dielectric properties

P.S. Sarath [a], Sohil Varghese Samson [a,b], Rakesh Reghunath [c], Mrituanjay Kumar Pandey [d], Józef T. Haponiuk [e], Sabu Thomas [f], Soney C. George [a,*]

[a] Centre for Nanoscience and Technology, AmalJyothi College of Engineering, Kanjirappally, Kottayam, Kerala, India
[b] Department of Mechanical Engineering, AmalJyothi College of Engineering, Kanjirappally, Kottayam, Kerala, India
[c] Department of Mechanical Engineering, NSS College of Engineering, Palakkad, Kerala, India
[d] Directorate of Extramural Research and Intellectual Property Right, Defence Research and DevelopmentOrganisation (DRDO), New Delhi, India
[e] Department of Polymer Technology, Gdansk University of Technology, Gdańsk, Poland
[f] International and Inter University Centre for Nanoscience and Nanotechnology, Mahatma Gandhi University, Kottayam, Kerala, India

ARTICLE INFO

Keywords:
Silicone rubber
Exfoliated graphite
Tribology
Dielectric performance

ABSTRACT

The effect of exfoliated graphite (EG) on the mechanical, tribological and dielectric properties of the silicone rubber (QM) composites has been systematically investigated and analysed. Morphological analysis of the composites helps to understand the interfacial interaction between the filler and the rubber matrix as well as wear mechanism respectively. An enhancement in the mechanical, tribological and dielectric properties was observed with an increase in filler loading and better performance was observed at 7 phr of filler loading. The improvement in performance is attributed to the better interaction between the QM chains and the EG layers as evident from the AFM and TEM analysis. It is also evident from the Kraus plot which supports the reinforcing effect of EG in QM matrix.

1. Introduction

Tailoring of elastomeric composites by the addition of fillers has gained wide popularity over the years. The fact that properties of elastomeric composites could be improved has led many researches to develop high performance composites using different elastomers and filler combinations [1–4]. Among the many types of fillers, graphite-based filler was used for this research work based on a detailed investigation by Sadasivuni et al. [5]. Silicone rubber has numerous applications in fields such as mechanical, electrical, thermal and insulation [6], but the area such as tribological aspects are yet to be explored. Research conducted by Lee and Ji [7] reveals that silica reinforced silicone rubber has resulted in improved dielectric strength. Further, varying the vinyl content in the rubber matrix has led to improved hardness and tracking resistance. Using dopamine coated barium titanate as fillers in silicone rubber, a new soft dielectric elastomer composite was successfully prepared by Jiang et al. [8]. It is observed that fillers were highly compatible in the rubber matrix and helped to improve the electro-mechanical properties. Du et al. [9] were successful in blending polydimethylsiloxane modified gelatinin siliconerubber to fabricate an asymmetric bilayer membrane having porous structure. These findings suggest an excellent bio-medical application of silicone rubber. The researchers promise that this membrane act as a substitute platform for skin regeneration because the mechanical properties, water uptake and water vapor permeability meets usual wound dressing material requirements. Surface treated halloysite nanotube (HNT) was incorporated into silicone rubber to study the effects of HNT loading on its mechanical and thermal properties [10]. Increased stiffness, tensile strength and imporved thermal stability were witnessed in the developed nanocomposite with increasing filler loading. Xu et al. [11] reported a feasilbe method in blending poly (vinylidene fluoride) and methyl vinyl silicone rubber to develop a thermoplastic vulcanizate. This vulcanizate showed excellent mechanical properties. Silicone rubber foam with enhanced mechanical performance was developed by using nanographite as filler [12]. Microcellular changes in the composites such as improved cell density and reduced mean cell diameter was obtained. These changes increased the compressive strength and enhanced the thermal stability of the silicone rubber/nanographite

* Corresponding author. Centre for Nanoscience and Technology, AmalJyothi College of Engineering, Kanjirappally, Kottayam, Kerala, India.
E-mail addresses: sarathps005@gmail.com (P.S. Sarath), sohiledu@gmail.com (S.V. Samson), rakeshreghunath@amaljyothi.ac.in (R. Reghunath), mkpandey@hqr.drdo.in (M.K. Pandey), jozef.haponiuk@pg.gda.pl (J.T. Haponiuk), sabuthomas@mgu.ac.in (S. Thomas), soneygeo@gmail.com (S.C. George).

https://doi.org/10.1016/j.polymertesting.2020.106601
Received 10 February 2020; Received in revised form 19 April 2020; Accepted 4 May 2020
Available online 14 May 2020
0142-9418/© 2020 Elsevier Ltd. This is an open access article under the CC BY-NC-ND license (http://creativecommons.org/licenses/by-nc-nd/4.0/).

MOST WIEDZY Downloaded from mostwiedzy.pl

foam.

Graphene, a wonder material of this era, has also been used as fillers in silicone rubber. The addition of graphene nonoplatelets in silicone rubber has enhanced the tensile strength, thermal conductivity and thermal stability [13]. Even graphene nanoribbon incorporation in silicone rubber has lead to the increase of thermal and mechanical properties of the nanocompoistes [14]. One of the latest methods of manufacturing technique is 3D printing. Quite surprisingly, carbon fiber reinforced silicone rubber composites were successfully 3D printed by Huang et al. [15]. These conductive composites were developed for strain sensor applications. Also, they were found to have excellent mechanical properties. Pylios et al. [16] used medical grade silicone rubber which is tested on pin-on-disc apparatus against titanium and Ultrahigh Molecular Weight Polyethylene (UHMWPE) to study the wear properties. Titanium pin produced less wear on the rubber composites when compared to UHMWPE under dry sliding conditions and under the effect of lubricants. The effects on the mechanical and tribological properties of different white carbon black were investigated by He et al. [17]. The prepared composites showed excellent mechanical and anti-wear properties.

However, very few works have been reported with QM reinforced graphite-based fillers when compared to other types of elastomers especially in the field of tribology. Therefore, silicone rubber with exfoliated graphite as reinforcing filler is selected for this research work. Later the studies were extended to tribological properties such as coefficient of friction, wear rate of the composites in detail and it is correlated with the morphological analysis of the worn surface.

2. Experimental details

2.1. Materials

The elastomer matrix used for this research work was silicone rubber (QM) 5060-U grade procured from KPCC Corporation, Korea. The reinforcing filler, exfoliated graphite (EG) was collected from Asbury Carbons, USA. Dicumyl peroxide (DCP), the curing agent was procured from Sigma Aldrich, Bangalore, India. Other ingredients and solvents used were of laboratory grade and were used without further purification.

2.2. Preparation of composites

Two-roll mixing technique was used for the preparation of composites. The rubber matrix, filler and the curing agent were thoroughly mixed according to the formulations given in Table 1. The mixing of each sample consumed about 20 min. Optimum cure time of the rubber vulcanizates was determined according to ASTM D-1646 in an oscillating disc type rheometer. The samples were press-cured for their respective cure time at 150 °C and post cured at 200 °C for 4 h ina hot air oven. The preparation layout of silicone rubber/exfoliated graphite composite (QMEG)is shown in Fig. 1.

2.3. Characterization and tests

2.3.1. Structural characterization

The structural characterization of composites was carried out by X-ray diffraction (XRD) analysis in Bruker AXS D8 advance X-ray diffractometer. X-ray source - Cu Kα radiation (λ = 0.154 nm).

2.3.2. Diffusion studies

The data obtained from solvent diffusion studies was used for investigating the reinforcing effect of the composites. Diffusion studies were performed as per the following procedure (at room temperature conditions). Circular samples were punched out from the compression moulded sheet using sharp edged steel die. The thickness of the samples was measured using micrometer screw gauge. Initial weight of the samples was noted in a precise electronic balance. Further, it was soaked in 25 ml toluene (solvent) in sorption bottles. At regular intervals, samples were taken out, its surface wiped off gently to remove the adhere solvent, weighed and placed back in the test bottles consuming around 30 s. The weighing was repeated till equilibrium was attained and the diffusion parameters were calculated.

2.3.3. Mechanical tests

The mechanical properties of the elastomeric composites were tested in a pneumatic universal testing machine, INSTRON-4411 with a grip separation of 30mmand cross head velocity of about 500 mm/min. Dumbbell specimens were punched out of the moulded sheet and thickness of the narrow portion was measured. Each specimen was placed tightly between the two grips whose upper grip being fixed and experiment was conducted. The tensile strength, elongation at break, modulus (tensile test as per ASTM D412) and tear strength (tear testing as per ASTM D624) values were recorded. The hardness measurements were carried out using a shore Adurometer (DPX-1000, Rex Gauge Co., USA) following the ASTM D2240 standard.

2.3.4. Tribological tests

To understand the tribological features of the developed composites, two types of wear tests were carried out on the filler reinforced elastomeric specimens in order to study their friction and wear properties – two body and three body wear tests.2.3.4.1. Two body wear tests.

Two body wear studies were conducted on pin-on-disc machine as per ASTM G99 standards as shown in Fig. 2. After noting the initial weight of the pin shaped specimens, they are subjected to an initial run-in period so that the specimen surface comes in complete contact with the disc surface. The pin gets rubbed against a rotating steel disc (EN -32) of hardness HRC 65 with a track diameter of 100 mm under loaded condition. Coefficient of friction between the pin and the disc is measured by the deflection occurring in the calibrated load cell. The experiment is conducted for different loads, sliding distances, and temperatures and the detailed experimental operating condition are listed in Table 2.

After completion of the tests, the specimen pins are cleaned with acetone and dried. Their final weights are noted for determining the weight loss from which the wear rates are calculated. The equipment monitor displays the generated tangential frictional force when the specimen starts to

rub the counter face and this force is recorded to calculate the coefficient of friction (μ) as follows:

$$\mu = F_f / F_n \quad (1)$$

Where F_f (frictionalforce) and F_n(normalload which is applied). The specific wear rate (W_S) is calculated by:

Table 1
Compounding ingredients of silicone rubber exfoliated graphite composites (Phr)[a].

Ingredients (phr)	QM	QMEG3	QMEG5	QMEG7	QMEG10	QMEG12	QMEG15
QM	100	100	100	100	100	100	100
EG	0	3	5	7	10	12	15
DCP	1.5	1.5	1.5	1.5	1.5	1.5	1.5

[a] Parts per hundred parts of rubber.

MOST WIEDZY Downloaded from mostwiedzy.pl

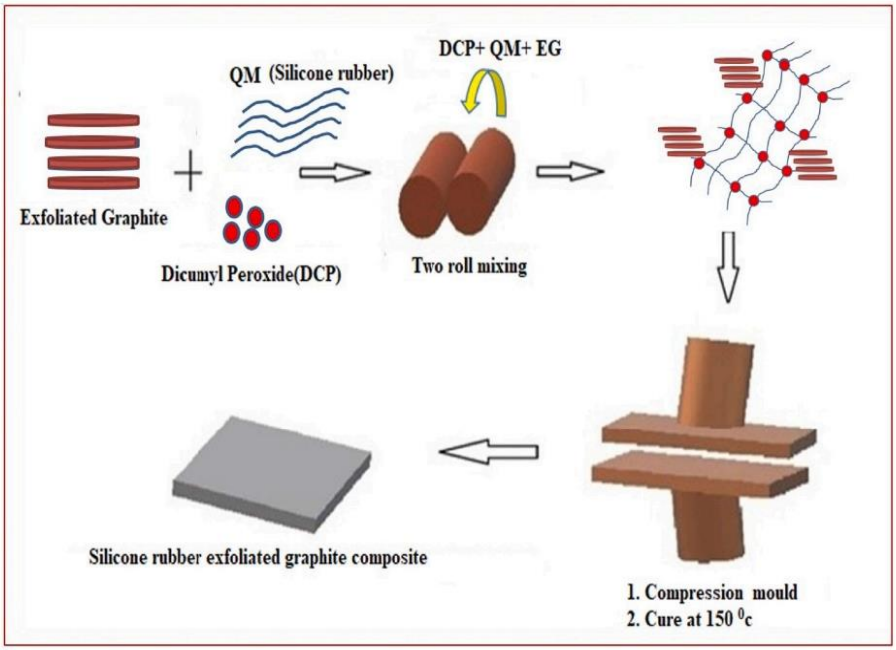

Fig. 1. Schematic representation of preparation of the QMEG composite.

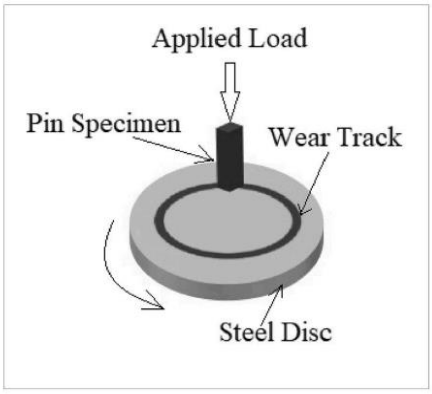

Fig. 2. Schematic representation of pin-on-disc test.

Table 2
Detailed experimental operating conditions.

Parameters	Operating Conditions
Temperature	Ambient conditions (temperature: 29 °C)
Relative humidity	55(±5) %
Test disc	Hardened ground steel (EN 31, hardness 60 HRC)
Roughness of EN-31	1.6 m Ra
Rubbing duration	1800s
Load	10 N,20 N and30 N
Sliding speed	1 m/s,2 m/s,3 m/s and 5 m/s
Sliding distance	1800 mm and 3600 mm
Pin size (ASTM G99 Std.)	30 mm × 10 mm × 10 mm

$$W_S = \Delta m / \rho F_n L \quad (2)$$

Here Δm is the weight loss, ρ is the composites' density, F_n is the applied load and L is the sliding distance (meters).

2.3.4.1. Three body wear tests. A dry rubber wheel abrasive wear test rig is used to conduct three body wear studies according to ASTM G65 as shown in Fig. 3. The test specimen of size 76 mm × 25 mm x 2 mm, gets abraded by using dry sand as the abrasive particle which is introduced in between the test specimen and the rotating wheel (rotated at a speed of 2 m/s) with a chorobutyl rubber tire in a controlled flow rate. The wheel rotates in such a way that its contact face moves in the direction of sand flow. The wear tests are carried out for different load conditions. Abrasive particles used are silica sand (AFS 50/70) of size 150–300 mm and the sand flow rate between rubber wheel and specimen is 375 ± 5 g/

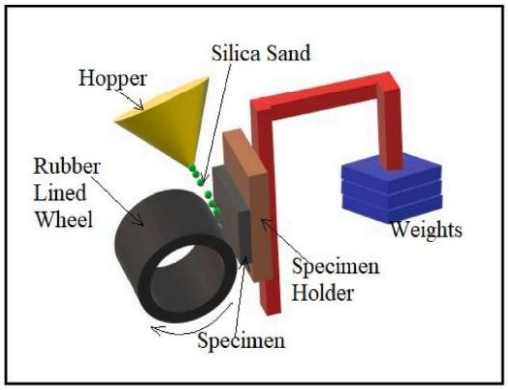

Fig. 3. Schematic diagram of dry sand/rubber wheel abrasive wear test rig.

MOST WIEDZY Downloaded from mostwiedzy.pl

min. The wear rate, determined from the measured weight loss values of the specimens, is further converted to wear volume. The specific wear rate (Ks) is calculated by the equation;

$$K_s = \frac{V}{Fn \times L} \quad (3)$$

Where, V- Volume loss (wear)

F_n- Applied Load

L - Sliding distance (meter)

2.3.5. Dielectric tests

Dielectric studies of the composites were performed in Agilent E4980A precision LCR meter (frequency range: 100 Hz to 2 MHz). AC conductivity, dielectric loss and dielectric permittivity (as per ASTM D150) values were obtained from these tests.

2.3.6. SEM(Scanning electron Microscopy)Analysis

The tensile fractured surface and the worn surface morphology of composites were analysed using TESCAN VEGA 3 SBH; (Thermal Emission) with resolution of 3 nm/30 KV. The samples to be analysed were sputter coated using Quorum SC7620 with Gold–Palladium.

3. Results and discussion

3.1. Structural characteristics - XRD analysis

Fig. 4 illustrates the X-ray diffraction patterns of neat QM, EG along with QMEG7composite. EG exhibits a high crystalline degree with a strong, sharp diffraction peak at $2\theta = 26.38^\circ$ with d –spacing of 3.37 Å. The sharp reflection at $2\theta = 26.4^\circ$ is once again observed in QMEG7, which implies that the individual EG sheets consist of multilayer graphite sheets with a d-spacing of 3.4 Å. Intrusion of polymer molecules does not change the structure of graphite, and hence its crystal structure is retained. Silicone rubber shows a broad peak at 11.28° with d-spacing value 7.84 Å. For the composite,as light change in peak position and d-spacing are observed.

The introduction of a filler into an elastomeric matrix leads to the formation of a reinforced composite materials. The extent of reinforcement depends on several factors such as filler loading, filler-filler interaction, polymer-filler interaction, hydrodynamic effect, degree of cross linking etc.[18]. Thus the vulcanization characteristics are also depends on these factors normally. The vulcanization characteristics of the composites could be studied by analyzing the cure characteristics given in Table 3. The minimum torque (M_L) values in the table present as the minimum viscosity and it represent the measure of mastication [19]. M_L values increased with increase in EG content and it indicate the building up of viscosity. The increase in viscosity with EG content reveals that filler restrict the movement of silicone chains and the processability becomes harder. It is clear from Table 3 that the maximum torque (M_H) values increased with increase in the concentration of EG and thereby the stiffness of the vulcanizate is improved. The details of the extent of crosslinking reactions, and the shear modulus of the vulcanizate can be infer from the M_H values. Moreover it also provide an idea about the filler-polymer interactions. Therefore it is easy to understand from M_H values that the extent of crosslinking, shear modulus as well as filler-polymer interactions are improved at higher dosage of EG. The differential torque, ΔS (i.e. MH – ML) represent the extent of crosslinking between silicone rubber and the curing agent. These results indicate that, ΔS for filled samples are higher than that of pure rubber. Thus ΔS increased with EG content. Scorch time (ts_2) is a parameter which measure the premature vulcanization of the composite and it evident from Table 3 that scorch safety increased with increase in the concentration EG. In order to get optimum physical properties the samples are usually vulcanized at optimum cure time (t90). As in the case of M_H and M_L, the t_{90}, also increased with increase in EG Content. The cure rate index (CRI) is a parameter which represent the fastness of curing process. The CRI values given in Table 2 showed that the highest values was observed for pure silicone rubber sample and the lowest for silicone rubber with higher filler content. Thus CRI values decreased with increase in EG content. This may be due to the improved surface area of EG that prevents the accelerating effect in vulcanization process [20].

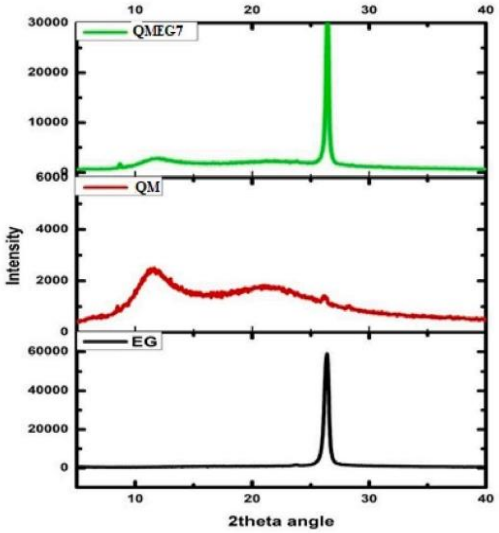

Fig. 4. X-ray powder diffraction patterns.

3.2. Mechanical properties

Silicone rubber has weak intermolecular forces among polymer chains. Thus, it has lower mechanical strength and this paves a way to improve its mechanical properties by incorporating fillers within its matrix. The various mechanical properties obtained for different EG filler loadings are shown in Table 4.

QMEG7 shows dispersion of EG with maximum tensile strength of 6.8 MPa which is almost 30% higher than QM. From the table, it is clear that tensile strength increases with filler loading up to 7phr and it decreases further. This reduction in value occurred because of agglomeration of EG particles. Agglomeration has affected dispersion and interaction of fillers within the rubber matrix. The effective dispersion of EG in matrix has facilitated uniform transfer of stress throughout rubber matrix. QMEG7 shows the optimum tensile strength, elongation at break and tear strength properties. This is because EG layers have been able to uniformly disperse in the elastomer matrix. Hardness values are also found to be increased continuously with EG filler concentrations as

Table 3
Cure characteristics of composites.

Sample	M_L (dNm)	M_H (dNm)	ΔS (dNm)	Scorch Time(ts_2) (min)	t_{90} (min)	Cure rate index(CRI) min^{-1}
QM	0.65	12.90	12.25	0.86	5.76	20.40
QMEG3	0.71	13.37	12.66	0.93	6.56	17.76
QMEG5	0.72	13.74	13.02	1.00	7.54	15.29
QMEG7	0.78	13.97	13.19	0.96	7.13	16.20
QMEG10	0.77	14.73	13.96	1.02	7.74	14.88
QMEG12	0.81	14.75	13.94	1.06	8.93	12.70
QMEG15	0.83	14.84	14.01	1.06	9.42	11.96

MOST WIEDZY Downloaded from mostwiedzy.pl

Table 4
Mechanical properties of composites.

Sample	Tensile strength (MPa)	Elongation at break (%)	Modulus at 100% (MPa)	Tear strength (N/mm)	Hardness (Shore A)
QM	4.747 ± 0.33	198 ± 12	2.36 ± 0.20	20.45 ± 1.24	51 ± 4
QMEG3	5.98 ± 0.12	241 ± 20	2.96 ± 0.25	24.81 ± 2.20	57 ± 4
QMEG5	6.589 ± 0.23	226 ± 16	3.53 ± 0.40	27.84 ± 3.10	63 ± 4
QMEG7	6.811 ± 0.21	221 ± 12	3.86 ± 0.30	30.22 ± 2.40	65 ± 2
QMEG10	6.184 ± 0.12	190 ± 18	4.21 ± 0.40	30.19 ± 2.34	67 ± 4
QMEG12	5.544 ± 0.32	150 ± 8	4.45 ± 0.40	29.82 ± 2.10	67 ± 2
QMEG15	5.446 ± 0.22	143 ± 10	4.87 ± 0.50	26.15 ± 3.20	69 ± 4

stiffening of elastomeric chains occurred with filler loading.

3.2.1. *Tensile fracture surface morphology*

A better knowledge of the interfacial adhesion between filler and rubber matrix can be obtained through the observation of tensile fractured surface as shown in Fig. 5. Fig. 5(a) shows the SEM image of neat EG with graphitic layers and Fig. 5(b) reveals silicone rubber with a very smooth surface. In the case of QMEG5 composites fracture surface appears to be much rougher and some voids noticed from the composites. But partially intercalated layers of the QMEG5 are visible in the SEM image. This is responsible for the enhancement of mechanical properties exhibited by QMEG5. Meanwhile, QMEG7 composites shows a better smooth surface with relatively low number of voids. It support its superior mechanical properties. Increased filler loading (QMEG10 composite), decreases the surface smoothness of the composites. This indicates that beyond 7 phr filler loading, agglomeration starts, it affect the dispersion and interaction between filler and matrix.

SEM images suggests that polymers are able to enter into the graphitic layers and forms interfacial interactions which has improved the mechanical properties of the composites. The dispersed EG, acts as a large number of stress concentration points in the QM matrix which absorbs energy and helps to transfer the load uniformly throughout the matrix as in the case of QMEG7 composite. Further it hinders crack growth under a strong external shock. Further QMEG composites reinforcement mechanism can be explained using Kraus plot (Fig. 6).

Based on Kraus equation as shown below [26],

$$\frac{V_{r0}}{V_{rf}} = 1 - m\left(\frac{f}{1-f}\right) \quad (4)$$

Where,V_{ro}-volume fraction of the swollen polymer in the fully swollen unfilled sample.

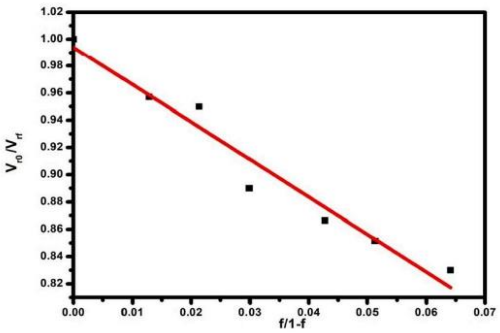

Fig. 6. Kraus plot of QMEGcomposites.

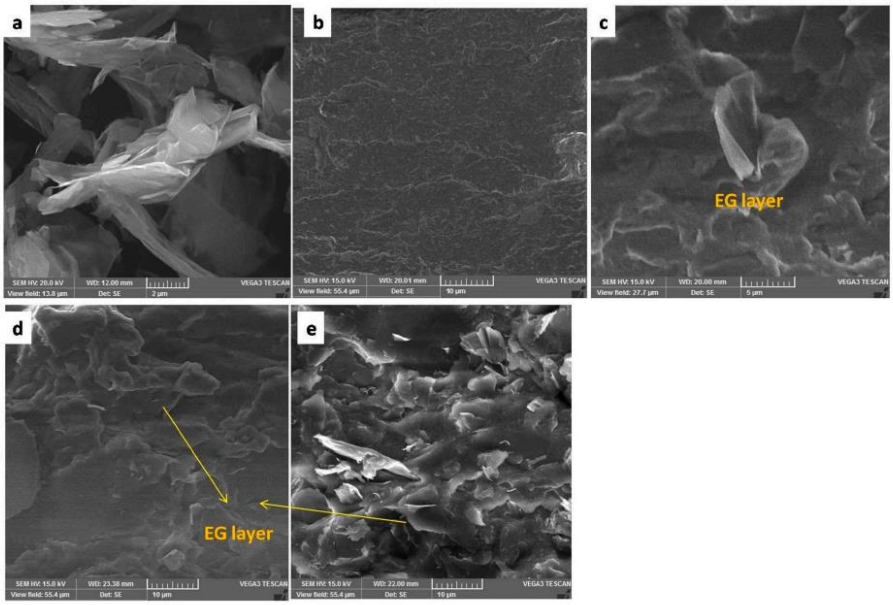

Fig. 5. Fracture surface SEM images (a) EG pure (b)QM(c) QMEG5 (d) QMEG7 and (e) QMEG10.

MOST WIEDZY Downloaded from mostwiedzy.pl

V_{rf}-volume fraction of the swollen reference polymer in the fully swollen filled sample

f - volume fraction of the filler

m - slope is a direct measure of the reinforcing capacity of the filler in the matrix.

Fig. 6 gives the plot of $\frac{V_{r0}}{V_{rf}}$ vs $\left(\frac{f}{1-f}\right)$. As the filler loading increases the value of $\frac{V_{r0}}{V_{rf}}$ decreases. Therefore, the composite with highest filler loading has the least value.

According to Kraus theory, higher the negative value of the slope, greater the reinforcement of the matrix with the filler. (V_{r0}/V_{rf}) is less than unity and the value of this ratio decreases with filler loading in QMEG composites. In QMEG composites (V_{r0}/V_{rf}) is 0.95 for 3 ph EG and 0.83 for 15 ph EG, indicate better reinforcement of EG with matrix [21]. As the reinforcement increases, the degree of transfer of stress from polymer matrix to filler will increase, which leads to an increase in the constraint zone of polymer chains.

3.3. Tribological properties

3.3.1. Friction and wear properties [Two body wear tests]

Fig. 7 provides information regarding the COF as a function of time (s) and the specific wear rate (mm^3/Nm) of the composites for different amount of filler loading.

Fig. 7(a) depicts the variation of coefficient of friction with respect to the sliding time. It is found that frictional coefficient values for all the composites shoot up initially and then a gradual decrease is observed to finally achieve almost stable values. It is also noticed that coefficient of friction of the EG filled composites is much lower than that of pure silicone rubber. Composite with 7 phr filler loading exhibited lowest COF value. However, QMEG10 composite quickly stabilized its COF value. Fig. 7(b) shows the variation of specific wear rate of composites with respect to graphite content. The specific wear rate of EG loaded composites is also found to achieve a lower value when compared to that of neat sample with lowest value for 7 phr loaded sample.

Thus, it is clear that EG reinforcement enhances the tribological properties of the composites. The self-lubricating property of graphite has in fact played a major role in achieving a lower COF and specific wear rate value. EG forms a transfer film on the frictional surface of the counterpart during rubbing which acts a lubricating film to help decrease these values. As the time increases, more and more stable film formation occurs [22]. A reduction in COF will also help to reduce the wear rate. Addition of filler concentration up to 7phr decreases the friction coefficient and specific wear rate after which friction coefficient and specific wear rate starts to increase indicates that the optimum limit – 7 phr has been reached.

3.3.1.1. Influence of normal load. The effect of applied load on COF and specific wear rate of the composites is analysed with the data shown in Fig. 8 (a) and (b.) As the load is increased, COF and wear rate of EG filled composites have a low value when compared to pure QM sample. At low loads (10 N) the COF and wear rate are quite high. Lower loads are unable to chip off the EG layers from the surface as such the applied load of 10 N is insufficient to break the interfacial adhesion existing between the EG filler and the matrix rubber. This leads to increased friction between the surface and in turn leads to higher wear rates. As the load reaches 30 N there is a drastic reduction in COF and increase in specific wear rate.

3.3.1.2. Influence of sliding velocity. Fig. 8 (c) and (d) represents the effect of filler reinforcement of composites on the COF and specific wear rates by varying the sliding velocity. As the EG content increases friction and wear properties decreases. Samples subjected to low sliding velocity (1 m/s) is characterised by higher friction and wear properties when compared to the sample values at higher sliding velocity (5 m/s). The values of COF and wear rates of composites with EG fillers are much lower to that of neat QM sample. Here also it is observed that 7 phr is the optimum value. When the specimen is rotated at 1 m/s, effective contact between the rubber and counter face takes place. Therefore, pure sample is observed to have high COF and wear rate values. However, with the addition of filler, EG gets peeled off from the rubber matrix for the applied load to form lubricant films thus reducing the contact area between the rubber and the counterpart leading to a reduction in these values. Meanwhile, at 5 m/s much films are not generated and even if any films are generated, this velocity might have affected the films stability to remain between the rubbing surfaces [23,24]. Overall, the addition of EG has helped to reduce the friction and wear properties appreciably.

3.3.1.3. Influence of temperature. Based on the results from the above two parameters, it was observed that 7 phr filler loading is the optimum filler loading for improved wear resistance. Therefore, QMEG7 composites is subjected to wear tests by varying the temperatures and the results are illustrated in Table 5

It is interesting to note that COF and specific wear rate are the lowest at 30 °C and the highest at 50 °C. Intermediate values are observed at 100 °C [Fig. 9]. This change in COF and specific wear rate might be due to the change in wear mechanism. The main wear mechanism operating though the system is adhesive wear which might be changed at 50 °C as there is a sudden rise in temperature. The changes occurring through a

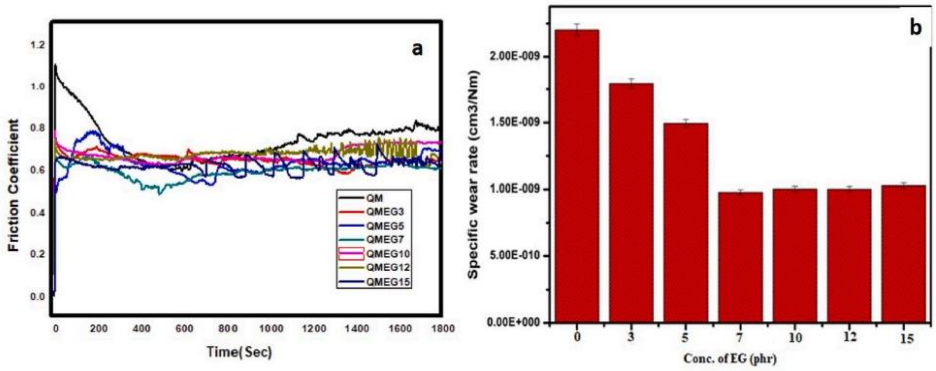

Fig. 7. (a) Friction coefficient of composites as a function of time **(b)** specific wear rate of the composites with various contents of EG (load-30 N, speed-2 m/s).

MOST WIEDZY Downloaded from mostwiedzy.pl

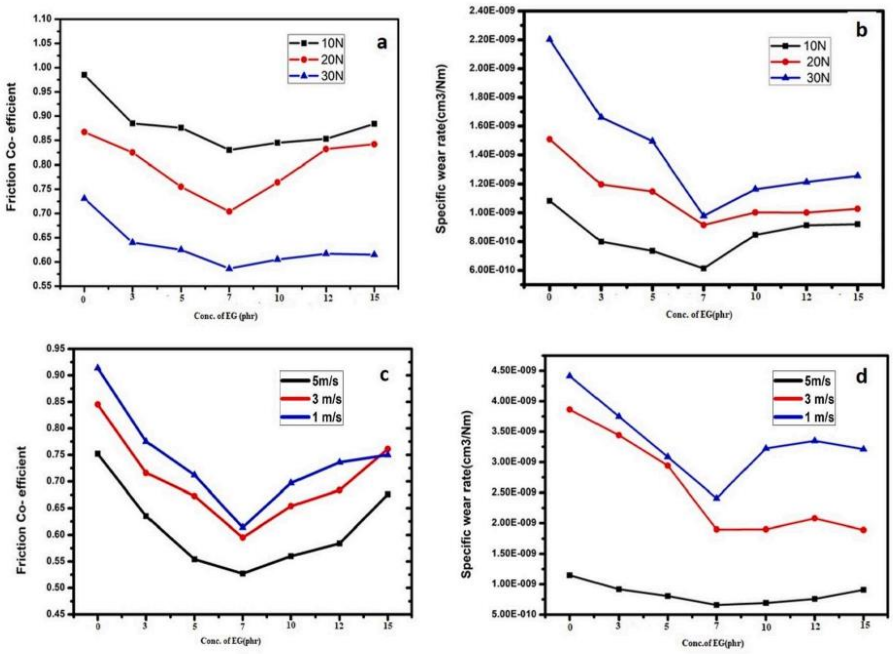

Fig. 8. **(a)** Friction coefficient **(b)** specific wear rate of composites with different loads (1800 m, RT,2 m/s)and **(c)** Friction coefficient **(d)** specific wear rate of the composites with different sliding velocity (30 N, RT, 1800 mm).

Table 5
COF and Specific Wear rate of QMEG7 composites with varying temperatures.

Temperature(°C)	Co efficient of friction	Specific wear rate × 10^6 (mm^3/Nm)
30	0.652	0.863
50	0.780	1.135
100	0.660	1.060

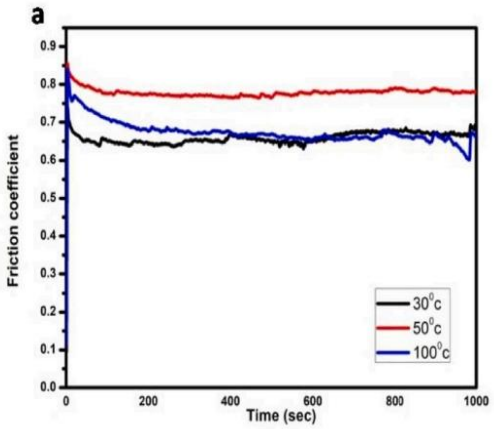

Fig. 9. Friction coefficient of QMEG7 composites as a function of temperature (30 N, 2 m/s, 1800 m).

series of actions such as shear failure of adhesive points, de-bonding of EG particles, lubricant film formation, destruction and reformation etc. Further rise in temperature rearrange the system so that mechanism is more or less similar to an adhesive wear. The difference in temperature leads to activation energy changes and which causes change in the wear behaviour of the material. Moreover, this suggests that the composite has undergone physical and mechanical changes which could be due to the viscoelastic nature of the elastomeric composites [25].

3.3.2. *Worn surface morphology*

In order to understand the wear behavior of the prepared composites, SEM examinations of the specimens after the pin on disc tests were employed. Worn surface morphology of the developed composites with different filler reinforcement after being subjected to two body wear tests is shown in Fig. 9. During the wear tests, deformation of rubber specimens occurs leading to energy loses which mainly arises due to the hysteresis friction. Further, formation and destruction of adhesive points between the rubbing surfaces develops adhesive friction. As such, bulk hysteresis and contact adhesiveness comes into picture regarding the friction in rubber [26,27]. Fig. 10 shows the worn surface morphologies of the silicone composites embedded with different amounts of EG after sliding in a circular path of 50 mm in radius for about 30 min at a sliding velocity of 2 m/s under a normal load of 30 N.Small craters and ridge like patterns are visible on the surface of QM along the sliding direction because pure rubber has low mechanical properties. Because of this it could be easily torn and ruptured. These patterns lead to an increase in adhesion friction force which further increases the friction and wear properties. Also, without any reinforcing fillers wear rate is quite high in pure rubber. But as the EG content increases the surface becomes more flattened out. SEM image of QMEG5 reveals that localized material removal starts to take place. EG layers starts to chip off and sufficient stable lubricating films could be formed due to the extensive chipping of

MOST WIEDZY Downloaded from mostwiedzy.pl

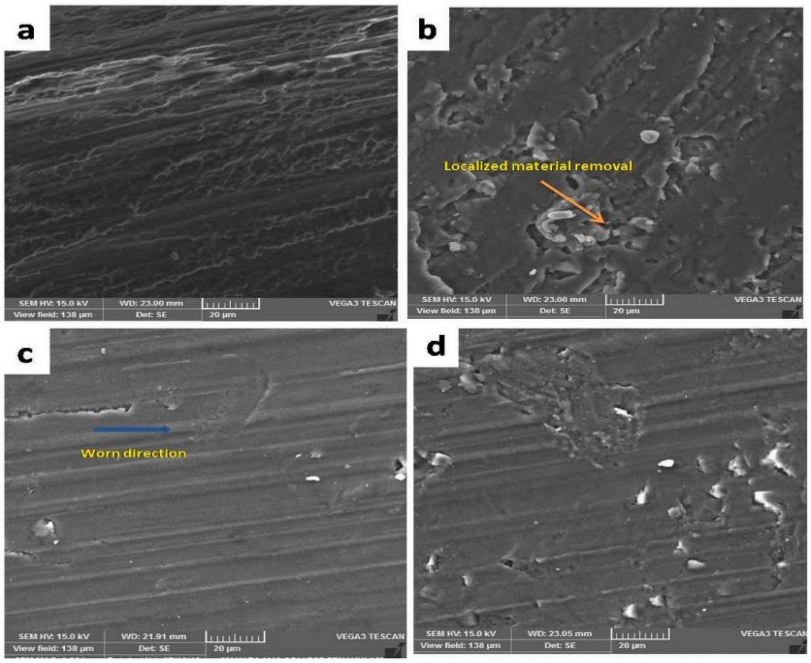

Fig. 10. SEM micrographs showing worn surface morphologies **(a)**QM**(b)**QMEG5**(c)**QMEG7 **(d)**QMEG10.

EG particles arising from slight abrasion of wear debris occurring between the rubbing surfaces. This leads to a decrease in adhesive friction.

However, almost a very neat surface morphology is present for the QMEG7 composite. Effective and stable lubricant film formation with the generation of sufficient chipped off EG particles have helped to reduce the friction and wear properties. This continuous stable film formation has reduced the real contact area of the rubbing surface which prevented further wear of the composite. Moreover, improved mechanical properties have been obtained for this composite when compared to neat rubber composite. This implies good dispersion of EG in the rubber matrix. Well dispersed filler within the rubber matrix leads to continuous and stable lubricant film formation. Since EG fillers have been easily chipped off, it indicates that poor interfacial adhesion exists and reducing the adhesive friction component. Further, with lesser number of interfacial adhesive points being created, results in reduced energy dissipations to shear the formed adhesive junctions. This results reduction in friction.

Addition of EG beyond the optimum value (7 phr) has affected this film formation. For composite with 10 phr EG surface morphology indicates material removal and shallow large crater during SEM examination. Beyond the optimum value, agglomeration has taken place and this has led to poor dispersion of EG within the composites. EG agglomerates have led to formation of strong interfacial adhesive junctions at the areas of agglomeration thus increasing the adhesive friction and hysteresis friction. From the SEM study it is concluded that wear of composites has occurred mainly due to adhesive wear. Initiation of adhesive wear starts with formation of interfacial adhesive junctions. When rubber starts to slide on rigid surface, with the applied load, deformation of rubber surface in contact takes place. The surface initially adheres together under dry sliding conditions. The relative sliding motion acts to shear the formed adhesive junctions and wear of the rubber material starts to occur. Therefore, wear mechanism involves the formation of adhesive junctions, shear failure of adhesive points, debonding of EG particles, lubricant film formation, destruction and reformation, and finally, adhesive wear [28].

Silicone rubber exfoliated graphite composites were prepared and evaluated by(High Resolution Transmission Electron Microscopy) HR-TEM, as shown in Fig. 11.HR-TEM image of QMEG7 indicates that fine dispersion of exfoliated graphite with layered structure in the QM matrix. The graphene layers of the EG clearly seen from the figure without any agglomeration. The better dispersion of EG in QM matrix due to good interfacial interaction between EG and QM. EG act as reinforcing agent in QM matrix. It helps to transfer stress uniformly throughout the matrix and protect from external shocks.

The AFM (Atomic Force Microscopy) analysis was used to study the surface roughens values of the QMEG composites. Fig. 12 illustrates the surface topographical features of QM, QMEG5, QMEG7 and QMEG10 composites in 2D and 3D view. In QMEG7 sample the distribution and dimensions of the heaps or hills are almost homogeneous, which indicates a good dispersion of EG in the QMmatrix. Addition of EG to the QM matrix increases the surface roughness Ra value. The improvement in mechanical and tribological properties compared to the gum samples can be correlated with AFM analyses. During tribological analyses, the homogeneous distribution of heaps and hills in QMEG7 sample helps to interact the counter surface uniformly. The SEM micrograph obtained from the QMEG7 vulcanisates showed a smooth surface. During tribological testing, the deformation rate QMEG7 was much lower than that of other composites. This distribution also helps to QMEG7 to form uniform transfer film in between material and counter surface, which improve the wear resistance of the material. In QMEG10, the surface roughness value was much higher around 77 nm which attributed to increased concentration of EG in QM matrix.

In roughness analysis, If Rms and Ra are similar, there is no layer deviation from the mean surface. The systems with Rms-Ra obtained a

MOST WIEDZY Downloaded from mostwiedzy.pl

MOST WIEDZY Downloaded from mostwiedzy.pl

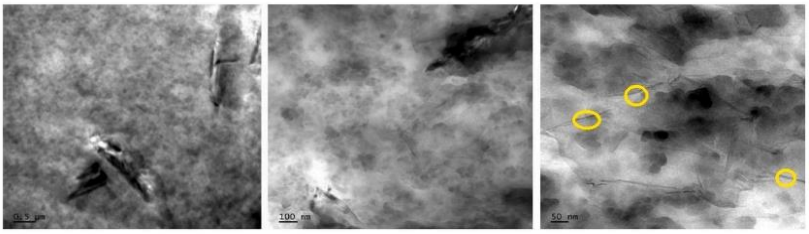

Fig. 11. TEM images of QMEG7 composite and yellow circle indicate the layers of EG. (For interpretation of the references to colour in this figure legend, the reader is referred to the Web version of this article.)

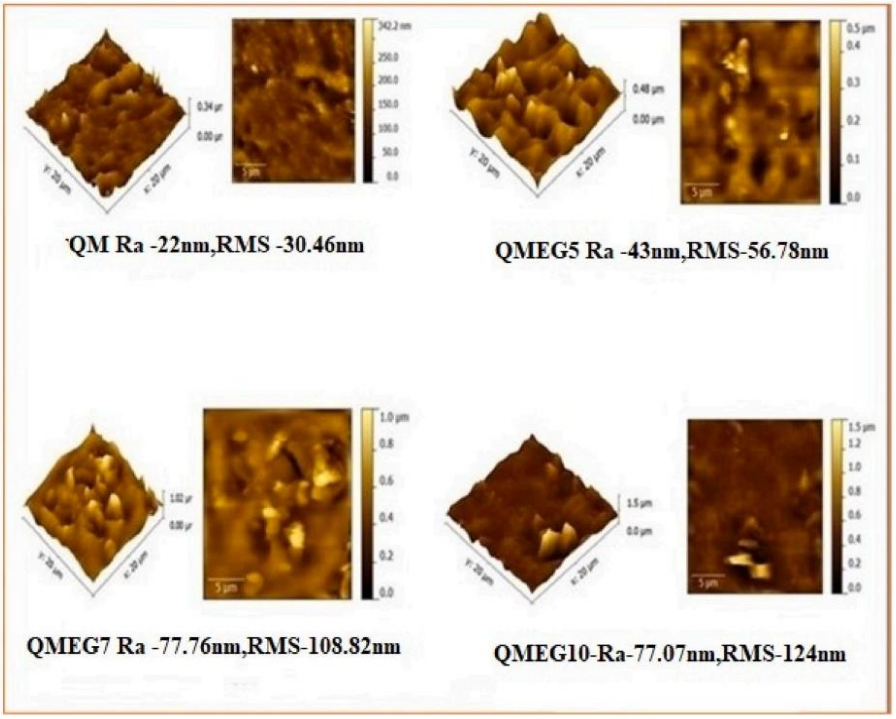

Fig. 12. AFM topography 2Dand3D images of silicon rubber exfoliated graphite composites with different EG content. (For interpretation of the references to colour in this figure legend, the reader is referred to the Web version of this article.)

higher value, it confirms the presence of filler particles on the surface [29]. From Table 6, it is clear that Rms-Ra value increased with filler loading. It confirms that EG comes on the surface of the composite and it interact with counter surface and produce thin film of lubricating film, which improve the material from wear resistance of the material.

Table 6
Roughness analysis of QMEG composites.

Sample	Ra (nm)	Rms (nm)	Rms-Ra(nm)
QM	22.7	30.46	7.76
QMEG5	42.99	56.78	13.79
QMEG7	77.76	108.82	31.06
QMEG10	77.07	124	46.93

3.3.3. Wear properties [Three body wear tests]

Wear volume and specific wear rates of QMEG7 composites with different loads are shown in Table 7. The data reveals that wear volume and specific wear rate have increased as the load increases with a more dramatic increase for the latter.

Here, wear increases with an increase in load. The rubber might have

Table 7
Wear volume and Specific wear rate of QMEG7 composite with different loads.

Load(N)	Wear volume(cm^3)	Specific wear rate $\times 10^4$ (cm^3/Nm)
2.94	1.1091	5.16
4.90	1.1686	9.25
9.80	1.2637	32.24

MOST WIEDZY Downloaded from mostwiedzy.pl

been induced with more stress with an increased load. This might have been substantial in weakening the interfacial interaction between the silicone rubber and the EG particles. As such, more EG particles and rubber were subjected to abrasive action further increasing the material removal rate. Moreover, as the load is increased more EG particles flake off and the high loads prevents the formation of stable lubricating film between the abrading surfaces by this flaked off EG particles.

3.4. Dielectric properties

The variations in electrical properties of the developed composites with the addition of fillers has been analysed. Fig. 13 (a) depicts the variation of AC conductivity as function of frequency and filler loading. The AC Conductivity (S/cm) of the developed composites is not only found to increase with an increase in frequency but also with filler loading. Composites with 15phr filler loading achieved higher values of conductivity. With more filler particles inside the filler material, the distance between the particles decreases and charges will be able to hop or tunnel [30] depending on the applied frequency. The increase in value with increased filler loading is due to better dispersion of EG which leads to micro capacitor network formations within the composites.

The material's ability to store an electric field in the polarisation of the medium is given by the measure of its dielectric permittivity and Fig. 13 (b) shows dielectric permittivity versus frequency and filler loading graph. It could be seen that for the neat QM sample, a slight decrease in the dielectric permittivity (E′) occurs with increasing frequency. A similar pattern can also be observed for QMEG3, QMEG5, QMEG7 and QMEG10 sample although the value of E′ increased slightly when compared to that of neat sample.

The elastomeric composites attained the percolation threshold (p_c) at filler loading of 12 phr and showed a sudden increase in dielectric constant at low frequencies. This implies that there were many EG particles separated by thin layers of QM. As the filler loading increases the permittivity increases at lower frequencies. The permittivity value increased with increasing the content of EG suggests the increased energy storage capacity of the developed composites [31–33]. However, it decreases with an increase in frequency. The number and the ability of the orientable dipoles to orient under applied electric field determines the dielectric permittivity value of the composites. At lower frequency, dipoles are able to orient under applied field and results in better filler-filler networks within the composites. Moreover, Maxwell–Wagner–Sillars relaxation [34] also occurs at low frequencies and therefore interfacial polarisation leads to an increase in permittivity initially. The polymer chains are unable to orient at higher frequencies and thus a decrease in value of the permittivity is observed. Fig. 13 (c) gives the variation of dielectric loss with frequency and filler loading. Dielectric loss represents extent of energy dissipation due to charge migration or conversion to thermal energy in the case of dielectric loss of QM composites, Energy dissipation is observed to be very low for all composites except QMEG15. Hence, QM composites with increased AC conductivity decreased dielectric loss and increased dielectric

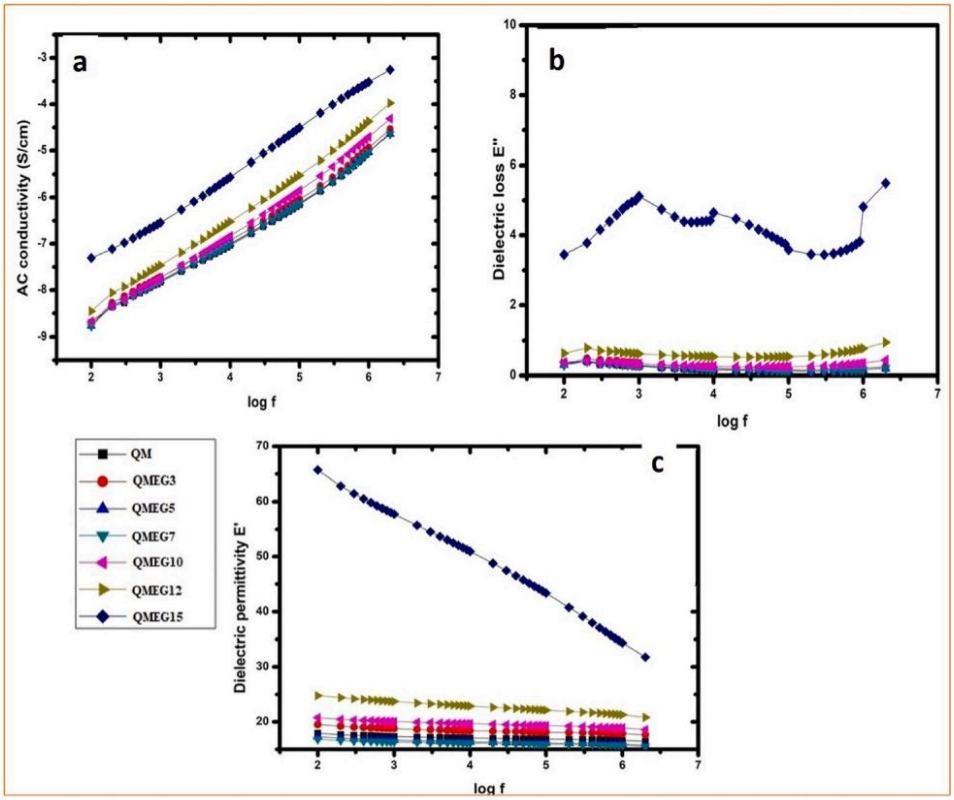

Fig. 13. Effect of EG loading and frequency on **(a)** AC Conductivity **(b)** Dielectric permittivity and **(c)** Dielectric loss of the composites.

MOST WIEDZY Downloaded from mostwiedzy.pl

MOST WIEDZY Downloaded from mostwiedzy.pl

permittivity has been developed. The resulting increase in dielectric properties is because of better adhesion between filler material and QM matrix [35,36].

4. Conclusion

Novel Silicone Rubber composites with Exfoliated Graphite as reinforcing fillers were successfully developed first time using simple two roll mixing technique. On investigating the composite properties, the experimental data reveals its excellent mechanical, tribological and dielectric properties and therefore it could be applied in automobile and aerospace applications.

- Silicone rubber with 7 phr of exfoliated graphite composite exhibited the highest mechanical properties as it evident from the fracture surface morphology of the composite. Coefficient of friction and specific wear rate reduced as the exfoliated graphite content increased. As the increased load reduces coefficient of friction but increases specific wear rate, while the increased sliding velocity increases both coefficient of friction and specific wear rate. COF and specific wear rate values were increased with increase in temperature upto 50 °C and then decrease. This might be due to the change in adhesive wear mechanism operating though the system at 50 °C as there is a sudden rise in temperature.
- Silicone rubber with 7 phr of exfoliated graphite composite has the lowest coefficient of friction value and silicone rubber with 10phr of exfoliated graphite composite sample quickly stabilized its friction value.
- Among the various composites, silicone rubber with 7 phr of exfoliated graphite composite recorded decreased friction and wear properties. A very neat worn surface morphology was also obtained for Silicone rubber with 7 phr of exfoliated graphite composite. Wear in the composite mainly occurred due to adhesive wear between the surfaces in contact.
- Under three body tests of silicone rubber with 7 phr of exfoliated graphite composite, wear volume and wear rate were found to increase as the load increases.
- AFM and TEM analysis confirms the better dispersion of EG particles, presence of EG particle on the composite surface form a lubricant film and improved wear resistance.
- Increased AC conductivity and dielectric permittivity, decreased dielectric loss were obtained with silicone rubber with 15phr of exfoliated graphite composites showing enhanced dielectric performance.

Therefore, incorporating EG as a reinforcing filler is found to be excellent in preparing filler reinforced elastomeric composites.

Declaration of competing interest

Authors have no conflict of interest.

CRediT authorship contribution statement

P.S. Sarath: Conceptualization, Data curation, Formal analysis, Investigation, Writing - original draft. **Sohil Varghese Samson:** Data curation, Formal analysis, Writing - original draft. **Rakesh Reghunath:** Conceptualization, Writing - original draft, Formal analysis, Visualization, Investigation. **Mrituanjay Kumar Pandey:** Visualization, Validation. **Józef T. Haponiuk:** Writing - review & editing, Supervision. **Sabu Thomas:** Conceptualization, Supervision, Writing - review & editing. **Soney C. George:** Conceptualization, Project administration, Resources, Supervision, Writing - review & editing.

Acknowledgment

The authors are especially grateful to DRDO (Order No: ERIP/ER/1504758/M/01/1667), New Delhi, India for providing the financial assistance. International and Inter University Centre for Nanoscience and Nanotechnology, Mahatma Gandhi University, Kottayam, Kerala, India and Rubber Park Airapuram, Kerala, India are also acknowledged here for various analyses.

Appendix A. Supplementary data

Supplementary data to this article can be found online at https://doi.org/10.1016/j.polymertesting.2020.106601.

Nomenclature

AFM	Atomic Force Microscopy
COF	Friction coefficient
DCP	Dicumyl peroxide
1D	One Dimensional
2D	Two dimensional
3D	Three Dimensional
EG	Exfoliated Graphite
HNT	Halloysite nanotube
M_H	Maximum Torque
M_L	Minimum Torque
QM	Silicone Rubber
QMEG	Exfoliated graphite/silicone rubber composite
Ra	Arithmetic average of the absolute values of surface height deviation taken from the mean plane
Rms	Root mean square average of surface height deviation taken from the mean data
SEM	Scanning electron Microscopy
TEM	Transmission electron microscopy
XRD	X-ray diffraction
UHMWPE	Ultrahigh Molecular Weight Polyethylene

References

[1] T. Jose, G. Moni, S. Salini, A.J. Raju, J.J. George, S.C. George, Multifunctional multi-walled carbon nanotube reinforced natural rubber nanocomposites, Ind. Crop. Prod. 105 (2017) 63–73, no. April.
[2] J. Abraham, M. Arif P, P. Xavier, S. Bose, S.C. George, N. Kalarikkal, S. Thomas, Investigation into Dielectric Behaviour and Electromagnetic Interference Shielding Effectiveness of Conducting Styrene Butadiene Rubber Composites Containing Ionic Liquid Modified MWCNT, Polym. (United Kingdom) 112 (2017) 102–115.
[3] M.G. Maya, S.C. George, T. Jose, L. Kailas, S. Thomas, Development of a flexible and conductive elastomeric composite based on chloroprene rubber, Polym. Test. 65 (2018) 256–263, no. September 2017.
[4] G. Moni, A. Mayeen, J. Abraham, T. Jose, M.G. Maya, R. Bhowmik, S.C. George, Flexible FKM/mRGO nanocomposites with excellent thermal, mechanical and electrical properties, Arab. J. Chem. 13 (1) (January 2020) 2142–2152.
[5] K.K. Sadasivuni, D. Ponnamma, S. Thomas, Y. Grohens, Evolution from graphite to graphene elastomer composites, Prog. Polym. Sci. 39 (4) (Apr. 2014) 749–780.
[6] SinEtsu, Characteristic properties of Silicone Rubber Compounds Meeting the increasingly diverse and sophisticated needs of industry with the unique properties of silicone rubbers, 2013.
[7] J.-H. Lee, W.Y. Ji, Electrical and mechanical properties of silicone rubber for high voltage insulation, Prop. Appl. Dielectr. Mater. 2003. Proc. 7th Int. Conf. 2 (2003) 591–594, vol. 2.
[8] L. Jiang, A. Betts, D. Kennedy, S. Jerrams, Improving the electromechanical performance of dielectric elastomers using silicone rubber and dopamine coated barium titanate, Mater. Des. 85 (2015) 733–742.
[9] W. Du, Z. Zhang, W. Fan, W. Gao, H. Su, Z. Li, Fabrication and evaluation of polydimethylsiloxane modified gelatin/silicone rubber asymmetric bilayer membrane with porous structure, Mater. Des. 158 (2018) 28–38.
[10] R. Berahman, M. Raiati, M. Mehrabi Mazidi, S.M.R. Paran, Preparation and characterization of vulcanized silicone rubber/halloysite nanotube nanocomposites:effect of matrix hardness and HNT content, Mater. Des. 104 (2016) 333–345.
[11] C. Xu, Y. Wang, B. Lin, X. Liang, Y. Chen, Thermoplastic vulcanizate based on poly (vinylidene fluoride) and methyl vinyl silicone rubber by using fluorosilicone rubber as interfacial compatibilizer, Mater. Des. 88 (2015) 170–176.

MOST WIEDZY Downloaded from mostwiedzy.pl

MOST WIEDZY Downloaded from mostwiedzy.pl

[12] J. Bai, X. Liao, E. Huang, Y. Luo, Q. Yang, G. Li, Control of the cell structure of microcellular silicone rubber/nanographite foam for enhanced mechanical performance, Mater. Des. 133 (2017) 288–298.

[13] Y. Song, J. Yu, L. Yu, F.E. Alam, W. Dai, C. Li, N. Jiang, Enhancing the thermal, electrical, and mechanical properties of silicone rubber by addition of graphene nanoplatelets, Mater. Des. 88 (2015) 950–957.

[14] L. Gan, S. Shang, C.W.M. Yuen, S.X. Jiang, N.M. Luo, Facile preparation of graphene nanoribbon filled silicone rubber nanocomposite with improved thermal and mechanical properties, Compos. B Eng. 69 (2015) 237–242.

[15] P. Huang, Z. Xia, S. Cui, 3D printing of carbon fiber-filled conductive silicon rubber, Mater. *Des.* 142 (2018) 11–21.

[16] T. Pylios and D. E. T. Shepherd, "Wear of medical grade silicone rubber against titanium and ultrahigh molecular weight polyethylene," J. Biomed. Mater. Res. B Appl. Biomater., vol. 84B, no. 2, pp. 520–523.

[17] Q. He, A. Li, Y. Zhang, S. Liu, Y. Guo, L. Kong, A study on mechanical and tribological properties of silicone rubber reinforced with white carbon black, Tribol. Mater. Surface Interfac. 12 (1) (2018) 9–16.

[18] J. Frohlich, W. Niedermeier, H.-D. Luginsland, The effect of filler–filler and filler–elastomer interaction on rubber reinforcement Composites: Part A 36 (2005) 449–460.

[19] S.C. George, K.N. Ninan, G. Groeninckx, S. Thomas, Styrene–butadiene rubber/natural rubber blends: morphology, transport behavior, and dynamic mechanical and mechanical properties, J. Appl. Polym. Sci. 78 (6) (2000) 1280–1303.

[20] G. Moni, T. Jose, S. Rajeevan, A. Mayeen, A. Rejimon, P.S. Sarath, S.C. George, Influence of exfoliated graphite inclusion on the thermal, mechanical, dielectric and solvent transport characteristics of fluoroelastomer nanocomposites, J. Polym. Res. 27 (3) (2020) 1–11.

[21] G. Kraus, Swelling of filler-reinforced vulcanizates, J. Appl. Polym. Sci. 7 (3) (1963) 861–871.

[22] L. Liu, F. Yan, F. Gai, L. Xiao, L. Shang, M. Li, Y. Ao, Enhanced tribological performance of PEEK/SCF/PTFE hybrid composites by graphene, RSC Adv. 7 (53) (2017) 33450–33458.

[23] L.L. Wang, L.Q. Zhang, M. Tian, Mechanical and tribological properties of acrylonitrile-butadiene rubber filled with graphite and carbon black, Mater. Des. 39 (2012) 450–457.

[24] L. Wang, L. Zhang, M. Tian, Effect of expanded graphite (EG) dispersion on the mechanical and tribological properties of nitrile rubber/EG composites, Wear 276–277 (2012) 85–93.

[25] A. Saffar, A. Shojaei, M. Arjmand, Theoretical and experimental analysis of the thermal, fade and wear characteristics of rubber-based composite friction materials, Wear 269 (1–2) (2010) 145–151.

[26] Hysteresis losses in the friction of lubricated rubber: david tabor. Rubber chemistry and technology. V. 33. No. 1, jan.–mar. 1960, p. 142–150. (Reprinted from the Proceedings of the first international skid prevention conference, Virginia council of high, Wear 3 (5) (1960) 405.

[27] J.A. Greenwood, D. Tabor, The friction of hard sliders on lubricated rubber: the importance of deformation losses, Proc. Phys. Soc. 71 (6) (1958) 989.

[28] 12 Adhesion and Adhesive Wear, in: G.W. Stachowiak, A.W. Batchelor (Eds.), Engineering TriBology, 24, Elsevier, 1993, pp. 613–635.

[29] C. Soney, George Regitha Rajan, Aprem Santhosh, The fabrication and properties of natural rubber-clay nanocomposites, Polym. Test. 51 (2016) 165–173. May.

[30] J.P. Giltrow, A relationship between abrasive wear and the cohesive energy of materials, Wear 15 (1) (1970) 71–78.

[31] M. Vaziri, R.T. Spurr, F.H. Stott, An investigation of the wear of polymeric materials, Wear 122 (3) (1988) 329–342.

[32] S. Capaccioli, M. Lucchesi, P.A. Rolla, G. Ruggeri, Dielectric response analysis of a conducting polymer dominated by the hopping charge transport Dielectric response analysis of a conducting polymer dominated by the hopping charge transport, J. Phys. Condens. Matter 10 (1998) 5595–5617.

[33] J. Abraham, L. Kailas, N. Kalarikkal, S.C. George, S. Thomas, Developing highly conducting and mechanically durable styrene butadiene rubber composites with tailored microstructural properties by a green approach using ionic liquid modified MWCNTs, RSC Adv. 6 (39) (2016) 32493–32504.

[34] S. Agrawal, K.S. Ojha, D. Sahu, Structural and dielectric studies of MWCNT reinforced microcellular silicone elastomer nanocomposite, Mater. Today Proc. 2 (9) (2015) 4516–4520.

[35] E. Tuncer, S.M. Gubanski, Electrical properties of filled silicone rubber, J. Phys. Condens. Matter 12 (8) (2000) 1873.

[36] M. Samet, V. Levchenko, G. Boiteux, G. Seytre, A. Kallel, A. Serghei, Electrode polarization vs. Maxwell-Wagner-Sillars interfacial polarization in dielectric spectra of materials: characteristic frequencies and scaling laws, J. Chem. *Phys.* 142 (19) (2015).

MOST WIEDZY Downloaded from mostwiedzy.pl

MOST WIEDZY Downloaded from mostwiedzy.pl

Publication -3:

A study on the influence of reduced graphene oxide on the mechanical, dynamic mechanical, and tribological properties of silicone rubber nanocomposites

Article summary

Graphene oxide (GO) was synthesized using Hummer's method, reducing it with hydrazine. Synthesized reduced graphene oxide (rGO) was characterized by FT-IR spectroscopy, X-ray diffraction spectroscopy, Raman spectroscopy, and X-ray photoelectron spectroscopy. An elastomeric nanocomposite was prepared by incorporating rGO in silicone rubber using a two-roll mill mixing method. The tribological study was conducted at a wear surface of hardened ground steel against different applied loads, sliding speed, and temperature using a pin on disk setup—addition of rGO results in an improvement of mechanical, tribological, and thermal properties of silicone rubber. The coefficient friction (COF) and specific wear rate of the nanocomposite decreased with rGO concentration, applied load, and temperature. Morphological analysis of SRrGO nanocomposites was deeply investigated by scanning electron microscopy (SEM), transmission electron microscopy (TEM), and atomic force microscopy (AFM). Worn surface analysis confirms that rGO forms a lubricant film on the counter surface, but it fails to create a strong adhesive film on the metal surface. The depth wear rate decreased by incorporating rGO in the Silicone rubber (SR) matrix.

Methodology

- Cure characteristics
- Mechanical properties
- Tribology
- Dielectric studies
- Thermal studies

MOST WIEDZY Downloaded from mostwiedzy.pl

Check for updates

Article

JOURNAL OF COMPOSITE MATERIALS

Journal of Composite Materials
2021, Vol. 55(15) 2011–2024
© The Author(s) 2020
Article reuse guidelines:
sagepub.com/journals-permissions
DOI: 10.1177/0021998320981608
journals.sagepub.com/home/jcm
SAGE

A study on the influence of reduced graphene oxide on the mechanical, dynamic mechanical and tribological properties of silicone rubber nanocomposites

PS Sarath[1], Grace Moni[1], Jinu Jacob George[2], Józef T Haponiuk[3], Sabu Thomas[4] and Soney C George[1]

Abstract

Graphene oxide (GO) was synthesized by modified Hummer's method and it reduced with hydrazine. Synthesized reduced graphene oxide (rGO) was characterized by FT-IR spectroscopy, X-ray diffraction spectroscopy, Raman spectroscopy, and X-ray photoelectron spectroscopy. An elastomeric nanocomposite was prepared by incorporating rGO in silicone rubber using two roll mill mixing method.Tribological study was conducted at a wear surface of hardened ground steel against different applied load, sliding speed and temperature using a pin on disk setup. Addition of rGO results in an improvement of mechanical, tribological and thermal properties of silicone rubber. The coefficient friction (COF) and specific wear rate of the nanocomposite decreased with rGO concentration, applied load, and temperature. Morphological analysis of SRrGO nanocomposites was deeply investigated by scanning electron microscopy (SEM), transmission electron microscopy (TEM), and atomic force microscopy (AFM). Worn surface analysis confirms that rGO forms a lubricant film on the counter surface but it fails to form a strong adhesive film on the metal surface. The depth wear rate decreased by the incorporation of rGO in the Silicone rubber (SR) matrix.

Keywords

Silicone rubber, reduced graphene oxide, tribology, friction coefficient

Introduction

Silicone rubber is widely used in different fields due to its exceptional properties such as chemical resistance, thermal stability, weatherability, biocompatibility and electrical insulation. Due to its low modulus, silicon rubber exhibit large deformations in small stress. The improvement in modulus of silicone rubber can be achieved by adding suitable fillers to it. Elastomeric materials are commonly used in different applications where they experience large deformations.Therefore applications of polymeric materials in such fields require knowledge of their tribological properties. Tribological properties of the material is largely depend on different parameters. Therefore it is significant to understand the tribiological parameters such as surface roughness, mechanism of adhesion, friction and wear, and physical and chemical interactions of lubricants in detail. Interacting surfaces must be understood for optimal function, long-term reliability of components, devices and economic viability.

[1]Centre for Nanoscience and Technology, Department of Basic Sciences, AmalJyothi College of Engineering, India
[2]Department of Polymer Science and Technology, Cochin University of Science and Technology, India
[3]Department of Polymer Technology, Chemical Faculty, Gdansk University of Technology, Poland
[4]International and Inter University Centre for Nanoscience and Nanotechnology, Mahatma Gandhi University, India

Corresponding author:
Soney C George, Centre for Nanoscience and Technology, Department of Basic Sciences, AmalJyothi College of Engineering, Kanjirappally, Kottayam, Kerala, India.
Email: soneygeo@gmail.com

MOST WIEDZY Downloaded from mostwiedzy.pl

Polymeric materials are viscoelastic in nature and their properties change with respect to time. Macroscopic properties of polymer depend on molecular structure and interactions and thereby one expects some correlation between tribological and mechanical properties. Polymeric materials are usually used as tribological materials such as virgin, composites,coatings and solid lubricants.[1] Polymer thin film monolayers are the new rapidly developing area, where the organic polymer molecule are used as surface lubricants. They are mainly used in memory storage devices, micromechanical systems and other high precision devices.[2,3] Evaluation of the tribological behaviour of polymers is relatively difficult due to the complex multiphase structures.[4] Graphene, a single-atom-thick film of carbon, offers a promising solution to control friction and adhesion in various applications, especially in micro- and nanoscale devices with moving contact.[5–9]

Invention of graphene and functional graphene becomes more attractive in the field of material science. The thermal, mechanical, optical and electrical properties of graphene are superior and hence it is a promising alternative to conventional fillers. A major challenge in this respect is the permutation of conventional reinforcing fillers like carbon black, silica, clays etc. In the elastomeric vulcanizates small amount of nanofillers are added (eg: graphene, CNT, GNP etc) to achieve desirable properties. Graphene oxide (GO) is one of the promising material for the mass production of graphene and the important advantage in this respect are the ease of accessibility of graphite and its processibility in aqueous solution. By the reduction of graphene oxide to reduced graphene oxide (rGO), functional groups such as epoxy and hydroxyl groups are removed and the electronic properties are partially restored. Several research reports are available in the field of elastomeric composites with graphene based fillers in silicon rubber,[10] emulsion styrene butadiene-rubber (SBR),[11,12] solution styrene-butadiene rubber[13–15] synthetic natural rubber (cis-1, 4-polyisoprene) and epoxidized natural rubber (ENR),[16] nitrile rubber[17] and fluro elastomers.[18]

There has been very little work done in this area of nanoparticle-filled polymer composites for tribological applications. However, in this work we have done a detailed study on the influence of concentration of fillers, sliding speed, temperature and applied load on the tribological properties of SRrGO nanocomposite on hardened ground steel (EN 31, hardness 60 HRC). We also investigated the mechanical, thermal and thermal conductivity properties of SRrGO nanocomposite as a function of concentration of reduced graphene oxide.

Experiments

Materials

Silicone rubber SH5060-U (HTV) was procured from KCC Corporation, Korea. It is a general-purpose grade with low level of vinyl content. Graphite (synthetic powder, particle size <20 μm, purity - 99%) and dicumyl peroxide (DCP) were supplied by Sigma Aldrich, Bangalore, India.

Preparation of reduced graphene oxide (RGO)

GO was synthesized from natural graphite by modified Hummers method.[19] Graphite oxide (2 g) is dispersed in distilled water (2 L) using ultra sonication for 1 h. Hydrazine monohydrate (2 μl for 2 mg of GO, 98%, Aldrich) was subsequently added to the suspension. Additional stirring with a Teflon-coated stirring bar in an oil bath held at 80°C for 2 h yielded a black precipitation of reduced graphene oxide powder. After cooling to room temperature, the powder was centrifuged. The resultant black precipitate is intensively washed with distilled water. The resulting black material was dried under oven at 80°C for 24 hours.[20]

Preparation of silicone rubber nanocomposites

The SR and RGO were thoroughly mixed in a two-roll mill followed by curing agent. DCP was added to the system. Formulation is given in Table 1. The total mixing of each sample took about 20 minutes. "ASTM D-1646" standard was used for the cure time analysis. The RGO/Silicone rubber samples were hot pressed at 150°C for the respective cure time and post cured at 200°C for 4 hours in a hot air oven. The schematic representation of the preparation of the composites is given in Figure 1.

Table 1. Formulation of mixes (Phr[a]).

Ingredients	SR	SRrGO0.5	SRrGO1	SRrGO1.5	SRrGO2	SRrGO2.5
SR	100	100	100	100	100	100
RGO	0	0.5	1	1.5	2	2.5
DCP	1.5	1.5	1.5	1.5	1.5	1.5

[a]Parts per hundred rubber.

MOST WIEDZY Downloaded from mostwiedzy.pl

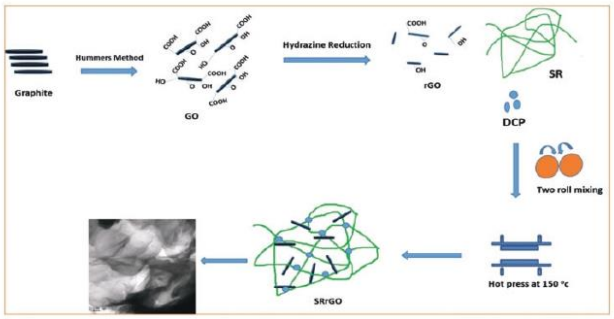

Figure 1. Schematic diagram of synthesis of SRrGO nanocomposites.

Characterization of rGO/SR nanocomposites

The synthesized rGO is analysed using FT-IR at a spectrum range of 500 – 4000 cm^{-1} and was analysed with Perkin Elmer analyser and Raman spectrometer (Horiba JobinYvon Lab Ram HR system). XRD spectra of rGO and nanocomposites were obtained from Bruker AXS D8. The cryocut specimens prepared using an ultramicrotome and nanocomposites were investigated by means of JEM-2100 HRTEM. The mechanical properties of the nanocomposites were analyzed on a pneumatic universal testing machine INSTRON-4411 with a cross head speed of about 500 mm/min according to ASTM D 412 at room temperature. Tear strength was also determined by the same instrument according to ASTM D624. Atomic force microscopy observations were carried out in air on as-received sample surfaces using Agilient 5500 AFM operated in contact mode. Measurements were carried out using standard triangular silicon nitride cantilever. Thermogravimetric analysis (TGA) was done using Perkin Elmer STA 6000, Diamond TG/DTA with a heating rate of 10°C/min from room temperature to 700°C under nitrogen atmosphere. Tribological properties of SRrGO nanocomposites studied using Ducom pin on disk tribometer. The behaviour of materials at extreme conditions studied with different applied load (5–15 N), sliding speed(2–5 m/s) and temperature (30°C–150°C). Dynamic mechanical analysis of the nanocomposites were measured over a wide temperature range from −130 to 40°C using a dynamic mechanical analyser (Perkin Elmer – DMA 8000) with a programmed heating rate of 10°C min^{-1}. Frequency and dynamic deformation were set to 1 Hz and 0.05%, respectively. The measurements were performed according to the procedure described in ASTM D 2231. Lee disc apparatus was used to study the thermal conductivities of the composites using ASTM D5470.

Results and discussions

Characterization of GO and rGO

FT-IR spectra of GO and rGO are shown in Figure 2 (a). GO shows an intense absorption peak at 1716 cm^{-1} corresponding to C = O stretching and a broad peak at 3448 cm^{-1} indicate the O-H stretching vibration. The broad peak of -OH coming from the C-OH groups. Peak at 1045 cm^{-1} is attributed as C-O stretching. The peak at 1160 cm^{-1} and 1625 cm^{-1} confirmed the C-O-C bending and C-OH bending. In the case of rGO, oxygen containing functional group such as hydroxyl, carbonyl was disappeared due to the successful reduction of GO. The peaks in 3448 cm^{-1}, 1045cm^{-1},1625cm^{-1} and 1716 cm^{-1} disappeared, and peak intensity decreased. This indicates the successful removal of oxygen-containing functional groups in GO. Figure 2(b) shows the Raman spectrum of synthesized GO and rGO. Raman spectroscopy is used for the structural elucidation of carbon materials. The I_D/I_G ratio of graphene oxide is 0.7852 and I_D/I_G ratio of reduced graphene oxide is 1.029.The rise in I_D/I_G ratio during reduction indicates the increased disorder in graphitic structure.[21]

Figure 3 Graphene oxide shows a diffraction peak at 10.9° with a d-spacing value 8.07 Å. Graphene oxide was reduced using hydrazine reagent and the peak at 10.9 Å (GO) disappeared and formation of broad peak around 26 Å (rGO) is observed. This is mainly due to exfoliation of graphitic layers and it leads to structural changes as revealed in XRD studies.[22]

The XPS (X-ray photoelectron spectroscopy) analysis of GO and rGO are shown in Figure 4. XPS spectrum of GO clearly indicates the degree of oxidation of carbon atoms of functional groups.

Table 2 shows the data obtained with the XPS spectrum of GO. The XPS spectrum of GO exhibited atomic ratio of carbon and oxygen (C/O) of Table 2.

MOST WIEDZY Downloaded from mostwiedzy.pl

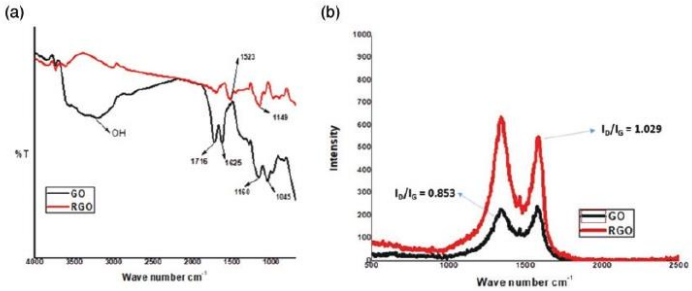

Figure 2. (a) FT-IR spectra (b) Raman spectra of GO and RGO.

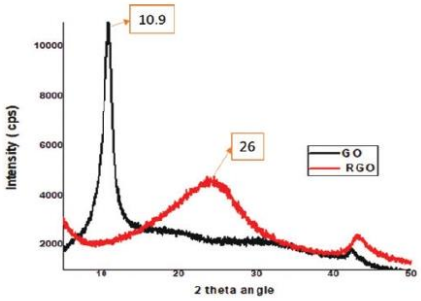

Figure 3. XRD spectra of synthesized GO and RGO.

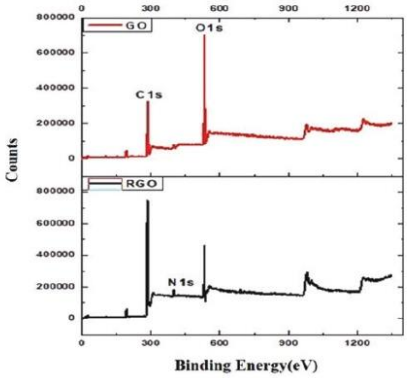

Figure 4. XPS spectra of GO and rGO.

The spectrum can be divided into five different peaks centred at 284.8, 286.6, 287.8 and 289 eV, which can be attributed to C = C, C–O, C = O, and O–C = O groups, respectively.[22]

After hydrazine reduction, C/O ratio increased from 1.33 to 2.85 (Table 3). This shows that most oxygenous groups have been removed by reduction. This was also confirmed by C1s spectra (Figure 2). It can be seen that intensity of the peak (C–C) decreased. There is also an additional component observed at 400 eV and these correspond to the carbon bound nitrogen (pyrazole) due to the reduction of hydrazine.[22]

The extent of curing can be understood by the maximum torque value M_H. From Table 4, it is clear that M_H decreased with filler loading. The minimum torque value M_L showed an increasing trend with filler loading and it gives an account of the improvement in viscosity of the compound. It also decreases with lower filler addition as in the case of tensile strength values. Tensile strength is mainly affected by the factors such as 1) inhomogenity, 2) the nature of physical form of the polymer and 3) its molecular orientation. When filler material is incorporated into the polymer matrix these factors will be adversely affected and that leads to a decrease in tensile strength.[23] ie, the incorporation of rGO has influenced the flexibility of the polymeric chains which affects the properties of the composites. The induction period of the composite or scorch time (t_{s2}) is decreased with filler loading and the optimum

Table 2. Data obtained from XPS analysis of graphene oxide (GO).[22]

Name	Peak BE (eV)	Atomic %
C1s	284.82	13.06
C1S	286.62	29.44
C1S	287.78	16.64
C1S	289.12	3.90
O1s	531.5	3.96
O1s	532.34	14.24
O1s	533.10	13.64
O1s	534.07	6.02

MOST WIEDZY Downloaded from mostwiedzy.pl

cure time (t_{90}) decreased initially with rGO loading upto 2phr and then it starts to increase. The decrease in cure time indicates that rGO act as an accelerator during curing.

Figure 5 show the XRD patterns of SR, rGO and SRrGO nanocomposites with different rGO loading. There is no noticeable shift in SR peak. SR showed a major diffraction peak at $2\theta = 12.1°$ and it shifted in SRrGO nanocomposites to 12.75°. But the diffraction peak of reduced graphene oxide is observed at $2\theta = 23.9°$ with a corresponding d-spacing of 0.374 nm. XRD profiles of SRrGO nanocomposites, such as SRrGO1 and SRrGO 2 exhibited a left shift with lower angle of diffraction such as 22.09° and 22.19° compared to pure rGO (23.9°) . The corresponding d- spacing values are 0.402 nm and 0.403 nm respectively. The decrease in angle of diffraction and an increase of d- spacing indicate the partial interaction of rGO with SR matrix.[24]

Transmission electron microscopy (TEM)

Figure 6 shows the TEM micrographs of SRrGO2 nanocomposites. The dark lines and the surrounding areas are rGO layers and aggregates, and the light area shows the rubber matrix. However, large agglomerates of rGO particles are not observed in the SRrGO2 nanocomposites. At lower magnification, the rGO appears to be well dispersed in the rubber matrix (shown in yellow circle) and inset shows magnified image of that region. Presence of some individual rGO layers clearly observed from the rubber matrix. Few stacks of rGO particles are visible at magnification. This shows partially to highly exfoliated morphology of rGO.

Table 3. Data obtained from XPS analysis of reduced graphene oxide (rGO).

Name	Peak BE (eV)	Atomic %
N1s	400.22	4.02
C1s	284.98	71.09
O1s	532.9	24.89

Figure 7 shows the EDS spectrum of SRrGO2 nanocomposite. To confirm the elemental composition of the sample, the nanocomposite sample was also tested with EDS. Table 5 listed the EDS result of SRrGO2. The result of EDS had proved that the sample

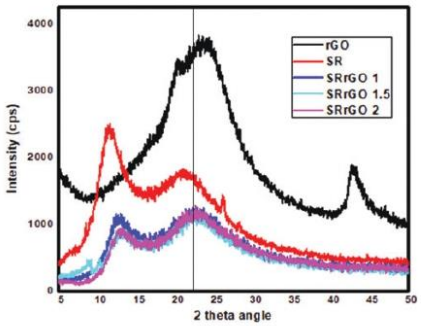

Figure 5. XRD patterns of SR, rGO and SRrGO nanocomposites with different rGO loading.

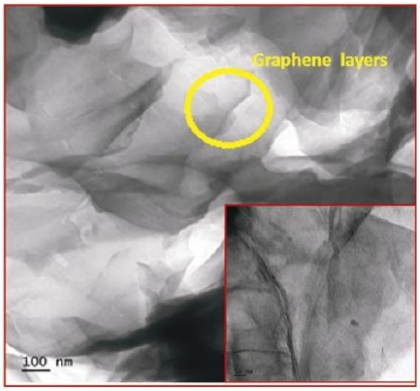

Figure 6. TEM images of SRrGO2 nanocomposite (inset shows magnified image of this region).

Table 4. Cure characteristics of SRrGO nanocomposites.

Sample	M_L Minimum torque (dNm)	M_H Maximum torque (dNm)	Scorch Time (ts_2) (min)	Cure time t_{90} (min)	CRI (min^{-1})
SR	0.65	12.90	0.86	5.76	20.40
SRrGO0.5	0.74	5.23	1.3	4.26	37.04
SRrGO1	0.76	4.33	1.18	2.78	62.50
SRrGO1.5	0.72	5.47	1.3	2.84	66.66
SRrGO2	0.66	6.88	1.43	2.58	86.95
SRrGO2.5	0.64	8.58	1.07	4.12	32.78

MOST WIEDZY Downloaded from mostwiedzy.pl

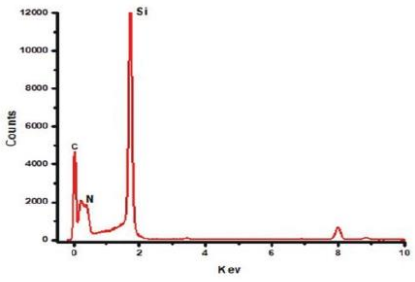

Figure 7. EDS spectrum of SRrGO2 nanocomposite.

Table 5. EDS data of SRrGO2 nanocomposite.

Element	Weight%	Atomic%
Si	85.94	74.60
C	10.86	18.90
N	3.20	6.50

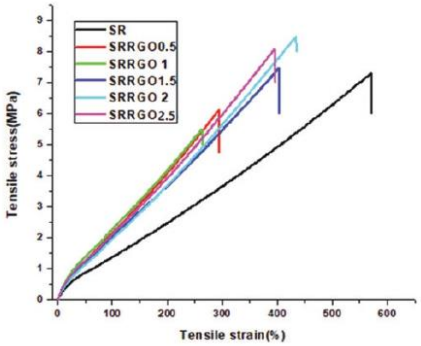

Figure 8. Stress- strain curves of SR containing varying amounts of rGO.

contained silicon (Si), carbon (C) and Nitrogen (N). In the EDS result, Si element had the highest content, and the content of C element was higher than N. It is also interest to note that ~3 weight percentage of nitrogen observed along with carbon and silicon. The presence of nitrogen is also oserved in XPS analysis.

Mechanical properties of SRrGO nanocomposites

The stress – strain curves of silicone rubber/rGO nanocomposites are shown in Figure 8. The incorporation of rGO causes rise in modulus of the nanocomposites. This indicates that rigidity of the nanocomposite grow with inclusion of rGO. Introduction of rGO also causes sharp decline in elongation at break and the possibility of retention was very weak. Tensile strength of nanocomposites decreases up to 1phr and then it starts to increase (Table 6). Maximum tensile strength obtained with 2 phr loading and above which it decreases. The improvement in mechanical properties confirms the reinforcing nature of rGO. This is mainly due to the π-π interaction between rGO and SR. The tear strength of vulcanizate also shows similar trend as that of tensile strength values. However, this improvement in mechanical properties also good enough for some application requiring mechanical integrity. There is weak van der Waals force of interaction between graphene layers and SR matrix. Besides this, there is weak pi-pi interaction between graphitic carbon and the vinyl group. This sort of interaction might be the reason for improved mechanical properties of the composites with higher rGO loading. The pictorial representation of the interaction between reduced graphene oxide and silicone rubber is shown in Figure 9.

Addition of rGO in SR matrix results in increased hardness value and decreased compression set value. This is because the addition of rGO causes an improvement of modulus of nanocomposites. The improvement in properties of the nanocomposites with low loading is due to high surface area of rGO, which makes large contacts points in the SR matrix and it leads to extensive interaction.[25]

Table 6. Mechanical properties of SRrGO nanocomposites.

Materials	Tensile strength (MPa)	Elongation at break (%)	Tear strength (N/mm)	Hardness (Shore A)	Compression set (%)
SR	7.31 ± 0.349	540 ± 3	20.45 ± 1.13	51	21
SRrGO0.5	5.94 ± 0.424	290 ± 2	18.75 ± 0.74	61	18
SR rGO 1	5.45 ± 0.190	250 ± 2	20.21 ± 1.40	66	16
SR rGO 1.5	7.17 ± 0.050	398 ± 3	24.43 ± 1.12	67	15
SR rGO 2	8.24 ± 0.173	425 ± 3	25.50 ± 0.95	68	12
SR rGO 2.5	7.65 ± 0.253	392 ± 4	24.12 ± 0.67	70	10

MOST WIEDZY Downloaded from mostwiedzy.pl

Figure 10 shows the tensile fracture surface of SRrGO nanocomposites. The scanning electron microscopic (SEM) image of neat SR shows a smooth rubbery failure. The reason for smoothness of the fractured surface is due to the uniform failure of the SR matrix. This is the clear indication of absence of mechanically weaker region in the matrix for crack initiation. The SEM morphology shows that rGO particles are homogeneously distributed throughout the matrix having good compatibility. Higher rGO loading results in agglomeration, in such cases the stress transfer is prevented by the agglomeration of filler particle in the polymer matrix and hence mechanical properties decreased.

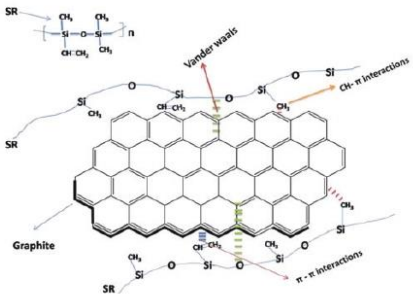

Figure 9. Schematic diagram of interaction between SR and reduced graphene oxide.

Thermo gravimetric analysis (TGA)

Thermal stability of SRrGO nanocomposites studied using thermo gravimetric analysis and the thermograms are shown in Figure 11. Thermal analysis of nanocomposites indicates that the nanocomposites were found to be stable up to ~400°C. Further increase in temperature results in decomposition of nanocomposites. Thermograms of SR shows that decomposition started at a temperature around 420°C due to the decomposition of the polymer network. Addition of rGO results in an improvement of thermal stability of the nanocomposites. The data obtained from the TGA curve is given in Table 7.

The nanocomposites with 2phr filler loading exhibit higher thermal stability. The heat insulation efficiency of rGO attributed to improve the thermal stability of the nanocomposites. Maximum weight loss (T_{max}) or degradation of maximum observed at temperature around 540°C. Figure 11 illustrate that, there is no significant weight change below 420°C and this indicates that nanocomposites are thermally stable upto 420°C. The thermal degradation of SRrGO nanocomposite improved due to the incorporation of rGO. Moreover, the SRrGO composite lost weight slowly during the TGA than neat SR, indicating that the composites with better dispersed rGO layers are more thermally stable. The higher bonding energy of the C = C

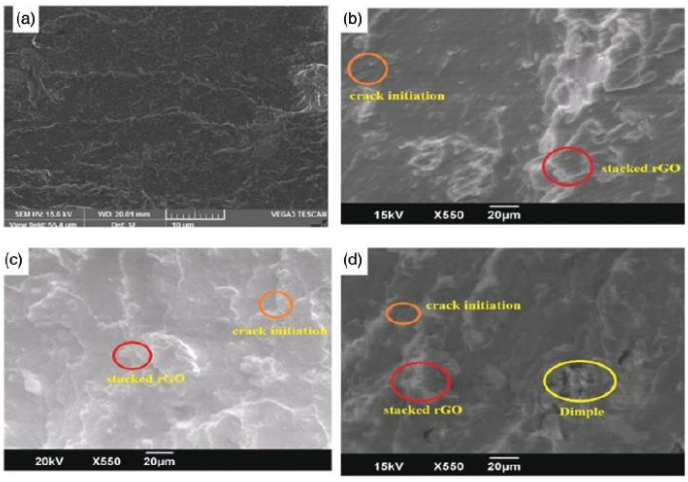

Figure 10. Tensile fracture surface of cured SRrGO nanocomposites (a) silicone rubber (b) 1.5phrSRrGO (c) 2phrrGO- silicone nanocomposites (d) 2.5phrrGO- silicone nanocomposite.

MOST WIEDZY Downloaded from mostwiedzy.pl

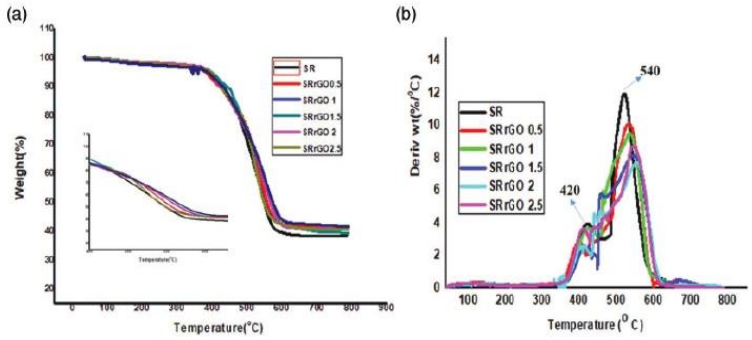

Figure 11. Thermal analysis of SRrGO nanocomposites.

Table 7. Data obtained from TGA curves of SRrGO nanocomposites.

Sample	T_{10}°c	T_{30}°c	T_{50}°c	T_{max}°c	Residue at Tmax (%)
SR	423	505	546	542	38
SR rGO 0.5	422	515	557	546	41
SR rGO 1	423	510	554	552	40
SR rGO 1.5	443	516	568	548	40
SR rGO 2	428	514	549	550	41
SR rGO 2.5	425	511	548	548	41

bond (607 kJ/mol) also would have contributed to the enhanced thermal stability.[26]

Dynamic mechanical analysis (DMA)

DMA measures the response of nanocomposite to an oscillatory deformation as a function of temperature. In this study, we analysed storage modulus (E′), loss modulus (E″), and mechanical loss factor (tanδ) of SRrGO nanocomposites as a function of temperature range from –130°C to 20°C as shown in Figure 12. It is useful to find out the molecular mobility transitions (Tg) in the system. This influence the overall properties of the nanocomposite. Figure 12(a) shows the plot of storage modulus of SR with different rGO loading as a function of temperature. For neat SR, the modulus increases between –130 and –120°C, and then reaches the modulus value of the semicrystalline sample. This rise in moduli can be attributed to the glass crystallization that may occur when the sample has reached enough molecular mobility.[27] It has been observed that storage modulus decreased with addition of rGO. This is due to the decrease in segmental mobility with addition of rGO and temperature. SRrGO nanocomposite samples that have been crystallized either from the melt (upon cooling) or from the glass (upon heating) present identical modulus values nearly at –50°C. Figure 12(b) shows that as the temperature increases, loss modulus decreases. This is because molecules might not get enough time to relax. Polymer exhibit glassy stage in low temperature region. The rise in temperature results in the drop down of elastic tensile modulus and the magnitude correspond to the glass – rubber transition.

In the case of SRrGO nanocomposite, it is important to study the effect of rGO on the flexibility of SR chains. In the case of SRrGO nanocomposites, these moduli decrease with increase in temperature. A typical sigmoidal decrease of E' is observed near –120°C for all samples. This reduction can be attributed to the α-relaxation that manifests cooperative segmental relaxation near the glass transition region. This modulus decrease is more pronounced for the neat silicone rubber because of the absence of crystalline phases in this case. These observations can be corroborated by the tan δ curves in Figure 12(c). Nanocomposites exhibits two relaxations located in the vicinity of –120 °C and –50°C. The peak around –120°C corresponds to the glass transition temperature of SR. Melting at –50°C causes the storage modulus, G', to decrease . Afterward the material exhibits rubbery elastic behavior.[11]

It is interesting to note that the temperature correspond to the maximum tan δ decreases when rGO concentration increases. This is attributed to the reduction in number of polymer chains during Tg. The tanδ curve of

MOST WIEDZY Downloaded from mostwiedzy.pl

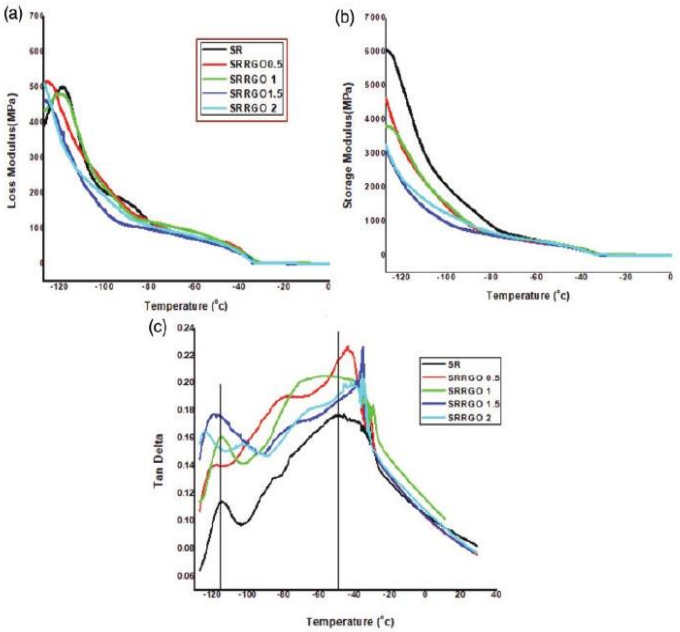

Figure 12. Variation in (a) storage modulus (b) loss modulus and (c) loss tangent (tanδ) as a function of temperature for SRrGO nanocomposites.

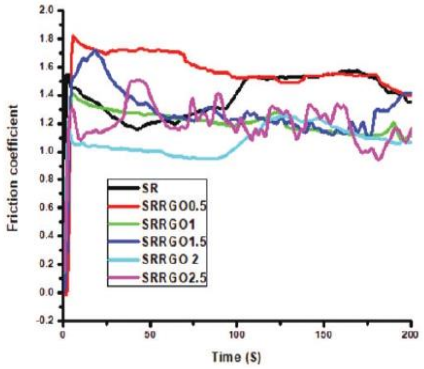

Figure 13. Friction coefficient vs time graph of SRrGO nanocomposites with different amounts of rGO.

nanocomposites is almost similar to that of neat SR except there is a slight reduction in peak height. Higher loading results in lower peak height which is attributed to the restriction of damping characteristics in SRrGO nanocomposites.

Tribological properties

The change in friction coefficient of SRrGO nanocomposites at an applied load of 5 N and speed of 2 m/s as a function of time is displayed in Figure 13. Neat SR exhibited high variation in tribological behaviour as compared to those of SRrGO1 and SRrGO2. Addition of rGO significantly reduces the friction coefficient. Lowest friction coefficient observed with SRrGO2.The mechanism involved in the tribological process is shown schematically in Figure 14. Case -1 shows the tribological studies of neat SR. In this case material comes in direct contact with perturbances at counter surface and thereby high wear rate occurred. But in the presence of rGO filler material (case -2) SRrGO nanocomposite exhibits a reduction in friction coefficient. It is attributed to the formation of lubricant film on the steel counter surface. This lubricant film protect the material which comes in contact with perturbances present on the metal surface.This prevent large material removal from the nanocomposite surface.

Effect of load. The variation of coefficient of friction and specific wear rate of the nanocomposite with rGO loading is shown in Figure 15. In sliding wear, load has an important role in friction and wear properties of the nanocomposites. Figure 15(a) shows a decline in coefficient of friction with respect to applied load. Composite sample slide against higher applied load result in larger deformation. Higher the frictional

MOST WIEDZY Downloaded from mostwiedzy.pl

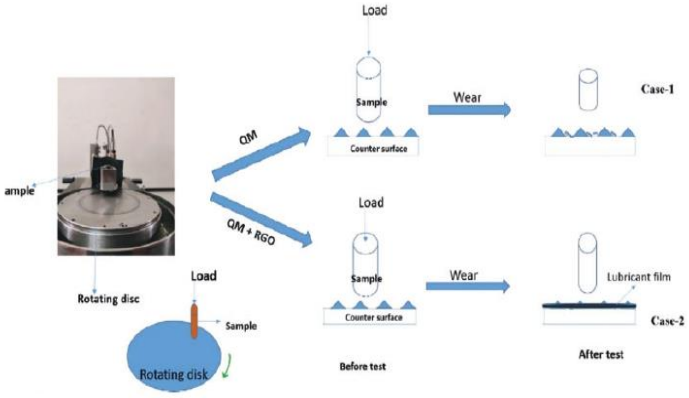

Figure 14. Schematic illustration of wear mechanism involved in two tribological conditions.

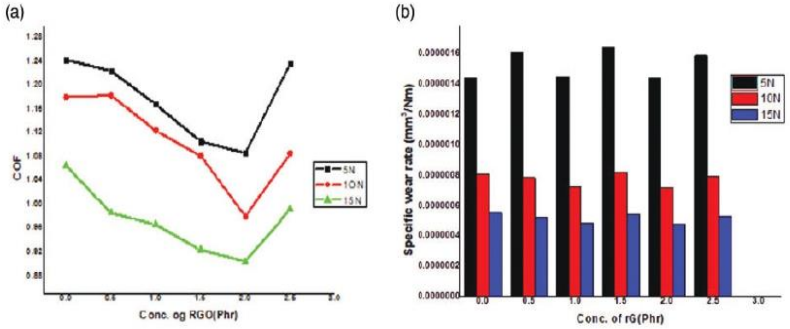

Figure 15. (a) Friction coefficient and (b) specific wear rate of SRRGO nanocomposites with a sliding speed of 2 m/s.

heat produced from the large deformation result in softening of the polymer. It also facilitate the material removal from the composite surface to the metal surface which comes into contact. The wear resistance properties of the nanocomposite can be remarkably improved by the addition of applied load.

Composite materials with rGO loading upto 2phr decreases the friction coefficient and specific wear rate, further addition of rGO has no added effect. The reason is that aggregation occurs and composite become rougher. This impart more asperities comes into composite surface. A steady decrease in the friction coefficient and specific wear rate value observed with applied load and better wear resistance was observed with 15 N. The tribological properties of the composite depends on the surface characteristics of reduced graphene oxide and interactions within the polymer matrix. Worn surface morphologies of the composites are shown in Figure 16.

Worn surface morphologies of SR indicates the localised removal of materials from the matrix. Addition of rGO results in formation of smooth surface and absence of wear depth. Surface roughness of both nanocomposites and the counter face is also considered to be a basic reason for degradation of wear resistance of graphene. There is also a possibility of atomic roughness of the nanocomposite surface that could assist the rupture of graphene and it induce adhesion on the counter face.[28] In adhesive wear mechanism, chemical bonds are formed at the two interacting surfaces that lead to tearing of graphene.[29]

Effect of sliding speed. Sliding speed also play a major role in friction and wear properties of SRrGO nanocomposites. Figure 17 shows the variation of coefficient of friction and specific wear rate against loading and sliding speed at a load of 10 N, respectively. The results show the average coefficient of friction and specific wear rate value. Figure 17(a) illustrate that at a constant load, friction coefficient decreases with increased rGO concentration upto 2 phr loading and further it starts to increase. Figure shows a clear indication that, both rGO concentration and sliding speed has

MOST WIEDZY Downloaded from mostwiedzy.pl

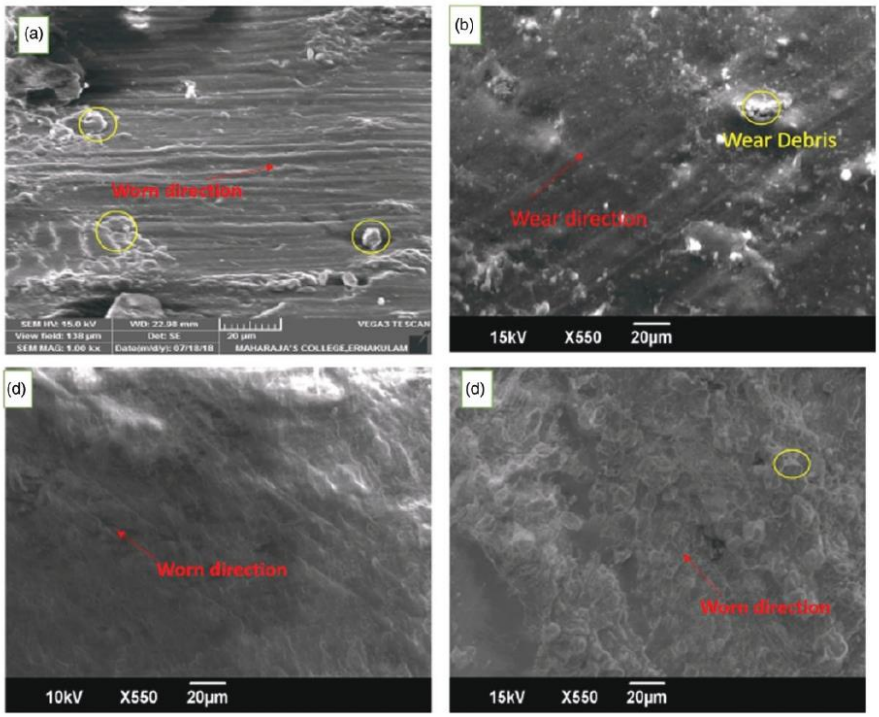

Figure 16. SEM micrographs showing worn surface morphologies (a) Silicone rubber, (b) 1.5 phr SRRGO (c) 2phrRGO- silicone nanocomposite,(d) 2.5phrRGO- silicone nanocomposite.

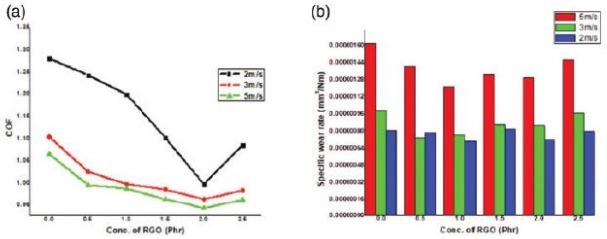

Figure 17. Friction coefficient (a) and specific wear rate (b) of the SRRGO nanocomposites with various contents of RGO as a function of sliding velocity (10 N, RT, 1800 m).

significant impact on the friction and wear characteristics of the SRrGO nanocomposites. Addition of rGO decreases the friction and wear properties but sliding speed increases the specific wear rate value for 3 m/s and further it decreased for 5 m/s. At a constant load, concentration above 2 phr rGO loading, the coefficient of friction and specific wear rate start to increase.

The worn surface morphology of nanocomposite clearly indicates that the rGO covered surface greatly improve the wear resistance properties. There is 20% decrease in the coefficient of friction of composite with 1phr filler loading. It is attributed that rGO exposed to the sliding interface act as a solid lubricant. The variation of depth wear rate with PV-factor of the

MOST WIEDZY Downloaded from mostwiedzy.pl

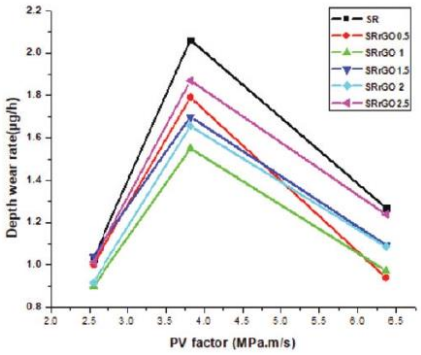

Figure 18. Depth wear rate of SRrGO nanocomposites.

nanocomposites are shown in Figure 18. Initially, the depth wear rate was found to be a low value and then it increased with rise in PV- factor. Following the sliding corresponding to 300 mm, the wear depth increased slowly. This is because the wear of the SR elastomer occurred first by the transfer of the elastomer to the harder mating surface and followed by removal of wear particles which led to a quick increase in the wear depth. The wear rate was generally small and stable when a steady-state condition was reached.

Effect of temperature. The effect of temperature on the friction and wear properties of SRrGO nanocomposites with different rGO loading is shown in Figure 19. As the temperature increases from 30–150°C the friction coefficient of the nanocomposites decreases.

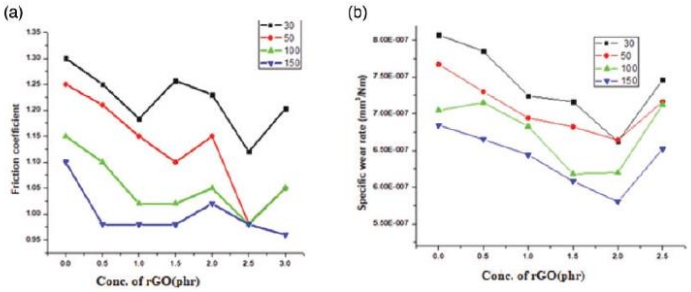

Figure 19. (a) Friction coefficients and (b) specific wear rate of SRrGO nanocomposites at different temperatures.

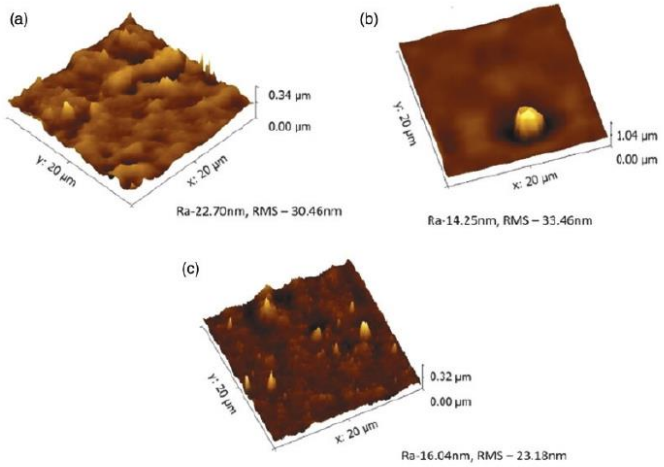

Figure 20. 3 D AFM topographies of SRrGO nanocomposites with varying concentrations of rGO(a) silicone rubber, (b)SRRGO1 (c) SRRGO2 silicone rubber nanocomposites.

MOST WIEDZY Downloaded from mostwiedzy.pl

This is due to the fact that frictional heat produced at the contact region and high heat surface leads to softening of the polymer and reduces the friction coefficient. As the temperature increases the specific wear rate also decreases and reaches maximum at 2 phr of rGO content and then decreases

AFM analysis

AFM analysis was used to find out the surface roughnes of SRrGOnanocomposites. In Figure 20 heaps or hills are almost homogeneous in the case of nanocomposites and this indicate the uniform distribution of rGO in the SR matrix. It also gives an insight into the local stiffness. Polymeric nanocomposite with homogenious surfaces can affect their properties of tribological, adhesion and degradation. Therefore surface topographical analysis of nanocomposite have importance in science and technonology. Root mean square roughness (Sq) and average surface roughness (Sa) of SRrGO2 are 16 nm and 23 nm respectively and that of SR are 22 nm and 30 nm respectively as shown in Table 8.

Sa and Sq values obtained for SRrGO1 nanocomposite were 14.25 nm and 33.46 nm.The decrease in surface rughness is a clear indication of improvement of wear resistance of the material. The difference in Sq-Sa values is found to be greater than zero and this is also a clear indication of dispersion of rGO in SR matrix.

Table 8. Surface roughness parameters of the SR nanocomposites obtained from AFM analysis.

Sample	Sq (nm)	Sa (nm)	Sq-Sa (nm)
SR	30.46	22.70	8.67
SRRGO 1	33.46	14.25	9.21
SRRGO 2	23.18	16.04	7.14

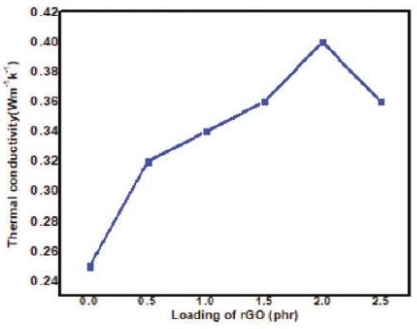

Figure 21. Thermal conductivity of SRrGO nanocomposites.

Thermal conductivity studies

The effect of filler loading on the thermal conductivity of SRrGO nanocomposites is shown in Figure 21. Thermal conductivity of the nanocomposites improved with addition of rGO and it forms a continuous conducting network within the matrix. The maximum thermal conductivity was 0.40 W/mk for 2 phr loading which is twice greater than the neat SR. Conductivity decreases with higher filler loading due to the agglomeration of the rGO in the SR matrix.

Conclusions

In this study, graphene oxide was synthesized using modified Hummers method, and it chemically reduced with hydrazine reagent. FT-IR, XRD, Raman and XPS measurements have been used to confirm the reduction of GO. Mechanical and tribological properties of the nanocomposites were enhanced by the addition of reduced graphene oxide. TEM images indicate the better dispersion of rGO in SR matrix. The friction and wear characteristics of the silicone rubber nanocomposites are measured using a pin-on-disc tester. The best wear resistant composite obtained with 2phr of rGO loading. Presence of rGO between the friction surfaces reduced contact between the material and hard metal surface by acting as lubricant film. The morphology analysis indicated that the addition of rGO decreased wear and resulted in a relatively smooth surface with fewer scars, thus indicating the presence of rGO that significantly reduced metal contact. Tribological properties of the composites with different sliding speed, load and temperature were investigated to optimize the composition of composite with wide range of conditions. Incorporation of rGO improved the mechanical properties as well as thermal conductivity of SRrGO nanocomposites as a result of improved interaction between rGO and SR matrix. Overall, the wear resistance of the composite improved by the addition of rGO as it evident from the depth wear rate analysis.

Declaration of Conflicting Interests

The author(s) declared no potential conflicts of interest with respect to the research, authorship, and/or publication of this article.

Funding

The author(s) disclosed receipt of the following financial support for the research, authorship, and/or publication of this article: The authors are especially grateful to DRDO (Order No:ERIP/ER/1504758/M/01/1667), New Delhi, India for providing financial assistance.

MOST WIEDZY Downloaded from mostwiedzy.pl

ORCID iD

Soney C George https://orcid.org/0000-0001-9590-3971

References

1. Myshkin NK, Petrokovets MI and Kovalev AV. Tribology of polymers: adhesion, friction, wear, and mass-transfer. *Tribol Int* 2005; 38: 910–921.
2. Hazel J, Lemieux M, Nguen T, et al. *Tribology issues and opportunities in MEMS* (Bhushan B (ed.) Dordrecht: Kluwer, 1998, pp.607–614.
3. Bhushan B. *Principles and applications of tribology*. 2nd ed. New York: IEEE Press, 1996, p.1125.
4. Bhattacharyya S, Sinturel C, Bahloul O, et al. Improving reinforcement of natural rubber by networking of activated carbon nanotubes. *Carbon* 2008; 46: 1037–1045.
5. Goldman AY. *Prediction of deformation properties of polymeric and composite materials*. Washington, DC: American Chemical Society, 1994.
6. Nilsson L, Andersen M, Balog R, et al. Graphene coatings: probing the limits of the one atom thick protection layer. *Acs Nano* 2012; 6: 10258–10266.
7. Nayak PK, Hsu CJ, Wang SC, et al. Graphene coated Ni films: a protective coating. *Thin Solid Films* 2013; 529: 312–316.
8. Pu JB, Mo YF, Wan SH, et al. Fabrication of novel graphene-fullerene hybrid lubricating films based on self-assembly for MEMS applications. *Chemical Communications* 2014; 50: 469–471.
9. Penkov O, Kim HJ, Kim HJ, et al. Tribology of graphene: a review. *International journal of precision engineering and manufacturing* 2014; 15: 577–585.
10. Zhu Y, Murali S, Stoller MD, et al. Microwave assisted exfoliation and reduction of graphite oxide for ultracapacitors. *Carbon* 2010; 48: 2118–2122.
11. Liu J, Tang J and Gooding JJ. Strategies for chemical modification of graphene and applications of chemically modified graphene. *J Mater Chem* 2012; 22: 12435–12452.
12. Valentini L, Bon SB and Pugno NM. Severe graphene nanoplatelets aggregation as building block for the preparation of negative temperature coefficient and healable silicone rubber composites. *Compos Sci Technol* 2016; 134: 125–131.
13. Malas A, Pal P, Giri S, et al. Synthesis and characterizations of modified expanded graphite/emulsion styrene butadiene rubber nanocomposites: mechanical, dynamic mechanical and morphological properties. *Compos Part B – Eng* 2014; 58: 267–274.
14. Sadhu S and Bhowmick AK. Preparation and properties of nanocomposites based on acrylonitrile-butadiene rubber, styrene-butadiene rubber, and polybutadiene rubber. *J Polym Sci B Polym Phys* 2004; 42: 1573–1585.
15. Mao Y, Wen S, Chen Y, et al. High performance graphene oxide based rubber composites. *Sci Rep* 2013; 3: 2508.
16. Das A, Jurk R, Werner Stöckelhuber K, et al. Nanoalloy based on clays: intercalated-exfoliated layered silicate in high performance elastomer. *J Macromol Sci Chem* 2008; 45: 144–150.
17. Sadasivuni KK, Ponnamma D, Thomas S, et al. Evolution from graphite to graphene elastomer composites. *Prog Polym Sci* 2014; 39: 749–780.
18. Yaragalla S, Chandran CS, Kalarikkal N, et al. Effect of reinforcement on the barrier and dielectric properties of epoxidized natural rubber-graphene nanocomposites. *Polym Eng Sci* 2015; 55: 2439–2447.
19. Park S, An J, Piner RD, et al. Aqueous suspension and characterization of chemically modified graphene sheets. *Chem Mater* 2008; 20: 6592–6594.
20. Park S, An J, Potts JR, et al. Hydrazine-reduction of graphite-and graphene oxide. *Carbon* 2011; 49: 3019–3023.
21. Bosq N, Guigo N, Persello J, et al. Melt and glass crystallization of PDMS and PDMS silica nanocomposites. *Phys Chem Chemical Physics* 2014; 16: 7830–7840.
22. Park S, Hu Y, Hwang JO, et al. Chemical structures of hydrazine-treated graphene oxide and generation of aromatic nitrogen doping. *Nat Commun* 2012; 3: 638.
23. Moni G, Mayeen A, Mohan A, et al. Ionic liquid functionalised reduced graphene oxide fluoroelastomer nanocomposites with enhanced mechanical, dielectric and viscoelastic properties. *Eur Polym J* 2018; 109: 277–287.
24. Zhang J, Xu Y, Liu Z, et al. A highly conductive porous graphene electrode prepared via in situ reduction of graphene oxide using Cu nanoparticles for the fabrication of high performance supercapacitors. *RSC Adv* 2015; 5: 54275–54282.
25. Agrawal N, Parihar AS, Singh JP, et al. Efficient nanocomposite formation of acyrlo nitrile rubber by incorporation of graphite and graphene layers: reduction in friction and wear rate. *Proc Mater Sci* 2015; 10: 139–148.
26. Kim ES, Kim EJ, Shim JH, et al. Thermal stability and ablation properties of silicone rubber composites. *J Appl Polym Sci* 2008; 110: 1263–1270.
27. Hu H, Zhao L, Liu J, et al. Enhanced dispersion of carbon nanotube in silicone rubber assisted by graphene. *Polymer* 2012; 53: 3378–3385.
28. Xu Q, Li X, Zhang J, et al. Suppressing nanoscale wear by graphene/graphene interfacial contact architecture: a molecular dynamics study. *ACS Appl Mater Interfaces* 2017; 9: 40959–40968.
29. Wang LF and Duan FL. Nanoscale wear mechanisms of few-layer graphene sheets induced by interfacial *adhesion*. *Tribol Int* 2018; 123: 266–272.

MOST WIEDZY Downloaded from mostwiedzy.pl

Publication -4:

Study the characteristics of novel ionic liquid functionalized graphene oxide on the mechanical and thermal properties of silicone rubber nanocomposites

Article summary

In the present work, we investigated the effect of ionic liquid (1 ethyl 3-methylimidazolium dicyanamide) modified graphene oxide (ILGO) on the mechanical and thermal behavior of silicone rubber (QM) nanocomposites. Silicone rubber nanocomposites (QMILGO) were prepared by the conventional two roll mixing method. The interactions of ILGO and silicone rubber nanocomposites have been investigated using Fourier- transform infrared spectroscopy, Raman spectroscopy, Dynamical mechanical analysis, and thermal conductivity measurements. The surface treatment of graphene oxide with IL resulted in significant changes in nanocomposites' mechanical and thermal properties, attributed to increased filler–polymer interaction. Studies show that the inclusion of ILGO led to an 18% improvement in mechanical properties and a 10% enhancement in thermal stability of QMILGO nanocomposites. Thermal conductivity studies and composites' dynamical mechanical analyses (DMA) indicate that QMILGO 1.5 nanocomposite obtained maximum thermal conductivity (28% improvement) and dynamic mechanical behavior compared to neat QM.

Methodology

- Cure characteristics
- Mechanical properties
- Tribology
- Dielectric studies
- Thermal studies

MOST WIEDZY Downloaded from mostwiedzy.pl

Journal of Polymer Research (2021) 28:446
https://doi.org/10.1007/s10965-021-02806-5

ORIGINAL PAPER

Study the characteristics of novel ionic liquid functionalized graphene oxide on the mechanical and thermal properties of silicone rubber nanocomposites

P. S Sarath[1,3] · David Pahovnik[2] · Petra Utroša[2] · Ozgun CanOnder[2] · Józef T. Haponiuk[3] · Sabu Thomas[4] · Soney C. George[1]

Received: 28 May 2021 / Accepted: 20 October 2021
© The Polymer Society, Taipei 2021

Abstract
In the present work, we investigated the effect of ionic liquid (1 ethyl 3-methylimidazolium dicyanamide) modified graphene oxide (ILGO) on the mechanical and thermal behaviour of silicone rubber (QM) nanocomposites. Silicone rubber nanocomposites (QMILGO) were prepared by the conventional two roll mixing method. The interactions of ILGO and silicone rubber nanocomposites have been investigated using Fourier- transform infrared spectroscopy, Raman spectroscopy, Dynamical mechanical analysis and thermal conductivity measurements. The surface treatment of graphene oxide with IL resulted in significant changes in the mechanical and thermal properties of nanocomposites, which can be attributed to increased filler–polymer interaction. Study show that the inclusion of ILGO led to an 18% improvement in mechanical properties and a 10% enhancement in thermal stability of QMILGO nanocomposites. Thermal conductivity studies and dynamical mechanical analyses (DMA) of composites indicate that QMILGO 1.5 nanocomposite obtained maximum thermal conductivity (28% improvement), and dynamic mechanical behaviour as compared to neat QM.

Keywords Silicone rubber · Ionic liquid · Thermal conductivity · Mechanical properties

Introduction

Silicone rubber is an inorganic polymer that has been widely used in different areas such as seal, adhesives, aviation, automobile, and aviation industries, etc. [1, 2]. But their poor mechanical and conductive (thermal and electrical) properties limit their industrial application; To overcome these shortcomings various fillers are used. Among them carbonaceous fillers are adopted to reinforce silicone rubber (QM) to achieve desirable rubber-like properties. The mechanical, and thermal properties of silicone rubber are all influenced by micro and nano fillers [3], Where the dominating reinforcing filler in silicone rubber was silica [4]. Graphene has potential application in rubber nanocomposites because of its size effects and unique

✉ Soney C. George
soneygeo@gmail.com; chemistrysoney2015@gmail.com

P. S Sarath
sarathps005@gmail.com

David Pahovnik
David.Pahovnik@ki.si

Petra Utroša
petra.utrosa@ki.si

Ozgun CanOnder
Ozgun.can.onder@ki.si

Józef T. Haponiuk
jozef.haponiuk@pg.edu.pl

Sabu Thomas
sabuthomas@mgu.ac.in

[1] Centre for Nanoscience and Technology, Department of Basic Sciences, Amal Jyothi College of Engineering, Kanjirappally, Kottayam, Kerala, India

[2] Department of Polymer Chemistry and Technology, National Institute of Chemistry, Hajdrihova 19, 1000 Ljubljana, Slovenia

[3] Department of Polymer Technology, Chemical Faculty, Gdansk University of Technology, G. Narutowicza Str. 11/12, 80-233 Gdansk, Poland

[4] International and Inter-University Centre for Nanoscience and Nanotechnology, Mahatma Gandhi University, Kottayam, Kerala, India

Published online: 29 October 2021

MOST WIEDZY Downloaded from mostwiedzy.pl

physicochemical properties [4]. GO is a monolayer material with a large surface area, high mechanical strength, conductivity, low-cost and good processibility that attracted researchers as a promising filler for polymer matrices [5]. Recently, GO has been widely used as a filler material in a large number of polymers, such as polymethylmethacrylate [6], polyvinyl alcohol [7], epoxy [8], polypropylene [9], and polyaniline [10] to enhance their mechanical properties, thermal, thermo electrical, and rheological properties. The major challenges in rubber composites are uniform filler dispersion in the rubber matrix and improved interfacial interaction between the filler and the rubber matrix. Liu et al. synthesized alkyl amine-modified GO/SBR composites, suggesting that the dispersion GO was substantially improved and demonstrated greater efficiency reinforcement for SBR [11]. In our previous work, we prepared exfoliated graphite (EG) /silicone rubber composite and investigated the mechanical, tribological, and dielectric properties. It has been found that the addition of EG resulted in an improvement in mechanical and tribological properties [2]. Ionic liquids (ILs) are salts in the liquid state with a low-melting point (< 100 °C). Owing to their tunable physicochemical properties, no flammability, high thermal stabilities, ILs have gained considerable attention as "green" alternatives to traditional organic solvents [12]. Recently, IL were used to modify the surface of GO to obtain better dispersion of GO in polymer matrices, which could thus further increase mechanical characteristics [13] electrical conductivity [14] and thermal stability [15]. Carbon nanomaterial–ionic liquid hybrids represent a very interesting class of materials because of their exceptional properties and potential use in a wide range of application fields. Owing to the specific interactions between ionic liquids (ILs) and carbon nanomaterials, the surface properties of the nanomaterials can be modified, leading to their improved dispersion, thus providing an alternative solution to the processing of these materials. Literature showed that graphene oxide (GO) contains a large number of oxygenated groups and it is synthesized from graphite using various methods. The work in this domain generally concerns itself with surface modification of GO which is needed to improve the compatibility with the polymer matrix. Several studies have explored the effects of functionalization on the GO surface. Room-temperature-vulcanized (RTV) silicone rubber reinforced with carbon nanotubes (CNTs), nanographite (GR), and CNT-GR hybrids was used for the development of new generation flexible devices, such as touch screens, flexible electronics, stretchable sensors, and actuatorsetc [16]. Graphene oxide (GO) contains a large number of oxygenated groups and it is synthesized from graphite using various methods. The work in this arena generally concerns itself with surface modification of GO is needed to improve the compatibility with the polymer matrix. Several studies have explored the effects of functionalization on the GO surface. More recent work in this area [17, 18] extends the methods by using, Ionic liquid (IL) to modify GO surface to obtain better dispersion in the matrix. IL having a wide range of interests associated with

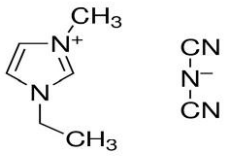

1-ethyl-3-methylimidazolium dicyanamide (IL)

their excellent chemical and thermal stability, good tribological and adsorption properties, ionic conductivity, etc.

The objective of this work was to study the effect of ionic liquid modified graphene oxide (ILGO) as a reinforcing filler in QM vulcanizates by preparing QM mixed with uniformly dispersed ILGO and characterizing its mechanical and thermal properties. The mechanical properties, dynamic mechanical properties, thermal conductivity, and thermal stability of QMILGO vulcanizate were then characterized and analysed.

Materials and methods

Materials

Graphite which is used for the synthesis of GO and IL which is used for the modification of GO, 1-ethyl-3-methylimidazolium dicyanamide is procured from Sigma Aldrich, Banglore, India.

Silicone rubber SH5060-U (HTV) was procured from KCC Corporation, Korea. It is a general-purpose grade with low level of vinyl content.

Modification of graphene oxide using ionic liquid (ILGO)

The modified Hummers method was used to synthesize graphene oxide [19, 20]. Graphene oxide surface was functionalized with 1-ethyl-3-methylimidazolium dicyanamide ILs. To prevent electrostatic contact between water and ionic liquid molecular, 1 g of KOH was dissolved. The solution was refluxed at 90 °C for 2 h to complete interaction between IL and an oxygen containing group of GO. Solution was washed with ethanol and deionized water (DIW) until neutral pH attained and dried in vacuum oven. It was dried at 80 °C for 24 h in a vacuum oven [21, 22]. The remaining functionalized ILGO with 1.0, 1.5, 2.0, and 2.5 g of IL was prepared using the same technique.

MOST WIEDZY Downloaded from mostwiedzy.pl

Preparation of QMILGO compound

Silicone rubber (100 g) was masticated for five minutes in an open two-roll mixing mill. Then modified graphene oxide (ILGO) was applied in various amounts (0.5, 1, 1.5, 2, and 2.5 g), with Dicumyl peroxide (1.5 g) serving as a curing agent according to our previous work [2].

Characterisation techniques

Fourier transform infrared (FT-IR) spectroscopy, X-ray diffraction (XRD) analysis, and Raman spectroscopic analysis were used to analyse the synthesised GO and ILGO. FTIR analysis was characterized using Perkin Elmer at a spectrum range of 4000- 500 cm^{-1}. The mechanical properties of the QMILGO nanocomposites were investigated using an INSTRON-4411 pneumatic universal testing system with a moving crosshead speed of about 500 mm/min.The samples' tear strength was determined using the ASTM D-1424 standard. Scanning electron microscopy (SEM) on an HR-SEM Zeiss Ultra plus instrument was used to examine the morphology of the samples (Carl Zeiss, Germany). The samples were coated with a 10 nm gold coating for charge dissipation during SEM analysis using a Gatan PECS 682. (Gatan, USA). On a DMA Q800, the dynamic mechanical analysis was carried out (TA Instruments, USA). Samples were cut into a rectangular shape (approximate length 13.0 mm, width 2.5 mm, and thickness 2.0 mm). The viscoelastic properties were measured at a frequency of 1 Hz, strain amplitude of 5 µm in a temperature range from −140 °C to 30 °C with the heating rate of 2 °C min^{-1}. The glass transition temperature (Tg) was observed as the peak of tan δ curve, and melting temperature (Tm) was observed as a drop-in storage modulus. The results are given as an average of three measurements, with a standard deviation. The thermal conductivities of the composites were studied using ASTM D5470 and Holmarc's Lee's Disc Apparatus (Model: HO-ED-M-03).

Results and discussions

The FTIR spectrum of GO, IL, and ILGO are displayed in Fig. 1. FTIR spectrum confirms a clear interaction between the IL and GO. GO exhibits a broad and wide absorption peak at 3600 cm^{-1} confirmed the presence of – OH (hydroxyl) stretching vibrations. The intensity of the peak decreases with IL concentration. The broadened OH stretching peak disappeared in ILGO2. FT- IR spectrum of GO shows characteristic carbonyl peaks at 1730 $cm^{-1}$and C = C stretching frequencies at 1539 cm^{-1}.Three distinct peaks at 2249, 2241 and 2139 cm^{-1} were observed, the first two peaks correspond to the anionic part of the IL with C≡N bond and the third one represents the stretching vibration of the C = N- bond present in the cationic part.

The characteristic Raman scattering peaks (Fig. 1b) of GO and IL-GO, including graphitic (G) and disorder (D) bands, are being directly detected at 1353 and 1586 cm1, but their strength ratio (I_D/I_G) is different. The I_D/I_G value of IL-GO rises from 0.88 to 1.02 as compared to GO, which could be due to the covalent bonding of IL and GO nano sheets as well as the structural defects inserted into GO [21].

The Raman spectra of QM and QMILGO nanocomposites are shown in Fig. 2. The QMILGO curve exhibits two significant peaks in the 1260 cm^{-1} and 1410 cm^{-1} regions,

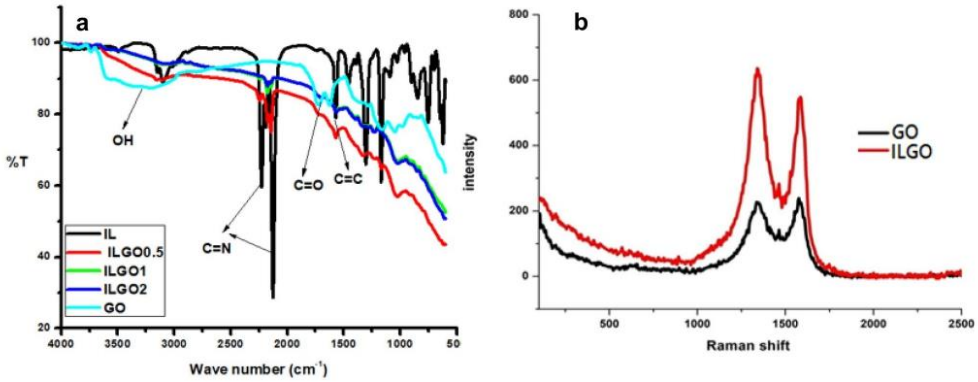

Fig. 1 (**a**) FT-IR spectra of GO, IL, and ILGO (**b**) Raman spectra of GO and ILGO

MOST WIEDZY Downloaded from mostwiedzy.pl

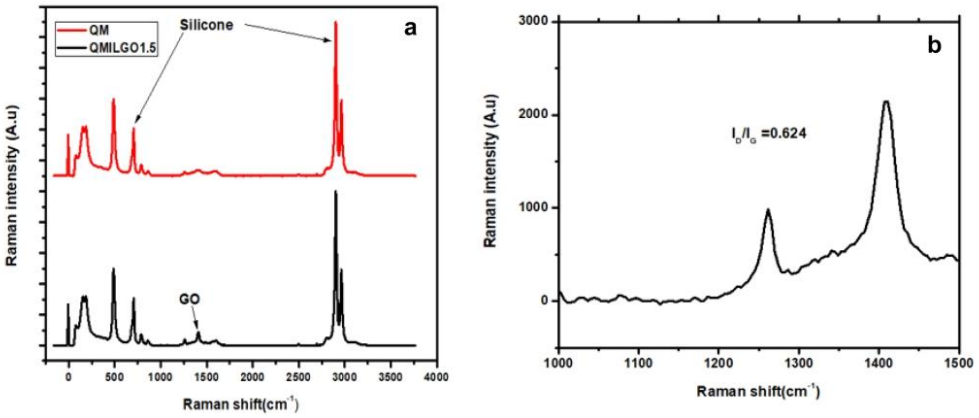

Fig. 2 Raman spectrum of QM and QMILGO nanocomposites (**a**) and (**b**) I_D/I_G ratio of QMILGO nanocomposite

which are assigned to the D and G bands of graphene, respectively. The G peak is stronger than the D peak, so the I_D/I_G ratio of QMILGO is 0.624 for some structure defects and the edge effects of narrow width of graphene sheets. The Raman spectra of QM has four sharp peaks at, 709, 490, 2918 and 2977 cm^{-1}, corresponding to stretching vibration of C–Si, symmetrical stretching vibration of Si-C_2, symmetrical stretching vibration of CH_3 and antisymmetrical stretching vibration of CH_3, respectively [23].

Cure analysis

The influence of ILGO on the rheometric properties of QM nanocomposites has been investigated. Table 1 summarises the curing characteristics of the studied materials as determined by the curing curves at T = 150 C and expressed in terms of scorch time, ts2, optimum cure time, t90, and cure rate index, CRI. The high specific surface area of GO results in high stiffness and torque values of the composite. Moreover, it is evident that incorporation of IL modified GO improves the vulcanization characteristics of QM especially scorch time.

Table 1 Cure Characteristics of the ILGO nanocomposites

Sample ID	ML (lbin)	M_H (lbin)	ts_2 (min)	t_{90} (min)	CRI (min^{-1})
QM	38.0	45.3	1.43	5.12	27.17
QMILGO0.5	37.5	58.7	2.07	4.67	38.46
QMILGO 1	34.1	37.5	2.39	4.3	52.36
QMILGO 1.5	32	35.2	2.07	4.11	49.09
QMILGO 2	37.9	60.3	2.08	4.03	51.89
QMILGO 2.5	36.8	40.7	2.14	4.89	36.66

(ts2) significantly increases with the incorporation of graphene aiding better process control. The addition of ILGO nanofillers increases the scorch time, which reflects the rubber's incipient vulcanization. According to Hernandez et al. [24] and Shanmugharaj et al. [25] adding carbon-based fillers can delay the onset of vulcanization because of the presence of functional groups such as carboxylic acid and oxygen on the surface of the nanofillers that absorb the basic accelerator additives In addition, as the filler loading has increased, the cure rate index, which reflects the vulcanization rate, has risen.

Mechanical properties of QMILGO nanocomposites

The stress–strain graph of QMILGO nanocomposites are shown in Fig. 3. The nanocomposite showed about 12% increment in tensile strength and tear strength respectively by the addition of 2.0 phr of modified filler and the values decreases considerably with further increase in filler content. The gum samples showed a tensile and tear strength of 7.10 and 19.78 MPa respectively and with ILGO loading the samples showed 10 -15% improvements in the properties (Table 2). Addition of neat graphene oxide (GO) resulted in decrease in mechanical properties and this might be due to the weak interaction between GO and QM. The large aspect ratio of ILGO might be the main reason of the improved modulus and tensile strength for QMILGO composites.

Figure 4 displays SEM pictures of the unfilled QM and the QMILGO nanocomposite's tensile cracked surfaces. The broken surface of the unfilled QM can be seen to be flat and smooth (Fig. 4a). In comparison to the unfilled QM, the surface of the QMILGO nanocomposite with 1.5 phr of ILGO (Fig. 4b, c) is quite rough. A study

MOST WIEDZY Downloaded from mostwiedzy.pl

Table 2 Mechanical properties of QMILGO nanocomposites with different ILGO concentration

Sample	Tensile strength (MPa)	Elongation at break (%)	Tear strength (N/mm)	Hardness (Shore A)	Compression set (%)
QM	6.86 ± 0.44	570 ± 30	20.45 ± 1.13	51	21
QMGO 1	6.10 ± 0.84	282 ± 20	17.93 ± 1.24	52	20
QMILGO0.5	6.49 ± 0.42	312 ± 22	19.45 ± 0.74	54	19
QMILGO 1	7.04 ± 0.29	382 ± 26	20.21 ± 1.40	56	17
QMILGO 1.5	7.48 ± 0.35	388 ± 18	22.43 ± 1.12	58	16
QMILGO 2	8.04 ± 0.27	415 ± 26	22.50 ± 0.95	58	14
QMILGO 2.5	7.84 ± 0.45	381 ± 24	20.12 ± 0.67	56	12

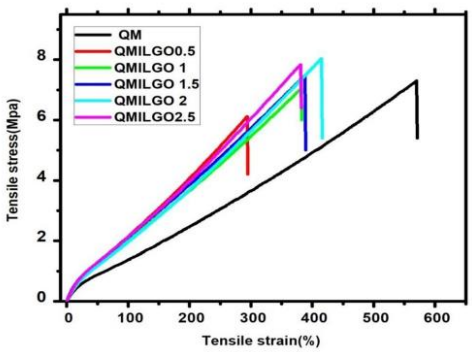

Fig. 3 Stress–Strain plot of QMILGO nanocomposites

has observed that the rough surface is due to the ILGO nanosheets being covered in a coating of rubber and not pulled out (Fig. 4d). These SEM images are similar to those found in the work of other researchers [26]. This demonstrates the nanofiller's deep interfacial interaction with the matrix yet again. The relatively homogenous dispersion of ILGO in the rubber matrix, as well as the strong interfacial interaction, are both beneficial to QMILGO nanocomposites' mechanical efficiency [27].

In the case of neat silicone rubber, the crack propagation is very easy because of the absence of reinforcing fillers in the matrix. But comes to the QMILGO case there is a filler-blocking effect was observed as the nanoparticle fractions increased as shown in Fig. 5.

To better understand the distribution of the nanoparticles within the rubber matrix, TEM analysis was performed (Fig. 6), which revealed a good dispersion of

Fig. 4 Scanning electron microscopic images of tensile fracture surface of (**a**) QM, (**b**) QMILGO1, (**c**) QMILGO1.5, (**d**) QMILGO2

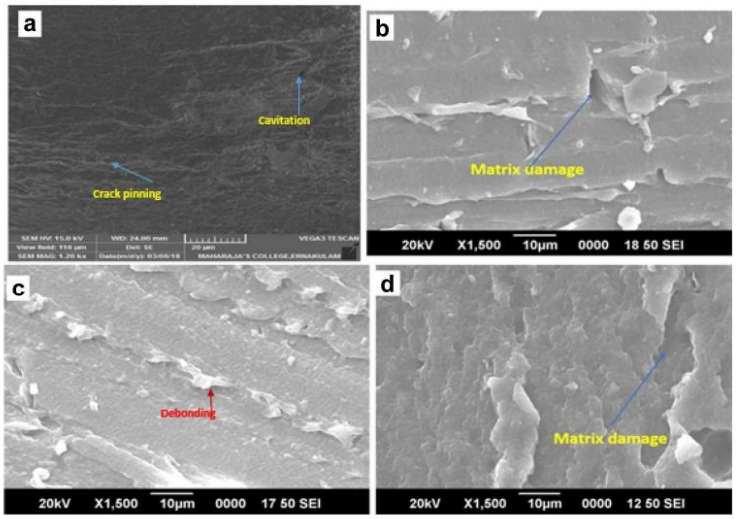

MOST WIEDZY Downloaded from mostwiedzy.pl

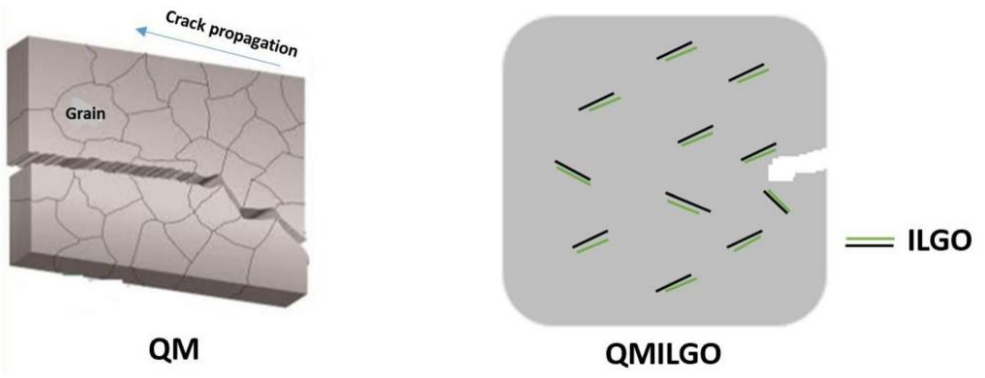

Fig. 5 Schematic diagram of the tensile fracture surface of QM and QMILGO nanocomposites

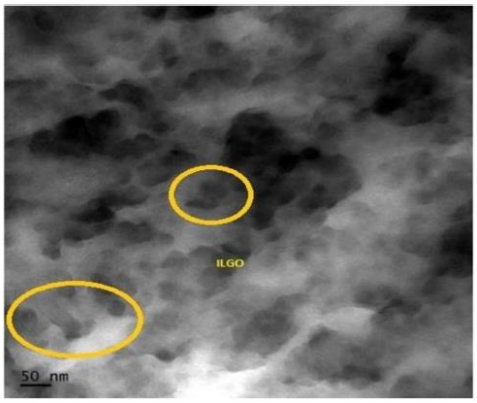

Fig. 6 TEM image of QMILGO1.5 nanocomposite

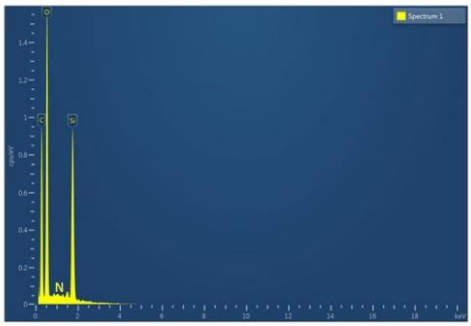

Fig. 7 EDX analysis of QMILGO1.5 nanocomposite

Table 3 Elemental Composition in QMILGO1.5 nanocomposite

Element	Line Type	Wt%	Atomic %
C	K series	40	47.99
N	K series	1.37	1.81
O	K series	50.48	45.79
Si	K series	8.15	4.21
Total:		100	100

Table 4 Data obtained from TGA curves of QMILGO nanocomposites with filler loading

Sample	T_{10} °C	T_{30} °C	T_{max} °C	Residue at Tmax (%)
QM	423	505	522	33.85
QMGO 1	440	510	530	34.10
QMILGO 0.5	447	513	530	34.22
QMILGO 1	457	528	534	35.38
QMILGO 1.5	463	528	554	42.13
QMILGO 2	465	532	552	39.90
QMILGO 2.5	464	530	536	37.06

the ILGO sheets within the QM matrix with no sign of agglomerates.

The energy-dispersive X-ray (EDX) analysis of QMILGO nanocomposite was shown in Fig. 7. It is used to investigate the distribution of desired elements in the QMILGO material. The existence of C, O, N, and Si elements (Table 3) in this analysis proves successful immobilization of ionic liquid on GO material, which is in good agreement with the FT-IR and Raman results.

MOST WIEDZY Downloaded from mostwiedzy.pl

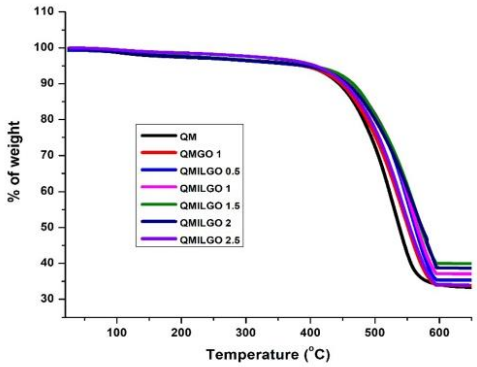

Fig. 8 TGA plot of QMILGO nanocomposites

Thermogravimetric analysis of QMILGO nanocomposites

Addition of neat graphene oxide (GO) on silicone rubber matrix resulted an improvement in the thermal stability of the composite. Inclusion of ILGO improved the thermal stability of silicone rubber nanocomposites as shown in Fig. 8. QMILGO1.5 exhibits better thermal stability compared with all other samples. The temperature corresponding to 10, and 30% of degradation was increased with an increase in filler content (Table 4). Because of the improved thermal stability ascribed by the inserted ILGO nanofiller, the residue of nanocomposites increases as the content of ILGO increases. The proper dispersion of the nanofillers in the QM matrix is responsible for the increase in thermal stability with filler filling. The nanofiller that is exfoliated in the QM matrix acts as a barrier, preventing thermal decomposition of nanocomposites by absorbing heat that is released before the QM matrix. As a result, increasing the nanofiller loading

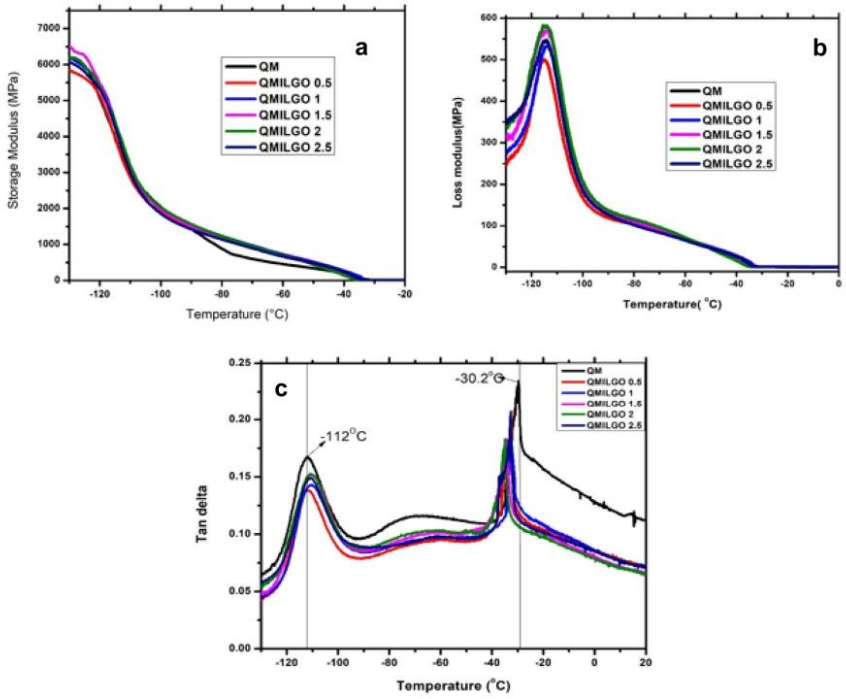

Fig. 9 Differences in (**a**) storage modulus, (**b**) loss modulus, and (**c**) delta (tan) for QM and QMILGO nanocomposites as a function of the temperature

MOST WIEDZY Downloaded from mostwiedzy.pl

Table 5 Data obtained from the dynamic mechanical analysis of QMILGO nanocomposites with filler loading

Sample	T_g (DMA) (°C)	T_m (DMA) (°C)
QM	−112.1 ± 0.6	−30.2 ± 0.5
QMILGO 0.5 mL	−111.6 ± 0.9	−34.3 ± 1.6
QMILGO 1.0 mL	−112.0 ± 0.9	−33.7 ± 0.7
QMILGO 1.5 mL	−111.5 ± 0.9	−35.1 ± 1.9
QMILGO 2.0 mL	−110.7 ± 0.4	−34.0 ± 2.1
QMILGO 2.5 mL	−111.5 ± 0.4	−34.9 ± 0.4

improves the thermal stability of the nanocomposites itself. The thermal degradation activity of GO/silicone nanocomposites was investigated by Wang and Dou the temperature for 50 percent degradation (T50) of GO/silicone nanocomposites was moved up to 67 °C and 86 °C, respectively, by adding 3 wt percent GO to the nitrogen and air atmospheres [27].

Dynamic mechanical analysis of QMILGO nanocomposites

Thermo mechanical properties of the nanocomposites were studied using DMA. The plot of storage modulus (E') of nanocomposites with different concentrations of ILGO as a function of temperature is shown in Fig. 9a. The values of E' drop between –120 °C to –90 °C, indicating a mechanical relaxation associated with glass transition, followed by rubbery region. Further softening of the samples is observed above –40 °C where another drop in the storage modulus occurs. The variance of E" as a function of temperature is shown in Fig. 9b. As temperature increases, an initial increase in loss modulus is observed as energy is dissipated due to glass transition, then loss modulus decreases as the material softens. Figure 9c depicts the influence of ILGO on nanocomposites' damping behaviour as a loss factor (tan delta). In addition to the relaxation behaviour of the composites, the tan delta value provides information on energy dissipation due to internal friction and molecular motions. As also indicated from the modulus drops, two transitions are observed. At –112 °C, tan delta reaches its first peak, which corresponds to the rubber's glass transition temperature (Tg).

Glass transition temperature (Tg) rises, with the addition of ILGO and the magnitude of tan delta decreases. This is probably due to filler imposing restrictions against molecular motion of polymer chains, therefore transition occurring at slightly higher temperature and having less energy dissipated. The second transition temperature at peak of tan delta at –33 °C can be attributed to crystalline melting temperature (T_m) of silicone rubber. A shift of T_m towards lower temperatures is observed with increasing concentration of ILGO, suggesting a disruption of crystalline structure by the addition of filler (Table 5).

Thermal conductivity

Polymer chains have a complex structure due to their complex morphology, the bulk polymer usually exhibits lower

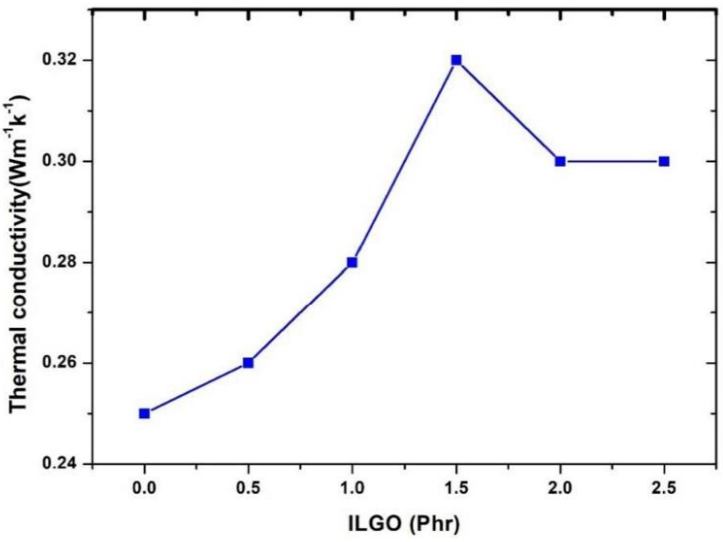

Fig. 10 Thermal conductivity of QMILGO nanocomposites as measured

MOST WIEDZY Downloaded from mostwiedzy.pl

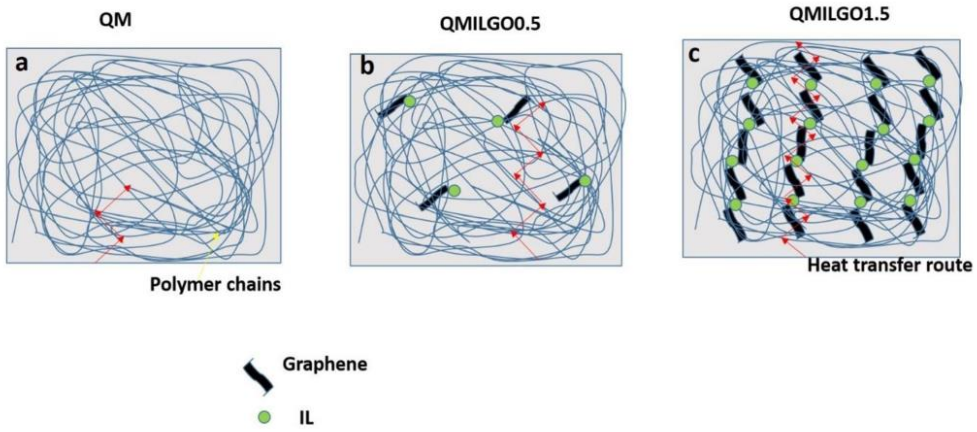

Fig. 11 Polymer nanocomposites schematic diagrams: The thermally conductive pathway is detected and shown in the red line in (**a**) QM (**b**) QMILGO0.5 with few inter-filler networks; and (**c**) QMILGO1.5 with inter-filler networks

thermal conductivity [28]. Therefore, morphology of a polymer has a major impact on its thermal conductivity. As amorphous domains dominate, the vibrational modes of the polymer become localised, as a result poor thermal conductivity obtained. Figure 10 depicts the influence of filler loading on the thermal conductivity of QMILGO nanocomposites.The inclusion of ILGO enhanced the thermal conductivity of the nanocomposites, forming a continuous conducting network within the matrix.Figure 11 depicts the thermal conductivity mechanism.

Neat silicone rubber exhibits thermal conductivity of 0.25 $Wm^{-1}\,k^{-1}$ (Fig. 11a). The thermal conductivity results show that the addition of ILGO shows remarkably improved (28%) conductivity of the composites. When the filler concentration was poor, no inter-filler networks emerged, as shown in Fig. 11b. Higher thermal conductivity of polymers could be achieved by improving inter-chain coupling strength. The thermal conductivity is determined by the filler-matrix interaction, or interfacial thermal resistance, as well as the distribution and geometric patterns of fillers [29, 30]. When the concentration of high conductivity fillers is adequate, they can form thermally conductive networks Fig. 11c.

Conclusions

Ionic liquid functionalized graphene oxide was successfully synthesized, and the composites were prepared using the two-roll mixing method. Current studies can show desirable interactions between graphene oxide and ionic liquid, which are largely due to the cation- cation–π–interactions between the cations of IL and the π- electrons of the graphitic structures in graphene oxide. Addition of 2 phr ILGO to the silicone rubber exhibited a prominent reinforcement effect as it evident from 17% increase in tensile strength. To reinforce the silicon rubber, non-surface modified GO nanoparticles and surface modified with ionic liquid were used. Mechanical experiments, as well as microstructure observations, are carried out in a systematic manner. The fracture of the composites was found to be continuously dominated by direct propagation of the main crack, micro-crack propagation with filler-blocking effect as the nanoparticle fractions increased. Thermal conductivity results show that ILGO addition significantly improves compound conductivity (28%) while compared to the neat QM. Moreover, the property enhancement is because of the homogeneous distribution of ILGO the QM matrix. This research paves a new path for improving graphene–polymer nanocomposites' overall efficiency by optimising interface structures.

Acknowledgements DRDO (Order No: ERIP/ER/1504758/M/01/1667), New Delhi, India is greatly acknowledged for the financial support.

References

1. Cherney EA (2005) Silicone rubber dielectrics modified by inorganic fillers for outdoor high voltage insulation applications. Annu Rep Conf Electr Insul Dielectr Phenomena CEIDP 2005(6):1–9. https://doi.org/10.1109/CEIDP.2005.1560607
2. Sarath PS et al (2005) Fabrication of exfoliated graphite reinforced silicone rubber composites-Mechanical, tribological and dielectric

MOST WIEDZY Downloaded from mostwiedzy.pl

properties. Polym Test 89. https://doi.org/10.1016/j.polymertesting.2020.106601
3. Chen J, Liu J, Yao Y, Chen S (2020) Effect of microstructural damage on the mechanical properties of silica nanoparticle-reinforced silicone rubber composites. Eng Fract Mech 235:107195. https://doi.org/10.1016/j.engfracmech.2020.107195
4. Su JF et al (2017) Preparation and physicochemical properties of microcapsules containing phase-change material with graphene/organic hybrid structure shells. J Mater Chem A 5(45):23937–23951. https://doi.org/10.1039/c7ta06980d
5. Krishnamoorthy K, Veerapandian M, Yun K, Kim SJ (2013) The chemical and structural analysis of graphene oxide with different degrees of oxidation. Carbon N Y 53:38–49. https://doi.org/10.1016/j.carbon.2012.10.013
6. Jang JY, Kim MS, Jeong HM, Shin CM (2009) Graphite oxide/poly(methyl methacrylate) nanocomposites prepared by a novel method utilizing macroazoinitiator. Compos Sci Technol 69(2):186–191. https://doi.org/10.1016/j.compscitech.2008.09.039
7. Xu Y, Hong W, Bai H, Li C, Shi G (2009) Strong and ductile poly(vinyl alcohol)/graphene oxide composite films with a layered structure. Carbon N Y 47(15):3538–3543. https://doi.org/10.1016/j.carbon.2009.08.022
8. Chen L et al (2012) Enhanced epoxy/silica composites mechanical properties by introducing graphene oxide to the interface. ACS Appl Mater Interfaces 4(8):4398–4404. https://doi.org/10.1021/am3010576
9. Yang Z, Peng H, Wang W, Liu T (2010) Crystallization behavior of poly(ε-caprolactone)/layered double hydroxide nanocomposites. J Appl Polym Sci 116(5):2658–2667. https://doi.org/10.1002/app
10. Zhao Y, Tang GS, Yu ZZ, Qi JS (2012) The effect of graphite oxide on the thermoelectric properties of polyaniline. Carbon N Y 50(8):3064–3073. https://doi.org/10.1016/j.carbon.2012.03.001
11. Liu X, Kuang W, Guo B (2015) Preparation of rubber/graphene oxide composites with in-situ interfacial design. Polymer (Guildf) 56:553–562. https://doi.org/10.1016/j.polymer.2014.11.048
12. Pringle JM, Ngamna O, Lynam C, Wallace GG, Forsyth M, MacFarlane DR (2007) Conducting polymers with fibrillar morphology synthesized in a biphasic ionic liquid/water system. Macromolecules 40(8):2702–2711. https://doi.org/10.1021/ma062483i
13. Kreyenschulte H et al (2012) Interaction of 1-allyl-3-methylimidazolium chloride and carbon black and its influence on carbon black filled rubbers. Carbon N Y 50(10):3649–3658. https://doi.org/10.1016/j.carbon.2012.03.037
14. Tasviri M, Ghasemi S, Ghourchian H, Gholami MR (2013) Ionic liquid/graphene oxide as a nanocomposite for improving the direct electrochemistry and electrocatalytic activity of glucose oxidase. J Solid State Electrochem 17(1):183–189. https://doi.org/10.1007/s10008-012-1858-5
15. Subramaniam K, Das A, Häußler L, Harnisch C, Stöckelhuber KW, Heinrich G (2012) Enhanced thermal stability of polychloroprene rubber composites with ionic liquid modified MWCNTs. Polym Degrad Stab 97(5):776–785. https://doi.org/10.1016/j.polymdegradstab.2012.02.001
16. Kumar V, Alam MN, Manikkavel A, Choi J, Lee DJ (2021) Investigation of silicone rubber composites reinforced with carbon nanotube, nanographite, their hybrid, and applications for flexible devices. J Vinyl Addit Technol 27(2):254–263. https://doi.org/10.1002/vnl.21799
17. Yang YK et al (2012) Non-covalently modified graphene sheets by imidazolium ionic liquids for multifunctional polymer nanocomposites. J Mater Chem 22(12):5666–5675. https://doi.org/10.1039/c2jm16006d
18. Subramaniam K, Das A, Steinhauser D, Klüppel M, Heinrich G (2011) Effect of ionic liquid on dielectric, mechanical and dynamic mechanical properties of multi-walled carbon nanotubes/polychloroprene rubber composites. Eur Polym J 47(12):2234–2243. https://doi.org/10.1016/j.eurpolymj.2011.09.021
19. Kosowska K, Domalik-Pyzik P, Nocuń M, Chłopek J (2018) Chitosan and graphene oxide/reduced graphene oxide hybrid nanocomposites – Evaluation of physicochemical properties. Mater Chem Phys 216:28–36. https://doi.org/10.1016/j.matchemphys.2018.05.076
20. Sarath PS, Moni G, George JJ, Haponiuk JT, Thomas S, George SC (2021) A study on the influence of reduced graphene oxide on the mechanical, dynamic mechanical and tribological properties of silicone rubber nanocomposites. J Compos Mater 55(15):2011–2024. https://doi.org/10.1177/0021998320981608
21. Moni G, Mayeen A, Mohan A, George JJ, Thomas S, George SC (2018) Ionic liquid functionalised reduced graphene oxide fluoroelastomer nanocomposites with enhanced mechanical, dielectric and viscoelastic properties. Eur Polym J 109:277–287. https://doi.org/10.1016/j.eurpolymj.2018.09.057
22. Moni G et al (2020) Influence of exfoliated graphite inclusion on the thermal, mechanical, dielectric and solvent transport characteristics of fluoroelastomer nanocomposites. J Polym Res. https://doi.org/10.1007/s10965-020-2040-x
23. Pino-Ramos VH, Alvarez-Lorenzo C, Concheiro A, Bucio E (2017) One-step grafting of temperature-and pH-sensitive (N-vinylcaprolactam-co-4- vinylpyridine) onto silicone rubber for drug delivery. Des Monomers Polym 20(1):33–41. https://doi.org/10.1080/15685551.2016.1231033
24. Hernández M, del Mar Bernal M, Verdejo R, Ezquerra TA, López-Manchado MA (2012) Overall performance of natural rubber/graphene nanocomposites. Compos Sci Technol 73(1):40–46. https://doi.org/10.1016/j.compscitech.2012.08.012
25. Shanmugharaj AM, Bae JH, Lee KY, Noh WH, Lee SH, Ryu SH (2007) Physical and chemical characteristics of multiwalled carbon nanotubes functionalized with aminosilane and its influence on the properties of natural rubber composites. Compos Sci Technol 67(9):1813–1822. https://doi.org/10.1016/j.compscitech.2006.10.021
26. Zhan Y, Yang X, Guo H, Yang J, Meng F, Liu X (2012) Cross-linkable nitrile functionalized graphene oxide/poly(arylene ether nitrile) nanocomposite films with high mechanical strength and thermal stability. J Mater Chem 22(12):5602–5608. https://doi.org/10.1039/c2jm15780b
27. Xing W, Wu J, Huang G, Li H, Tang M, Fu X (2014) Enhanced mechanical properties of graphene/natural rubber nanocomposites at low content. Polym Int 63(9):1674–1681. https://doi.org/10.1002/pi.4689
28. Xiong X, Wang J, Jia H, Fang E, Ding L (2013) Structure, thermal conductivity, and thermal stability of bromobutyl rubber nanocomposites with ionic liquid modified graphene oxide. Polym Degrad Stab 98(11):2208–2214. https://doi.org/10.1016/j.polymdegradstab.2013.08.022
29. Xu X, Chen J, Zhou J, Li B (2018) Thermal Conductivity of Polymers and Their Nanocomposites. Adv Mater 30(17):1–10. https://doi.org/10.1002/adma.201705544
30. Bartlett MD et al (2017) High thermal conductivity in soft elastomers with elongated liquid metal inclusions. Proc Natl Acad Sci U S A 114(9):2143–2148. https://doi.org/10.1073/pnas.1616377114

Publisher's Note Springer Nature remains neutral with regard to jurisdictional claims in published maps and institutional affiliations.

MOST WIEDZY Downloaded from mostwiedzy.pl

Publication -5:

Study the effect of fumed silica on the mechanical, thermal, and tribological properties of silicone rubber nanocomposites

Article summary

This study explored the mechanical, thermal, and tribological properties of silicone rubber (QM) / Fumed silica ($FSiO_2$) nanocomposites. The mechanical properties of silicone rubber were increased by optimizing the silica content of the composite. The effects of applied load, temperature, and sliding speed on the tribological behavior of the samples were evaluated. The addition of $FSiO_2$ significantly reduced the friction coefficient of the composite. Surface wear analysis of the nanocomposite revealed that the nanoparticles have a positive rolling effect. The strengthening properties of the compound improve significantly as the diffusion of $FSiO_2$ increases, resulting in a more significant improvement in the tensile and dynamic material properties and a substantial reduction in the friction coefficient (25 percent) and specific wear rate (Ws). The silica-filled surface of the rubber is relatively smooth, with few grooves and ridges, and the reinforcing fillers seem to have anti-wear properties

Methodology

- Cure characteristics
- Mechanical properties
- Tribology
- Dielectric studies
- Thermal studies

MOST WIEDZY Downloaded from mostwiedzy.pl

Journal of Polymer Research (2022) 29:53
https://doi.org/10.1007/s10965-022-02905-x

ORIGINAL PAPER

Study the effect of fumed silica on the mechanical, thermal and tribological properties of silicone rubber nanocomposites

Sarath P.S[1,5] · Vishnu Prasad[2] · David Pahovnik[3] · Sabu Thomas[4] · Józef T. Haponiuk[5] · Soney C. George[1]

Received: 14 September 2021 / Accepted: 10 January 2022
© The Polymer Society, Taipei 2022

Abstract
This study explored the mechanical, thermal, and tribological properties of silicone rubber (QM) / Fumed silica ($FSiO_2$) nanocomposites. The mechanical properties of silicone rubber were increased by optimizing the silica content of the composite. The effects of applied load, temperature, and sliding speed on the tribological behavior of the samples were evaluated. The addition of $FSiO_2$ significantly reduced the friction coefficient of the composite. Surface wear analysis of the nanocomposite revealed that the nanoparticles have a positive rolling effect. The strengthening properties of the compound improve significantly as the diffusion of $FSiO_2$ increases, resulting in a more significant improvement in the tensile and dynamic material properties and a substantial reduction in the friction coefficient (25 percent) and specific wear rate (Ws). The silica-filled surface of the rubber is relatively smooth, with few grooves and ridges, and the reinforcing fillers seem to have anti-wear properties.

Keywords Silicone rubber · Tribology · Fumed silica · Thermal · Mechanical properties

Introduction

Silicone rubber (QM) is a highly desirable polymeric material with excellent weather and thermal stability, oxidation resistance, and dielectric characteristics [1, 2]. Tribology is an interdisciplinary area, and it is mainly dealt with friction, wear, and lubrication of contacting surfaces in relative motion [3]. Xue et al. [4] explored ATH(aluminum hydroxide) and SiO_2 filled HTVSIR (high temperature vulcanized silicone rubber) composites as an electrical insulator. The influence of the filler type and geometry of ATH and SiO_2 on various HTVSIR properties was explored. Once silica is combined with elastomers, the unique properties are merged with the superior properties of inorganic fillers. Stiffness, processability, elasticity, thermal strength, and mechanical stability are all improved [5]. Fumed silica is distinguished by its small particle size, large surface area, and chain structure in the manometer range. It is synthesized by the

✉ Soney C. George
soneygeo@gmail.com

Sarath P.S
sarathps005@gmail.com

Vishnu Prasad
vishnuprasad193@gmail.com

David Pahovnik
David.Pahovnik@ki.si

Sabu Thomas
sabuthomas@mgu.ac.in

Józef T. Haponiuk
jozef.haponiuk@pg.edu.pl

[1] Centre for Nanoscience and Technology, Department of Basic Sciences, Amal Jyothi College of Engineering, Kanjirappally, Kottayam, Kerala, India

[2] Department of Mechanical Engineering Automobile, Amal Jyothi College of Engineering, Kanjirappally, Kerala 686518, India

[3] Department of Polymer Chemistry and Technology, National Institute of Chemistry, Hajdrihova 19, 1000 Ljubljana, Slovenia

[4] International and Inter-University Centre for Nanoscience and Nanotechnology, Mahatma Gandhi University, Kottayam, Kerala, India

[5] Department of Polymer Technology, Chemical Faculty, Gdansk University of Technology, G. Narutowicza Str. 11/12, 80-233 Gdansk, Poland

Published online: 21 January 2022

MOST WIEDZY Downloaded from mostwiedzy.pl

high-temperature hydrolysis of silicon tetrachloride vapor in a hydrogen–oxygen flame [6].According to He et al. [7], the nano-alumina surface modified with vinyl tri-methoxy silane (VTMS) acts as a molecular bridge between the silicone rubber matrix and the nano-alumina filler to improve the interfacial connection. The overall effect of the charge dispersion's thermal conductivity, tensile strength, and mechanical properties are enhanced by VTMS, lowering the dielectric constant and dielectric losses of the created mixture. Xu et al. used a silane coupling agent (KH550) and 4,4'-diphenylmethane diisocyanate (MDI) to modify the surface of graphene oxide [8]. The MDI-modified GO composites surpassed the KH550 modified GO composites in electrical insulation and light loss in the UV visible region. However, thermal conductivity is more excellent in composites loaded with KH550 modified GO. Chen, Liu, and Huang tried to introduce divinyl-hexa[(trimethoxysilyl) ethyl]-POSS (DVPS), and fumed silica into silicone rubber system employed as the cross-linker and the correspondingly, improved filler. It was found that the synergistic influence of POSS and fumed silica on the thermal stability, and mechanical properties of silicone rubber are very well established [9].

We recently investigated the reinforcement effect of carbonaceous materials added to silicone rubber, such as exfoliated graphite [10] and reduced graphene oxide [11]. Song et al. investigated the thermomechanical and electrical properties of silicone rubber composites as a function of GNP quantities [12]. The functional group attached to the surface of GNP and concentration helps form a thermally conductive network. The friction coefficient, mechanical load carrying capacity, and wear rate of the materials ensure the credibility of tribologically loaded components for commercial processes [13]. Fumed silica is a commonly used material in semiconductor polishing, paint rheology control, and silicone rubber reinforcement [14]. The structural integrity of the fumed silica particle is believed to contribute to its effectiveness in every case. Diani and Gall [13] and Paul and Mark [14] used vinyl ethoxy silane to modify silica surfaces and improve PDMS bonding. Biogenic opaline silica short fibers changed with vinyltrimethoxysilane were effective superior reinforcing fillers for PDMS [15]. Numerous factors influence polymer wear, including internal factors such as interface adhesion, mechanical properties, self-lubricating properties of nanofillers, and external factors such as environment, wear mode, load force, mating surface characteristics, speed, and lubrication, among others [16].

Rubber friction is influenced by the viscoelastic properties of the rubber and the topography of the opposing surface; fortunately, only a few studies have looked into the influence of the rubber surface topography [17]. This research aims to examine the role of fumed silica in improving the mechanical and tribological properties of silicone rubber as a function of silica concentration.

Materials and methods

Materials

The fumed silica was purchased from Sigma Aldrich, Banglore, India. Silicone rubber [SH5060-U (HTV) was purchased from Korea KCC Corporation. It is a general-purpose grade with a low level of vinyl content.

Composite preparation

A two roll mixing procedure was employed for the preparation of composite materials [10]. According to the formulations (Table 1), different loadings of fumed silica ranging from 0 to 10 phr (parts of silica per hundred parts of rubber by weight) were mechanically mixed with QM. A schematic diagram of composite preparation is shown in fig. 1. Samples were hot-pressed at 150 °C and post-cured at 200 °C for 4 hours.

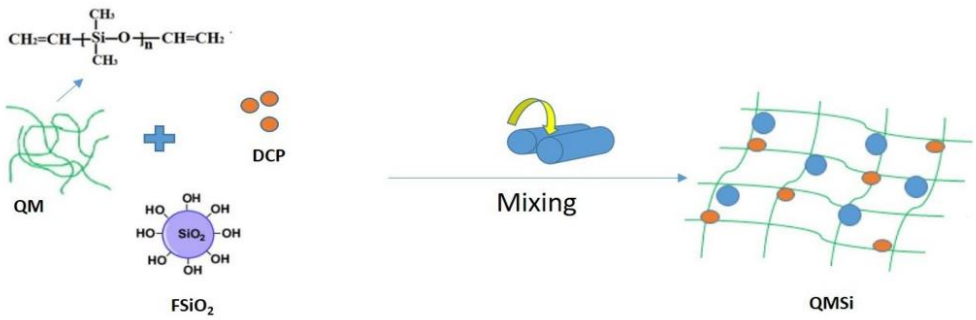

Fig. 1 Schematic diagram of composite preparation

MOST WIEDZY Downloaded from mostwiedzy.pl

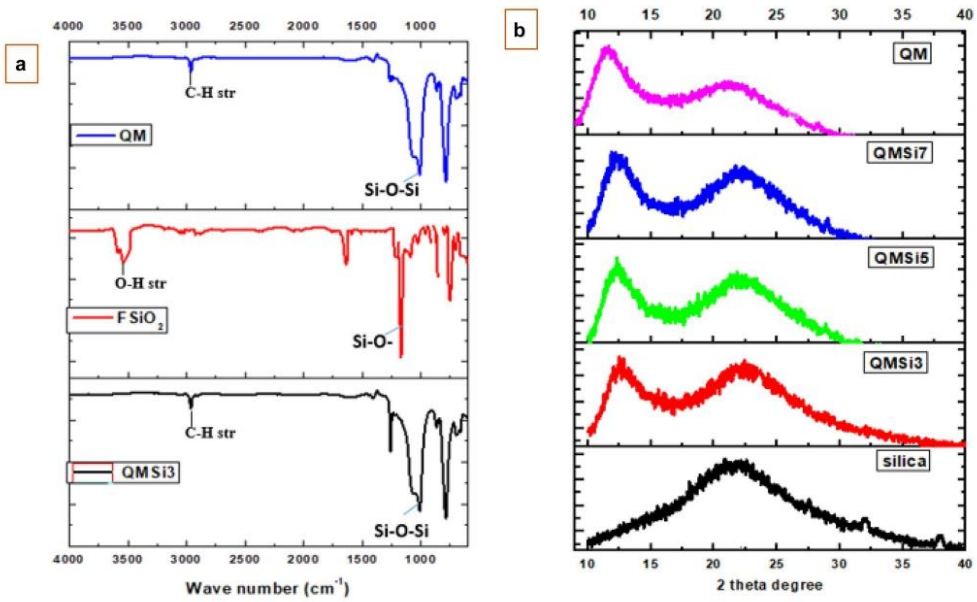

Fig. 2 (**a**) FT-IR spectrum of fumed $FSiO_2$, QM, and QMSi 3(**b**) XRD patterns of QM, fumed silica, and QMSi nanocomposites with different silica loading

Results and discussions

In Fig. 2(a), Fumed silica shows the characteristic peak of -OH str around 3400 $cm^{-1}$and bending 1250 cm^{-1}. These peaks are disappeared in the composites. These changes indicate that most silanol on the surface of fumed silica had participated in bonding during the cross-linking process of QMSi [18]. Table 2 shows the asymmetric and symmetric C-H stretching, and symmetric C-H deformation vibrations of Si-CH_3 are responsible for the sharp bands at 2962 cm^{-1}, 2898 cm^{-1}, and 1260 cm^{-1}, respectively. Peaks at 1612 cm^{-1} and 1415 cm^{-1} are attributed to the QM C=C stretching and C-H deformation vibrations of CH_2=CH. The most vital bands, between 1260 cm^{-1} and 1110 cm^{-1}, are related to the Si–O-Si stretching vibration of the silicone rubber cross-linked networks [19, 20].

In Fig. 2(b), the crystalline peaks at 12.5° and broad, amorphous peaks at 22.5° were in reasonable compliance with XRD characterization for silicone rubber and fumed silica [21]. XRD patterns of fumed silica in Fig. 2(b) reveal that broadband at 2θ = 22.5°, which is typical of amorphous materials without long-range order, and the corresponding d- spacing was 4.23^0 angle. The other small two peaks observed around 34° and 38 degree corresponding to the phases of zeolite includes analcime (Cubic; JCPDS No. 70–1575) [22, 23]. The fumed silica is a mixture of amorphous and crystalline silica, as evidenced by the sharp

Table 1 Compounding ingredients of QMSi nanocomposite

Sample	QM	Fumed silica ($FSiO_2$)	Dicumyl Peroxide (DCP)
QM	100	0	1.5
QMSi 1	100	1	1.5
QMSi 2	100	2	1.5
QMSi 3	100	3	1.5
QMSi 5	100	5	1.5
QMSi 7	100	7	1.5
QMSi10	100	10	1.5

phr*- parts per hundred rubber

Table 2 FT -IR analysis of QM, $FSiO_2$, and QMSi composites

Functional group	Wavenumber (cm^{-1})
Silanol Si–OH	3400
C-H str	2962
CH_3 sym. Stretch	2898
Si–O-Si	1110
Si-CH_3	1260

MOST WIEDZY Downloaded from mostwiedzy.pl

Table 3 X-Ray diffraction analysis of QM, $FSiO_2$, and QMSi composites

Sample	2-theta(deg)	d(ang.)	FWHM (deg)	Height(cps)
Fumed silica	20.97	4.23	9.99	644
QM	21.43	4.14	4.98	283
QMSi3	21.87	4.06	9.28	569
QMSi5	21.62	4.10	9.64	643
QMSi7	21.60	4.11	9.62	659

diffraction peak shown in Fig. 2(b). In the XRD patterns of composites, the disappearance of a sharp crystalline peak at 34° and 38° confirmed the minimal amount of crystalline silica [24].

The values of X-ray diffraction analysis of QM, $FSiO_2$, and QMSi composites are shown in Table 3. The QM showed weak diffraction peaks even at low $FSiO_2$ content, corresponding to a d-spacing of 4.11 angstrom. The diffraction peaks were enhanced, and the peaks intensity decreased as the $FSiO_2$ content was raised. The d-spacings changed from 4.23 A^0 to 4.11 A^0 when the silica content was increased from 1 to 7 Phr. It demonstrates the formation of intercalated nanocomposites and partially exfoliated and partially intercalated nanocomposites [20].

Cure characteristics of QMSi nanocomposites

The influence of the mass fraction of $FSiO_2$ on the curing characteristics of di-cumyl peroxide (DCP) cured QMSi nanocomposites at 150 °C is shown in Table 4. The minimum elastic torque (M_L) of composite QMSi1 is the highest, followed by composite QMSi 2 and QMSi 3. M_L values were related to the viscosity and ability to process compounds. This indicates that the QMSi1 and QMSi2 compounds have better consistency and process capability than others. In contrast, the highest maximum elastic torque (M_H) value was obtained by QMSi 10 compound. The M_H value represents the cross-linking process during the vulcanization process. The M_H value represents the mechanism of cross-linking during vulcanization. It is shown in Table 4 that the QMSi10 composite has the most incredible torque difference ($M_H - M_L$). The degree of cross-linking that developed during curing manifests in the torque variation, correlated to the composite's shear modulus. Silica with a larger surface area creates high compound viscosities due to more bonded polymer and filler connections.

Dynamic mechanical properties of QMSi

Figure 3 shows the dynamical mechanical analysis of silicone rubber nanocomposites. The microscopic relaxation behavior of polymer molecules can be revealed through DMA analysis. In polymeric materials, a drop in the transition peak height can be accompanied by changes in cross-linking density. The peak values of tan δ of QM drop as the silica content of the polymer increases, as seen in Fig. 3(c). However, the QM tan δ displays a restricted glass transition temperature range, demonstrating the produced silica network's good homogeneity. In Fig. 3(b), QMSi3 has the highest loss modulus that increases with the filler volume fraction. The involvement of the matrix phase, the shear forces in the glassy polymer layer near the filler, the rupture and reconstruction of the filler network and glass bridges, and the surrounding polymer chains are all sources of energy dissipation of these compounds. For all samples, the contribution of the polymer matrix is similar; therefore, in those samples filled with interacting silica particles, the higher G″ values observed in these deformed states may be related to the energy generated by the deformation through the glass layer dissipate connected more effectively. The non-interacting filler compounds show the most substantial changes, with the maximum being somewhat apparent in the intermediate deformation domain. Fillers in the polymer matrices have an enormous impact on the materials dynamic response, causing dynamic mechanical properties to depend on dynamic strain amplitude [6]. The most commonly accepted explanation for these findings is the Payne effect [25], i.e., as strain amplitudes rise, the filler system

Table 4 Cure characteristics of composites

Sample	M_L (dNm)	M_H (dNm)	ΔS (dNm)	Scorch Time(ts_2) (min)	Optimum cure time t_{90} (min)	Cure rate index (min^{-1})
QM	5.19	23.55	18.36	0.75	4.63	25.77
QMSi1	1.02	14.07	13.05	0.89	4.78	25.71
QMSi 2	1.56	16.07	14.51	0.77	4.92	24.10
QMSi 3	2.07	17.73	15.66	0.83	4.65	26.18
QMSi 5	3.81	22.45	18.64	0.74	6.05	18.83
QMSi 7	5.14	23.78	18.64	0.77	4.49	26.88
QMSi 10	9.80	34.02	24.22	0.67	5.29	21.65

MOST WIEDZY Downloaded from mostwiedzy.pl

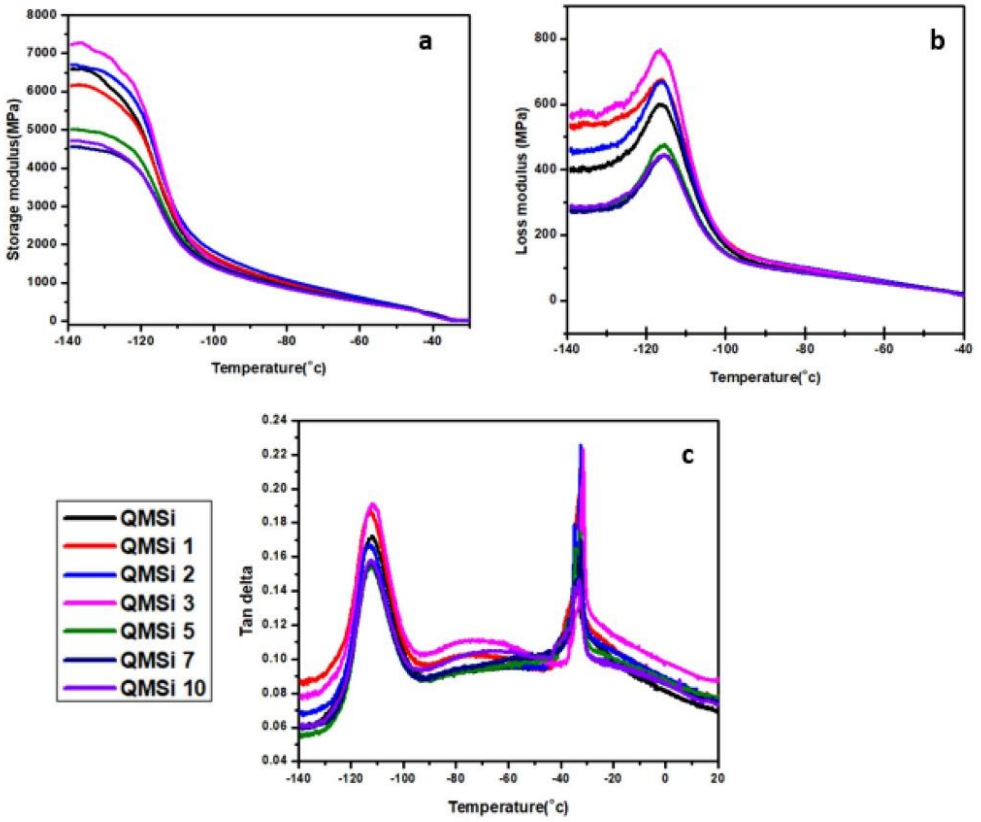

Fig. 3 Variation in (**a**) storage modulus (**b**) loss modulus and (**c**) loss tangent (tanδ) as a function of temperature for QMSi nanocomposites

breaks down, resulting in non—linearity in the elastic modulus. Figure 3(a) depicts the unexpected decrease in storage modulus, which dominates the polymer composite's behavior filled with fumed silica [6]. Increased filler interconnection develops at greater concentrations of filler content due to poor adhesion and lack of contacts between the polymer and the silica surface, enabling the development of large aggregates that typically feature some bound polymer with reduced movement. The breakup of these aggregates under strain relieves the contained rubber, providing bulk flexibility and causing the structure's nonlinear dynamic response. The expansion of the glass transition (Tg) is the most notable change in the dynamic response affected by interacting fillers. These changes are consistent with prior research that suggests enormously diverse dynamics for the glass transition temperature. Interconnected silica particles improve the physicochemical characteristics of the polymeric matrix.

The mechanical characteristics of silicone rubber have been studied by using different amounts of fumed silica. The predominance of dispersion and compatibility of nano-silica with the rubber accounts for the observed reinforcement effect of fumed silica in silicone rubber. Table 5 shows the comprehensive mechanical properties and tensile stress vs. strain behavior of QMSi composites. Fumed silica successfully reinforces QM, that nano-sized silica disperses more homogeneously and strengthens the rubber [26].

The vulcanizate's strength rises steadily as the amount of fumed silica in it rises, then falls to a certain level after reaching its maximum value. The tensile strength of silicone rubber reaches a maximum of 8.36 MPa when 3phr of fumed silica is used. The elastic modulus of vulcanized rubber, or its ability to resist deformation, is expressed by its hardness. In general, when the fumed silica content of vulcanized rubber increases, the tear resistance increases

MOST WIEDZY Downloaded from mostwiedzy.pl

Table 5 Mechanical characteristics of QMSi nanocomposites

Sample	Tensile strength (MPa)	Elongation at break (%)	Tear strength (N/mm)	Hardness (Shore A)
QM	6.21 ± 0.349	540 ± 30	20.45 ± 1	51
QMSi1	6.12 ± 0.42	200 ± 20	24.60 ± 2	54
QMSi 2	6.68 ± 0.26	244 ± 32	27.48 ± 3	58
QMSi3	8.36 ± 0.24	228 ± 40	31.74 ± 2	58
QMSi 5	7.24 ± 0.33	236 ± 16	30.46 ± 3	62
QMSi 7	7.13 ± 0.42	224 ± 24	28.11 ± 2	64
QMSi 10	6.58 ± 0.36	158 ± 30	30.10 ± 3	66

initially, then falls. The tear strength of silicone rubber achieved the highest value of 31.74 N/mm for 3 phr loaded fumed silica. Fumed silica needs to interact with the QM matrix via a two-layer interfacial structure consisting of an adsorbed rubber layer and abounded rubber layer. Polymer-filler interactions include direct contacts resulting from chain adsorption and secondary interactions resulting from chain entanglements [27]. The inclusion of fillers in the polymer matrices has a significant impact on the dynamic responsiveness of the final compounds, causing dynamic mechanical characteristics to be dependent on dynamic strain amplitude. The most generally recognized hypothesis links nonlinear characteristics in the modulus of elasticity to the disruption

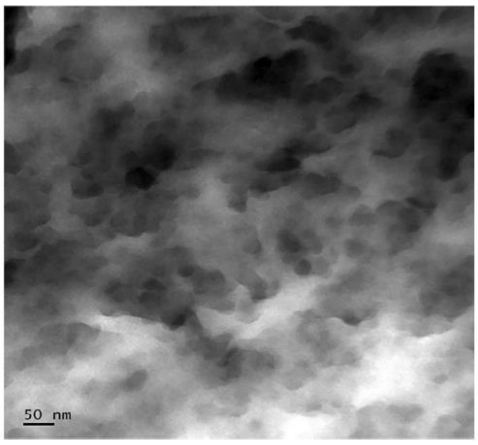

Fig. 4 Transmission electron microscope (TEM) image of QMSi3 nanocomposite

of the filler network as strain amplitudes increase. The substantial reduction in storage modulus after 3phr characterizes the behavior of the polymeric composite loaded with silica, as shown in Fig. 3(a). Significant filler connectivity occurs because of the poor dispersion and lack of contacts between the polymer matrix and the silica surface, creating

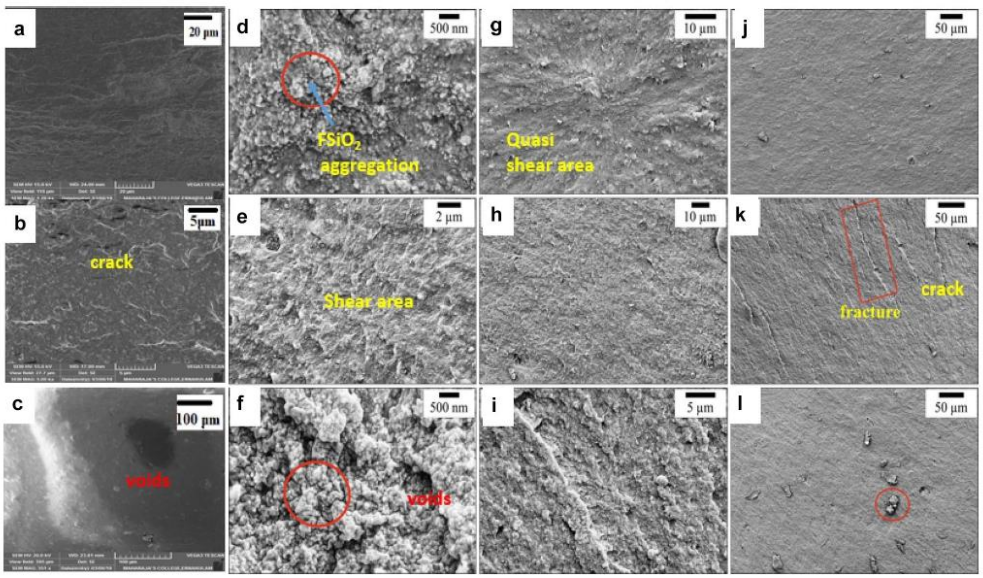

Fig. 5 Tensile fracture surface of cured QMSi nanocomposites (**a-c**) QM,(**d-f**) 5phr silica (**g-i**) 3phr silica, (**J-l**) 1phr silica—silicone nanocomposites

MOST WIEDZY Downloaded from mostwiedzy.pl

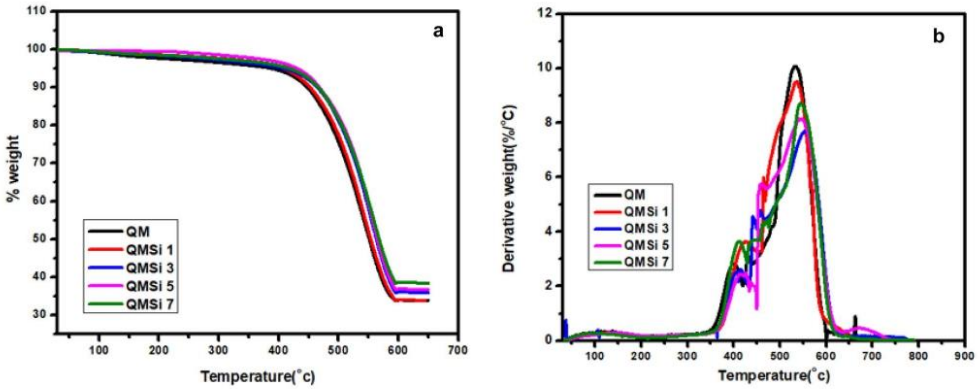

Fig. 6 Thermogravimetric analysis of QMSi nanocomposites

agglomerates holding bound polymer with limited mobility. The bound rubber is released when these agglomerates break down under the applied strain, restoring bulk mobility and causing the compound's nonlinear dynamic response.

TEM images can be used to determine the extent of filler dispersion in the composite directly. The fumed silica is uniformly distributed as much smaller units in sample QMSi3, as shown in Fig. 4. It's worth noting that fumed silica aggregates are spherical and monodispersed particle aggregates, while aggregates are linked by physical interactions [27].

Figure 5 shows the morphologies of tensile fracture surfaces of QM with 1,3 and 5 phr loaded fumed silica. Scanning electron microscopy (SEM) was utilized to investigate the surface characteristics to acquire a more substantial insight into the wear process. In the case of 5 phr loaded samples attributed to silica aggregates, many bright areas could be seen. They are in size range from a few nanometer range to micrometers. We can see the cracks and voids that occurred in the QM system after tensile testing.

In comparison to neat QM and other composites, QMSi3 appears to have the most homogeneous filler dispersion, minimal shear regions, and lower void formation. QMSi1 is substantially more damaged than QMSi3, and the shear area has many voids, but QMSi 5 has the most severe silica aggregation. This might be the reason for the lower tensile properties of QM with higher $FSiO_2$ loading.

Thermogravimetric analysis (TGA)

Silicone rubber has traditionally been regarded as a specialty rubber for many high and low operating temperatures [28]. Thermogravimetric analysis of silicone rubber loaded with fumed silica (1,3,5 and 7 Phr) is shown in Fig. 6 and the values are tabulated in Table 6. Degradation temperatures of the QMSi composites were 433 °C and 440 °C, which was both higher than the silicone rubber. The contributing factors for the enhancement in thermal stability of composites were most likely as follows: (1) the active centers of the silicone leading chains' degradation probably had become inactive when they approached the filler, and (2) interactions between the filler and silicone rubber enhanced the chemical and physical cross-linking points, preventing the unzipped degrading of QM chains [29]. The initial decomposition temperature (Ti) of QMSi, is found to be 410 °C. In the thermal disintegration of the composites, only one degradation phase was clearly visible. Initially, the T_{10} weight loss characteristic temperatures increased from 410 °C for QM to 450 °C for QMSi 5. Because all of these composites lost 50% of their initial mass, their characteristic deteriorated temperatures improved from 550 °C for QM to 567 °C for QMSi 7. The typical temperatures of 10% weight loss of these fumed silica filled silicone rubbers (420 °C for QM and 454 °C for QMSi7) were clearly greater than those of the standard neat silicone rubbers [28].

Table 6 Thermogravimetric analysis of QMSi nanocomposites

Sample	T_{10}°C	T_{50}°C	T_{max}°C	Residue at Tmax (%)
QM	420	550	533	33.85
QMSi1	430	554	536	34.10
QMSi3	445	563	538	35.38
QMSi 5	450	565	540	38.64
QMSi 7	454	567	545	42.13

MOST WIEDZY Downloaded from mostwiedzy.pl

Thermal analysis using the first derivative method confirms that the addition of fumed silica improves the thermal stability of the nanocomposites.

Tribological properties

The friction coefficient shoots up during the friction test, reaching a high of 1.42 for the tidy QM, and with the inclusion of fumed silica, the friction coefficient effectively decreases. Owing to the increased hardness of the vulcanized rubber, mainly with the application of fumed silica, the friction coefficient of the vulcanized rubber strengthened by fumed silica was lower than those of the silicone rubber. The experimental rubber is difficult to distort, and the protrusions on the worn surface cannot be forced against it. Furthermore, the excellent hardness of the rubber surface is matched by its high stiffness, and vulcanized rubber has fewer wrinkles and good anti-wear and anti-friction capabilities. The average distance between the surfaces of the two materials is directly proportional to the surface roughness of a steel counter, which significantly impacts the creation of the transfer film [30]. The difference in the friction coefficient regarding the sliding time is depicted in Fig. 7. The friction coefficient(COF) values for all composites grow at first, then progressively drop to reach virtually stable values [10].

Effect of load

The influence of load on the wear and friction properties of QMSi composites is depicted in Fig. 8. The COF for all composites decreases significantly with increasing normal load. The COF of QMSi composite is considerably high at low loads (5 N); however, the scenario changes dramatically when fumed silica is introduced, particularly for the

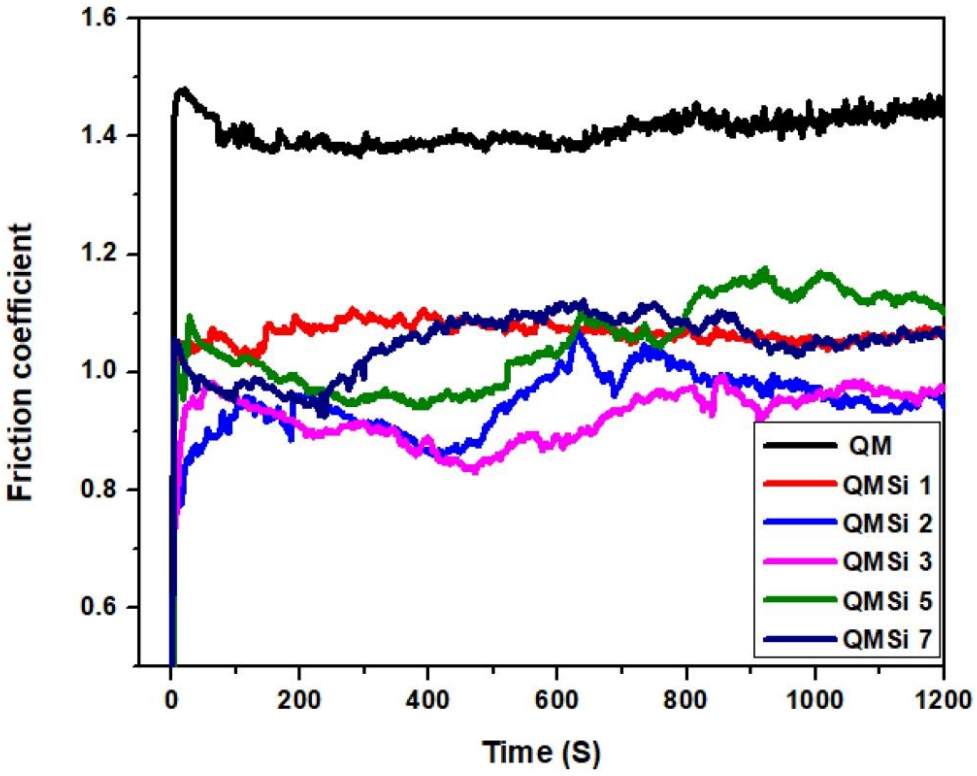

Fig. 7 Friction coefficient vs. time graph of QMSi nanocomposites with different amounts of silica

MOST WIEDZY Downloaded from mostwiedzy.pl

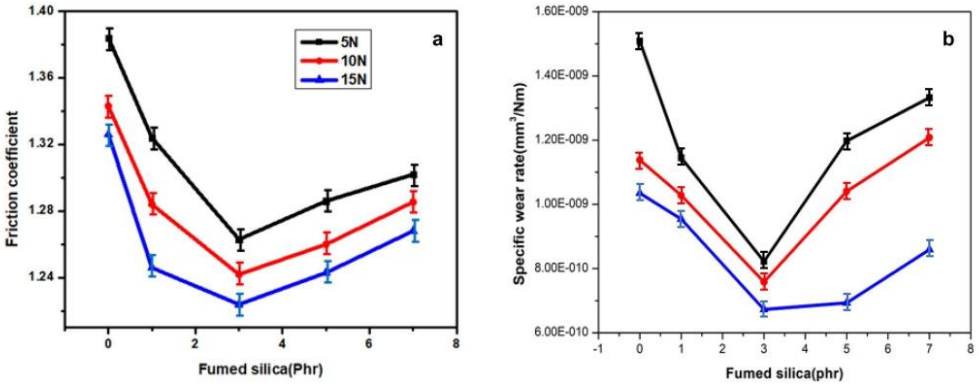

Fig. 8 (**a**) Friction coefficient and (**b**) Specific wear rates of QMSi nanocomposites

nanocomposite [26]. The variation of applied load on the tribological performance of composite graphically presented in Fig. 8. As applied load increases, the frictional heat produced during sliding in the contact area also increases. Figure 8(a) represents COF of the composite decreased with increased load, and 15 N load exhibited the lowest friction coefficient due to silica reinforcement in the QM matrix. At high applied load, the temperature between composite and counter surface may increase, which causes softening of the matrix and the reduction of COF and specific wear rate. In Fig. 8(b) Specific wear rate was found to be rapidly increased with applied load.

Effect of sliding speed and temperature

This study examines the impact of temperature and sliding speed on the frictional properties of the QMSi composites. The variation of COF concerning temperature and velocity is represented in Fig. 9. Figure 9(a) shows the coefficient of friction (COF) value obtained for QMSi composite material at various sliding speeds. The COF decreased with increasing sliding velocity for all materials, the concept known as "velocity weakening" [26]. When considering a lesser velocity of 2 m/s, the COF decreases as the temperature rises. QMSi3 composite obtained the

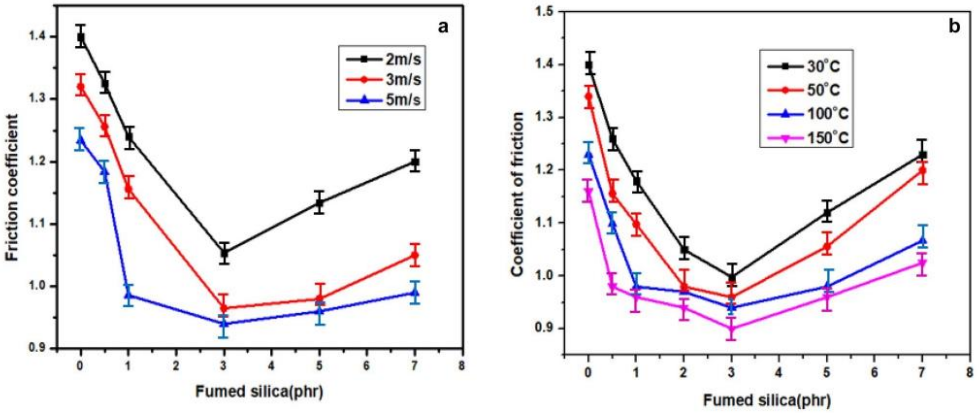

Fig. 9 Coefficient of friction QMSi nanocomposites as a function of sliding speed (**a**) and temperature (**b**)

MOST WIEDZY Downloaded from mostwiedzy.pl

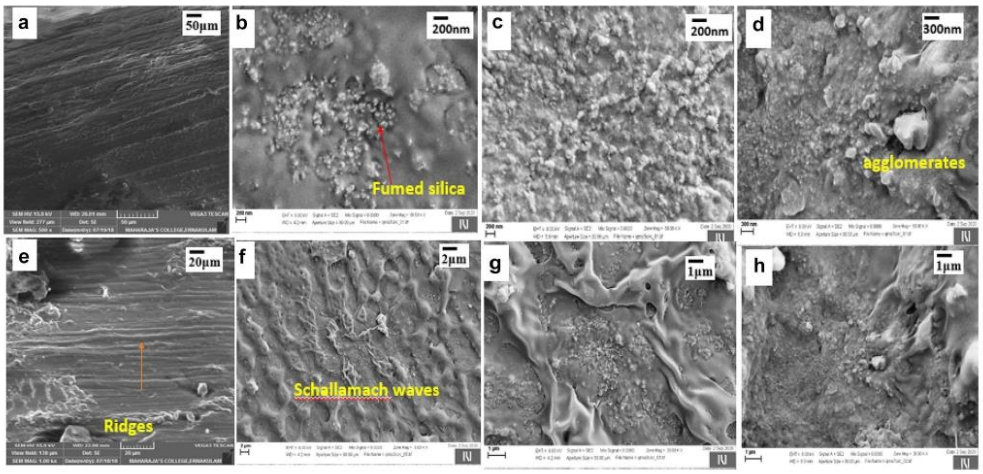

Fig. 10 worn surface of cured QMSi nanocomposites (**a** & **e**) QM (**b** & **f**) QMSi1 (**c** & **g**) QMSi3 (**d** & **h**) QMSi5 silicone nanocomposites

lowest COF; nevertheless, silica increased COF. The surface conditions of the composites have a significant impact on friction and wear behavior. A significant drop in COF was noticed when pin wear was measured at 30–150 OC [31]. Figure 9(b) illustrates that COF decreases in moving from 30 to 150 °C. From the results, it is clear that there is temperature dependence on the friction and wears properties. QMSi composites, test temperature of 150 °C gives the better performance, i.e., lower friction. It's worth noting that at 150 °C, the COF and specific wear rate are the lowest, while at 30 °C, they're the highest. At 100 °C, intermediate values are recorded [Fig. 9(b)]. However, the magnitude is low in all of these examples, ranging from 1.4 to 0.95. At both of these temperatures, the disc's friction layer is mostly made up of loose particles that can be twisted while sliding in the contact zones, causing a mild abrasive interaction on the disc counterface. A temperature rise may cause a thermal softening of the disc counter face, increasing particle transfer to the disc surface [31]. Changes occur due to a series of events such as adhesive point shear failure and reformation. The temperature variation generates differences in activation energy, which modifies the material's wear mechanism. Furthermore, owing to the viscoelastic nature of rubber composites, this shows that perhaps the composite has undergone physical and mechanical changes.

Figure 10 displays SEM pictures of vulcanized rubber worn scars strengthened with fumed silica. Vulcanized rubber reinforced with fumed silica has much less wear surface deformations and abrasion than silicone rubber, which is evident. The surface of the worn rubber loaded with fumed silica seems to be relatively smooth, with few hollows and ridges. It should always be noted that the tribological properties measured are not the same. In this work, the micro tribometer is used to regulate friction in Nanopositioning. The effect of some key control factors on friction is reported, including applied loads, sliding velocity, and temperature. A greater understanding of the acquired characteristics necessitates a better characterization of the microstructures and characteristics of the bulk surfaces. The area of contact also became temperature-independent during sliding, being ruled primarily by the mechanical properties of the rubber and only marginally reliant on the sliding velocity [32].

The experiments at various conditions yielded a lot of information about the nature of the friction layer for the pin and disc materials. Figure 10 shows the worn pattern of the

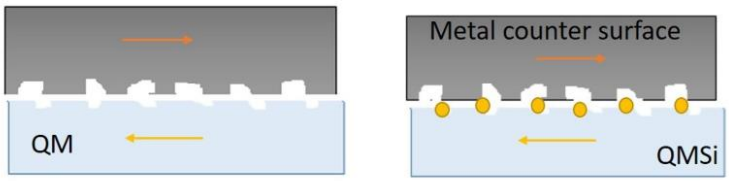

Fig. 11 Tribological rolling effect of $FSiO_2$ nanoparticle in QM matrix

MOST WIEDZY Downloaded from mostwiedzy.pl

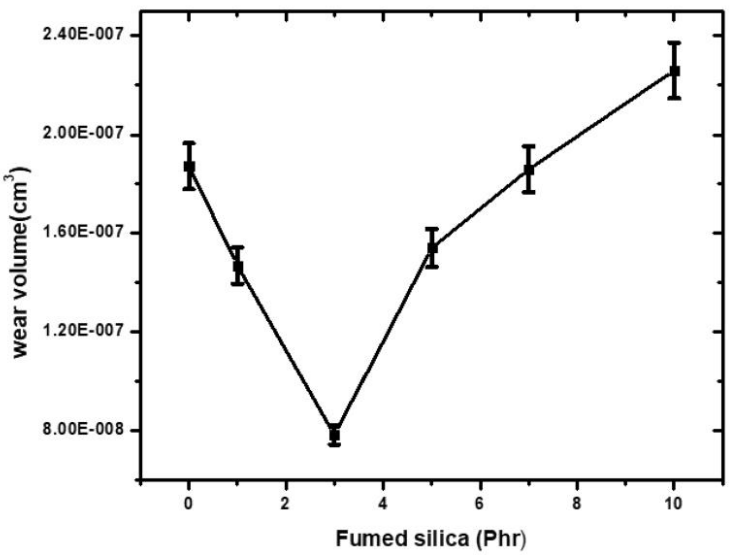

Fig. 12 Variation of wear volume loss against fumed silica loading

neat QM vulcanizate produced at 10 N, 2 m/s respectively. Based on the findings and analyses, the shape of ridges and their particular orientation concerning the worn direction appear surprising. During testing, the ridges are all bent back, and the material is removed by abrasion from the underside of the ridges [33]. Schallamach [34] reported that the origin of the abrasion pattern is not fully understood. Still, it is most probably the consequence of the combination of rubber material's high elasticity and high friction coefficient characteristics. Wear analysis of composite under 10 N load and 3000 m distance shows a significant quantity of voids formed in neat QM. However, voids are restricted and limited due to the wear resistance afforded by reinforced $FSiO_2$. Matrix phase wear was reduced owing to the $FSiO_2$ reinforcement. As a result, the worn surface is smoother, with fewer micro fractures and voids [35]. The fumed silica and the matrix both suffered from interfacial degradation. Surface morphology of the 3-5Phr loaded composites, in addition to the fine and discontinuous cracks, many fine granular wear particles were allocated [36]. Even though the scenario was different for the QMSi3 composition, the QMSi3 rear edges were partially damaged. According to these findings, a positive rolling impact of nanoparticles has been hypothesized for both material combinations. This rolling effect aided in diminishing the frictional coefficient while sliding, decreasing shear stress and interface temperature [30]. Mechanism of the positive rolling effect of nanoparticles as depicted in Fig. 11. Due to its superior surface energy, many neighboring fumed silica primary particles aggregate together, with collective widths of roughly 200 nm. Furthermore, extensive nanoscale pore geometries may be seen in the inside of the material. Due to the apparent reinforcing nature of the fumed silica, this porous feature can attain exceptional tribological performance.

Three-body testing

The dry abrasion technique was used to study the abrasive wear pattern of composites as per ASTM G65. The test specimen was pressed against a revolving wheel at a given force with a lever arm while a controlled flow of abrasives abrades the test surface is investigated in this study. According to ASTMG65, the tests were performed with a load of 10 N and a speed of 200 rpm for 4 min. Figure 12 shows the composite wear volume loss as a function of $FSiO_2$ loading at a set rubber wheel speed of 200 rpm and a constant abrading distance and load (5 N). At initial filler loading, composites decreased wear volume loss, which steadily increased with loading over 3Phr. Due to the resistance provided by $FSiO_2$ particles, the wear rate was reduced at more significant $FSiO_2$ loadings. Because abrasive particles first come into contact with a low-modulus matrix on the composite's surface, wear rate was substantial at lower $FSiO_2$ loadings; however, with higher $FSiO_2$ loadings, wear rate was low [37]. The use of $FSiO_2$ improves the particulate hardness value, preventing abrasive particles from penetrating the composite. The $FSiO_2$ then acts as a reinforcing agent in

MOST WIEDZY Downloaded from mostwiedzy.pl

the QM matrix, providing further abrasive wear resistance. As a result, the $FSiO_2$ loaded composite was more resistant to abrasive wear [35]. Deep furrows results from higher filler content, and the micro-plowing and transverse bending impact of sharp quartz abrasives cause the composite to wear out the most. Surface hardness was among the most critical elements determining a substance's wear resistance, and a more rigid surface will have more excellent wear resistance.

Conclusions

In this study, the mechanical and tribological properties of fumed silica reinforced silicone rubber were investigated. The pin-on-disc test configuration was used for the friction and wear analysis of composites. The experiments were carried out at various temperatures, loads, and sliding speeds. The investigation revealed that filler significantly impacts all rheological parameters of compounds and the mechanical characteristics of vulcanizates. The viscosity of the compounds and the modulus of the vulcanizates increase significantly as filler concentrations increase, but tear strength, elongation at break, and compression set improve only slightly. The interactions between the filler and silicone rubber enhanced the chemical and physical cross-linking points, preventing the unzipped degrading of silicone rubber chains. Due to the extremely high stiffness and rigidity of the rubber surface, a small quantity of fumed silica could significantly decrease the coefficient of friction and specific wear rate of QMSi composites. The coefficient of friction and specific wear rate of QMSi composites are affected considerably by applied load and sliding velocity. As the applied load and sliding speed rise, the coefficient of friction of all composite materials declines. The area of contact also became temperature-independent during sliding, being ruled primarily by the mechanical properties of the rubber and only marginally reliant on the sliding velocity. The friction and wear properties of silicone rubber with 3 phr fumed silica composite was the lowest of all the composites evaluated. The addition of $FSiO_2$ results in a positive rolling effect, and this will improve the tribological properties of the composite, and a similar effect is also observed with the dry abrasion results.

Acknowledgements DRDO (Order No: ERIP/ER/1504758/M/01/1667), New Delhi, India, is greatly acknowledged for its financial support.

Declarations

Conflicting Interests The authors declared no potential conflicts of interest with respect to the research, authorship, and or publication of this article.

References

1. Xue L, Zhang Y, Zuo Y, Diao S, Zhang J, Feng S (2013) Preparation and characterization of novel UV-curing silicone rubber via thiol-ene reaction. Mater Lett 106:425–427. https://doi.org/10.1016/j.matlet.2013.05.084
2. Diao S, Jin K, Yang Z, Lu H, Feng S, Zhang C (2011) The effect of phenyl modified fumed silica on radiation resistance of silicone rubber. Mater Chem Phys 129(1–2):202–208. https://doi.org/10.1016/j.matchemphys.2011.03.077
3. Friedrich KB, Lu ZB, Hager AM (1995) Recent advances in polymer composites' tribology. 190:139–144
4. Xue Y, fei Li X, hai Zhang D, sheng Wang H, Chen Y, fa Chen Y (2018) Comparison of ATH and SiO2 fillers filled silicone rubber composites for HTV insulators. Compos Sci Technol 155:137–143. https://doi.org/10.1016/j.compscitech.2017.12.006
5. Najam M et al (2020) Influence of silica materials on synthesis of elastomer nanocomposites: A review. J Elastomers Plast 52(8):747–771. https://doi.org/10.1177/0095244319888768
6. Mora-Barrantes I, Rodríguez A, Ibarra L, González L, Valentín JL (2011) Overcoming the disadvantages of fumed silica as filler in elastomer composites. J Mater Chem 21(20):7381–7392. https://doi.org/10.1039/c1jm10410a
7. He S et al (2018) Performance improvement in nano-alumina filled silicone rubber composites by using vinyl tri-methoxysilane. Polym Test 67(March):295–301. https://doi.org/10.1016/j.polymertesting.2018.03.023
8. Xu Y, Gao Q, Liang H, Zheng K (2016) Effects of functional graphene oxide on the properties of phenyl silicone rubber composites. Polym Test 54:168–175. https://doi.org/10.1016/j.polymertesting.2016.07.013
9. Chen D, Liu Y, Zhang H, Zhou Y, Huang C, Xiong C (2013) Influence of Polyhedral Oligomeric Silsesquioxanes (POSS) on Thermal and Mechanical Properties of Polydimethylsiloxane (PDMS) Composites Filled with Fumed Silica. J Inorg Organomet Polym Mater 23(6):1375–1382. https://doi.org/10.1007/s10904-013-9939-1
10. Sarath PS et al (2020) Fabrication of exfoliated graphite reinforced silicone rubber composites - Mechanical, tribological and dielectric properties. Polym Test 89:106601. https://doi.org/10.1016/j.polymertesting.2020.106601
11. Sarath PS, Moni G, George JJ, Haponiuk JT, Thomas S, George SC (2021) A study on the influence of reduced graphene oxide on the mechanical, dynamic mechanical and tribological properties of silicone rubber nanocomposites. J Compos Mater 55(15):2011–2024. https://doi.org/10.1177/0021998320981608
12. Song Y et al (2015) Enhancing the thermal, electrical, and mechanical properties of silicone rubber by addition of graphene nanoplatelets. Mater Des 88:950–957. https://doi.org/10.1016/j.matdes.2015.09.064
13. Lingaraju D, Ramji K, Devi MP, Lakshmi UR (2011) Mechanical and tribological studies of polymer hybrid nanocomposites with nano reinforcements. 34(4)705–712
14. Boldridge D (2010) Morphological characterization of fumed silica aggregates. Aerosol Sci Technol 44(3):182–186. https://doi.org/10.1080/02786820903499462
15. Silva VP, Gonçalves MC, Yoshida IVP (2006) Biogenic silica short fibers as alternative reinforcing fillers of silicone rubbers. J Appl Polym Sci 101(1):290–299. https://doi.org/10.1002/app.23324
16. Tangpong SXXW (2013) Review : Tribological behavior of polyethylene-based nanocomposites. 578–597. https://doi.org/10.1007/s10853-012-6844-x

MOST WIEDZY Downloaded from mostwiedzy.pl

17. Ido T, Yamaguchi T, Shibata K, Matsuki K, Yumii K, Hokkirigawa K (2019) Sliding friction characteristics of styrene butadiene rubbers with varied surface roughness under water lubrication. Tribol Int. https://doi.org/10.1016/j.triboint.2019.01.015
18. Yue Y, Zhang H, Zhang Z, Chen Y (2013) Polymer-filler interaction of fumed silica filled polydimethylsiloxane investigated by bound rubber. Compos Sci Technol 86:1–8. https://doi.org/10.1016/j.compscitech.2013.06.019
19. Luo YY, Wang YQ, Zhong JP, He CZ, Li YZ, Peng Z (2011) Interaction Between Fumed-Silica and Epoxidized Natural Rubber. J Inorg Organomet Polym Mater 21(4):777–783. https://doi.org/10.1007/s10904-011-9539-x
20. Chen D, Liu Y, Huang C (2012) Synergistic effect between POSS and fumed silica on thermal stabilities and mechanical properties of room temperature vulcanized (RTV) silicone rubbers. Polym Degrad Stab 97(3):308–315. https://doi.org/10.1016/j.polymdegradstab.2011.12.016
21. Siyuan Y, Jincheng W, Junhua W (2016) Investigation on the application properties of epoxy resin and glass fiber in RTV mold rubber. E-Polymers 16(6):437–445. https://doi.org/10.1515/epoly-2016-0188
22. Abdelrahman EA (2018) Synthesis of zeolite nanostructures from waste aluminum cans for efficient removal of malachite green dye from aqueous media. J Mol Liq 253(2017):72–82. https://doi.org/10.1016/j.molliq.2018.01.038
23. Bagci C, Kutyla GP, Kriven WM (2017) Fully reacted high strength geopolymer made with diatomite as a fumed silica alternative. Ceram Int 43(17):14784–14790. https://doi.org/10.1016/j.ceramint.2017.07.222
24. Wang W et al (2012) Synthesis of silicon complexes from rice husk derived silica nanoparticles. RSC Adv 2(24):9036–9041. https://doi.org/10.1039/c2ra20986a
25. Payne AR (1962) The dynamic properties of carbon black loaded natural rubber vulcanizates. Part II. J Appl Polym Sci 6(21):368–372. https://doi.org/10.1002/app.1962.070062115
26. Wang LL, Zhang LQ, Tian M (2012) Mechanical and tribological properties of acrylonitrile-butadiene rubber filled with graphite and carbon black. Mater Des 39:450–457. https://doi.org/10.1016/j.matdes.2012.02.051
27. Aranguren MI, Mora E, MacOsko CW (1997) Compounding fumed silicas into polydimethylsiloxane: Bound rubber and final aggregate size. J Colloid Interface Sci 195(2):329–337. https://doi.org/10.1006/jcis.1997.5143
28. Jana R, Mukunda P, Nando G (2003) Thermogravimetric analysis of compatibilized blends of low density polyethylene and poly(dimethyl siloxane) rubber. Polym Degrad Stab 80(1):75–82. https://doi.org/10.1016/s0141-3910(02)00385-3
29. Wang S, Long C, Wang X, Li Q, Qi Z (1998) Synthesis and properties of silicone rubber/organomontmorillonite hybrid nanocomposites. J Appl Polym Sci 69(8):1557–1561. https://doi.org/10.1002/(sici)1097-4628(19980822)69:8%3c1557::aid-app10%3e3.3.co;2-8
30. Friedrich K, Zhang Z, Schlarb AK (2005) Science and Effects of various fillers on the sliding wear of polymer composites. 65:2329–2343. https://doi.org/10.1016/j.compscitech.2005.05.028
31. Jayashree P, Turani S, Straffelini G (2020) Effect of temperature and sliding speed on the dry sliding behavior of a SiC-graphite composite against martensitic steel," *Wear*, vol. 450–451, no. February, 203242. https://doi.org/10.1016/j.wear.2020.203242
32. Hemette S, Cayer-Barrioz J, Mazuyer D (2021) Thermal effects versus viscoelasticity in ice-rubber friction mechanisms. Tribol Int 162(no. June):107129. https://doi.org/10.1016/j.triboint.2021.107129
33. Sarath PS, Reghunath R, Thomas S, Haponiuk JT, George SC (2021) An investigation on the tribological and mechanical properties of silicone rubber/graphite composites. J Compos Mater 55(26):3827–3838. https://doi.org/10.1177/00219983211031634
34. Schallamach AGVGV (1953) The velocity and temperature dependence of rubber friction. Proc Physical Soc Section B 66(5):386
35. Manoharan S, Suresha B, Bharath PB, Ramadoss G (2014) Investigations on Three-Body Abrasive Wear Behaviour of Composite Brake Pad Material. Plast Polym Technol 3. [Online]. Available: www.seipub.org/papt
36. Dong CL, Yuan CQ, Bai XQ, Yan XP, Peng Z (2015) Tribological properties of aged nitrile butadiene rubber under dry sliding conditions $. Wear 322–323:226–237. https://doi.org/10.1016/j.wear.2014.11.010
37. Mahesh V, Joladarashi S, Kulkarni SM (2021) Three body abrasive wear assessment of novel jute/natural rubber flexible green composite. J Thermoplast Compos Mater 1–11. https://doi.org/10.1177/08927057211017185

Publisher's Note Springer Nature remains neutral with regard to jurisdictional claims in published maps and institutional affiliations.

MOST WIEDZY Downloaded from mostwiedzy.pl

Publication -6:

Tribological performance of ionic liquid modified graphene oxide/silicone rubber composite and the correlation of properties using machine learning methods

Article summary

This study investigates and predicts the tribological properties of an imidazolium ionic liquid modified graphene oxide (ILGO) with silicone rubber (QM) composite. The pin on the disc tribometer was utilized to conduct experimental tribological property analysis, with load, sliding velocity, and temperature as changing parameters. The coefficient of friction (COF) of QMILGO1.5 was 42 percent lower than that of pure QM. The study found that ionic liquid serves as a self-lubricating layer for graphene, establishing a solid graphene-to-ionic liquid interface bond with the rubber matrix. The experimental data were utilized for training artificial neural networks (ANNs), which were then used to predict the COF of the nanocomposites for values for which the experiment was not performed. The produced composite's predictions of friction coefficient utilizing the ANN technique were quite close to experimental results. The work's fundamental goal is to buy experimentation verifies the COF of functionalized graphene oxide (ILGO) with silicone rubber composite, use the actual experimental values to train a deep neural network using Multilayer perceptron, and then use the trained network to predict the values of COF for which obtaining the values by experimentation was difficult.

Methodology

- Ionic liquid modification of GO
- Tribology
- ANN method

MOST WIEDZY Downloaded from mostwiedzy.pl

Received: 1 December 2021 | Revised: 25 January 2022 | Accepted: 5 February 2022
DOI: 10.1002/pen.25936

RESEARCH ARTICLE

POLYMER ENGINEERING AND SCIENCE WILEY

Tribological performance of ionic liquid modified graphene oxide/silicone rubber composite and the correlation of properties using machine learning methods

Sarath P. S[1,2] | **Therese Yamuna Mahesh**[3] | **Mrituanjay Kumar Pandey**[4] | **Józef T. Haponiuk**[2] | **Sabu Thomas**[5] | **Soney C. George**[1]

[1]Centre for Nanoscience and Technology, Department of Basic Sciences, Amal Jyothi College of Engineering, Kottayam, Kerala, India

[2]Department of Polymer Technology, Gdansk University of Technology, Gdansk, Poland

[3]Department of Electronics and Communication Engineering, Amal Jyothi College of Engineering, Kottayam, Kerala, India

[4]Directorate of Extramural Research and Intellectual Property Right, Defence Research and Development Organisation (DRDO), New Delhi, India

[5]Department of Chemical Sciences, University of Johannesburg, Doornfontein 2028, Johannesburg, South Africa

Correspondence
Soney C. George, Centre for Nanoscience and Technology, Department of Basic Sciences, Amal Jyothi College of Engineering, Kanjirappally, Kottayam, Kerala, India.
Email: soneygeo@gmail.com

Abstract

This study investigates and predicts the tribological properties of an imidazolium ionic liquid modified graphene oxide (ILGO) with silicone rubber (QM) composite. The pin on the disc tribometer was utilized to conduct experimental tribological property analysis, with load, sliding velocity, and temperature as changing parameters. Coefficient of friction (COF) of QMILGO1.5 was 42% lower than that of pure QM. Study found that ionic liquid serves as a self-lubricating layer for graphene, establishing a solid graphene-to-ionic liquid interface bond with the rubber matrix. The experimental data were utilized for training artificial neural networks (ANNs), which were then used to predict the COF of the nanocomposites for values for which the experiment was not performed. The produced composite's predictions of friction coefficient utilizing the ANN technique were quite close to experimental results. The work's fundamental goal is to buy experimentation verifies the COF of functionalized graphene oxide (ILGO) with silicone rubber composite, use the actual experimental values to train a deep neural network using Multilayer perceptron, and then use the trained network to predict the values of COF for which obtaining the values by experimentation was difficult.

KEYWORDS
graphene oxide, ionic liquids, multilayer perceptron, silicone rubber, tribology

1 | INTRODUCTION

Silicone rubber (QM) is a synthetic elastomer with a solid silicone-oxygen chemical structure that contributes to its excellent properties, high chemical and thermal stability, and biocompatibility.[1] As a result, QM has various applications in medical devices, sealing, gas, aerospace industries, flexible electronics, and electrical insulators.[2–6] However, to improve the mechanical strength and stiffness, QM usually requires reinforcement. In this case, carbon nanomaterials have been introduced to overcome some of the inherent limitations of fillers to produce multifunctional polymeric materials with exceptional properties.[7–9] Marlinda et al. developed a resistive pressure sensor based on graphene incorporated natural rubber latex (NR/G) composite fabricated in a simple solution casting method. The pressure sensor shows high sensitivity (~0.2 kPa^{-1}), high cycle stability, and selective response to the applied pressure.[10] A recent systematic review investigated the surface modification of graphene compounds as one of the foremost vital techniques to provide superior

 © 2022 Society of Plastics Engineers.

MOST WIEDZY Downloaded from mostwiedzy.pl

graphene polymer nanocomposites.[11] Graphene is the most promising two-dimensional material with an sp^2 hybridized carbon atom.[12] Graphene is used in different areas such as sensor, water sensitive shape memory material, tribology, multi-functional behavior.[13–15] The work in this arena generally concerns itself with surface modification of GO to enhance the compatibility with the compound matrix. More recent work in this area extends the methods by using, Ionic liquid (IL) to modify the GO surface to obtain better dispersion in the matrix.[16–18] IL has a wide range of interests associated with its excellent chemical and thermal stability, good tribological and adsorption properties, ionic conductivity, etc. Wang et al. explore the impact of GO size on the thermal stability of GO/silicone nanocomposites.[19] Diani and Gall demonstrate that we can predict the % recovery in sliding wear from our brittleness measure including polyvinylidene fluoride, poly(methylmethacrylate), and polyphenylsulfone in their formula.[20] Xu et al. study the performance of casting polyurethane (CPU) compounding with modified Ultra-high molecular weight polyethylene (UHMWPE) is enhanced the mechanicalproperties as well as its surface self-lubricating performance.[21] Researchers explored the potential of IL because of its high chemical and thermal stability, nonflammability, etc. Many reports are available with ILs modified GO and their reinforcing effect, but most of the work reported is related to electrochemical applications.[22,23] This research aims to look into methods for improving the tribological properties of silicone rubber nanocomposites and using multilayer perceptron to predict tribological parameters.

A simple setup has been employed here to study the frictional properties of silicone rubber nanocomposites. The multilayer perceptron with backpropagation is used to classify and predict outputs. This computing method can represent the complex relationship between input and output. The input data received by the ANN system processes the data and classifies it at the output. Experimental findings were not well correlated with mathematical models for tribological studies. Furthermore, estimating such properties using pure mathematical formulae takes a long time. For this reason, Artificial neural networks (ANN) have proven to be a successful tool for predicting specific tribological properties as an alternative.

This work is unique because it intends to examine and predict the tribological features of a novel imidazolium ionic liquid modified graphene oxide (ILGO) with silicone rubber (QM) composite. We also applied artificial neural networks (ANNs) trained using the experimental results to predict the COF and specific wear rate of the nanocomposites for values for which the experiment was not performed.

2 | MATERIALS AND METHODS

2.1 | Materials

Sigma Aldrich provides the graphite for GO synthesis and the ionic liquid (IL) 1-ethyl-3-methylimidazolium dicyanamide for GO modification. KCC Corporation in Korea supplied the silicone rubber SH5060-U (HTV). It's a general-purpose grade with a low percentage of vinyl.

2.2 | Synthesis of graphene oxide (GO)

A modified Hummers' technique was used to produce graphene oxide.[24] Natural graphite was oxidized to graphite oxide using concentrated H_2SO_4 in this procedure. To the resulting solution, KMnO4 was introduced to the mixture, thoroughly mixed with deionized water (DIW) for 20 min at 90°C and followed by slow addition of H_2O_2. It was centrifuged and washed with dilute hydrochloric acid and DIW until neutral pH was obtained. It was dried in an oven at 80°C for 24 h.

2.3 | Modification of graphene oxide with an ionic liquid (ILGO)

Ultrasonication was used to disperse synthesized GO (1 g) in 1000 ml water for 2 h, 0.5 g of 1-ethyl-3-methylimidazolium dicyanamide was added to the solution. Then, 1 g of KOH was dissolved in the corresponding solution to prevent electrostatic interaction between water and ionic liquid molecules. The solution was refluxed at 90°C for 2 h. Finally, the obtained ILGO was washed with DIW and ethanol. In a vacuum oven, it was dried at 80°C for 24 h. The remaining modified ILGO with 1.0, 1.5, 2.0, and 2.5 g of IL were made using the same process.[14]

TABLE 1 Compounding ingredients of QMILGO nanocomposite

Sample	QM	Ionic liquid modified graphene oxide(ILGO)	Dicumyl peroxide (DCP)
QM	100	0	1.5
QMILGO 0.5	100	0.5	1.5
QMILGO 1	100	1	1.5
QMILGO 1.5	100	1.5	1.5
QMILGO 2	100	2	1.5
QMILGO 2.5	100	2.5	1.5

MOST WIEDZY Downloaded from mostwiedzy.pl

2.4 | Preparation of nanocomposite

In a two-roll open mixing mill, the nanocomposites were made by varying the concentration of ILGO as 0.5, 1.0, 1.5, 2.0, and 2.5 with 100 phr of rubber and DCP as the crosslinking agent as per ASTM D 3184 (Table 1). The resulting mixture was then cured at 150°C in a hydraulic press before post-curing at 200°C. The composite preparation is represented graphically in Figure 1.

2.5 | Characterization techniques

The synthesized GO and ILGO were characterized using Fourier transform infrared (FTIR) spectroscopy, X-ray diffraction (XRD), and Raman spectroscopic analysis. Over a spectrum range of 4000–500 cm^{-1}, the Perkin Elmer instrument was used to characterize FTIR analysis. For XRD analysis, a Bruker AXS D8 advanced X-ray diffractometer was used. Cu K radiation (=0.154 nm) was used as the X-ray source in this experiment. The worn surface of the nanocomposites was examined using an SEM-EDS JEOL Model JSM– 6390LV microscope with an 8 nm resolution (Acc V 3.0 KV, WD 6 mm, SEI). Tribological properties of the nanocomposite were studied using a Pin on disc instrument, which was commercially available from Ducom Company. Pin-shaped specimen was fixed to a sample holder using screws. Pin-on-disc experiments were carried out with a hardened ground steel disc at a sliding speed of 2–5 m/s (EN 31, hardness 60 HRC). Weights were measured before and after the wear test with an accuracy of 0.1 mg, and pins and discs were washed in acetone. It was held firmly perpendicular to the rotating counter disc's flat surface. The specimen was tested against smooth hardened steels at various loads, sliding speeds, and temperatures under the ASTM G99 standard. The details of wear analysis were explained in our previous work.[25]

2.5.1 | Experimental procedure

The effects of load, sliding velocity, and temperature on the difference in tribological behavior of the pin-shaped composite sample against the steel counter surface were investigated in three experimental campaigns.

1. The first campaign looked at the effect of a load sliding at 2 m per second over a distance of 3600 m in rotational motion. Three constant normal loads of 5, 10, and 15 N were chosen.
2. The second campaign looked at the effect of velocity in rotational motion with a constant load of 10 N over a distance of 3600 m. Three sliding velocities were chosen at 2, 3, and 5 m/s.
3. The impact of temperature was the focus of the third campaign. Four different temperatures were chosen to study the wear on the QMILGO surface: room temperature (30°C–150°C). The surface of the QMILGO samples was polished before testing, resulting in a surface roughness Ra of 65 9 nm. The samples were washed with ethanol rather than being dried. Each experiment was carried out twice, and the results were tallied.

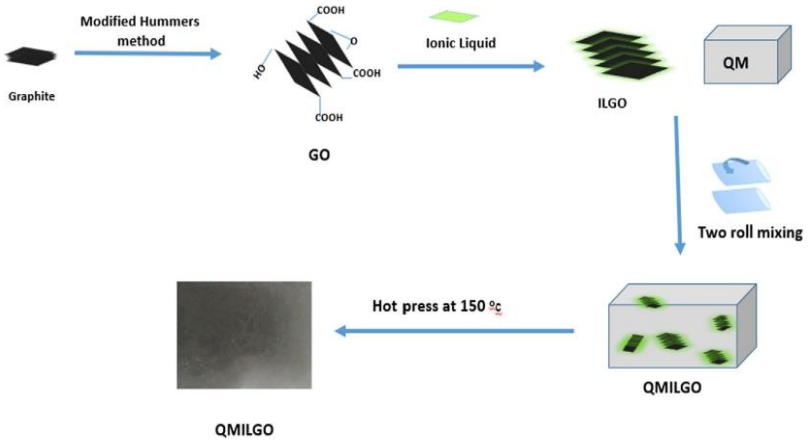

FIGURE 1 Schematic representation of the synthesis of QMILGO composite

MOST WIEDZY Downloaded from mostwiedzy.pl

2.6 | Perceptron criterion

The multilayer perceptron is described by 'W' weight vectors and five hidden layers. For an m dimensional input, assume N number of patterns. Let us take the jth pattern denoted as vector (X_j), and the multilayer perceptron will generate the output y_j. If it is a single class problem then there are two outputs, if it is a multi-class classification problem, it should contain multiple outputs. Consider an M class classifier (means M number of classes). If there are M number of classes then there should be M number of outputs. Outputs are denoted as y_{1j}, y_{2j} ... y_{Mj}. y_{Mj} means output M in the response to the input pattern j. Input forms a point in m dimensional space, and each of the points is indicated by one pattern and each of the patterns will belong to one of the m classes.

A linear equation can be written as

$$g(X) = W^t X + W_o, \tag{1}$$

where X is the feature vector, assume that the feature vector X is of dimension d. The weight vector is called W, and the bias or threshold weight is called Wo. As shown in Equation (1), the perceptron criterion is defined as follows: When the output has two classes, X belongs to the class W_1 if $g(X)$ is higher than 0, and class W_2 if $g(X)$ would be less than zero.

$$g(X)\begin{cases} > 0 \rightarrow X \in W_1 \\ < 0 \rightarrow X \in W_2 \\ = 0 \rightarrow X \text{ is on the decision boundary} \end{cases}. \tag{2}$$

2.7 | Verification of the experimental data and prediction using AI for COF

The experimental results of the coefficient of friction for the used samples were predicted using a multi-layer perceptron classifier network. The classifier uses backpropagation to research a multi-layer perceptron to classify the examples. A basic heuristic is used to set up the network. During the training period, the network parameters are monitored and revised. In this network, the activation function is sigmoid. When the class is numeric, the output nodes become non-threshold linear units. The random number generator is started with the seed. The training data is shuffled, and the initial weights of the internode connections are set with random numbers. A momentum of 0.3 is applied to the weight updates. A nominal to binary filter is used to pre-process the instances as minor attributes are in the data. A wildcard 'a' = (attribs + classes)/2 = (4 + 6)/2 = 10/2 = 5 was used to select the number of hidden layers. As calculated, five hidden layers are used. The numerical attributes and nominal attributes are normalized to improve network performance. This is done with the help of the nominal to binary filter. The binary values are between −1 and 1. A batch size of 100 was set to do the processing. Figure 2 shows the architecture of the MLP network with all the four features of a sample given as input. The red node shows the hidden layers. The orange nodes are the output nodes. The labels on the output node show the class to which the output node belongs.

2.8 | Experimental conditions

The experiment to train a multilayer perceptron classifier was done using 24 instances of data. The samples used

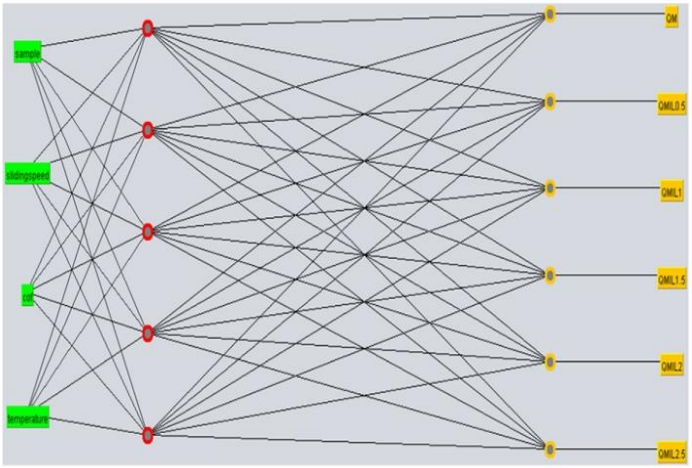

FIGURE 2 Architecture of MLP used for classification, showing the four input features of an input sample, five hidden layers, and six output layers

MOST WIEDZY Downloaded from mostwiedzy.pl

are silicone rubber (QM) and ionic liquid-modified graphene oxide. Four attributes were considered for pre-processing the data for further classification. They are the load in newtons, sliding distance in meters, speed in meters/sec, ILGO in phr.

The classifier uses the gradient descent minimization technique. The sigmoid function is the activation function to provide gradient information. The trained network predicted the friction coefficient by varying the load, velocity, and temperature on the test set. The Mean Absolute Error (MAE) is a metric for determining how close forecasts or predictions are to the actual outcomes of each event.[26]

The formulae determine MAE

$$\mathrm{MAE} = \frac{1}{n}\sum_{i=1}^{n}|f_i - y_i| = \frac{1}{n}\sum_{i=1}^{n}|e_i|, \tag{3}$$

where f_i is the prediction and y_i Is the true value. The absolute error $e_i = |f_i - y_i|$.

Given the percentage of sample, sliding distance, coefficient of friction, temperature as input to the MLP, the network is trained for the six classes QM, QMILGO0.5, QMILGO1, QMILGO 1.5, QMILGO2, and QMILGO2.5. The trained network was used to predict the COF by varying the test set's load, velocity, and temperature.

3 | RESULTS AND DISCUSSIONS

3.1 | Characterization of GO and ILGO

The FT-IR spectrum of GO, IL, and ILGO are displayed in Figure 3A. GO exhibits a broad and wide absorption peak at 3600 cm^{-1}, which confirmed the presence of – OH (hydroxyl) stretching vibrations. The intensity of the peak decreases with IL concentration. The broadened OH stretching peak was disappeared in ILGO2.

The structural information of the ionic liquid-modified graphene oxide was studied using Raman spectroscopy Figure 3B. FT-IR spectrum of GO shows characteristic carbonyl peaks at 1730 $cm^{-1}$and C=C stretching frequencies at 1539 cm^{-1}. At 2249, 2241, and 2139 cm^{-1}, three different peaks were found, the very first two from which belong to the anionic portion of the IL with the C=N bond, and the third of which represents the stretching vibration of the C=N- bond existing in the cationic part.[27] The Raman spectra of GO and IL-GO can be seen in Figure 3B, which show their normal Raman scattering peaks, such as the graphitic (G) and disorder (D) bands, at 1353 and 1586 cm^{-1}, respectively. Small shifts in the ILGO Raman bands suggest chemical interactions between the IL and the GO, such as charge transfer or chemical bond modifications in the ILGO interactions. The I_D/I_G value of ILGO increases from 0.88 to 1.02 compared to GO, which can be attributed to the chemical bonding of IL and GO sheets and the structural defects introduced into GO.[22]

3.2 | Structural characteristics by XRD

X-Ray Diffraction (XRD) gives the structural information for polymers and composites. Pre-exfoliation characteristics of IL-modified GO by XRD are shown in Figure 4. GO has a sharp peak at two thetas 11.5°, but when IL was added, the peak intensity was reduced, and a slight left shift was observed, indicating that the ionic moiety

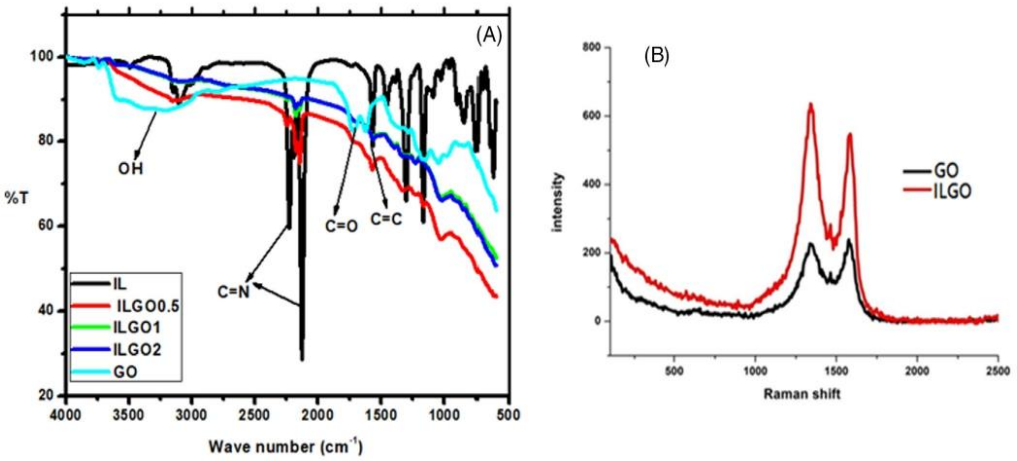

FIGURE 3 (A) FT-IR spectra of GO, IL, and ILGO (B) Raman spectra of GO and ILGO

MOST WIEDZY Downloaded from mostwiedzy.pl

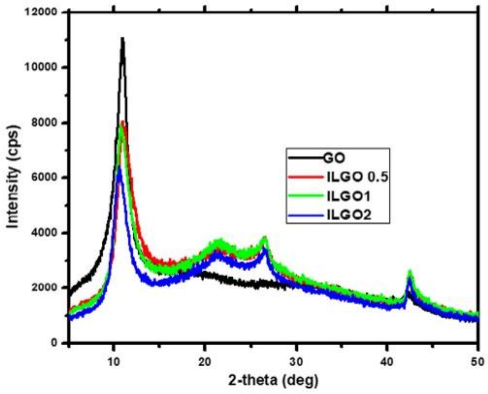

FIGURE 4 XRD spectrum of GO and ionic liquid modified graphene oxide samples

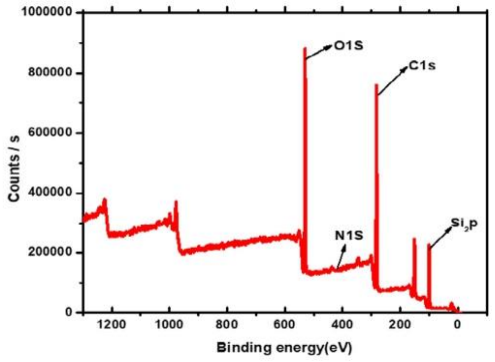

FIGURE 5 XPS spectrum of QMILGO1.5 nanocomposite

TABLE 2 Elemental composition from XPS analysis

Name	Peak BE	Atomic %
O1s	529	25.02
C1s	282	55.16
Si2p	99	19.29
N1s	398	0.53

interacts with GO. There is also a broad diffraction peak observed for ILGO samples around 2θ = 23°and 27° for the ILGO sample. The QMILGO samples display a broader amorphous peak with increasing IL content; the location of the peak maximum is slightly shifted to lower 2θ values.[28]

3.3 | XPS analysis of QMILGO nanocomposite

Figure 5 shows the QMILGO sample's XPS spectra, which show carbon bonds and C–C in aromatic rings (approximately 282 eV). The percentage of various elements present is given in Table 1, and the nitrogen presence indicates the successful incorporation of imidazolium ionic liquid in the polymer composite.[29] A single peak at 400.0 eV was attributed to the imidazolium group.

XPS was used to investigate the surface composition of the synthesized nanocomposites. Four dominant peaks can be seen in QMILGO, corresponding to C1s, N1s, O1s, and Si2p photoelectrons (Table 2).

3.4 | Tribological properties

Figure 6 depicts the friction coefficient evolution over time, with the COF displaying distinct characteristics under various slip states. As the concentration of IL increased, the friction coefficients decreased. Because of solid cation–cation interactions, IL-containing imidazolium cation can be adsorbed onto the conjugated - structure of carbon nanomaterials.[30]

The addition of functionalized graphene reinforcements to polymer composites is expected to increase their tribological properties. To evaluate the wear rates of polymer composites, the device program registered the frictional force of the composites, and wear was measured manually. The QM/polymer and QMILGO/polymer composites provide friction coefficients of 1.35 and 0.84, respectively. ILGO act as a reinforcing agent resulted in a decrease of COF about 40% in the friction coefficient of the composite.

3.5 | Worn surface analysis

Worn surface morphologies analyze the wear, scars, and grooves formed on the surfaces of the composites, which offers an insight into how the material behaves in the process of wear. Figure 7 depicts the worn surface morphologies of composites containing various quantities of ILGO. Figure 7A shows that ridges formed on the contact surfaces of QM more rapidly than those in the ILGO filled condition. Asperities in the steel counter surface quickly removed the material from the soft polymer, as shown in Figure 7B, but groove depths vary from place to place. Figure 7C shows repeated stress on the QMILGO0.5 composite surface since the observation of groove damage occurs on the worn region of the

MOST WIEDZY Downloaded from mostwiedzy.pl

composite. Material separation in the shape of agglomerates and material cutting can be seen at higher magnification.[31] However, since the polymers are sliced by a counterface disc, transferred to the steel surface, and its surface is covered with the transferred polymer, Figure 7D–F has a smoother surface than the previous sample. Because rising normal load often causes a rise in temperature at the frictional surface, adhesion appears to be dominant in this case.

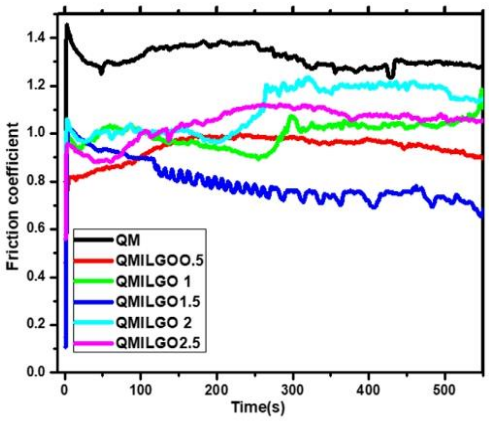

FIGURE 6 Friction coefficient of the QMILGO nanocomposites (10 N, 2 m/s)

3.6 | The effect of load

Figure 8 depicts tribological reliability as a function of a load of QMILGO composite under a constant speed of 3 m/s and a load ranging from 5 N to 15 N. The effect of load on the evolved composite's coefficient friction was investigated by feeding load at various conditions (5 N, 10 N, and 15 N) although maintaining a steady speed of 2 m per second and a distance of 3600 m. When the load increases, COF is found to decrease. It was primarily due to the development of a lubricant film, which smoothens the material that comes into contact with the metal surface, as well as the frictional heat produced.[14,32,33]

As applied load increases, the frictional heat produced during sliding in the contact area increases. The coefficient of friction was predicted for loads of 20 N and 30 N, as shown in Figure 8C. Figure 8A shows that the composite's COF decreased as the load increased, with the 15 N load having the minimum friction coefficient. This is probably due to the opposite surface's uniform film formation. High applied loads soften the matrix, resulting in a reduction in COF. As a result, adhesion and transferring films, rather than abrasion, became the dominant wear types.

According to Archard, the wear volume is assumed to increase with the actual contact area, sliding distance, and the uncertainty of the formation of debris particles. The trend of the results illustrates that wear resistance increases with the addition of ILGO. Wear resistance is

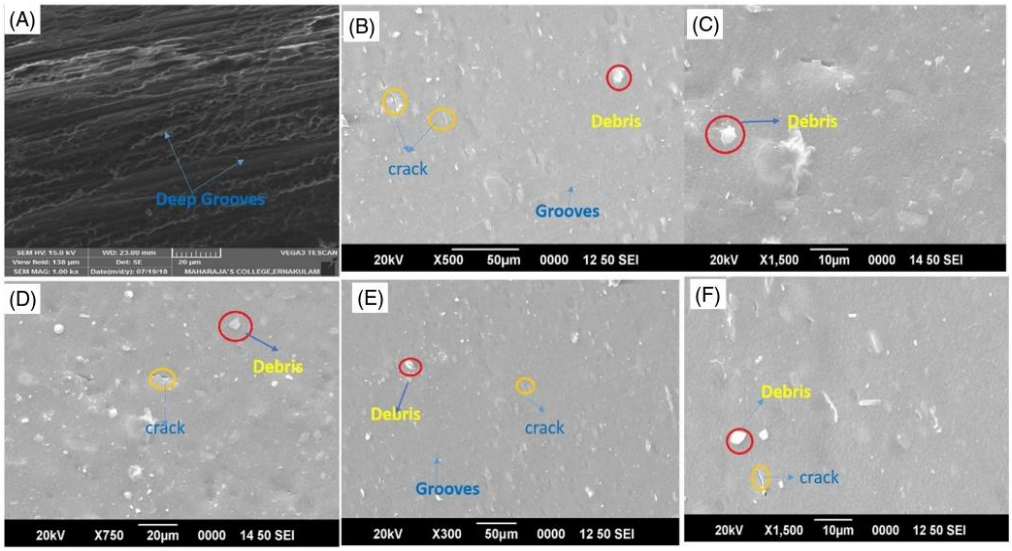

FIGURE 7 Worn surface morphologies of (A) QM, (B, C) QMILGO1, (D, E) QMILGO1.5, (F) QMILGO2

MOST WIEDZY Downloaded from mostwiedzy.pl

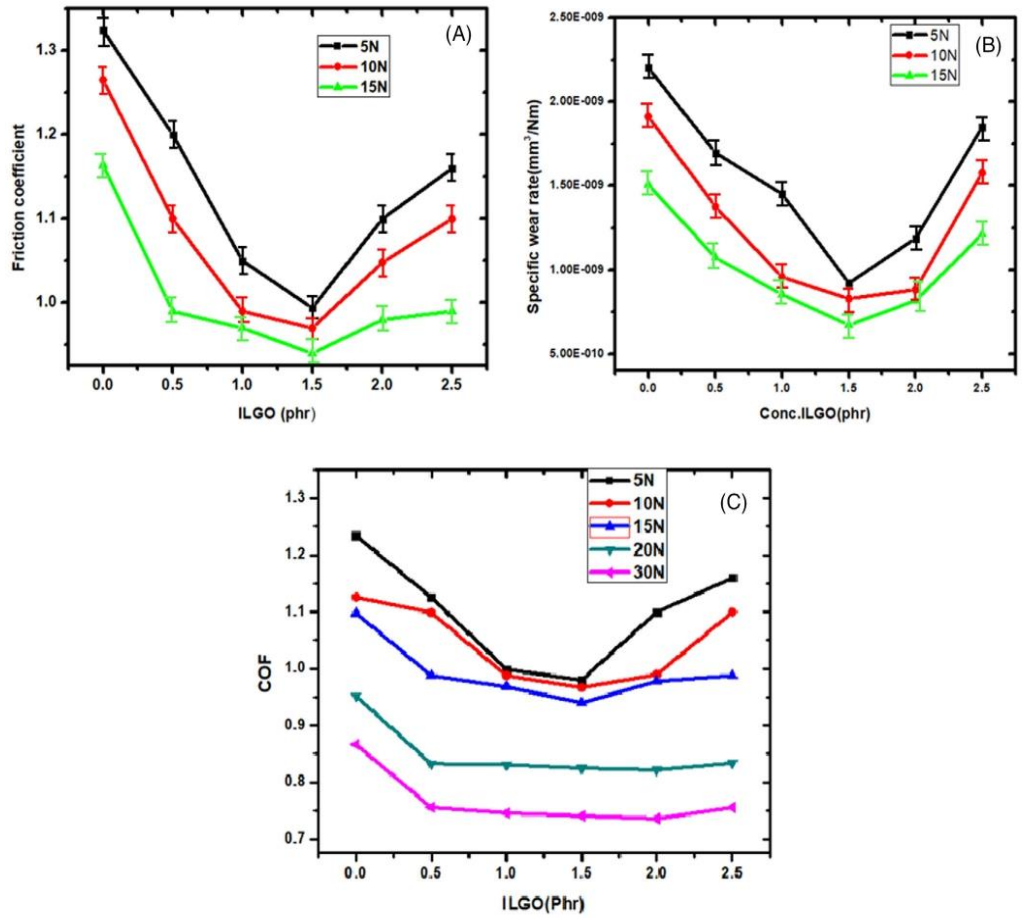

FIGURE 8 (A) friction coefficient and (B) specific wear rates of QMILGO nanocomposites as a function of load (C) measurement of friction coefficients under higher loads

substantially higher in QMILGO, compared to QM. The influence of the ILGO is also pertinent in the tribological properties of the nanocomposites. When ILGO particles are used as a filler, the optimum content (1.5 phr) was needed to attain a noticeable reduction in wear rate.[34]

3.7 | The effect of sliding speed

The impact of sliding velocity on the tribological efficiency of graphene oxide-modified Ionic liquid silicone rubber (QMILGO) composites was studied under constant load (10 N) and temperature at 25°C in Figure 9. It was mainly used to explore the tribological performance at different lubricant regimes. Figure 9A shows the variation of friction coefficient concerning ILGO content and stepwise increase in sliding speed (2 m/s to 5 m/s). Data for 2 m/s are denoted by solid black lines and 5 m/s are shown as green lines. The composite's COF and specific wear rates decreased up to a particular value and then rose when the sliding velocity was grown from 2 to 5 m/s (Figure 9B). This offers clear evidence that the lubricating film's lifting effect is more pronounced at higher speeds.[35] This may be because as the sliding speed increased, the number of adhesive points decreased, resulting in less adhesive friction force and a lower wear rate.

The network was trained for different speeds using the given 18 experimental instances. Many wear mechanisms (abrasion, oxidation, delamination, and thermal

MOST WIEDZY Downloaded from mostwiedzy.pl

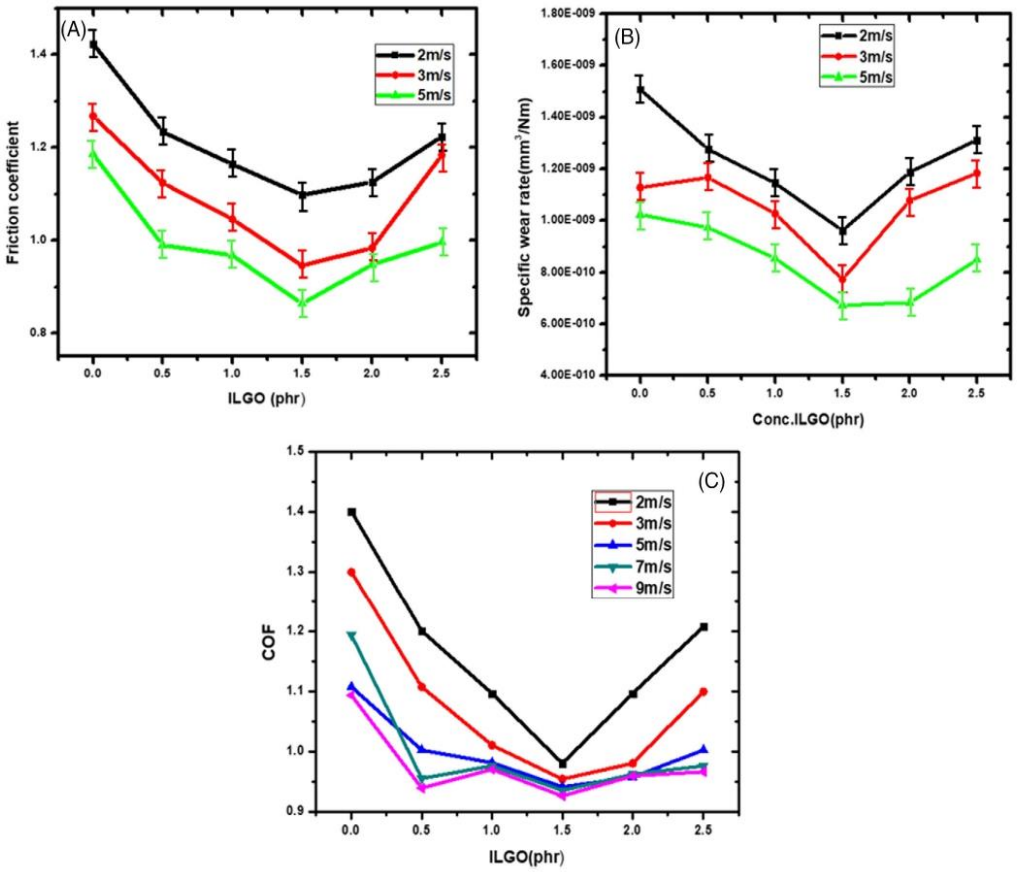

FIGURE 9 (A) friction coefficient and (B) specific wear rates of QMILGO nanocomposites as a function of sliding speed (C) predicted friction coefficient values at a higher sliding speed

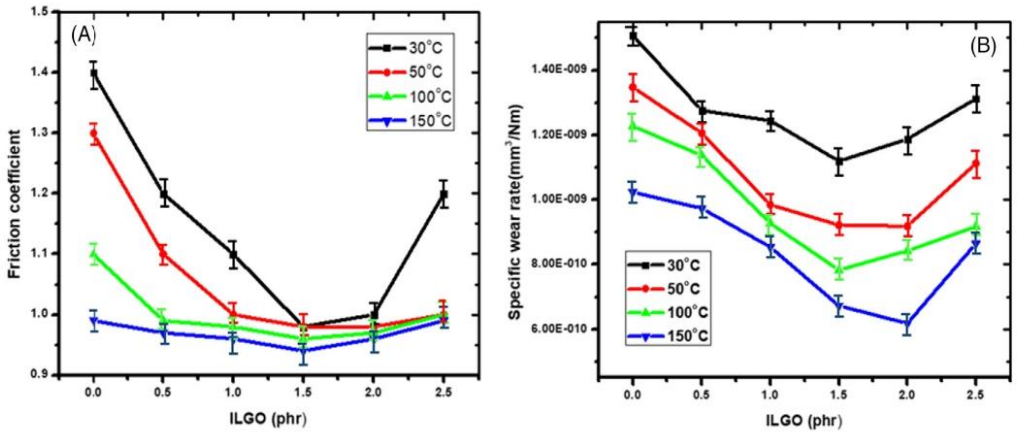

FIGURE 10 (A) coefficient of friction and (B) specific wear rates of QMILGO nanocomposites as a function of temperature

MOST WIEDZY Downloaded from mostwiedzy.pl

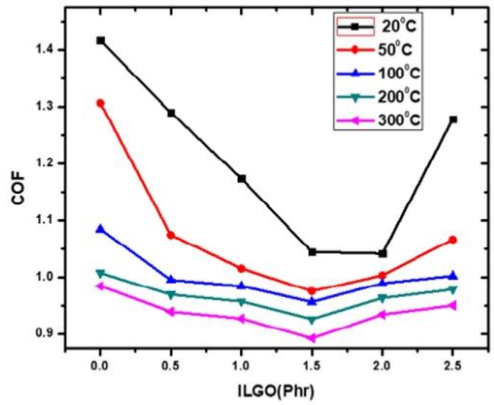

FIGURE 11 ANN predicted COF of different temperature conditions

assisted fatigue) simultaneously at higher sliding speeds (2–9 m/s). Because of the complexities of the wear mechanism and the lubricant impact of ILGO, determining the unique influence of each mechanism is difficult.[36] ILGO prevent direct solid–solid action was mitigated due to the lubricant film formation.

3.8 | The effect of temperature

Figure 10 depicts the effect of temperature on the composites' tribological performance. The initial stage frictional coefficient decreases and attains a stable value. As the temperature rises, the friction coefficient decreases, the elastomer becomes more elastic and the hysteresis friction component decreases. As the temperature rose, the composite's special wear rate fell. High temperature

TABLE 3 Error values and correlation coefficient of train and test data

Parameter varied for testing	Samples used for testing	Mean absolute error of training data	Correlation coefficient of test data	Mean absolute error for test data
Load	12 samples with varying load	0.0676	0.998	0.0089
Speed	12 samples with varying load	0.0641	0.9955	0.125
Temperature	18 samples with varying temperature	0.0498	0.9889	0.0145

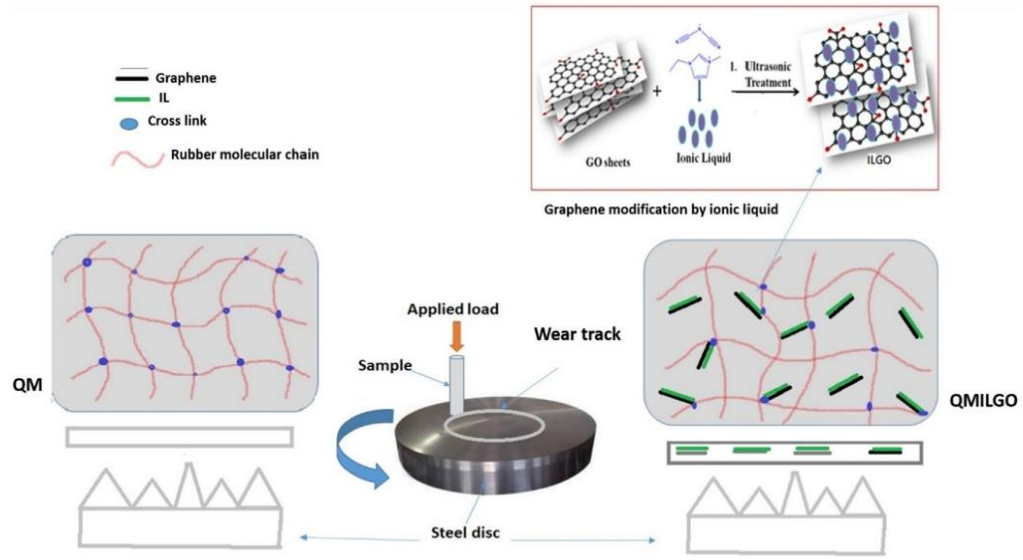

FIGURE 12 Schematic diagram of improvement in tribological properties of silicone rubber by the introduction of ILGO

MOST WIEDZY Downloaded from mostwiedzy.pl

shows a remarkable change in the COF and specific wear rate.

This might be attributed to the higher temperature surroundings and loading that enhance the temperature between composite and counterface. This resulted in the softening of matrix and eventually reducing the COF and the specific wear rate.

3.8.1 | Predictions at different temperatures

Figure 11 gives a comparative graph of the prediction at temperatures of 20, 200, and 300 degrees. The mean absolute error of the test set using the trained MLP classifier is 0.0145. The coefficient of friction was predicted at 20, 200, and 300 degrees using the trained network.

The frictional results of QMILGO composite, tested in different temperature conditions at applied loads (10 N) and sliding speeds (3 m/s), were obtained using ANN for test durations of 30 min. Figure 11 demonstrates the prediction profile created after training the ANN to forecast the friction coefficient dependent on the training dataset collected. The experimental and simulated data are well-matched in Figure 11. However, when comparing the ANN results to the experimental values of the QMILGO composite, there is a subtle distinction. During the test, the COF of the composite material did not remain stable. This was primarily due to the asperities' frequent changes in contact. The development of an ILGO layer on the contact surface is caused by the sliding of harder material on the composite surface. Experiment data becomes more complicated as a result of this.

Table 3 gives a high degree of correlation of test data. The low values of MAE using the training data indicate the correct classification, whereas the MAE of the test data indicates how closely the predicted value follows the actual value.

Figure 12 depicts an effective methodology for enhancing the tribological characteristics of QMILGO composites. When the load is applied to the counterpart and the virgin QM, transfer film is quickly distorted or develops any defects, gradually losing its lubrication. IL, on the other hand, not only improves graphene compatibility in the QM matrix but also produces a dense adhesive layer on the graphene surface after surface functionalization, which can minimize the adhesive force between the composite and the counter surface under high friction conditions by preventing direct contact.[37] Better interfacial interaction results in stress transfer, protect micro-cracks from spreading, and avoids the destruction of interfaces triggered by reciprocating motion.

In conclusion, ionic liquid surface modification of graphene improved the tribological properties of QMILGO composites due to strong graphene matrix interaction and IL lubrication effects.

4 | CONCLUSIONS

The pin-on-disc method is used to achieve experimental results for the COF and wear rate of QMILGO composites. The developed model performed well in predicting friction coefficient, particularly in the steady-state region. The results of single-layer ANN models with many neurons were better. Based on both the experimental findings and the ANN. Strong graphene matrix interaction and IL lubricating effects played an important role in improving the tribological characteristics of QMILGO composites through ionic liquid modification of the graphene surface. The composition of the QMILGO nanocomposite with 1.5 phr ILGO provides the best wear resistance predictions (i.e., the lowest specific wear resistance). The applied load, sliding velocity, and temperature affect the friction coefficient and wear rate of composites. The experiment demonstrated that ionic liquid surface modification of graphene improved the tribological properties of QMILGO composites by enhancing graphene matrix interaction and IL lubrication effects, and the results were validated using a trained Neural network, which also predicted COF values for various temperature, speed, and load conditions.

ACKNOWLEDGMENT

For financial aid, the authors are thankful to DRDO (Order No:ERIP/ER/1504758/M/01/1667) in New Delhi, India.

ORCID

Soney C. George https://orcid.org/0000-0001-9590-3971

REFERENCES

[1] S. C. Shit, P. A. Shah, *Natl. Acad. Sci. Lett.* **2013**, *36*, 355. https://link.springer.com/content/pdf/10.1007/s40009-013-0150-2.pdf (accessed: June 2021).

[2] J. Stieghorst, D. Majaura, H. Wevering, T. Doll, *ACS Appl. Mater. Interfaces* **2016**, *8*(12), 8239.

[3] H. Zhang, Y. Lin, D. Zhang, W. Wang, Y. Xing, J. Lin, H. Hong, C. Li, *Curr. Appl. Phys.* **2016**, *16*(12), 1695.

[4] C. Y. Chen, N. W. Pu, Y. M. Liu, S. Y. Huang, C. H. Wu, M. D. Ger, Y. J. Gong, Y. C. Chou, *Compos. Part B Eng.* **2017**, *114*, 395.

[5] Z. He, Y. Chen, J. Yang, C. Tang, J. Lv, Y. Liu, J. Mei, W. M. Lau, D. Hui, *Compos. Part B Eng.* **2017**, *129*, 58.

[6] H. Yang, X. F. Yao, Z. Zheng, L. H. Gong, L. Yuan, Y. N. Yuan, Y. H. Liu, *Compos. Sci. Technol.* **2018**, *167*(June), 371.

MOST WIEDZY Downloaded from mostwiedzy.pl

[7] N. Kumar, A. T. Kozakov, A. V. Sidashov, A. V. Nicolskii, *J. Mol. Liq.* **2019**, *296*, 111813.

[8] C. Gómez-Navarro, J. C. Meyer, R. S. Sundaram, A. Chuvilin, S. Kurasch, M. Burghard, K. Kern, U. Kaiser, *Nano Lett.* **2010**, *10*(4), 1144.

[9] Y. Zhu, S. Murali, W. Cai, X. Li, J. W. Suk, J. R. Potts, R. S. Ruoff, *Adv. Mater.* **2010**, *22*(35), 3906. https://doi.org/10.1002/adma.201001068

[10] A. R. Marlinda, N. H. Kamaruddin, A. W. Fadilah, M. Said, N. A. Hamizi, M. R. Johan, *Polym. Eng. Sci.* **2021**, *61*(5), 1476.

[11] T. Ramanathan, A. A. Abdala, S. Stankovich, D. A. Dikin, M. Herrera-Alonso, R. D. Piner, D. H. Adamson, H. C. Schniepp, X. Chen, R. S. Ruoff, S. T. Nguyen, I. A. Aksay, R. K. Prud'Homme, L. C. Brinson, *Nat. Nanotechnol.* **2008**, *3*(6), 327.

[12] D. A. C. Brownson, D. K. Kampouris, C. E. Banks, *J. Power Sources* **2011**, *196*(11), 4873.

[13] Z. Zhang, S. Lu, R. Cai, W. Tan, *Nano Today* **2021**, *38*, 101202.

[14] P. S. Sarath, G. Moni, J. J. George, J. T. Haponiuk, S. Thomas, S. C. George, *J. Compos. Mater.* **2021**, *55*(15), 2011.

[15] K. K. Sadasivuni, D. Ponnamma, S. Thomas, Y. Grohens, *Prog. Polym. Sci.* **2014**, *39*(4), 749.

[16] Y. K. Yang, C. E. He, R. G. Peng, A. Baji, X. S. du, Y. L. Huang, X. L. Xie, Y. W. Mai, *J. Mater. Chem.* **2012**, *22*(12), 5666.

[17] H. Kreyenschulte, S. Richter, T. Götze, D. Fischer, D. Steinhauser, M. Klüppel, G. Heinrich, *Carbon N. Y.* **2012**, *50*(10), 3649.

[18] K. Subramaniam, A. Das, D. Steinhauser, M. Klüppel, G. Heinrich, *Eur. Polym. J.* **2011**, *47*(12), 2234.

[19] G. Zhang, F. Wang, J. Dai, Z. Huang, *Materials (Basel)* **2016**, *9*(2), 92. https://doi.org/10.3390/ma9020092

[20] A. Amin, R. Sarkar, C. N. Moorefield, G. R. Newkome, *Polym. Eng. Sci.* **2013**, *53*(10), 2166. https://doi.org/10.1002/pen.23485

[21] B. Xu, B. Yin, Q. Li, X. Kuang, H. Jia, *Polym. Eng. Sci.* **2021**, *61*(7), 2033. https://doi.org/10.1002/pen.25719.

[22] X. Xiong, J. Wang, H. Jia, E. Fang, L. Ding, *Polym. Degrad. Stab.* **2013**, *98*(11), 2208. https://doi.org/10.1016/j.polymdegradstab.2013.08.022.

[23] X. Fan, L. Wang, *J. Colloid Interface Sci.* **2015**, *452*, 98.

[24] L. Shahriary, A. A. Athawale, *Int. J. Renew. Energy Environ. Eng.* **2014**, *02*(01), 58.

[25] P. S. Sarath, S. V. Samson, R. Reghunath, M. K. Pandey, J. T. Haponiuk, S. Thomas, S. C. George, *Polym. Test.* **2020**, *89*(April), 106601. https://doi.org/10.1016/j.polymertesting.2020.106601

[26] T. Rajmohan, K. Palanikumar, J. P. Davim, A. A. Premnath, *J. Thermoplast. Compos. Mater.* **2016**, *29*(2), 161.

[27] G. Moni, A. Mayeen, A. Mohan, J. J. George, S. Thomas, S. C. George, *Eur. Polym. J.* **2018**, *109*, 277. https://doi.org/10.1016/j.eurpolymj.2018.09.057.

[28] H. Gu, Z. Xie, T. Li, S. Zhang, C. Lai, P. Zhu, K. Wang, L. Han, Y. Duan, Z. Zhao, X. Yang, L. Xing, P. Zhang, Z. Wang, R. Li, J. J. Yu, X. Wang, P. Yang, *Sci. Rep.* **2016**, *6*(January), 1.

[29] M. Klepić, K. Setničková, M. Lanč, M. Žák, P. Izák, M. Dendisová, A. Fuoco, J. C. Jansen, K. Friess, *J. Memb. Sci.* **2020**, *597*, 117623. https://doi.org/10.1016/j.memsci.2019.117623

[30] Y. Song, J. Yu, L. Yu, F. E. Alam, W. Dai, C. Li, N. Jiang. *Mater. Des.* *88*(June), 950, **2015**. https://doi.org/10.1016/j.matdes.2015.09.064.

[31] T. Fukushima, A. Kosaka, Y. Ishimura, T. Yamamoto, T. Takigawa, N. Ishii, T. Aida, *Science (80-).* **2003**, *300*(5628), 2072.

[32] A. Mukhopadhyay, *Polym. Test.* **2016**, *52*, 167. https://doi.org/10.1016/j.polymertesting.2016.04.013.

[33] P. S. Sarath, R. Reghunath, S. Thomas, J. T. Haponiuk, S. C. George, *J. Compos. Mater.* **2021**, *55*(26), 3827. https://doi.org/10.1177/00219983211031634.

[34] G. Shi, M. Q. Zhang, M. Z. Rong, B. Wetzel, K. Friedrich, *Wear* **2003**, *254*(7–8), 784. https://doi.org/10.1016/S0043-1648(03)00190-X.

[35] F. Zhao, L. Zhang, G. Li, Y. Guo, H. Qi, G. Zhang, *Carbon N. Y.* **2018**, *136*, 309. https://doi.org/10.1016/j.carbon.2018.05.002.

[36] T. R. Prabhu, *Mater. Des.* **2015**, *77*, 149. https://doi.org/10.1016/j.matdes.2015.03.059.

[37] H. Wang, H. Zhang, J. Zhang, Y. Zhao, *Compos. Sci. Technol.* **2019**, *170*(May 2018), 109. https://doi.org/10.1016/j.compscitech.2018.11.041.

SUPPORTING INFORMATION

Additional supporting information may be found in the online version of the article at the publisher's website.

How to cite this article: S. P. S, T. Y. Mahesh, M. K. Pandey, J. T. Haponiuk, S. Thomas, S. C. George, *Polym. Eng. Sci.* **2022**, 1. https://doi.org/10.1002/pen.25936

MOST WIEDZY Downloaded from mostwiedzy.pl

Publication -7:

Fabrication, characterization, and properties of silane functionalized graphene oxide/ silicone rubber nanocomposites

Article summary

This work used octadecyl trichlorosilane (ODTS) to create a novel silane-modified graphene oxide (SiGO). Further, varied concentrations of silane-modified graphene oxide were used to make silicone rubber (QM) nanocomposite using the open two roll mixing mill. The composites were studied for their mechanical, thermal, and tribological properties. The results showed that a small amount of silane-modified graphene oxide significantly increased the mechanical and tribological performances. Under dry sliding, silane-modified graphene oxide significantly reduced wear and friction to the silicone matrix. Nanocomposites have a lower wear rate than neat silicone rubber; their friction coefficient is almost 36% less than pure silicone rubber: the higher the load and temperature conditions, the more significant the difference in friction and properties. Wear mechanisms were revealed by Scanning Electron Micrographs of the worn surface. The transfer film formation on the counter surface and acceptable wear debris improved the nanocomposite's friction and wear resistance characteristics.

Methodology

- Silane modification of GO
- Tribology
- Mechanical properties
- Thermal properties

MOST WIEDZY Downloaded from mostwiedzy.pl

Received: 14 November 2021 | Revised: 9 February 2022 | Accepted: 12 February 2022
DOI: 10.1002/app.52299

ARTICLE

Applied Polymer SCIENCE WILEY

Fabrication, characterization and properties of silane functionalized graphene oxide/silicone rubber nanocomposites

Pampayil Sasikumar Sarath[1,2] | **Sabu Thomas**[3] | **Józef T. Haponiuk**[2] | **Soney C. George**[1]

[1]Centre for Nanoscience and Technology, Department of Basic Sciences, Amal Jyothi College of Engineering, Kottayam, India

[2]Department of Polymer Technology, Chemical Faculty, Gdansk University of Technology, Gdansk, Poland

[3]International and Inter-University Centre for Nanoscience and Nanotechnology, Mahatma Gandhi University, Kottayam, India

Correspondence
Soney C. George, Centre for Nanoscience and Technology, Department of Basic Sciences, Amal Jyothi College of Engineering, Kanjirappally, Kottayam, Kerala, India.
Email: soneygeo@gmail.com

Funding information
Defence Research and Development Organisation, Grant/Award Number: ERIP/ER/1504758/M/01/1667

Abstract

In this work, octadecyl trichlorosilane (ODTS) was used to modify the surface of graphene oxide. Further, varied concentrations of silane-modified graphene oxide were used to make silicone rubber nanocomposite. The mechanical, thermal, and tribological properties of the composite were studied. The results showed that a small amount of silane-modified graphene oxide significantly increased the mechanical and tribological performances. Under dry sliding, silane-modified graphene oxide to the silicone matrix significantly reduced wear and friction properties. Nanocomposites have a lower wear rate than neat silicone rubber; their friction coefficient is almost 36% less than pure silicone rubber: the higher the load and temperature conditions, the more significant the difference in friction and properties. Wear mechanisms were revealed by scanning electron micrographs of the worn surface. The transfer film formation on the counter surface and acceptable wear debris improved the nanocomposites friction and wear resistance characteristics.

KEYWORDS

graphene oxide, mechanical properties, silane functionalization, silicone rubber, tribology

1 | INTRODUCTION

Silicone rubber (QM) is a commonly used industrial material because of its excellent physical properties, chemical inertness, wide operating temperature range, ultraviolet, ozone, aging, and materials appropriate for environmental applications.[1–3] Traditionally, the QM has been used in applications requiring high thermal stability, dielectric strength, or fire resistance. However, researchers are currently working on developing silicone materials with multifunctional features. As a result of the evolution of current technologies, there is a growing demand for high thermal conductivity rubber materials with good mechanical properties that can be used in extreme conditions. This places a high value on research in this field.[4–10] Graphene is two-dimensional and one-atom-thick nanomaterial made up of sp^2 -hybridized carbon atoms first isolated in 2004.[11] Graphene, the most promising material of the decade, has sparked widespread interest in various applications. It has tremendous potentiality as a reinforcement in polymer composites because of its remarkable mechanical, thermal, and electric properties.[4,12] Yang et al. used a combination of solution and co-coagulation method to develop graphene-silicone rubber nanocomposites. Silicone rubber-graphene composites as well as vast strain sensing range and a high strain sensitivity properties have been greatly enhanced.[13] XU et.al studied the influence of

 © 2022 Wiley Periodicals LLC.

MOST WIEDZY Downloaded from mostwiedzy.pl

different processing conditions on electrical and mechanical properties of graphene-filled-silicone rubber composites.[14] Kumar et al. also demonstrated that using carbon nanotubes (CNTs) as a nanofiller in an silicone rubber matrix improves the mechanical and electrical properties.[15] In recent years, the chemical modification of graphene oxide has been an essential topic in academia. This is mainly accomplished by selecting proper reagents due to the active oxygen functionalities associated to graphene oxide (GO). Such modifications improve the compatibility of GO in various systems, and this modified graphene offers prospective uses in polymer composites, energy-related materials, field-effect transistors, and lubricant coatings, among others.[16–18] Ge et al. synthesized diisocyanate functionalized graphene oxide (FGO) and as the amount of FGO filler increased, the thermal conductivity of the silicone rubber was continuously enhanced.[19] Bai et al. studied the effect of rGO (reduced graphene oxide) reduction degree on the reinforcement in silicone rubber and it was observed that rGO reinforcement increased with degree of reduction of graphene oxide. The oxidation of the side group of silicone rubber chains was slowed by rGO, which has a good barrier effect.[20] Ren et al. studied the thermal conductivity of silane-functionalized graphene nanoplatelets (GNPs) reinforced silicone rubber. It was found by Raman mapping that the silane-functionalized GNPs could be dispersed uniformly into the silicone rubber matrix, leading to an increase of Young's modulus and a considerable enhancement in the thermal conductivity.[21] Gan et al. studied the effect of silicone rubber's vinyl concentration on the mechanical properties of the composites they produced. The GO sheets were found to be equally distributed throughout the QM matrix and thereby it improved the thermal and mechanical properties of the composites tremendously.[22] The weak van der Waals interaction between atomically thick neighboring lamellae, superior mechanical strength, impressive thermal conductivity, and high surface area of graphene makes it a promising candidate for tribological applications. Nanoelectronics, lubrication, drug delivery, gas sensing, catalysis, and photovoltaics have used graphene's large surface area. The total strengthening of these carbon materials to the QM matrix is determined mainly by their dispersion level and the interfacial interaction between both the polymer and filler.[23,24] Sivakumar et al. show the possible usage of a waste carbon source transformed to GO, which can be employed as a nano-additive directly.[25]

This research aims to find out how silane functionalized graphene oxide affects the mechanical, thermal, and tribological properties of QM composites. Friction and wear of polymers under tribological contacts/contacting surfaces are the fundamental reasons, which are inescapable. As a result, new additives must be developed to improve lubricant efficiency and reduce the concerns above.

2 | EXPERIMENTAL

2.1 | Materials

The graphite and octadecyl trichlorosilane was purchased from Sigma Aldrich, Bangalore, India, and SH5060-U (HTV) silicone rubber was purchased from Korea KCC Corporation. It is a general-purpose grade with a low level of vinyl content.

2.2 | Preparation of QMSiGO composite

Silicone rubber (100g) was masticated for five minutes in an open two-roll mixing mill. Then modified graphene oxide (SiGO) was added in various amounts (0.25, 0.5, 1 and 2 g), with Dicumyl peroxide (1.5 g) serving as a curing agent. it is hot pressed at 150 degree centigrade corresponding to the cure time obtained by the rheometer. The composite was further post cured for 4 hours. Schematic diagram of the composite preparation is shown in Figure 1.

2.3 | Characterization techniques

Fourier transform infrared (FT-IR) spectroscopy, X-ray diffraction (XRD) analysis, and Raman spectroscopic analysis was used to analyze the synthesized GO and SiGO. FTIR analysis was characterized using Perkin Elmer at a spectrum range of 4000–500 cm^{-1}. The mechanical properties of the QMILGO nanocomposites were investigated using an INSTRON-4411 pneumatic universal testing system with a moving crosshead speed of about 500 mm/min. The samples' tear strength was determined using the ASTM D-1424 standard. The tensile fractured surface and the worn surface morphology of composites were collected and analyzed using Scanning electron microscopy (SEM) on an HR-SEM Zeiss Ultra plus instrument was used to examine the morphology of the samples (Carl Zeiss, Germany). The samples were coated with a 10 nm gold coating for charge dissipation during SEM analysis using a Gatan PECS 682 (Gatan, USA). On a DMA Q800, the dynamic mechanical analysis was carried out (TA Instruments, USA). Differential scanning calorimetry was performed using a Mettler Toledo DSC 1 (Mettler Toledo, Switzerland). The viscoelastic

MOST WIEDZY Downloaded from mostwiedzy.pl

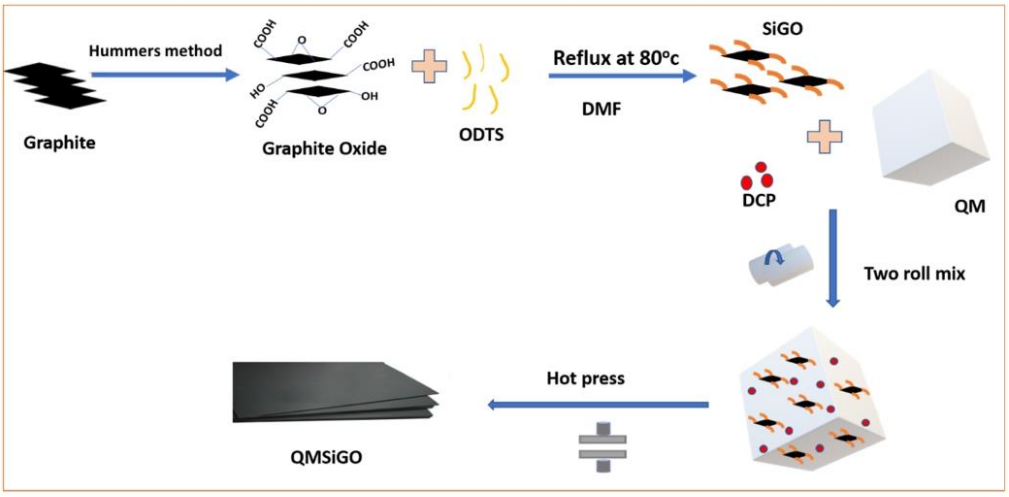

FIGURE 1 Schematic showing the preparation of QMSiGO nanocomposite [Color figure can be viewed at wileyonlinelibrary.com]

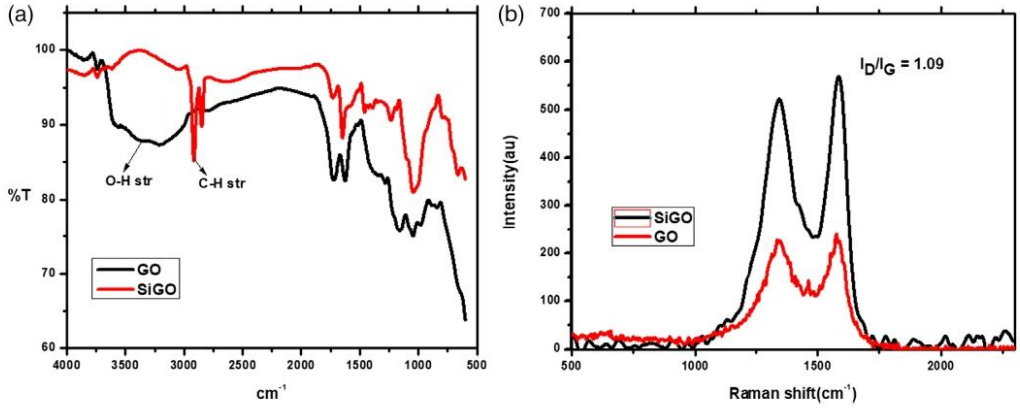

FIGURE 2 (a) FT-IR spectrum of GO and SiGO and (b) Raman spectra of GO and SiGO [Color figure can be viewed at wileyonlinelibrary.com]

properties were measured at a frequency of 1 Hz, strain amplitude of 5 μm in a temperature range from −140 to 30°C with the heating rate of 2°C min^{-1}. The glass transition temperature (T_g) was observed as the peak of the tan δ curve, and melting temperature (T_m) was marked as a drop-in storage modulus. The results are given an average of three measurements with a standard deviation. The thermal conductivities of the composites were studied using ASTM D5470 and Holmarc's Lee's Disc Apparatus (Model: HO-ED-M-03).

2.4 | Functionalization of the graphene nanoparticles

GO was made by oxidizing natural graphite powder.[26,27] The resultant GO was modified with Octadecyl trichlorosilane (ODTS). GO (2 g) was dispersed in 200 ml of N, N dimethylformamide (DMF) and dispersed through ultrasonication for about 30 min. ODTS) (2.0 ml) was added to a suspension. The mixture was stirred under a nitrogen atmosphere at room temperature reflux for 2 h. The

MOST WIEDZY Downloaded from mostwiedzy.pl

TABLE 1 Formulation of mixers

Sample	Weight of QM(Phr)	Weight of SiGO(Phr)	DCP (Phr)
QM	100	0	1.5
QMSiGO 0.25	100	0.25	1.5
QMSiGO 0.5	100	0.5	1.5
QMSiGO 1	100	1	1.5
QMSiGO 2	100	2	1.5

Note: Phr, parts per hundred rubber.

TABLE 2 Stretching frequencies and corresponding functional groups

Stretching frequency	Functional group
1337, 3412 cm^{-1}	O—H (carboxyl)
1720 cm^{-1}	C=O carbonyl
1092 cm^{-1}	C—O (epoxy or alkoxy)
1627 cm^{-1}	C=C
2918 and 2848 cm^{-1}	$-CH_2$ stretching

precipitate was collected by centrifugation and then washed with DMF, ethanol, and water. It was then dried and converted into powder form. The resulting functionalized GO material is obtained and referred to as SiGO.

3 | RESULTS AND DISCUSSIONS

Figure 2 shows that the FT-IR spectra of pristine GO show O—H (carboxyl) at 1337 and O—H at 3412 cm^{-1} originated from the carboxylic acid. The spectra also confirm various functionalities in carboxylic acid and carbonyl moieties at 1720 cm^{-1}, as shown in Table 2. After silane treatment, the intensities of IR peaks associated with oxygen functions drop dramatically or disappear. The FT-IR spectra of SiGO show two new peaks at 2918 and 2848 cm^{-1} resulting from the $-CH_2$ stretching of the octadecyl chain together with the peak at 720 cm^{-1}, confirming the silane modification on the surface of GO.

Figure 2b shows the Raman spectra of GO, SiGO. Two main features generally represent Raman spectra of graphitic materials: The G mode, originating from the first-order scattering of E_{2g} photons by graphitic sp^2 carbon atoms, and the D band, emerging from a breathing mode of k-point photons with A_1g symmetry due to defects, are the two principal features of graphitic Raman spectra.[28] The D band of GO is located at 1350 cm^{-1} with a broader peak in the current study due to oxidation, suggesting the loss of the in-plane sp^2 feature and the creation of imperfections in the sheets. Due to solitary, double bonds that vibrate at higher frequencies than the D- band,

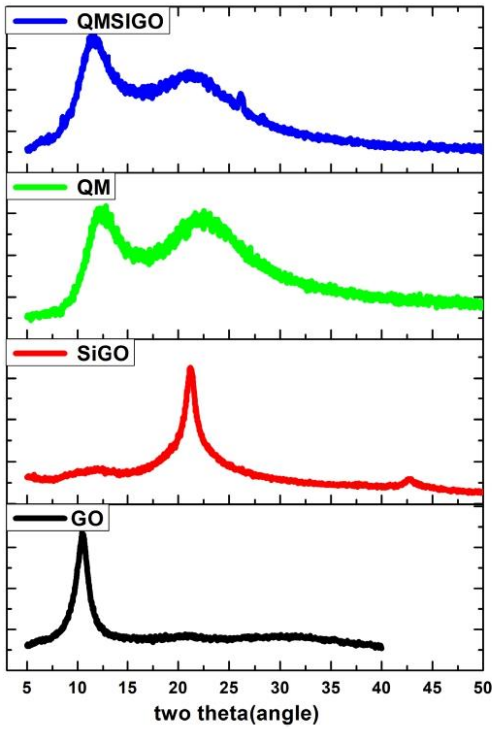

FIGURE 3 XRD spectrum of GO, SiGO, QM, and QMSiGO nanocomposite [Color figure can be viewed at wileyonlinelibrary.com]

the G- band of GO became more dominant and shifted to 1598 cm^{-1}. The Raman spectrum of SiGO is in line with the graphene, indicating a successful functionalization.

The XRD patterns of Graphene oxide, SiGO, and QMSiGO nanocomposite are illustrated in Figure 3. The evaluation of XRD patterns of GO and SiGO revealed that the characteristic peak of GO at 2θ – 10.54°(d = 0.83 nm) was gone in SiGO, whereas new peaks formed at 2θ-21.20 (d = 0.41 nm) and 43.03 (d = 0. 21 nm) for SiGO. These

MOST WIEDZY Downloaded from mostwiedzy.pl

TABLE 3 Cure characteristics of QMSiGO composites

Sample	M_L dNm	M_H dNm	ΔM dNm	Scorch time ts_2 (min)	Cure time t_{90} (min)	Cure rate index (min^{-1})
QM	5.34	8.46	3.12	2.81	4.26	68.97
QMSiGO 0.25	6.12	9.12	3.42	2.58	3.84	78.74
QMSiGO 0.5	6.24	9.84	3.60	2.38	3.70	76.07
QMSiGO 1	6.84	11.24	4.40	1.97	3.19	81.97
QMSiGO 2	6.74	8.64	1.90	2.42	3.84	70.42

findings demonstrated that the lattice geometry of GO altered during the silylation process and the implementation of the surface's attached functional groups, implying that the GO sheets were completely exfoliated.[29] Silicone rubber shows a diffraction peak around 11.28° (d spacing of 0.78 nm) and a broad peak at 21.43° (d = 0.41 nm). On the other hand, in the XRD pattern of QMSiGO nanocomposite, the addition of SiGO results in a slight left shift observed at a peak around 2θ- 21.6°. The nanocomposites show similar peaks to the pure sample, but the two-theta value was altered to a lower value by adding silane-modified graphene oxide. Exfoliation of graphene oxide in the QM matrix is responsible for the drop in peak intensity and the change in the value of 2 theta at lower levels.[30]

3.1 | Cure characteristics

Table 3 shows the characteristic parameters of QM compound vulcanization. Minimum torque (M_L) is a measure of the rubber vulcanizates' stiffness; maximum torque (M_H) represents the extent of cross-linking (modulus) of the nanocomposites. It is generally correlated to hardness, stiffness, or modulus of a rubber compound. However, M_H value for QMSiGO 2 is lower, which could be owing to lesser crosslinking. The maximum torque (M_H) increased with the addition of SiGO. When both silane coupling agents were employed, the results were better than when they were not. The rubber chain's crosslinking concentration has increased. ΔM shows the difference between M_H and M_L, and minimum torque (ts_2) is the main cure parameter, slightly changed with the addition of fillers, implying that the fillers have no impact on the precuring time. During the rheometric experiments, the minimum torque (M_L) matched to the viscosity of the uncured rubber compounds. As a result, the kind of curing method had an effect on the viscosity of the uncured QM compounds loaded with SiGO. The viscosity of the SiGO filled rubber compounds was significantly higher than that of QM. This was due to the use of SiGO with a very large specific surface area, which raised the viscosity and stiffness of the rubber compounds. It should be observed that the uncured QM compounds containing SiGO had a lower M_L and hence a lower viscosity than the reference sample QM. ΔM is commonly associated with cross-linking networks and interactions between filler and rubber. Compared to the pure QM, the degree of cross-linking of the rubber composite improved by adding SiGO due to the development of filler-filler networks.[31]Table 1 depicts the variance in cure time of QM and SiGO filled silicone rubber composites at various filler loadings. The cure time for SiGO served silicone rubber composite decreases with increasing filler loading, showing a significant increase in cure rate; however, the cure time for SiGO filled silicone rubber compound reduces with increasing loading until 1 phr, after which $\mathbf{t_{90}}$ gradually increases with SiGO loading. QM compounds including SiGO had a significantly shorter optimal vulcanization time than pure QM. When compared with the nea QM. system, using SiGO resulted in a significantly greater cure rate. This was owing to the SiGO's accelerated action. The curing rate of rubber composite is influenced by many filler-related parameters, such as particle size, surface area, surface reactivity, and moisture content of fillers.[32] The scorch time (ts_2) for SiGO filled silicone rubber composite reduces with increasing loading up to 1phr, after which $\mathbf{ts_2}$ increases as SiGO loading increases. The values of both the minimum and maximum torque of the fillers filled QM compounds grew as the SiGO filler loading increased, as shown in table 2. This suggested that adding filler to the rubber matrix increased the viscosity and modulus of the rubber composites.

3.2 | Mechanical properties

The table 4 shows the changes in tensile strength and elongation at the break of the QMSiGO composite when different amounts of SiGO are added. Nanofillers can strengthen the stiffness of the polymer matrix while weakening its toughness. Figure 4 shows a small quantity of filler added to the polymer will vulcanize with the filler as the cross-linking point, increasing the polymer's cross-linking density and tensile strength.[33] Table 4 demonstrates that the addition of small amounts of SiGO (1 phr) resulted in a

MOST WIEDZY Downloaded from mostwiedzy.pl

TABLE 4 Mechanical properties of QMSiGO nanocomposites with different SiGO concentration

Sample	Tensile strength	Elongation at break	Modulus at 100% (MPa)	Tear strength	Hardness (shore A)	Poisson ratio
QM	6.40 ± 0.34	380 ± 30	2.28	18.45 ± 1.13	56	0.49
QMGO 1	6.10 ± 0.84	262 ± 20	2.13	17.93 ± 1.24	52	0.48
QMSiGO 0.25	6.82 ± 0.54	280 ± 30	2.33	20.54 ± 0.74	58	0.47
QMSiGO 0.5	6.86 ± 0.40	290 ± 20	2.36	21.26 ± 1.40	57	0.45
QMSiGO 1	7.06 ± 0.05	274 ± 30	2.39	22.05 ± 1.12	60	0.44
QMSiGO 2	6.80 ± 0.17	260 ± 26	2.36	20.50 ± 0.95	58	0.44

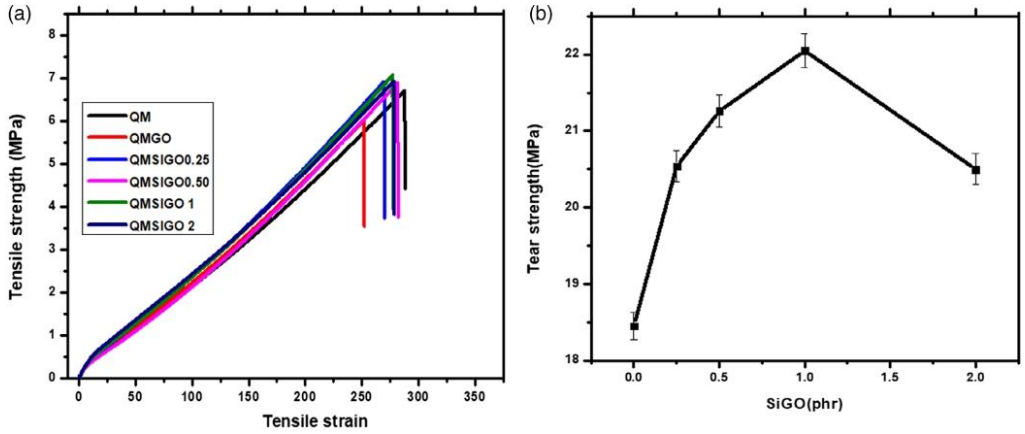

FIGURE 4 (a) Stress–strain curve and (b) tear strength of QMSiGO nanocomposites [Color figure can be viewed at wileyonlinelibrary.com]

significant increase in modulus, demonstrating the strong reinforcing effect of these fillers. When there is an excessive amount of filler, the interaction between polymer chain segments weakens and the tensile strength decreases. This might be the reason for the lower tensile strength of QMSiGO2. By enhancing interaction between the polymer matrix and the nanoparticles, the specific surface area can improve the stiffness of the polymer matrix.

Furthermore, good interaction between the filler and the polymer can improve tensile strength. The addition of unmodified GO to silicone rubber reduces tensile strength in QMGO, owing to the existence of highly polar functions bound to the surface of GO, which makes the interaction very weak. Whereas substituting SiGO enhances mechanical properties. This suggests that silane modification of graphene oxide improves filler-matrix compatibility. Tensile results reveal that silane functionalization groups significantly improve the interfacial adhesion between the filler and the host matrix. The morphological study of the tensile fracture surface using a scanning electron microscope also confirms this result. With the addition of SiGO, the hardness values of the composite improve considerably. Modulus at 100% increases with SiGO concentration, with QMSiGO1 obtaining the greatest value of all. The addition of SiGO to QM, increased the stiffness of the emerging nanocomposites. This could be due to the fact that the filler partially occupies the free volume portion, preventing polymer chains from freely rotating. When a load is applied, the stress is distributed evenly throughout the matrix, which improves the tensile and tear strength. But the filler, on the other hand, refuses QM to undergo rearrangement to accept additional stress, resulting in decreased elongation.[25] The evolution of the Poisson's ratio (v) Equation 1, in both unfilled (a) and filled (b) QMSiGO nanocomposites is shown in table 4. it is decreases with filler loading. We can observe a small linear decrease of v from 0.49to 0.44 in the case of filled rubbers.

$$\text{Poissons ratio}(v) = \text{lateral strain}/\text{Longtitudinal strain} \quad (1)$$

MOST WIEDZY Downloaded from mostwiedzy.pl

Figure 5 shows that silane-modified graphene oxide has good homogeneity and dispersion in composites, with no visible aggregates or voids. This is owing to the interfacial solid compatibility of SiGO and matrix. When compared with QMSiGO nanocomposites, crack propagated easily across the matrix in the case of neat QM. The fracture surface of QMSiGO2 composites appears rougher, and some gaps are visible in the composites. QMSiGO1 composites, on the other hand, have a smoother texture and a lower number of holes. Its exceptional mechanical qualities are supported by it. Increased filler loading reduces the smoothness of the composites' surface. Several factors influence tensile strength, including (1) filler dispersion, (2) polymer structure, and (3) molecular alignment. By dispersing the load evenly across the matrix material and minimizing the availability of stress localized sites, more evenly distributed will solve the defects.[30]

3.3 | Dynamic mechanical analysis

The dynamical mechanical study demonstrates synergistic intercalation due to solid network architecture. The storage modulus (G′) and loss factor (tan d) experiments are shown in Figure 5. Figure 6a shows the storage moduli (E′) of QM and QMSiGO composites from −130 to 30°C. The storage modulus of QMSiGO composites is higher than that of pure QM, indicating that SiGO has a reinforcing effect on QM, as seen in the figure. This demonstrates that silane modification promotes the dispersion of fillers in QM matrixes. With the addition of filler, the storage modulus of QMSiGO composites increases.[31] The increased intermolecular bonding caused by the more excellent dispersion of SiGO in the QM matrix results in a larger storage modulus for QMSiGO 1. SiGO's increased reinforcement allows for better heat and stress transport while maintaining matrix adherence. The higher the storage modulus, the higher the stiffness, indicating that composition QMSiGO 1 has a higher stiffness than QM.

In most cases, the storage modulus is utilized to determine the elastic characteristics of a polymeric-based material. The curves illustrate that the storage modulus has a high value at low temperatures and then steadily drops as the temperature rises. DMA analysis is a valuable tool for revealing the microscopic relaxation motion of polymer molecules. It is known that the temperature at which tan delta reaches its maximum is considered to be the glass transition temperature (T_g) of the material.

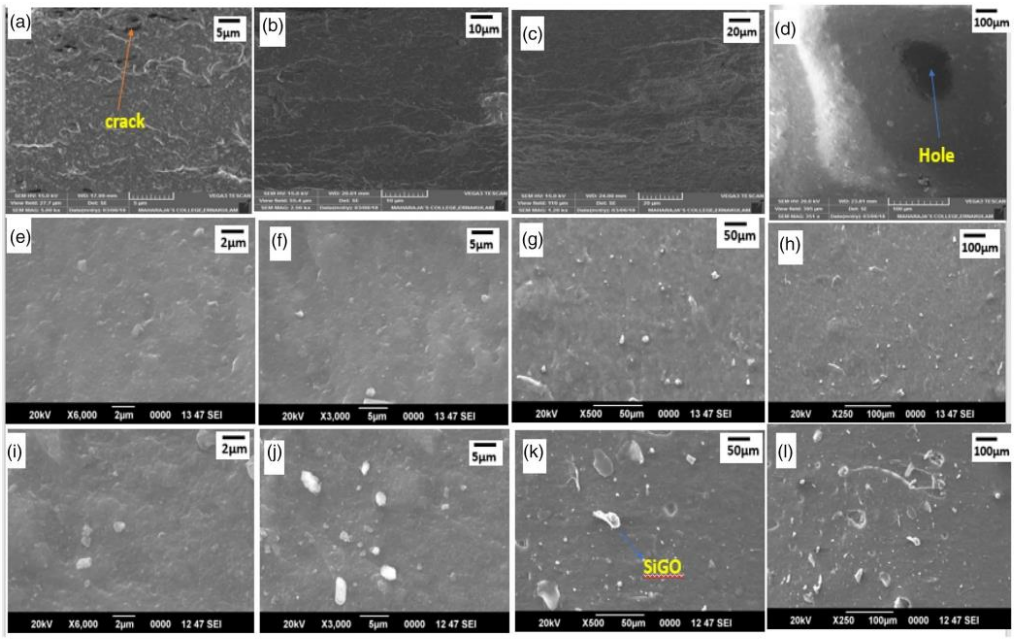

FIGURE 5 SEM picture of the tensile stretch section of pure (a-d) QM, (e-f) QMSiGO1 and (i-l) QMSiGO2 nanocomposites [Color figure can be viewed at wileyonlinelibrary.com]

MOST WIEDZY Downloaded from mostwiedzy.pl

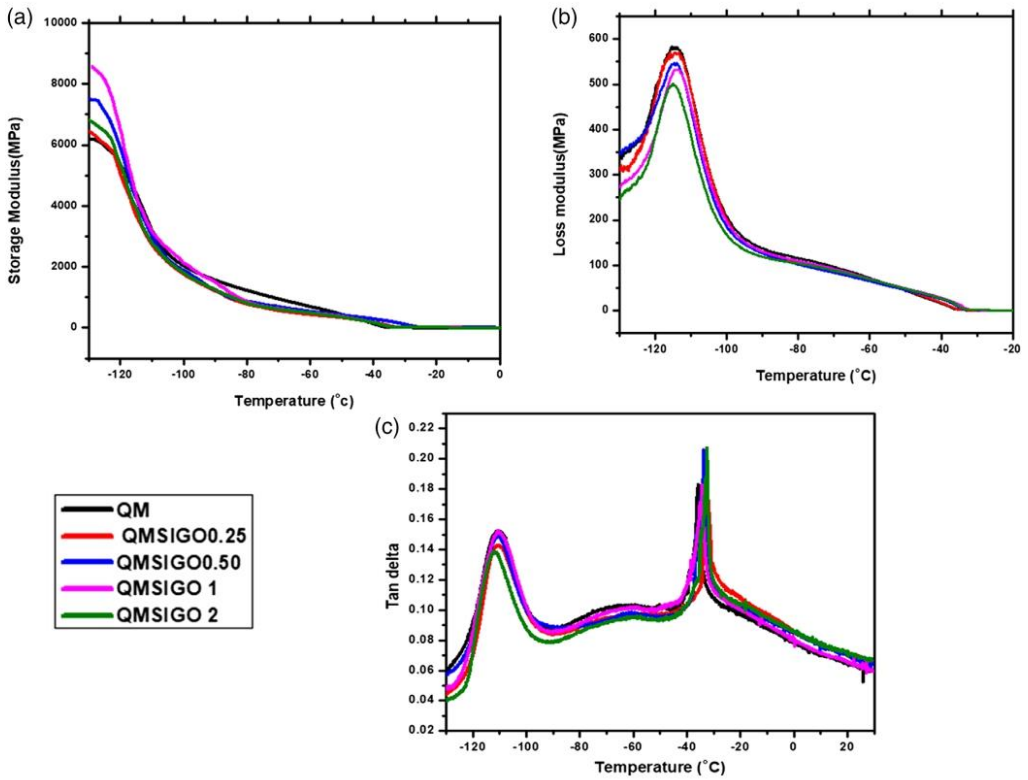

FIGURE 6 Differences in (a) storage modulus, (b) loss modulus, and (c) (tan) delta for QM and QMSiGO nanocomposites as a function of the temperature [Color figure can be viewed at wileyonlinelibrary.com]

The shift from the glassy to rubbery state happens in the intermediate region of the curves (around −112°C. This area denotes the beginning of chain mobility.[34] The T_g did not vary appreciably when the SiGO was introduced or when the crosslinking density was changed. These findings suggest that QMSiGO can operate at a wide variety of temperatures.[35] This pattern is consistent across all compositions and is related to the matrix's strengthening of filler components.

The loss modulus is a measurement of energy dissipation, but it is also a measure of a material's hardness or stiffness as a modulus. Figure 6b QMSiGO 1 has a lower loss modulus than QM. Owing to the difference in coefficients of thermal expansion of polymer and fillers, typical values of loss modulus due to filler particle-particle slippage are resisted at low temperatures. More heat was dissipated as a result of particle-particle slippage. The peak values of loss modulus grow as the amount of SiGO in the silicone (QM) matrix increases. The loss modulus has a high peak value, indicating broken intermolecular bonding.[36] QMSiGO 1 composites have a substantially lower tan delta Figure 6c than QM composites. In amorphous polymers, a drop in the α-transition peak height can be linked to increased cross-linking density. In Figure 6c, β- the transition peak observed around −30°C temperature of melting (T_m). Furthermore, silane modification of graphene surface leads to the lowering the tan delta of QMSiGO 1 composite, the less likely it is to re-agglomerate and form a tight network architecture. According to the literature, the insertion of any nanocarbon decreases the peak value of tan delta.[37]

3.4 | Differential scanning calorimetry

Figure 7 illustrates the DSC thermogram of nanocomposites. The samples were heated from −80 to −20°C at a rate of 10°C min^{-1}. The endothermic peak of

MOST WIEDZY Downloaded from mostwiedzy.pl

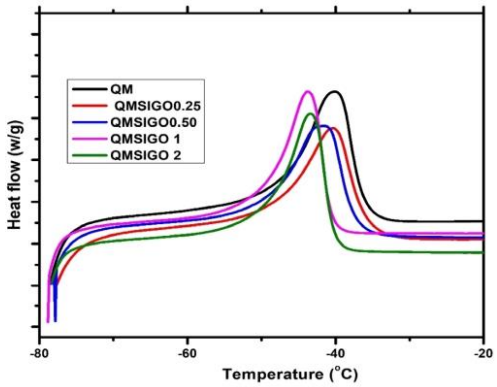

FIGURE 7 DSC thermogram of silicone rubber nanocomposites [Color figure can be viewed at wileyonlinelibrary.com]

second heating was used to determine the T_m. Despite repeated heating, the temperature remains constant during melting. Melting is an endothermic process that necessitates heat absorption. Despite repeated heating, the temperature remains constant during melting. During this time, the energy added is used to melt the crystalline areas, not to enhance the kinetic energy of the chains already in the melt.[38] The DSC melting temperatures for QMSiGO samples and the QM are shown in Table 5. The melting temperatures, Tm, of the neat QM (−40°C) and QMSiGO samples (−41.3°C) are not distinguishable.

3.5 | Thermogravimetric analysis

TGA plot showing the variation of weight% of the QMSiGO sample with an increase in temperature is given in the Figure 8. Silicone rubber has significantly higher heat stability than other synthetic rubbers. TGA footprints of unfilled silicone rubber and silicone rubber filled with 0.25–2 phr of filler (silane modified graphene oxide) are tabulated in Table 6. The filled silicone rubber decomposition temperatures were higher than the unfilled silicone rubber. The following are most likely the explanations for the increase in decomposition temperatures of loaded silicone rubber: When the active centers of the silicone molecular chain came into touch with the filler, it may have become inactive.[39] The thermal stability of the QM nanocomposites was not affected by the presence of SiGO up to 400°C. The table reveals that introducing signs into the QM matrix improves the thermal stability of the nanocomposites observed.

TABLE 5 DSC melting temperature (T_m) for QMSiGO nanocomposites

Sample	T_m (DSC) (°C)
QM	−40.2
QMSiGO 0.25	−41.3
QMSiGO 0.5	−43.7
QMSiGO 1	−43.3
QMSiGO 2	−43.2

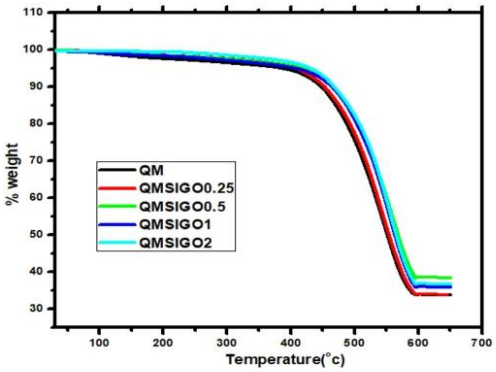

FIGURE 8 (a) TGA plot of QMSiGO nanocomposites [Color figure can be viewed at wileyonlinelibrary.com]

Compared with pure silicone rubber, the filled rubber's initial degradation temperature was higher. The increased initial decomposition temperature of the QMSiGO composite could be attributed to SiGO's thermal solid stability.[40] For example, the T_{50} of QM is 546°C, but it is 552°C for the composite with 2 phr. There is a marginal temperature difference of around 6°C.

3.6 | Tribological properties

Tribological properties of the nanocomposite studied using a Pin on disc instrument (Ducom). Pin-shaped specimen was fixed to a sample holder using screws. Pin-on-disc experiments were carried out with a hardened ground steel disc (EN 31, hardness 60 HRC) at various loads and temperatures under the ASTM G99 standard. In the tribological experimental data above (Figure 9), the composite's coefficient of friction (COF) concerning the time at various filler concentrations is displayed. As the sliding distance grew, the friction coefficient gradually shot up. This was because as the sliding distance increased, small wear particles formed between both the

MOST WIEDZY Downloaded from mostwiedzy.pl

Sample	T_{10} (°C)	T_{30} (°C)	T_{max}	Residue at T_{600} (%)
QM	423	505	510	34
QMSiGO 0.25	423	508	515	34
QMSiGO 0.5	428	516	530	40
QMSiGO 1	430	514	535	38
QMSiGO 2	434	511	540	37

TABLE 6 Thermogravimetric results of silcone rubber nanocomposites

QM elastomer surface and the disc. As a result, the actual contact area increased, and the friction coefficient increased.[41] There is an initial increase in COF value, and it reaches maximum, then it starts to fall and gets the maximum value of 1.43, and finally, it forms a plateau. The pure QM has the highest COF value, around 1.43, and the lowest friction coefficient value of all the composites, QMSiGO 1 composite exhibit.[42]

3.6.1 | Effect of load

Figure 10a.b shows the effect of load on the tribological performance of QMSiGO composites under applied load from 5 to 15 N. Pin on disc experiment were performed under room temperature (30°C) condition and sliding speed of 2 m/s. The frictional heat produced in the contact area increases as the applied load increases. As a result of the high deformation on the composite surface, the temperature between both the composite and the counter steel surface may rise, causing matrix softening and a drop in COF and specific wear rate, as shown in Figure 10b. The composite's COF dropped as the load rose, as seen in Figure 10a.

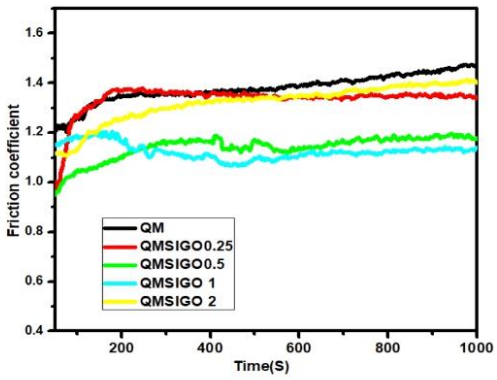

FIGURE 9 Friction coefficient of the QMSiGO nanocomposites (10 N, 2 m/s) [Color figure can be viewed at wileyonlinelibrary.com]

The steady-state values of COF versus time for QMSiGO composites under various applied stress conditions are shown in Figure 10a. In this picture, the error bars are from three replicates. The load substantially affects the COF of QMSiGO composites, as shown in this figure. The COFs for all composites exhibit a declining trend as the load increases. When the load is increased to 15 N, the COF of QMSiGO drops to 1.15. Figure 10b depicts the effect of load on the wear and friction parameters of QMSiGO composites. With increasing average load, the COF of all composites reduces significantly. Compared to a pure QM sample, the COF and wear rate of SiGO loaded composites decrease as the load increases. Compared to the 15 N load, the COF and wear rate are relatively high at low loads (5 N). Lower loads cannot chip off the SiGO layers from the surface. Therefore, as the applied load increases, the interfacial adhesion between the SiGO filler and the matrix rubber is broken. As a result, there is less friction between the surfaces, resulting in lower specific wear rates. When the load reaches 15 N, the COF and specific wear rate drop dramatically. The frictional heat produced during sliding in the contact area increases as the applied force increases. This also results in lower friction and wear rates.[3]

3.6.2 | Effect of temperature

Figure 11 depicts the average friction coefficient under various temperature environments with a sliding velocity of 2 m/s. Pin on disc experiment were performed under load 10 N and sliding speed of 2 m/s. A steady-state friction coefficient range was used to obtain the mean friction coefficient. The data demonstrated that as the hardness of the filler improved, the friction coefficient lowered. The hardness of the QM elastomer was influenced by temperature. However, it did not have a pronounced effect on the friction coefficient. Irrespective of the temperature condition, the average friction coefficient decreased when the filler loading increased. The coefficient of friction is shown to be substantially temperature-dependent, decreasing from 1.35 to 1 between 30 and 150°C. The friction coefficient decreased slowly and did not smooth out as the temperature increased. The wear rate decreases as the

MOST WIEDZY Downloaded from mostwiedzy.pl

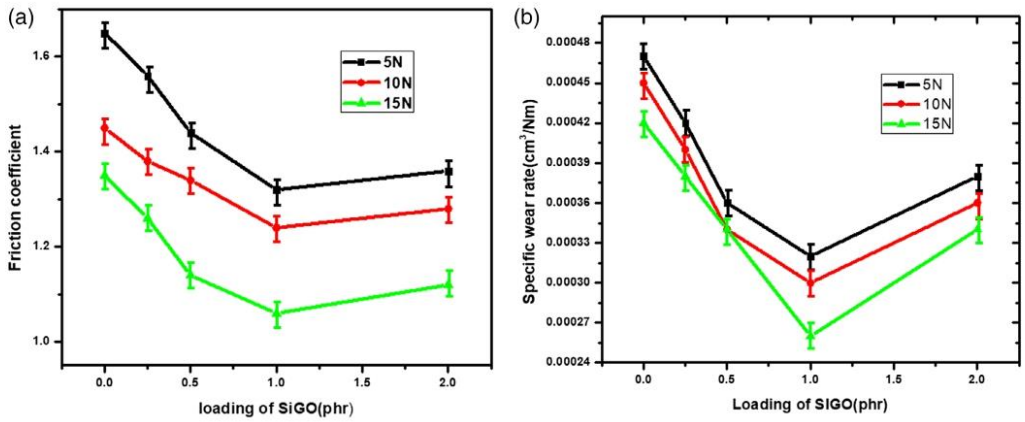

FIGURE 10 Coefficient of friction and specific wear rates of QMSiGO composites as load function (temperature-30°C, speed -2 m/s) [Color figure can be viewed at wileyonlinelibrary.com]

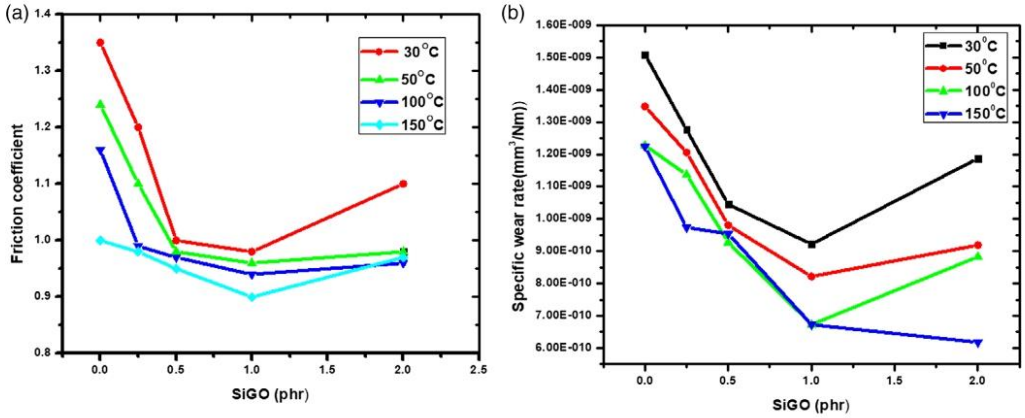

FIGURE 11 Coefficient of friction and specific wear rates of QMSiGO composites as a function of temperature (load -10 N, speed -2 m/s). Worn surface morphology of QMSiGO nanocomposites [Color figure can be viewed at wileyonlinelibrary.com]

temperature rise with the accumulated friction heat. The compounds have a low friction coefficient and wear rate at high temperatures. Heating the chamber from 25 to 150°C resulted in temperature-dependent friction measurements. Figure 11 shows a representative friction coefficient curve as a function of filler concentration. COF falls when the temperature rises from 30 to 150°C, as seen in Figure 11. It is evident that friction and wear characteristics are temperature-dependent. A test temperature of 150°C improves the performance of QMSiGO 1 composites, resulting in lower friction. It's significant to mention that the COF and specific wear rate are lowest at 150°C, while they are highest at 30°C. However, all of these examples have a small magnitude, ranging from 1.4 to 0.95. The disc's friction layer comprises loose particles that can be twisted while sliding in the contact zones at both temperatures, resulting in a mild abrasive interaction on the disc counterface.

The Figure 12 shows the worn surface morphologies of QM and QMSiGO composites. From Figure 12, the wear track generated on QMSiGO was wide. Just a few granular wear debris was found outside of the wear track. As seen in Figure 12, more significant wear debris developed at the wear track extremities. Scratch grooves were found in the worn paths, leading to debris build-up at the endpoints. The QMSiGO wear tracks were relatively

MOST WIEDZY Downloaded from mostwiedzy.pl

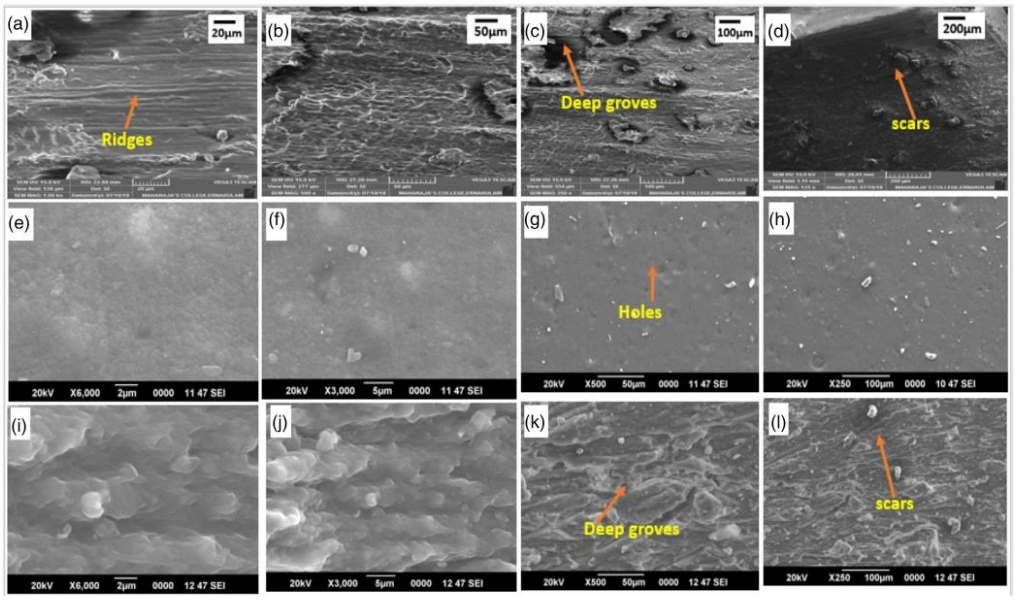

FIGURE 12 Worn surface morphologies of pure (a-d) QM, (e-f) QMSiGO1 and (i-l) QMSiGO2 nanocomposites [Color figure can be viewed at wileyonlinelibrary.com]

smooth, showing that the QMSiGO 1 surface was easily conformed to the sphere's surface during the running procedure. A careful examination of the wear tracks found several light particles embedded in or localized on the wear tracks. Rubber's visco-elastic characteristic allows it to withstand significant deformation without rupturing. Stretching and twisting chemical chains make this feasible. During sliding contact with other sliding bodies, shear stress arises on the rubber's surface. The massive internal damping energy that has been stored as a result of repetitive loading is now abruptly released. Schallamach was the first to notice this phenomenon, known as the Schallham wave.[43,44]

3.7 | Thermal conductivity

Figure 13 shows the change in thermal conductivity values of silicone rubber with different amounts of silane functionalized graphene oxide. Graphene has high thermal conductivity and an ultra-high surface area. The thermal conductivity of polymer composites depends primarily on the interaction between the thermally conductive filler and the polymer matrix.[33] When the filler content reaches 1 phr, the thermal conductivity of composites filled with silane-modified GO (0.263 W m^{-1} K^{-1}) is equal to that of

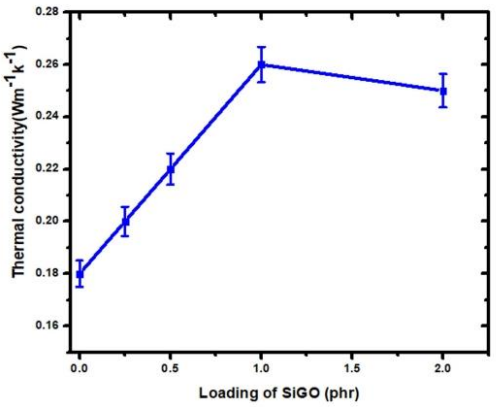

FIGURE 13 Thermal conductivity of QMSiGO nanocomposites as measured [Color figure can be viewed at wileyonlinelibrary.com]

pure phenyl silicone rubber (0.184 W m^{-1} K^{-1}). It exceeds the heat conductivity. This is because the ODTS modification improves the graphene dispersion in the QM matrix. The thermal conductivity of QMSiGO composites increases up to 1phr SiGO loading, after which it begins to decrease.

MOST WIEDZY Downloaded from mostwiedzy.pl

Because of the high filler content, aggregation develops in the matrix, and as the filler content rises, the space between graphene layers rises. These gaps are filled by air, reducing the filler-filler interaction and lowering thermal conductivity.[31] A phonon is the most common heat transport method.[45] As a result, the heat transmission of the composite is controlled by reducing phonon scattering and acoustic impedance mismatch at the filler-polymer matrix interface.[46] The compatibility and interfacial interaction of the GO and QM matrix are improved by silane-modified graphene oxide, reducing an acoustic impedance mismatch. As a result, the QMSiGO nanocomposite's thermal conductivity has enhanced even further.[47]

4 | CONCLUSIONS

In conclusion, we synthesized octadecyl trichlorosilane-modified graphene oxide. FTIR spectroscopy, Raman spectroscopy, and X-ray diffraction analysis confirmed the surface modification of graphene oxide. The two-roll mixing mill method used to incorporate silane-modified GO into the silicone matrix. The results revealed that the silicone rubber matrix and silane-modified graphene oxide have good compatibility and interfacial interaction, which was confirmed by the morphological studies of the tensile fracture surface. QMSiGO1composite possesses superior tensile, tear, and dynamic mechanic properties. The pin-on-disc tests were conducted under different load and temperature conditions. As the applied stress and temperature rise, the coefficient of friction of all composite materials diminishes. In comparison to all other composites evaluated, QMSiGO 1 exhibits the lowest friction (36%) and wear characteristics. Improvements in mechanical properties corroborate the filler material's reinforcing nature, strengthening the composite while smoothing the surface with high frictional heat, resulting in lower friction and wear properties. With the addition of 1 phr SiGO, the thermal conductivity of silicone rubber improves by over 44%. Overall, adding silane-modified graphene oxide to silicone rubber significantly improves its overall characteristics.

ACKNOWLEDGMENT

For financial aid, the authors are thankful to DRDO (Order No: ERIP/ER/1504758/M/01/1667) in New Delhi, India.

AUTHOR CONTRIBUTIONS

P. S Sarath: Formal analysis (lead); investigation (lead). **Józef T. Haponiuk:** Investigation (supporting); supervision (supporting); writing – review and editing (supporting). **Soney C. George:** Conceptualization (lead); formal analysis (equal); investigation (equal); supervision (equal); writing – review and editing (equal). **Sabu Thomas:** Supervision (lead); validation (lead); writing – review and editing (supporting).

DATA AVAILABILITY STATEMENT

The data that support the findings of this study are available on request from the corresponding author. The data are not publicly available due to privacy or ethical restrictions.

ORCID

Pampayil Sasikumar Sarath https://orcid.org/0000-0001-9222-5714

Soney C. George https://orcid.org/0000-0001-9590-3971

REFERENCES

[1] P. S. Sarath, S.V. Samson, R. Reghunath et al., *Polymer Testing* **2020**, *89*, 106601.
[2] P. S. Sarath, R. Jacob, T. Jose, J. T. Haponiuk, S. Thomas, S. C. George, *Int. J. Membr. Sci. Technol.* **2020**, *7*, 25.
[3] P. S. Sarath, G. Moni, J. J. George, J. T. Haponiuk, S. Thomas, S. C. George, *J. Compos. Mater.* **2021**, *55*, 2011.
[4] Y. Song, J. Yu, L. Yu, F. E. Alam, W. Dai, C. Li, N. Jiang, *Mater. Des.* **2015**, *88*, 950.
[5] L. Xue, Y. Zhang, Y. Zuo, S. Diao, J. Zhang, S. Feng, *Mater. Lett.* **2013**, *106*, 425.
[6] L. Bokobza, *J. Appl. Polym. Sci.* **2004**, *93*, 2095.
[7] R. Anyszka, D. Strzelecki, *Tribol. Ind.* **2015**, *37*, 154.
[8] R. Anyszka, D. M. Bieli, M. Imiela, M. Siciński, T. Gozdek, D. Strzelecki, *Tribol. Ind.* **2016**, *38*, 332.
[9] J. Liu, X. Gong, R. Zhang, *IOP Conf. Ser.: Mater. Sci. Eng.* **2018**, *301*, 012029.
[10] B. Du, Thermal conductivity and dielectric properties of silicone rubber nanocomposites. in *Progress in Rubber Nanocomposites*, Woodhead Publishing, Amsterdam **2017**, p. 495.
[11] K. S. Novoselov, A. K. Geim, S. V. Morozov, D. Jiang, Y. Zhang, S. V. Dubonos, I. V. Grigorieva, A. A. Firsov, *Science* **2004**, *306*(5696), 666.
[12] L. Gan, S. Shang, C. W. M. Yuen, S. X. Jiang, N. M. Luo, *Composites, Part B* **2015**, *69*, 237.
[13] Z. Zheng, H. Yang, X. F. Yao, *Tribol. Trans.* **2020**, *63*, 205.
[14] H. Xu, L. X. Gong, X. Wang, L. Zhao, Y. B. Pei, G. Wang, Y. J. Liu, L. B. Wu, J. X. Jiang, L. C. Tang, *Compos. Part A Appl. Sci. Manuf.* **2016**, *91*, 53.
[15] V. Kumar, D. J. Lee, *J. Appl. Poly. Sci.* **2017**, *134*, 44407.
[16] A. K. Geim, K. S. Novoselov, *Nanosci. Technol.* **2009**, *6*, 11. https://doi.org/10.1142/9789814287005_0002
[17] S. Park, R. S. Ruoff, *Nat. Nanotechnol.* **2009**, *4*, 217.
[18] D. R. Dreyer, S. Park, C. W. Bielawski, R. S. Ruoff, *Chem. Soc. Rev.* **2010**, *39*, 228.
[19] T. Ge, M. Zhang, K. Tang, H. Tang, *Mater. Chem. Phys.* **2020**, *252*, 123250.
[20] Y. Bai, H. Cai, X. Qiu, X. Fang, J. Zheng, *High Perform. Polym.* **2015**, *27*, 997.

MOST WIEDZY Downloaded from mostwiedzy.pl

[21] H. Ren, E. Cunha, Z. Li, L. Wang, I. A. Kinloch, D. Yi, A. Kretinin, Q. Sun, Z. Fan, R. J. Young, *J. Mater. Sci.* **2022**, *57*, 2683.
[22] L. Gan, S. Shang, S. X. Jiang, *Composites, Part B* **2016**, *84*, 294.
[23] J. D. Fowler, M. J. Allen, V. C. Tung, Y. Yang, R. B. Kaner, B. H. Weiller, *ACS Nano* **2009**, *3*, 301.
[24] B. M. Yoo, H. J. Shin, H. W. Yoon, H. B. Park, *J. Appl. Polym. Sci.* **2014**, *131*, 1.
[25] B. Sivakumar, N. Ranjan, S. Ramaprabhu, M. Kamaraj, *Tribol. Int.* **2020**, *142*, 105990.
[26] X. Jiao, Y. Qiu, L. Zhang, X. Zhang, *RSC Adv.* **2017**, *7*, 52337.
[27] D. C. Marcano, D. V. Kosynkin, J. M. Berlin, A. Sinitskii, Z. Sun, A. Slesarev, L. B. Alemany, W. Lu, J. M. Tour, *ACS Nano* **2010**, *4*, 4806.
[28] S. Samanta, S. Singh, R. R. Sahoo, *RSC Adv.* **2015**, *5*, 61888.
[29] S. Fathalipour, M. Mardi, *Mat. Sci. Eng.: C*, **2017**, *79*, 55.
[30] G. Moni, A. Mayeen, A. Mohan, J. J. George, S. Thomas, S. C. George, *Eur. Polym. J.* **2018**, *109*, 277.
[31] Z. Zhang, P. Chen, W. Nie, Y. Xu, Y. Zhou, *Polymer* **2020**, *203*, 122772.
[32] L. C. Sim, C. K. Lee, S. R. Ramanan, H. Ismail, K. N. Seetharamu, *Polym. Plast. Technol. Eng.* **2006**, *45*, 301.
[33] Y. Xu, Q. Gao, H. Liang, K. Zheng, *Polym. Test.* **2016**, *54*, 168.
[34] S. H. Masood, W. Q. Song, *Mater. Des.* **2004**, *25*, 587.
[35] L. Guo, X. Yang, F. Dong, Y. Qian, J. Guo, X. Lin, H. Shaghaleh, W. Liu, X. Xu, S. Wang, S. Liu, *Mater. Chem. Phys.* **2020**, *247*, 122868.
[36] K. S. Boparai, R. Singh, *Encyclopedia of Materials: Composites*, 1st ed., Vol. 1, Elsevier Ltd, Amsterdam **2018**, p. 774. https://doi.org/10.1016/B978-0-12-803581-8.11409-2.
[37] M. J. Wang, *Rubber Chem. Technol.* **1998**, *71*, 520.
[38] M. F. At, Investigation of Polymers with Differential Scanning Calorimetry Contents Introduction Thermal Properties of a Polymer Heat Capacity
[39] S. Wang, C. Long, X. Wang, Q. Li, Z. Qi, *J. Appl. Polym. Sci.* **1998**, *69*, 1557.
[40] X. Wang, W. Dou, *Thermochim. Acta* **2012**, *529*, 25.
[41] C. Lian, K. H. Lee, C. H. Lee, *Tribol. Trans.* **2018**, *61*, 238.
[42] Q. He, A. Li, Y. Zhang, S. Liu, Y. Guo, L. Kong, *Tribol. Mater. Surf. Interfaces* **2018**, *5831*, 1.
[43] A. Mukhopadhyay, *Polym. Test.* **2016**, *52*, 167.
[44] A.G.V.G.V. Schallamach, *Proc. Phys. Soc. B*, **1953**, *66*, 386.
[45] J. Shen, T. Li, Y. Long, N. Li, M. Ye, *Soft Mater.* **2013**, *11*, 326.
[46] N. M. Barkoula, B. Alcock, N. O. Cabrera, T. Peijs, *Polym. Polym. Compos.* **2008**, *16*, 101.
[47] Y. Hu, J. Shen, N. Li, H. Ma, M. Shi, B. Yan, W. Huang, W. Wang, M. Ye, *Compos. Sci. Technol.* **2010**, *70*, 2176.

How to cite this article: P. S. Sarath, S. Thomas, J. T. Haponiuk, S. C. George, *J. Appl. Polym. Sci.* **2022**, e52299. https://doi.org/10.1002/app.52299

MOST WIEDZY Downloaded from mostwiedzy.pl

Publication -8:

Study the synergistic effect of fumed silica and reduced graphene oxide insertion on the thermal, mechanical, tribological, and solvent transport properties of silicone rubber nanocomposites

Abstract

This study explored the effects of hybrid nanofillers such as fumed silica ($FSiO_2$) and reduced graphene oxide (rGO) on the mechanical, thermal, solvent transport, and tribological properties of silicone rubber nanocomposite (QMSirGO). A pin-on-disc test system was used to investigate the friction and wear properties of QMSirGO nanocomposites, which were significantly influenced by the applied load, temperature, and rGO concentration. Study shows that better graphene oxide dispersion in the matrix paved the way for improved tensile and dynamic mechanical properties and lowered the coefficient of friction (COF) and specific wear rate (Ws) values. Compared to silicone rubber (QM), the friction coefficient of the QMSirGO1.5 composite was reduced by around 40%. The mechanism involves the formation of a lubricant layer, which smooths the material surface that comes into contact with the metal surface. In the solvent transport study, we investigated the effect of solvents' structure, molecular size, filler concentration, and the transport mechanism of composites, and the extent of reinforcement was evaluated using Kraus equations.

Methodology

- Preparation of hybrid silicone rubber nanocomposite
- Study the mechanical, thermal and tribological properties
- Analyse the tensile fracture surface and worn surface

MOST WIEDZY Downloaded from mostwiedzy.pl

Received: 8 January 2022 | Revised: 14 April 2022 | Accepted: 30 April 2022
DOI: 10.1002/app.52820

RESEARCH ARTICLE

Applied Polymer SCIENCE WILEY

Study the synergistic effect of fumed silica and reduced graphene oxide insertion on the thermal, mechanical, tribological, and solvent transport properties of silicone rubber nanocomposites

Pampayil Sasikumar Sarath[1,2] | **David Pahovnik**[3] | **Petra Utroša**[3] | **Ozgun Can Onder**[3] | **Sabu Thomas**[4] | **Józef T. Haponiuk**[2] | **Soney C. George**[1]

[1]Centre for Nanoscience and Technology, Amal Jyothi College of Engineering, Kottayam, India
[2]Department of Polymer Technology, Chemical Faculty, University of Technology, Gdansk, Poland
[3]Department of Polymer Chemistry and Technology, National Institute of Chemistry, Ljubljana, Slovenia
[4]International and Inter-University Centre for Nanoscience and Nanotechnology, Mahatma Gandhi University, Kottayam, India

Correspondence
Soney C. George, Centre for Nanoscience and Technology, Amal Jyothi College of Engineering, Kanjirappally, Kottayam, Kerala, India.
Email: soneygeo@gmail.com

Funding information
Defence Research and Development Organisation, Grant/Award Number: ERIP/ER/1504758/M/01/1667

Abstract
This study explored the effects of hybrid nanofillers such as fumed silica ($FSiO_2$) and reduced graphene oxide (rGO) on the mechanical, thermal, solvent transport, and tribological properties of silicone rubber nanocomposite (QMSirGO). A pin-on-disc test system was used to investigate the friction and wear properties of QMSirGO nanocomposites, which were significantly influenced by the applied load, temperature, and rGO concentration. Study shows that better graphene oxide dispersion in the matrix paved the way for improved tensile and dynamic mechanical properties and lowered the coefficient of friction and specific wear rate (Ws) values. Compared to silicone rubber (QM), the friction coefficient of the QMSirGO1.5 composite was reduced by around 40%. The mechanism involves the formation of a lubricant layer, which smooths the material surface that comes into contact with the metal surface. In the solvent transport study, we investigated the effect of solvents' structure, molecular size, filler concentration, and the transport mechanism of composites, and the extent of reinforcement was evaluated using Kraus equations.

KEYWORDS
friction, mechanical properties, thermal properties, wear and lubrication

1 | INTRODUCTION

Silicone rubber (QM) has distinctive qualities originating from its unique molecular structure.[1] It has been widely employed to substitute petrochemical goods in various companies, including aerospace, automobiles, construction, electronics, medical, and food processing. The unique hydrogen bonding interactions among silica surfaces, silanol groups, and the polydimethylsiloxane chain significantly impact this interaction coefficient.[2–6] Graphene is a two-dimensional substance with outstanding electron transport, mechanical properties, and a large surface area that has attracted scientific attention.[5] Graphene has also been considered a strategic candidate to strengthen polymeric materials for a wide variety of uses such as structures, automotive, filtration, packaging, electronics, aerospace, electromagnetic interference (EMI) shielding, and so on.[6–10] Stacked graphene materials have piqued researchers due to their anti-friction, anti-wear, and good self-lubricating qualities. In earlier research, we

 © 2022 Wiley Periodicals LLC.

MOST WIEDZY Downloaded from mostwiedzy.pl

used reduced graphene oxide (rGO) to create silicone rubber nanocomposite, which improved silicone rubber's mechanical, tribological, and thermal properties.[3] Zhao et al. established a new approach for manufacturing graphene–SiO_2 hybrid fillers using hydrogen bonding self-assembly interaction, which considerably improves natural rubber composites' mechanical and thermal properties.[11] The investigation of solvent sorption characteristics of a composite material helped to understand the behavior of nanocomposites in a chemical environment and the morphology and interfacial interaction of the system.[12] Nanofiller-based polymer composites have emerged as one of the most appealing areas in material research.[13]

It is critical to understand polymer transport mechanisms better to make major improvements in areas like seals and o-rings.[14] The diffusion is a dynamical parameter that is affected by various factors. The free volume within the matrix, the nature of the polymer, cross-link density, nature of fillers, penetrant size, temperature, and degree of reinforcement are all factors to consider. Rubber-based nanocomposites are of critical importance in polymer science. Silicone rubber is utilized in a variety of applications, including automobiles, sealants, and adhesives. Different nanoforms, such as carbon nanotubes,[15] nanofibers, and silica nanoparticles,[16] can be incorporated into silicone elastomers to increase their mechanical, thermal, dynamic, and barrier properties.

Nanoscience and nanotechnology provide remarkable chances to combine breakthrough nanoscale fillers with polymer materials to produce polymer nanocomposites with fascinating features.[17] Advances in improving the mechanical and tribological properties of polymer nanocomposites have received much interest because polymer nanocomposites exhibit lightweight, high strength, thermal stability, anti-wear, and solvent resistance.[18–20] In practice, friction between rubber composite components such as tyres, wiper blades, conveyor belts, and seals, among others, is critical. Rubber friction is relatively high when compared to other polymers or plastics. Friction and wear are two significant issues that affect performance and machine productivity. As a result, this is an area with high research potential.[21] Torbati-Fard et al. study the effects of the surface modification of silica by low-molecular-weight hydroxyl-terminated polybutadiene are compared with those of bis(3-triethoxysilylpropyl)tetrasulfide (TESPT) on the mechanical, viscoelastic, and tribological properties of styrene-butadiene rubber vulcanizates.[22] Liu et al. examined the molecular mechanism of improving the mechanical and tribological properties of nitrile rubber (NBR) by adding nano-SiO_2.[23,24]

According to earlier research, adding fumed silica ($FSiO_2$) to the silicone rubber reduced the friction coefficient considerably.[16] The nanoparticles exhibit a beneficial rolling effect, according to the surface wear study of the nanocomposite. Out of all the composites tested, the 3 phr fumed silica loaded composite had the lowest friction coefficient. So in this work, we varied the graphene oxide concentrations while keeping the $FSiO_2$ concentration at 3 phr in all composites. Akhilesh et al. developed nanocomposites of ethylene propylene diene monomer (EPDM) rubber and silicone rubber blends by reinforcing with nano-silica. Because of the efficient filler network that resists solvent penetration. Solvent transport study shows that the KorsmeyerPeppas model provided the most excellent fit for solvent sorption in nanosilica-reinforced EPDM—silicone rubber nanocomposites.[25]

This research aimed to study the synergistic effect of fumed silica and rGO on the mechanical, tribological, thermal, and solvent transport properties of the QMSirGO nanocomposites. The study also expanded to investigate the tribological properties of the QMSirGO nanocomposites. Graphene-based hybrid combinations have recently been suggested as potential candidates for use as hybrid fillers in high-performance polymer nanocomposites. In our previous work, addition of fumed silica in silicone rubber matrix there is a great improvement in the mechanical, thermal and tribological properties.[16] While these achievements are amazing, there is still little research on the synergistic effect of graphene and silicon dioxide ($FSiO_2$) hybrids in elastomer composites especially in the case of tribological studies. This study also looks into the effect of different solubility parameter on the diffusion transport characteristics and evaluate the compatibility and reinforcing effects of silica and graphene as fillers in the QM matrix. In state-of-the-art, no studies on the diffusion behavior of fumed silica and graphene through the QM rubber matrix have been published.

2 | MATERIALS AND METHODS

The fumed silica was purchased from Sigma Aldrich, Bangalore, India and SH5060-U (HTV) silicone rubber was purchased from Korea KCC Corporation. It is a general-purpose grade with a low level of vinyl content. Graphene was produced by modified Hummer's method with graphite as the starting material. Details of the materials used are included in the supplementary materials (Appendix S1). The properties of rGO, silicone rubber and fumed silica are placed in Tables S1–S3 (Appendix S1), respectively.

2.1 | Composite preparation

The silicone rubber and fumed silica (3 phr) were thoroughly mixed in a two-roll mill for 2 min followed by

MOST WIEDZY Downloaded from mostwiedzy.pl

adding rGO (mix for 2 min) then incorporate the curing agent. According to the formulation is given in Table 1. The total mixing of each sample took about 20 min. "ASTM D-1646" standard was used for the cure time analysis. The QMSirGO samples were hot pressed at 150°C for the respective cure time and post cured at 200 °C for 4 h in a hot air oven. The schematic representation of the preparation of the composites is given in Figure 1.

2.2 | Characterization techniques

Fourier transform infrared (FT-IR) spectroscopy, X-ray diffraction (XRD) analysis, and Raman spectroscopic analysis were used to analyze the synthesized GO and ILGO. FTIR analysis was characterized using Perkin Elmer at a spectrum range of 4000–500 cm^{-1}. The mechanical properties of the QMILGO nanocomposites were investigated using an INSTRON-4411 pneumatic universal testing system with a moving crosshead speed of about 500 mm/min. The samples' tear strength was determined using the ASTM D-1424 standard. Scanning electron microscopy (SEM) on an HR-SEM Zeiss Ultra plus instrument was used to examine the morphology of the samples (Carl Zeiss, Germany). The samples were coated with a 10 nm gold coating for charge dissipation during SEM analysis using a Gatan PECS 682. (Gatan, USA). On a DMA Q800, the dynamic mechanical analysis was carried out (TA Instruments, USA). Samples were cut into a rectangular shape (approximate length 13.0 mm, width 2.5 mm, and thickness 2.0 mm). The viscoelastic properties were measured at a frequency of 1 Hz, strain amplitude of 5 μm in a temperature range from −140 to 30°C with the heating rate of 2°C min^{-1}. The glass transition temperature (T_g) was observed as the peak of tanδ curve, and melting temperature (T_m) was observed as a drop-in storage modulus. The results are given as an average of three measurements, with a standard deviation. The thermal conductivities of the composites were studied using ASTM D5470 and Holmarc's Lee's Disc Apparatus (Model: HO-ED-M-03). The detailed explanation of solvent transport experiment and tribological studies are given in supporting information (Appendix S1).

TABLE 1 Compounding ingredients of QMSirGO nanocomposite

Sample	QM	Fumed silica ($FSiO_2$)	Reduced graphene oxide (rGO)	Dicumyl peroxide (DCP)
QMSi	100	3	0	1.5
QMSirGO 0.5	100	3	0.5	1.5
QMSirGO 1	100	3	1	1.5
QMSirGO 1.5	100	3	1.5	1.5
QMSirGO 2	100	3	2	1.5
QMSirGO 2.5	100	3	2.5	1.5

Abbreviations: phr, parts per hundred rubber; QM, silicone rubber; QMSirGO, mechanical, thermal, solvent transport, and tribological properties of silicone rubber nanocomposite.

3 | RESULTS AND DISCUSSIONS

Figure 2 illustrates the FT-IR spectrum of GO, rGO, and $FSiO_2$ nanoparticles. The presence of multiple oxygen-containing functional groups in the FT-IR spectrum of

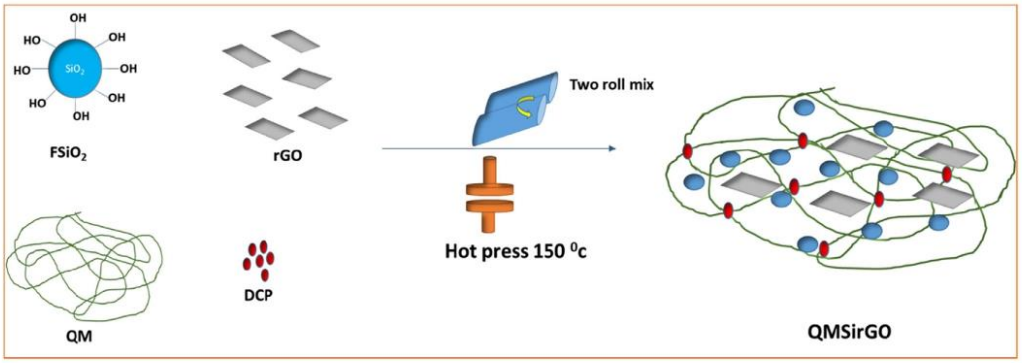

FIGURE 1 Schematic representation of the preparation of QMSirGO nanocomposites. QMSirGO, mechanical, thermal, solvent transport, and tribological properties of silicone rubber nanocomposite [Color figure can be viewed at wileyonlinelibrary.com]

MOST WIEDZY Downloaded from mostwiedzy.pl

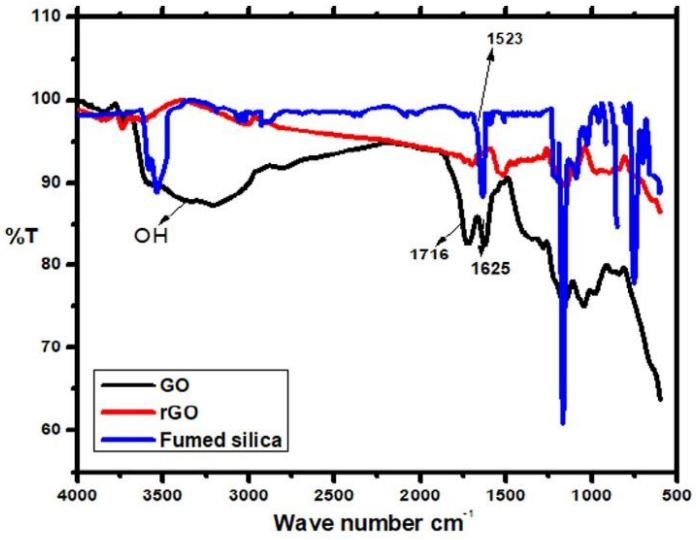

FIGURE 2 FT-IR spectrum of GO, rGO, and $FSiO_2$ nanoparticles. FT-IR, Fourier transform infrared; rGO, reduced graphene oxide [Color figure can be viewed at wileyonlinelibrary.com]

GO confirms the formation of GO nanosheets. Stretching of the hydroxyl (OH) group is responsible for the broad peak from 3200 to 3500 cm^{-1}. The peaks observed at 1236 and 1280 cm^{-1} correlate to epoxy (C—O) stretching, skeletal vibration of unoxidized graphitic domains, and (C—OH) stretching, respectively. Stretching of (C═O) functional groups is responsible for the broad peaks at 1730 and 2361 cm^{-1}.[26] In the case of rGO, oxygen-containing functional groups such as (—OH) and (C═O) disappeared due to the successful reduction of the hydrazine reagent. In FT-IR spectrum of rGO, Peaks at 3448, 1045, 1625, and 1716 cm^{-1} vanished. This indicates that oxygen-containing functional groups in GO were successfully removed.[3] This fumed silica exhibits a peak around 3500 cm^{-1} corresponding to the Si—OH group and around 1200 cm^{-1} corresponding to the Si—O—Si group.[27] Raman spectrum and FT-IR spectrum of graphite oxide and rGO are shown in Figure S1.

Figure 3 shows a broad peak around $26A^0$ (rGO). This is primarily the expulsion of graphitic layers that causes structural changes revealed by XRD studies.[28] XRD technique was used to confirm the chemical reduction of graphene oxide and are shown in Figure S2. X-ray photoelectron spectroscopy was used for the chemical analysis of GO and rGO are shown in Figure S3. The detailed chemical analysis of GO and rGO are shown in Tables S4 and S5, respectively. The diffraction peak in neat QM is roughly 12.1°, whereas it is 12.75° in QMSirGO peaks. But on the other hand, it was noticed at 2θ–23.5°, with a corresponding d-spacing of 0.374 nm. When compared to pure rGO (23.9°), XRD characteristics of QMSirGO nanocomposites such as QMSirGO1 and QMSirGO2 showed a left shift with a comparatively low angle of diffraction such as 22.09°and 22.19°.[3] The diffraction peak at $2\theta = 42.26°$ indicates a short-range order in stacked graphene layers.[29] In the case of QMSirGO composites, silicone rubber polymer chains diffused through the graphene layers and obtained an exfoliated structure. This results in better interaction of polymer chain with the filler materials and disappearance of peak around 42.

For QMSirGO nanocomposites, parameters such as maximum torque (M_H) and minimum torque (M_L), cure time, torque difference, scorch time, and cure rate index were investigated to optimize the curing system. Table 2 summarizes the typical cure data of DCP-cured QMSirGO nanocomposite at 150°C. It was also discovered that as rGO content increases, the cure time of the samples increases, showing high-scorch safety.[30] The scorch time (ts) designates the onset of vulcanization at a specific temperature and thus denotes the processing time limit. Cure time (tc90) is the time taken during the vulcanization stage for the desired cross-linking level. The results show that when the filler loading increases, the QMSirGO composite's cure time (tc90) reduces, indicating an increase in cure rate.

In general, the curing rate of rubber compounds is regulated by several filler-related concerns, such as particle size, surface reactivity, and moisture content of fillers.[31] A rubber compound's maximum torque (M_H) is usually proportional to its hardness. It was discovered that the increased hardness is caused by silica and rGO

MOST WIEDZY Downloaded from mostwiedzy.pl

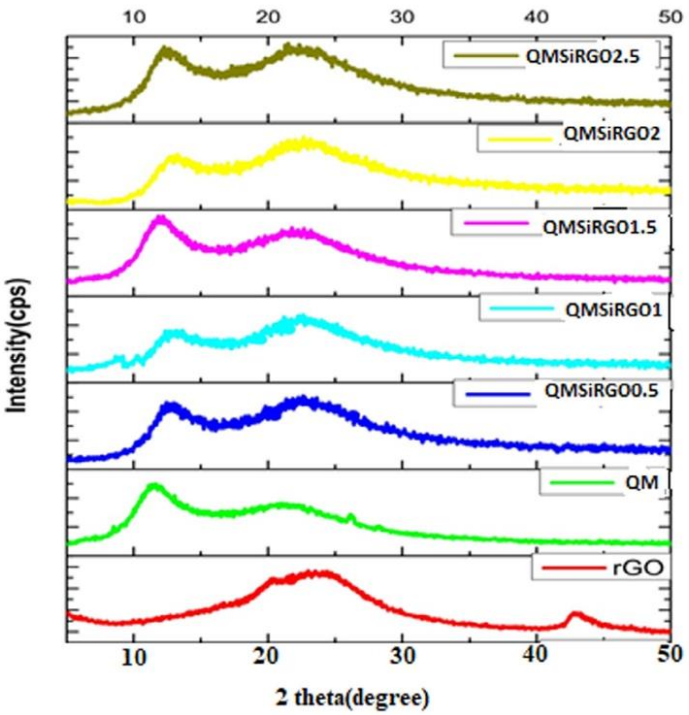

FIGURE 3 XRD spectrum of QMSirGO nanocomposites. QMSirGO, mechanical, thermal, solvent transport, and tribological properties of silicone rubber nanocomposite; XRD, X-ray diffraction. [Color figure can be viewed at wileyonlinelibrary.com]

particles in silicone rubber. As a result of this discovery, the molecular connection between the fillers and the silicon rubber matrix has increased.M_L value steadily increases with filler loading from silicone rubber QM (5.19 dNm) to QMSirGO2.5 (5.34 dNm). The incorporation of rGO affected the sliding movement of the elastomeric chains, affecting the composites' properties. Polymer and filler interphase show better interaction resulting in a rise in the density of vulcanizates (ΔS) value. The upward trend of torque differences with the addition of rGO to the QM could be ascribed to the reinforcement.

3.1 | Mechanical properties

Table 3 shows the impact of silica and rGO on the tensile, tear, and hardness parameters of QMSirGO composites. The inclusion of rGO enhanced the composite's tensile properties, while the addition of silica and rGO significantly improved the composite's tear strength and hardness. Stress–strain graph of QMSirGO nanocomposites is shown in Figure 4. The tensile modulus of silica-filled QM composites generated by rGO was lower. It was due to silica's activity as a reinforcing agent and rGO as a plasticizer. The improvement in mechanical properties confirms the reinforcing nature of rGO. There is weak π–π interaction between graphitic carbon and the vinyl group. This interaction might be the reason for improved mechanical properties of the composites with higher rGO loading.[3]

3.2 | Tensile fracture surface analysis

In comparison, both the QMSi and QMSirGO composites, as shown in Figure 5, have good homogeneity and dispersion in the composites, with no visible aggregates or voids, particularly for the QMSirGO composite. This is because of the good interfacial compatibility between $FSiO_2$ and matrix-based rGO fillers and strong interfacial interactions, which not only reduce the incidence. Defects, as well as increasing the interfacial contact area and good fit uniform dispersion, will benefit the final performance of the mixtures.[32] A better knowledge of the interfacial adhesion between filler and rubber matrix can be obtained by observing tensile fractured surfaces, as shown in Figure 5. Figure 5a shows the SEM image of

MOST WIEDZY Downloaded from mostwiedzy.pl

TABLE 2 Cure characteristics of QMSirGO nanocomposites

Sample	M_L (dNm)	M_H (dNm)	ΔS (dNm)	Scorch time(ts_2) (min)	Optimum cure time t_{90} (min)	Cure rate index (min^{-1})
QMSi	5.19	24.52	19.33	0.74	5.09	23.09
QMSirGO 0.5	5.24	24.59	19.35	0.75	4.40	27.40
QMSirGO 1	5.25	24.75	19.50	0.76	4.87	24.21
QMSirGO 1.5	5.28	24.95	19.67	0.75	4.63	25.77
QMSirGO 2	5.32	25.56	20.24	0.78	4.83	24.69
QMSirGO 2.5	5.34	25.55	20.21	0.77	5.03	23.47

Abbreviation: QMSirGO, mechanical, thermal, solvent transport, and tribological properties of silicone rubber nanocomposite.

TABLE 3 Mechanical properties of QMSirGO nanocomposites

Sample	Tensile strength (MPa)	Elongation at break (%)	Tear strength (N/mm)	Hardness (shore A)
QM	6.82 ± 0.34	340 ± 30	20.45 ± 1.13	51 ± 1
QMSi	6.95 ± 0.34	286 ± 20	27.34 ± 2.24	54 ± 2
QMSirGO 0.5	7.25 ± 0.67	277 ± 40	27.24 ± 2.06	56 ± 1
QMSirGO 1.5	7.32 ± 0.66	246 ± 26	28.05 ± 1.82	56 ± 2
QMSirGO 2	7.1 ± 0.24	261 ± 30	28.63 ± 1.64	58 ± 1
QMSirGO 2.5	6.90 ± 0.36	256 ± 20	31.59 ± 1.84	62 ± 2

Abbreviations: QM, silicone rubber; QMSirGO, mechanical, thermal, solvent transport, and tribological properties of silicone rubber nanocomposite.

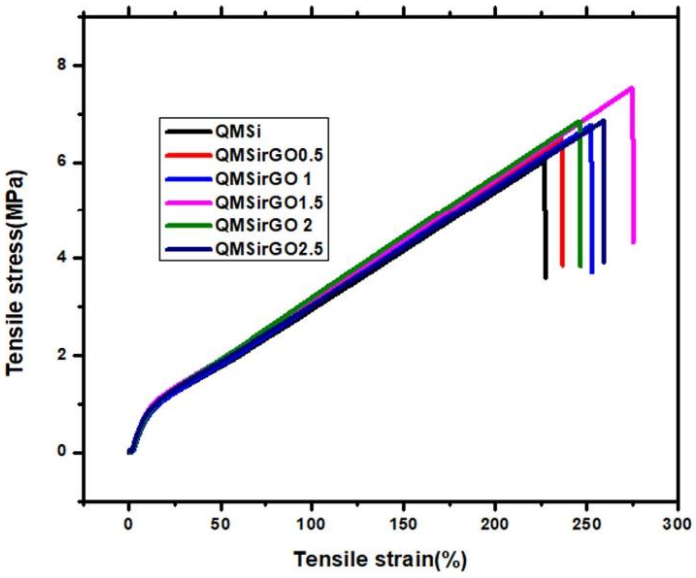

FIGURE 4 Stress–strain graphs of QMSirGO nanocomposites. QMSirGO, mechanical, thermal, solvent transport, and tribological properties of silicone rubber nanocomposite [Color figure can be viewed at wileyonlinelibrary.com]

the tensile fracture surface of QMSirGO nanocomposites. In the case of QMSirGO2 composites fracture surface appears much rougher, and some voids are noticed from the composites. Meanwhile, QMSirGO1 composites show a better smooth surface with relatively few holes. It supports its superior mechanical properties. Increased filler loading decreases the surface smoothness of the composites. Tensile strength is influenced by several aspects,

MOST WIEDZY Downloaded from mostwiedzy.pl

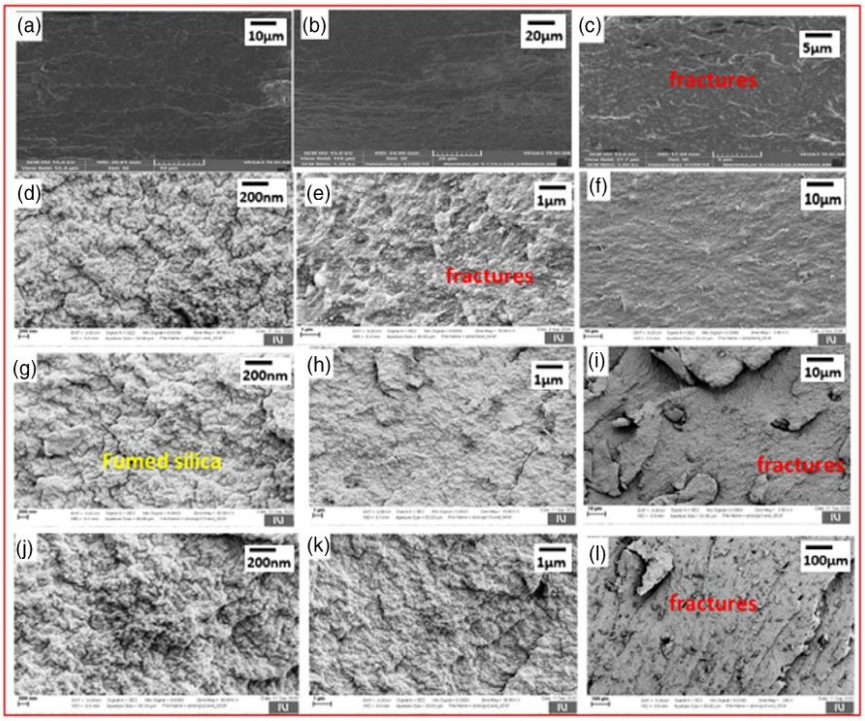

FIGURE 5 Tensile fracture surface of cured QMSi nanocomposites (a–c) QM, (d–f) QMSi, (g–i) QMSirGO 1.5, and (j–l) QMSirGO2 nanocomposites. QM, silicone rubber; QMSirGO, mechanical, thermal, solvent transport, and tribological properties of silicone rubber nanocomposite [Color figure can be viewed at wileyonlinelibrary.com]

including (1) filler dispersion, (2) structure of the polymer, and (3) its molecular alignment. Including more equally distributed will correct the faults by distributing the load equally throughout the matrix material and reducing the availability of stress localized centers.[33]

3.3 | Transmission electron microscopy

One of the most significant components in producing effective nanocomposite is nanofillers' well dispersion and distribution in the polymeric matrix. The diffusion of rGO in the silicone rubber matrix is observed using transmission electron microscopy (TEM). Figure 6 shows the TEM images of all the nanocomposites. The TEM images showed that the rGO was effectively dispersed in the polymer matrix. The dispersion of rGO grows as the concentration of rGO increases without aggregation. 1.5 phr of rGO nanocomposite had the most homogenous and well-dispersed structure.

3.4 | Dynamical mechanical analysis of QMSirGO nanocomposites

The dynamic mechanical characteristics of QMSirGO composites are shown in Figure 7. Storage Module of QMSirGO (E') Compounds from −130 to 30°C are shown in the Figure 7a. The figure shows that the storage modulus of QMSirGO composites is higher than that of pure QM, indicating that rGO has a reinforcing effect on QM. The storage modulus (E') of nanocomposites of various rGO quantities as a function of temperature is shown in Figure 7a. The value (E') declines between −120 and −90°C, indicating a mechanical relaxation associated with glass transformation, followed by a rubber area. Above −40°C, the samples soften further, resulting in another decline in the storage modulus. Figure 7b shows the variation of E" as a function of temperature. As the temperature rises, the loss modulus increases at first as energy is released owing to the glass transition, then reduces as the material relaxes. The loss factor (tanδ) is the ratio of viscous behavior to elastic behavior.

MOST WIEDZY Downloaded from mostwiedzy.pl

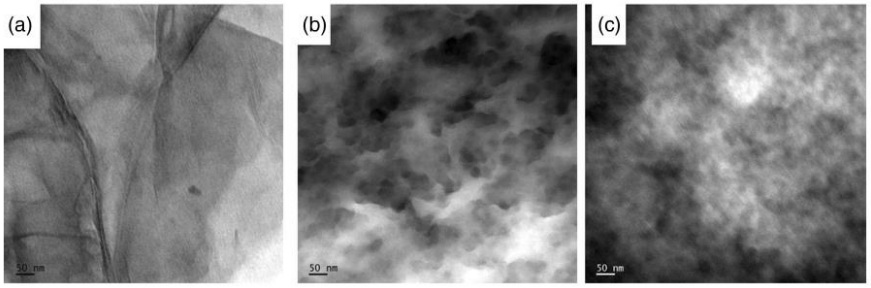

FIGURE 6 TEM micrographs of QMSirGO 0.5, QMSirGO 1.5, and QMSirGO 2.5 nanocomposite. QM, silicone rubber; QMSirGO, mechanical, thermal, solvent transport, and tribological properties of silicone rubber nanocomposite; TEM, transmission electron microscopy

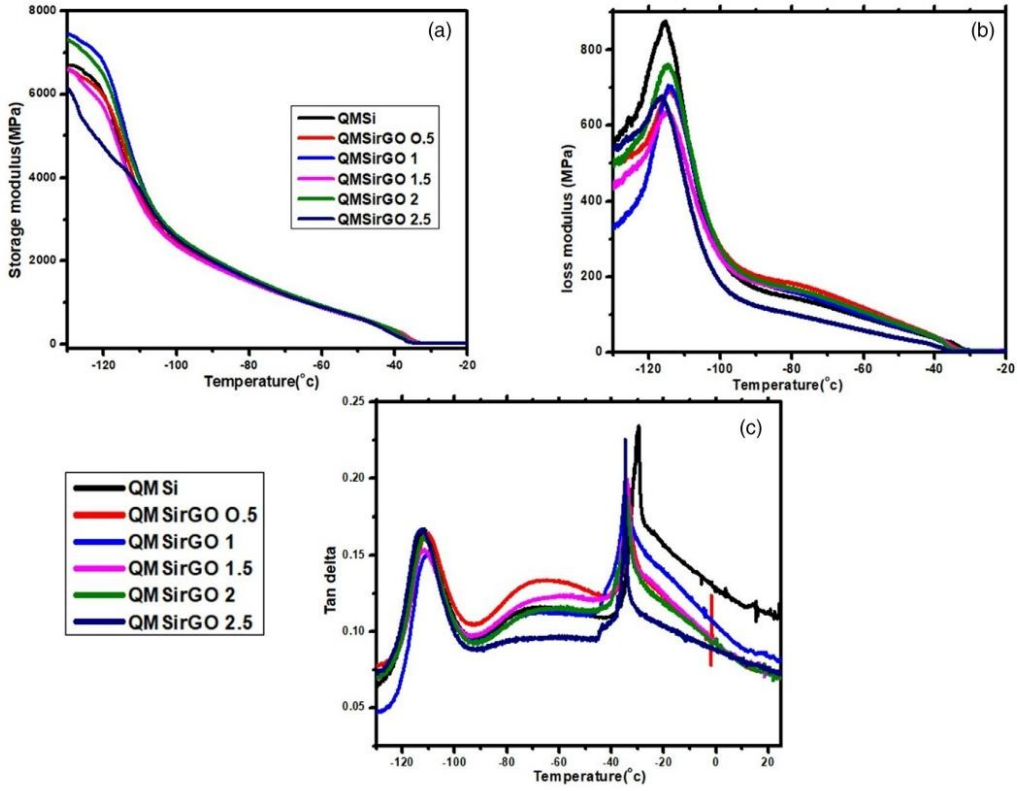

FIGURE 7 Variation in (a) storage modulus, (b) loss modulus, and (c) loss tangent (tanδ) as a function of temperature for QMSirGO nanocomposites. QMSirGO, mechanical, thermal, solvent transport, and tribological properties of silicone rubber nanocomposite [Color figure can be viewed at wileyonlinelibrary.com]

MOST WIEDZY Downloaded from mostwiedzy.pl

The experimental values of loss factor as a function of temperature are shown in Figure 7c—the ratio increases with the temperature reaching a peak and then drops down. The loss factor is related to the energy absorption capacity when a cyclic load is applied, and it goes through a peak at the glass transition (glassy phase to rubbery phase). The higher the peak, the more significant the energy dissipation (also referred to as damping). The decreasing height of the tanδ peak with increasing graphene concentration relates to increasing elastic behavior and less damping. The damping decreased because the introduction of graphene reduced the mobility of the polymer chains, consequently reducing the composite's capacity to absorb energy by polymer chain sliding. The tan delta value offers information about the energy dissipation due to internal friction and molecular movements and the composites' relaxation behavior. Two transitions are visible, as indicated by the modulus dips. Tan delta gets its first peek at −112°C, the glass transition point of rubber (T_g). It is noted that the amount of the rGO loading a slight increase in the glass transition temperature observed. This may be due to the change in the average relaxation time of the chains in the vicinity of the nanoplatelets. Second peek around −32°C, corresponding to the melting temperature (Tm).

3.5 | Diffusion studies

The characterization of polymers requires a thorough understanding of solvent transport and material barrier properties. Some widely used laboratory organic solvents with different solubility parameter values are transported through silicone rubber nanocomposites. The three solvents employed were benzene, toluene, and xylene, and their solubility parameter values varied greatly. The influence of diffusion on liquid molecule size and shape is crucial for understanding the free-volume model diffusion system and predicting its behavior.[34] In the ambient temperature range, silicone rubber (QM) reinforced $FSiO_2$ aromatic solvent resistance, and rGO nanocomposites were investigated using hexane, benzene, and toluene. The microstructure-assisted solvent resistance property of fabricated composites is evident from the morphological analysis.[35]

3.5.1 | Effect of filler

The addition of rGO to the QMSi matrix significantly impacts the solvent diffusivity (benzene, toluene, and xylene) in the resultant composites, as shown in Figure 8. The QMSi sample has the highest diffusivity, while QMSirGO 2.5 has the lowest. While increasing rGO content, different transport parameters such as diffusion, permeation, and sorption constants were moderated. Because the concentration gradient of the penetrant in the composite is substantial, the swelling continues at a relatively rapid rate of solvent uptake. The absorption rate of the solvent reduces as the concentration gradient of the penetrating molecules diminishes. It is also evident

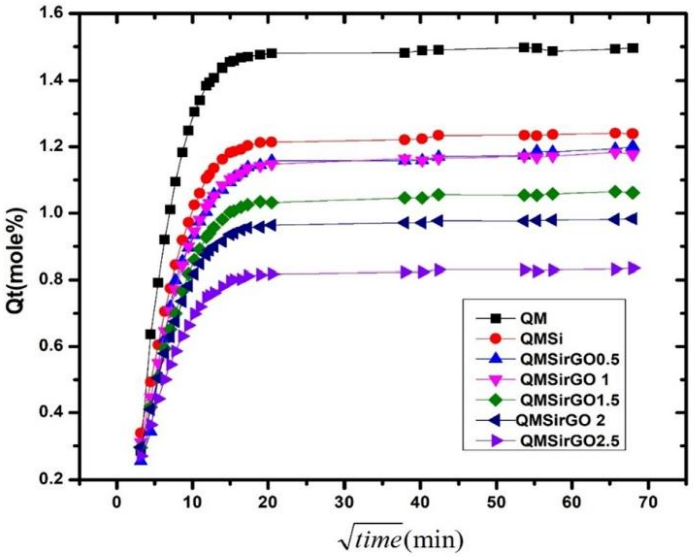

FIGURE 8 Sorption curves of QMSirGO nanocomposites with varying concentrations of rGO and toluene solvents. QMSirGO, mechanical, thermal, solvent transport, and tribological properties of silicone rubber nanocomposite; rGO, reduced graphene oxide [Color figure can be viewed at wileyonlinelibrary.com]

MOST WIEDZY Downloaded from mostwiedzy.pl

from the graph that the equilibrium uptake goes down when the filler loading becomes up. The inclusion of rGO in the silicon rubber matrix has dramatically affected the sorption. The process can be explained in terms of the free volume concept. It is clear from the plot that the amount of solvent uptake decreases as the filler load increases. The reduction in the free volume of the nanocomposites generated by the introduction of rGO causes a decline in solvent uptake. After the vulcanization process, the polymer chains' long-range segmental mobility is controlled, but the polymer's local segmental motion is unaffected; however, when the reinforcing filler material is applied, it creates physical cross connections between the filer and the matrix, resulting in restricted local segmental mobility and improved solvent resistivity.[36]

Filler dispersion is critical in managing the performance of polymer-based composites in general. The nanofiller's good dispersion in the matrix enhances the surface area of the reinforcing phase, resulting in better improvements in the nanocomposites' solubility resistance characteristics.

The amount of rGO required to build an extensive network structure and show homogeneous distribution is relatively low at low concentrations of rGO. As a result, the solvent molecules can quickly move through the QM matrix, as observed in Figure 9a. In QMSi, the network structure $FSiO_2$ is broad, and the dispersion is uniform. As a result, solvent molecules can pass through the matrix, as shown in Figure 9b. rGO particles form a local filler–filler network in the rubber matrix. As a result, soluble molecule transport is restricted, observed in Figure 9c.

Table 4 shows the results of the diffusion coefficient (D), sorption coefficient (S), and permeation coefficient (P) calculations. The low transport coefficients of nanocomposites, when compared with QMSi, demonstrate their superior solvent resistance. The involvement of nanofillers with a large aspect ratio as an effective barrier to solvent mobility and the confinement of intermolecular mobility of rubber chains by nano reinforcing can be explained by the diminution of transport coefficients values with rGO concentration. Because of its molecular size compared to the other two solvents, xylene had the lowest diffusion coefficient values of all the solvents examined.[35]

3.5.2 | Effect of nature of the solvent

Aromatic hydrocarbons such as benzene, toluene, and xylene have been used in extensive sorption studies of nanocomposites. The sorption of benzene's solvent is high, and it decreases as the solvent's molecular weight increases, as shown in Figure 10. Because the high molecular weight of xylene makes transport through the polymer problematic, the high molecular weight xylene polymer matrix demonstrated poor sorption compared to toluene and benzene. Furthermore, by reducing the physical volume, the potential for penetration of the solvent molecule present in the polymer matrix is lowered due to better filler-polymer interaction.

The ease of transfer becomes more difficult as the molecular size of the solvent grows. In the case of nanocomposites, it becomes more difficult due to the existence of filler material. As a result, as the penetration size increases, the solubility spread diminishes. This is explained by free volume theory,[37] which states that a molecule's diffusion rate is substantially influenced by the ease with which polymer chains interchange locations with solvent molecules. As the penetrant size grows more significant, the ease of exchange decreases, especially in full matrices, decreasing solvent absorption. Another explanation for limited solvent uptake is the high activation energy required for a big penetrant molecule.[38] This could also be due to changes in the polymer and solvent solubility parameters. The diffusion coefficients declined as the filler content increased, with benzene having the most excellent value, followed by toluene and xylene. The diffusion coefficient of benzene is highest for pure silicone rubber, which may contribute to the molecular weight of benzene. Regardless of the

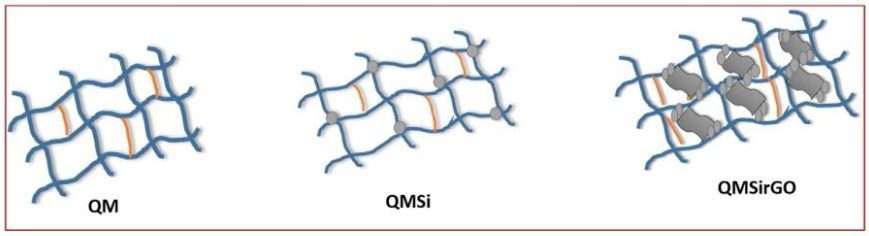

FIGURE 9 Schematic diagram of interaction QM, $FSiO_2$, and rGO. QM, silicone rubber, rGO, reduced graphene oxide [Color figure can be viewed at wileyonlinelibrary.com]

MOST WIEDZY Downloaded from mostwiedzy.pl

TABLE 4 D, S, and P values for QMSirGO nanocomposites with rGO concentration in various solvents

Solvent	Sample	D x 10^3 (cm^2 s^{-1})	S	P x 10^3 (cm^2 s^{-1})
	QM	7.410	1.054	7.813
	QMSi	7.031	1.053	7.409
	QMSiRGO 0.5	7.118	1.032	7.347
	QMSiRGO 1	6.866	1.011	6.943
	QMSiRGO 1.5	6.365	1.024	6.524
	QMSiRGO 2	5.900	1.012	5.973
	QMSiRGO 2.5	5.410	0.984	5.813
Solvent	**Sample**	**D x 10^3 (cm^2 s^{-1})**	**S**	**P x 10^3 (cm^2 s^{-1})**
	QM	6.519	1.228	8.007
	QMSi	6.213	1.219	7.576
	QMSiRGO 0.5	5.276	1.162	6.131
	QMSiRGO 1	6.016	1.136	6.834
	QMSiRGO 1.5	5.487	1.125	6.170
	QMSiRGO 2	5.989	1.079	6.464
	QMSiRGO 2.5	5.646	1.056	6.364
Solvent	**Sample**	**D x 10^3 (cm^2 s^{-1})**	**S**	**P x 10^3 (cm^2 s^{-1})**
	QM	6.144	1.060	6.512
	QMSi	5.897	1.044	6.335
	QMSiRGO 0.5	5.643	1.044	5.890
	QMSiRGO 1	5.528	1.044	5.696
	QMSiRGO 1.5	5.424	1.033	5.603
	QMSiRGO 2	5.246	1.028	5.264
	QMSiRGO 2.5	4.762	1.020	4.858

Abbreviations: QM, silicone rubber; QMSirGO, mechanical, thermal, solvent transport, and tribological properties of silicone rubber nanocomposite.

system studied, tortuosity is an impediment and pore network connection issue, as addressed by various scholars.[39,40] Figure 11 depicts the creation of a tortuous route in nanocomposites as filler loading increases. The solvents' structure and molecular size also substantially impacted the diffusion properties. As filler loading increases, the molecular mass (Mc) falls while the cross-link density (v) increases, showing that rGO in the QMSi matrix is more reinforcing.

Nanosized fillers in polymers result in a better interface between polymeric chains and rGO, resulting in better reinforcement and minor swelling.

The Kraus plot explains how the reduction in solvent uptake is linked to greater reinforcing.

Based on the Kraus equation as shown below,[4]

$$\frac{V_{r0}}{V_{rf}} = 1 - m\left(\frac{f}{1-f}\right), \quad (1)$$

where V_{ro}-volume fraction of the swollen polymer in the fully swollen unfilled sample.

V_{rf}–volume fraction of the swollen reference polymer in the fully swollen filled sample.

f–volume fraction of the filler.

m–the slope is a direct measure of the reinforcing capacity of the filler in the matrix.

Figure 6 gives the plot of $\frac{V_{r0}}{V_{rf}}$ versus $\left(\frac{f}{1-f}\right)$. As the filler loading increases, the value $\frac{V_{r0}}{V_{rf}}$ decreases. Therefore, the composite with the highest filler loading has the most negligible value.

The Vro/Vrf ratio represents the level of elastomer swelling inhibition caused by the presence of filler. The regression line indicates rGO's higher reinforcing capacity. The Kraus plot (Figure 12) shows a negative slope, indicating that the interaction with rGO and QMSi has enhanced.[14,35] TEM images of QMSirGO nanocomposites show that, When the concentration of rGO increases the interphase comes in contact decreases. Therefore, the amount of solvent uptake decreases as the filler load increases. This is also evident from the Kraus analysis negative slope, indicating that rGO's higher reinforcing

MOST WIEDZY Downloaded from mostwiedzy.pl

capacity. All these evidence confirms that interactions between the fillers and polymer improved.

Table 5 shows the calculated molecular mass (Mc) and cross-link density (υ) results. A declining trend for Mc is found as the rGO concentration in QMSi increases.

An increase in molecular weight between crosslinks (Mc) is accompanied by a decrease in cross-linking density, followed by a reduction in swelling ratio. It is evident from the table that the gum sample has the highest value of crosslinks (Mc) and increased solvent sorption. QM sample has the highest Mc value, which denotes the presence of polymer chains far away from each other, making the solvent transport process easier. The addition of fumed silica decreases the crosslink density. When rGO is added, the even distribution of filler in the QM matrix results in enhanced interaction between the network chains. The chains become more and nearer, which restricts the mobility of the polymer matrix, and hence the solvent absorptivity decreases. However, the molecular weight between crosslinks (Mc) of the material increases with rGO loading, indicating the better reinforcing nature of rGO in the QMSi matrix.[40] Because of the improved connection between the polymer and the rGO, the penetration of solvent molecules is reduced. The slope of the plot log(Qt/Q∞) vs. log t gives the value of n, indicating the transport mechanism, and its y-intercept is the value of k. The n values obtained from the preceding equation are $n = 1/2$ in the table, indicating that the diffusion process is Fickian.[41]

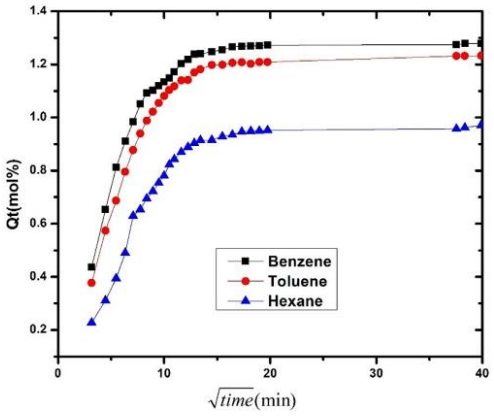

FIGURE 10 Diffusion curves of QMSirGO 1.5 nanocomposites using different aromatic solvents. QMSirGO, mechanical, thermal, solvent transport, and tribological properties of silicone rubber nanocomposite [Color figure can be viewed at wileyonlinelibrary.com]

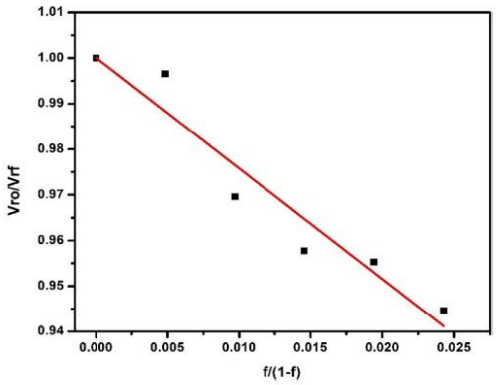

FIGURE 12 The plot of Vro/Vrf versus f/(1−f) of QMSirGO composites using toluene as the solvent. QMSirGO, mechanical, thermal, solvent transport, and tribological properties of silicone rubber nanocomposite [Color figure can be viewed at wileyonlinelibrary.com]

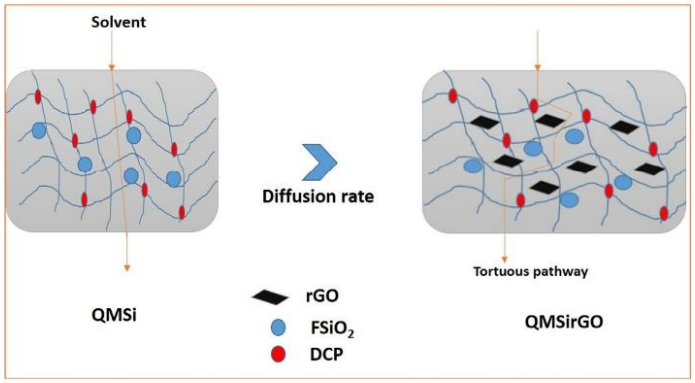

FIGURE 11 A schematic illustration of solvent diffusion through QMSi and QMSirGO nanocomposites. QMSirGO, mechanical, thermal, solvent transport, and tribological properties of silicone rubber nanocomposite [Color figure can be viewed at wileyonlinelibrary.com]

MOST WIEDZY Downloaded from mostwiedzy.pl

TABLE 5 Molecular weight between cross-links (mc), cross-link density(υ), n and k values of QMSirGO composites for the transport of toluene

Sample ID	Mc (g/Mol)	$\upsilon \times 10^4$ (Mol/cc)	n	k (min^{-1})
QM	3646	1.37	0.497	0.475
QMSi	2301	2.17	0.543	0.320
QMSirGO 0.5	2278	2.19	0.523	0.377
QMSirGO 1	2107	2.37	0.511	0.334
QMSirGO 1.5	2033	2.46	0.508	0.354
QMSirGO 2	2019	2.48	0.502	0.354
QMSirGO 2.5	1954	2.56	0.508	0.351

Abbreviations: QM, silicone rubber; QMSirGO, mechanical, thermal, solvent transport, and tribological properties of silicone rubber nanocomposite.

FIGURE 13 Thermogravimetric analysis of QMSirGO nanocomposites. QMSirGO, mechanical, thermal, solvent transport, and tribological properties of silicone rubber nanocomposite [Color figure can be viewed at wileyonlinelibrary.com]

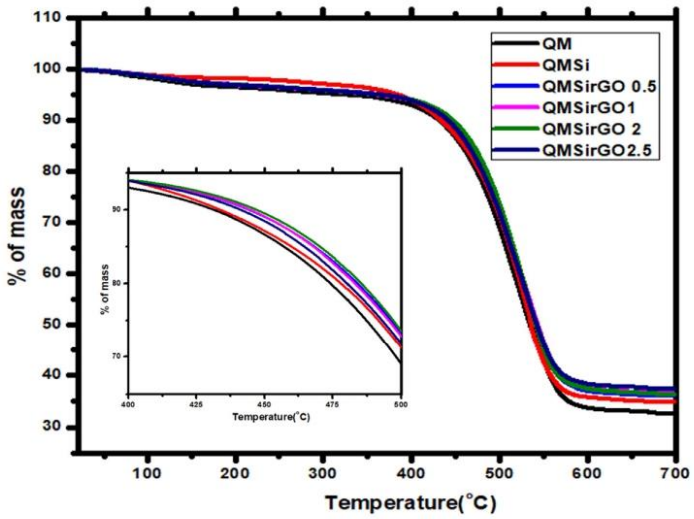

TABLE 6 Thermal characteristics of QMSirGO nanocomposites

Sample	T_{10}°C	T_{50}°C	T max	Residue at 700°C (%)
QM	415	505	532	32.46
QMSi	423	530	538	33.85
QMSirGO 0.5	447	532	540	34.64
QMSirGO 1	457	536	540	35.54
QMSirGO 2	465	540	542	37.40
QMSirGO 2.5	464	542	542	38.24

Abbreviations: QM, silicone rubber; QMSirGO, mechanical, thermal, solvent transport, and tribological properties of silicone rubber nanocomposite.

3.6 | Thermogravimetric analysis of QMSirGO nanocomposites

The thermal stability of QMSirGO composites was evaluated using TGA in an air atmosphere, and the findings are presented in Figure 13. The decomposition temperature at T_{10} (10% decomposition of the sample), center temperature (T_{50}), and char residue of thermal degradation are the key thermal parameters, and the results are given in Table 6. In the case of QMSirGO nanocomposites, T_{10} and T_{50} temperatures rise, most likely due to an increase in small organic molecules.

MOST WIEDZY Downloaded from mostwiedzy.pl

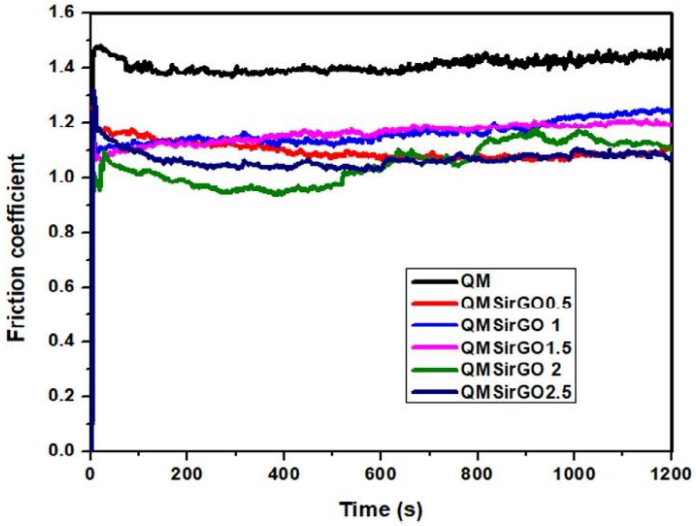

FIGURE 14 Friction coefficient vs. time graph of QMSirGO nanocomposites with different amounts of rGO loading. QMSirGO, mechanical, thermal, solvent transport, and tribological properties of silicone rubber nanocomposite.; rGO, reduced graphene oxide [Color figure can be viewed at wileyonlinelibrary.com]

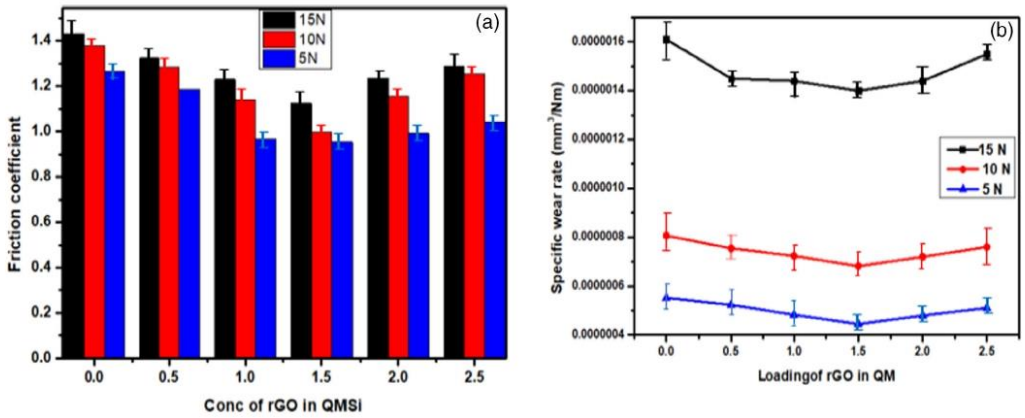

FIGURE 15 (a) Coefficient of friction and (b) specific wear rates of QMSirGO nanocomposites as a function of load. QMSirGO, mechanical, thermal, solvent transport, and tribological properties of silicone rubber nanocomposite. [Color figure can be viewed at wileyonlinelibrary.com]

There is a remarkable improvement in the thermal stability of QMSi as compared to QM. This is mainly due to the better thermal stability of $FSiO_2$. The central temperature of thermal deterioration follows the same pattern. QMSirGO 2.5 has the most extraordinary center temperature due to the largest retard effect of the QM molecular chain. The higher the central temperature, the more chain is constrained by the graphene and silicate layers. This confirmed that the fumed silica/graphene oxide composite had the best reinforcing effect.

3.7 | Tribological properties of QMSirGO nanocomposites

Two body wear studies were conducted on pin-on-disc machine as per ASTM G99 standards. The experiment is conducted for different loads, and temperature conditions and the details of experimental operating conditions are listed in Table S6. Figure 14 shows the value of the friction coefficient increases rapidly with the process of the friction test, and the maximum is 1.42 for the neat

MOST WIEDZY Downloaded from mostwiedzy.pl

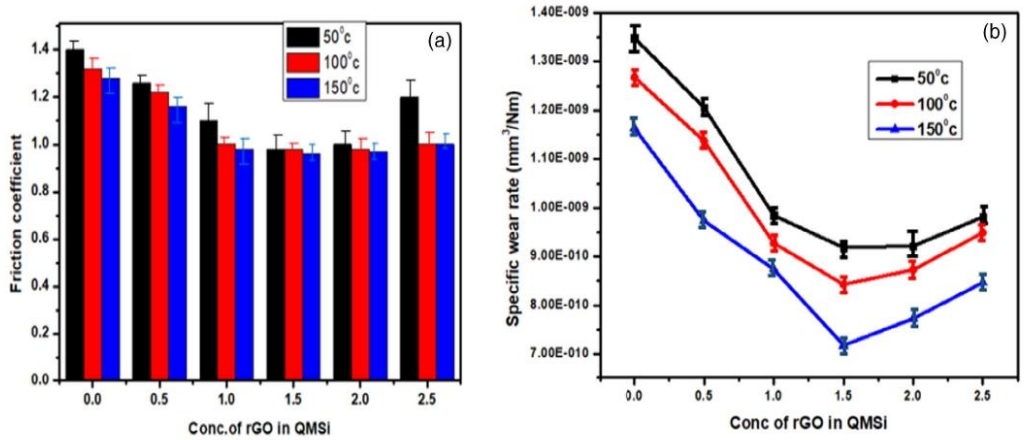

FIGURE 16 (a) Coefficient of friction and (b) specific wear rates of QMSirGO nanocomposites as a function of temperature. QMSirGO, mechanical, thermal, solvent transport, and tribological properties of silicone rubber nanocomposite [Color figure can be viewed at wileyonlinelibrary.com]

QM. Then the friction coefficient decreases gradually with the addition of fumed silica and rGO. The friction coefficient of the vulcanized rubber reinforced by the fumed silica was smaller than that of the silicone rubber, which was due to the high hardness of the vulcanized rubber with the addition of fumed silica. The incorporation of rGO and $FSiO_2$ resulted in a decrease in friction coefficient of about 40% in the friction coefficient of the composite. This imparts more asperities to contact the composite surface and increases the friction coefficient. The segregated network hinders the crosslinking reaction at higher filler content and makes the composite rougher, giving rise to poor mechanical properties.

Figure 15 shows the effect of the applied load on the wear rate of QMSirGO nanocomposites. The load was fed at various conditions (5, 10, and 15 N) while keeping a constant speed of 2 meters per second and a distance of 3600 meters to evaluate the influence of load on the developed composite's coefficient friction. Figure 15a shows that the friction coefficient decreases when the load increases. It was primarily due to forming a lubricant layer, which smooths the material that comes into contact with the metal surface and reduces the frictional heat generated. The wear rate enhances with different slopes for all specimens as the normal load increases from 5 to 15 N. The variation of wear rate with applied load is ascending; however, it is not linear. Due to the polymer's complex nature of the polymer, it is not easy to understand the friction and wear nature of polymer compared to metal or ceramics. Composite sample slide against higher applied load results in more considerable deformation. Higher frictional heat produced from the extensive deformation results in the polymer's softening. It also facilitates the material removal from the composite surface to the metal surface, which comes into contact. The wear properties of the nanocomposite increased by the addition of applied load. Figure 15b shows how composite materials with rGO loadings of up to 1.5 phr reduce the specific wear rate; however, the specific wear rate increases as more rGO is added. The friction coefficient is reduced due to the improved reinforcing and lubricating nature of rGO concentrations up to 1.5 phr. This is because TEM pictures indicate uniform dispersion of rGO at 1.5 phr, and additional inclusion of rGO causes aggregation of rGO and roughening of the composite surface. This introduces more irregularities in the composite surface's interaction with the metal surface. With 15 N, there was a consistent drop in the friction coefficient and specific wear rate value, and better wear resistance.

Figure 16 shows the variation of coefficient of friction (COF) and specific wear rate of the composites with varying temperatures. Elastomers are viscoelastic materials. Thus, their behavior depends on temperature, which could be the ambient temperature or the generated temperature at the surface by the frictional heating. The effect of temperature on the friction and wear properties of QMSirGO nanocomposites with different rGO loading is shown in Figure 16; as the temperature increases from 30 to 150°C, the friction coefficient of the nanocomposites decreases. This is due to the fact that frictional heat produced at the contact region and high heat surface leads to softening of the polymer and reduces the friction coefficient. As the temperature increases, the specific wear rate also decreases and reaches the maximum at 1.5 phr of rGO content and then decreases.

MOST WIEDZY Downloaded from mostwiedzy.pl

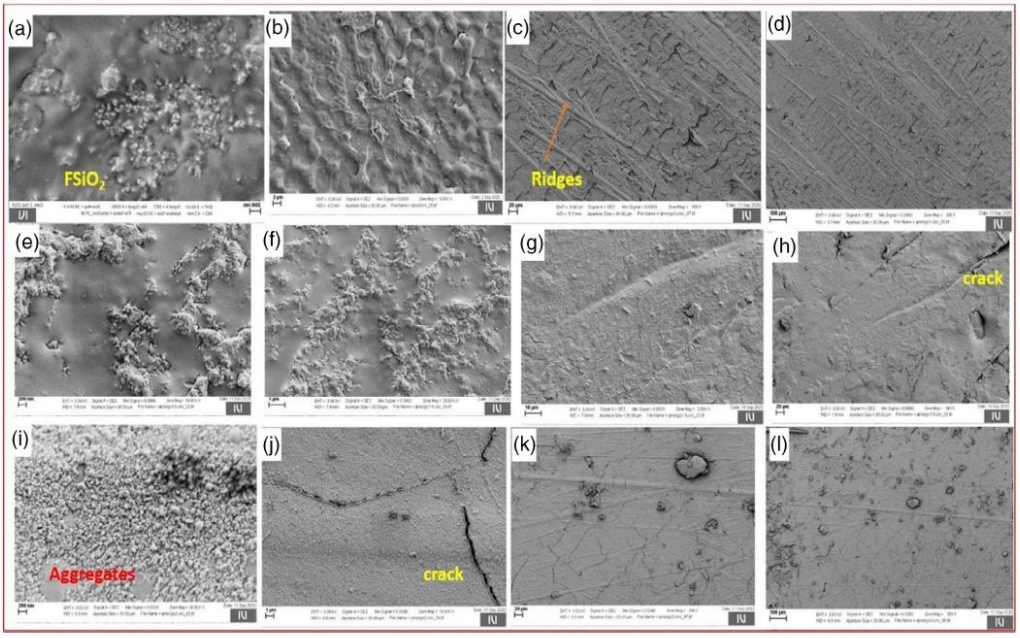

FIGURE 17 Worn surface of cured QMSirGO nanocomposites (a–d) QMSi (e–h) QMSirGO1.5 (i–l) QMSirGO2 nanocomposites. QMSirGO, mechanical, thermal, solvent transport, and tribological properties of silicone rubber nanocomposite [Color figure can be viewed at wileyonlinelibrary.com]

It affects the strength of the elastomers' mechanical properties, wear, and friction-resistant them. When two materials slide against each other because of friction, the mechanical energy converts to the heat; therefore, at the counterface, particularly at the contact spots, the temperature is higher than the bulk. This is because frictional heat produced at the contact region and high heat surface leads to softening of the polymer and reduces the friction coefficient. The frictional heating is attributed to the plastic deformation, hysteresis, dispersion, and viscous flow. Besides, it might be due to the breakdown of adhesive bonds. Figure 16b also shows the similar trend, that is, silicone rubber with rGO loadings of up to 1.5 phr decreases the specific wear rate; further addition of rGO, the specific wear rate starts to increase. As the temperature increases, the specific wear rate also decreases and reaches a lower value at 1.5 phr of rGO content and then drops.

3.8 | Worn surface analysis of QMSirGO nanocomposites

Figure 17 demonstrate SEM images of the worn surface of rubbers after wear under constant applied load and velocity. Generally, ridges and furrows are formed on the surface of elastomers. As can be seen from the figures, a series of ridges are created on the abraded surface of QMSirGO. These features are called wear patterns (Schallamach waves) formed because of nucleation and developments of micro-cracks in elastomers when sliding under stress. Their geometry (size and shape) characterizes the wear process. The formed ridges are well defined and equally spaced. The formed parallel ridges stretched particles, and small voids are observed on the worn surface of QMSirGO, which are characteristic of the frictional wear mechanism. Hence, the wear mechanism is adhesive or frictional wear under the low applied load. Worn surface morphologies of QMSi indicate the localized removal of materials from the matrix. Addition of rGO results in the formation of a smooth surface and the absence of wear depth. The surface roughness of both nanocomposites and the counterface is also considered a basic reason for the degradation of wear resistance of graphene. There is also a possibility of atomic roughness of the nanocomposite surface that could assist the rupture of graphene and induce adhesion on the counterface.

MOST WIEDZY Downloaded from mostwiedzy.pl

4 | CONCLUSIONS

The mechanical, thermal, solvent transport, and tribological properties of silicone rubber reinforced with fumed silica and rGO were systematically studied. The appropriate proportion of fumed silica in rubber should be managed at 3 phr (optimal), and various concentrations of rGO added. The vulcanized rubber improved tensile strength (10%), tear strength (35%), elongation rate, and tribological properties. The solvent transport properties of QMSirGO nanocomposites loaded with rGO and silica were studied using benzene, toluene, and xylene as solvents. The elastomer nanocomposites' barrier properties were improved by adding nanofillers. The solvents' structure and molecular size also substantially impacted the diffusion properties. As filler loading increases, the molecular mass (Mc) falls while the cross-link density (v) increases, showing that rGO in the QMSi matrix is more reinforcing. The pin-on-disc test setup was adopted for the friction and wear investigation of QMSirGO nanocomposites. The tests were performed under a different range of loads and temperature conditions. The COF of all composite materials decreases as the applied load and temperature increase. QMSirGO1.5 composite has the least friction and wears properties of all the composites tested. The filled composites developed transfer films on the counter faces. However, the transfer film on the smoothest counterface covers the asperities completely. The coverage of asperities with transfer film was thorough with the rougher counterfaces. With the addition of 1.5 phr rGO nanoparticles to QMSi, the bond strength of the transfer film to the counterfaces of the surface increased, and thus the wear rate decreased.

AUTHOR CONTRIBUTIONS

Pampayil Sasikumar Sarath: Investigation (lead); writing – original draft (lead). **David Pahovnik:** Formal analysis (equal); validation (lead); writing – review and editing (supporting). **Petra Utroša:** Formal analysis (lead); investigation (equal); visualization (supporting); writing – review and editing (supporting). **Ozgun Can Onder:** Formal analysis (lead); writing – review and editing (supporting). **Sabu Thomas:** Methodology (supporting); supervision (lead); writing – review and editing (supporting). **Józef T. Haponiuk:** Formal analysis (supporting); supervision (equal); writing – review and editing (supporting).

ACKNOWLEDGMENT

For financial aid, the authors are thankful to DRDO (Order No: ERIP/ER/1504758/M/01/1667) in New Delhi, India.

DATA AVAILABILITY STATEMENT

The data that support the findings of this study are available from the corresponding author upon reasonable request.

ORCID

Soney C. George https://orcid.org/0000-0001-9590-3971

REFERENCES

[1] S. C. Shit, P. Shah, *Natl. Acad. Sci. Lett.* **2013**, *36*, 355.
[2] P. S. Sarath, R. Jacob, T. Jose, J. T. Haponiuk, S. Thomas, S. C. George, *Int. J. Membr. Sci. Technol* **2020**, *7*, 25.
[3] P. S. Sarath, G. Moni, J. J. George, J. T. Haponiuk, S. Thomas, S. C. George, *J. Compos. Mater* **2021**, *55*, 2011.
[4] P. S. Sarath, S. V. Samson, R. Reghunath, M. K. Pandey, J. T. Haponiuk, S. Thomas, S. C. George, *Polym. Test* **2020**, *89*, 106601.
[5] H. Kim, A. A. Abdala, C. W. Macosko, *Macromolecules* **2010**, *43*, 6515.
[6] V. C. Tung, M. J. Allen, Y. Yang, R. B. Kaner, *Nat. Nanotechnol* **2009**, *4*, 25.
[7] W. L. Song, M. S. Cao, M. M. Lu, S. Bi, C. Y. Wang, J. Liu, J. Yuan, L. Z. Fan, *Carbon N. Y* **2014**, *66*, 67.
[8] P. K. S. Mural, A. Banerjee, M. S. Rana, A. Shukla, B. Padmanabhan, S. Bhadra, G. Madras, S. Bose, *J. Mater. Chem. A* **2014**, *2*, 17635.
[9] T. S. Muzata, S. Bose, *Polymer* **2020**, *188*, 122127.
[10] P. K. S. Mural, M. Sharma, G. Madras, S. Bose, *RSC Adv* **2015**, *5*, 32078.
[11] S. Zhao, S. Xie, P. Sun, Z. Zhao, L. Li, X. Shao, X. Liu, Z. Xin, *RSC Adv* **2018**, *8*, 17813.
[12] G. Moni, T. Jose, S. Rajeevan, A. Mayeen, A. Rejimon, P. S. Sarath, S. George, *J. Polym. Res* **2020**, *27*, 72.
[13] J. Abraham, H. J. Maria, S. C. George, N. Kalarikkal, S. Thomas, *Phys. Chem. Chem. Phys* **2015**, *17*, 11217.
[14] S. C. George and S. Thomas, "API-15S - Recommended practice for qualification of spoolable reinforced plastic line pipe," vol. *26*, **2006**. http://fartrouven.pt/doc/api_rp_15s-2006_489.pdf.
[15] L. Vast, Z. Mekhalif, A. Fonseca, J. B. Nagy, J. Delhalle, *Compos. Sci. Technol* **2007**, *67*, 880.
[16] S. V. Prasad, D. Pahovnik, S. Thomas, J. T. Haponiuk, S. C. George, *J. Polym. Res* **2022**, *29*, 1.
[17] H. Wu, W. P. Fahy, S. Kim, H. Kim, N. Zhao, L. Pilato, A. Kafi, S. Bateman, J. H. Koo, *Prog. Mater. Sci* **2020**, *111*, 100638.
[18] P. S. Sarath, S. Thomas, J. T. Haponiuk, S. C. George, *J. Appl. Polym. Sci.* **2022**, *139*, 52299.
[19] P. S. Sarath, T. Y. Mahesh, M. K. Pandey, J. T. Haponiuk, S. Thomas, S. C. George, *Polym. Eng. Sci.* **2022**, *62*, 1473.
[20] Z. Ji, L. Zhang, G. Xie, W. Xu, D. Guo, J. Luo, B. Prakash, *Friction* **2020**, *8*, 813.
[21] A. Tiwari, N. Miyashita, N. Espallargas, B. N. J. Persson, *J. Chem. Phys* **2018**, *148*, 224701.
[22] N. Torbati-Fard, S. M. Hosseini, M. Razzaghi-Kashani, *Polym. J* **2020**, *52*, 1223.
[23] X. Liu, X. Zhou, F. Kuang, H. Zuo, J. Huang, *Tribol. Lett.* **2021**, *69*, 1.

MOST WIEDZY Downloaded from mostwiedzy.pl

Conclusions

The present study includes a systematic and detailed investigation into the mechanical, thermal, and tribological behavior of graphene-based silicone rubber nanocomposites as a function of nanofiller concentration. Tribological studies focus on investigating the effect of operating parameters such as applied load, sliding velocity, and temperature on the behavior of silicone rubber nanocomposites. Silicone rubber filled with natural graphite, exfoliated graphite, reduced graphene oxide, ionic liquid modified graphene oxide, and silane-modified graphene oxide fabricated by the simple two-roll mixing method were well explored in all aspects. In brief, the nanocomposites' nanofiller loading's cure kinetics, morphology, mechanical behavior, solvent transport characteristics, viscoelasticity, thermal behavior, and dielectric response were investigated in detail.

Natural graphite, the foundation material for all graphene derivatives, is inexpensive and possesses superior thermal and mechanical stability and electrical conductivities. They also work as a lubricant due to their loosely packed architecture. The study shows that adding graphite improved the tribological performance of QMG composites. The QMG20 has superior mechanical, tribological, and thermal conductivity than other silicone rubber graphite composites. The worn surface morphology of the composite shows a smooth surface, indicating that the presence of graphite significantly reduced the metal contact. Lubricant film formed on the counter surface prevents the asperities in contact with the composite surface. This results in a decreased coefficient of friction and specific wear rate.

Silicone rubber with 7 phr of exfoliated graphite composite recorded decreased friction and wear properties. The study found that adhesive wear between the surfaces in contact was the primary cause of wear in the composite. AFM and TEM analysis confirm the better dispersion of EG particles on the composite surface form a lubricant film and improved wear resistance. Silicone rubber composites with 15phr of exfoliated graphite composites improved dielectric performance by increasing AC conductivity and dielectric permittivity and lowering the dielectric loss.

The improved wear-resistant of the composite was obtained with 2phr of rGO loading. The rGO between the friction surfaces reduced contact between the material and hard metal surface by acting as a lubricant film. The morphology analysis indicated that adding rGO

MOST WIEDZY Downloaded from mostwiedzy.pl

decreased wear and resulted in a relatively smooth surface with fewer scars, thus indicating the presence of rGO significantly reduced metal contact. Tribological properties of the composites with different sliding speeds, loads, and temperatures were investigated to optimize composite composition with a wide range of conditions. Incorporating rGO improved nanocomposites' mechanical properties and thermal conductivity due to enhanced interaction between rGO and silicone rubber matrix. Overall, the wear resistance of the composite was enhanced by the addition of rGO, as is evident from the depth wear rate analysis

The desirable interactions between graphene oxide and the ionic liquid 1-ethyl-3-methylimidazolium dicyanamide are most likely caused by cation–π-interactions between the IL's cations the π- electrons of graphitic structures at the graphene oxide surface. The experiment demonstrated that ionic liquid surface modification of graphene improved the tribological properties of QMILGO composites by enhancing graphene matrix interaction and IL lubrication effects. In addition to 1.5 phr ILGO, the resulting QMILGO nanocomposite exhibited a prominent reinforcement effect (17% increase in tensile strength) and 28% improvement in thermal conductivity compared to the neat QM. Moreover, the property enhancement was because of the homogeneous distribution of ILGO on the inside of the QM matrix. The thermal conductivity results reveal that adding ILGO significantly improves the conductivity (by 28%). In the next stage, we used experimental data for training artificial neural networks (ANNs), which were then used to predict the COF of the nanocomposites for values for which the experiment was not performed. The results were validated using a trained Neural network, which predicted COF values for various temperature, speed, and load conditions. The produced composite's predictions of friction coefficient utilizing the ANN technique were quite close to experimental results.

The effect of fumed silica on the mechanical, thermal, and tribological properties was evaluated. The study shows that adding fumed silica significantly improved silicone rubber's mechanical properties and optimized the composite's silica content. The effect of tribological parameters such as applied load, temperature, and sliding speed was evaluated. The addition of $FSiO_2$ significantly reduced the friction coefficient of the composite. Surface wear analysis of the nanocomposite revealed that the nanoparticles have a positive rolling effect. The strengthening properties of the compound improve significantly as the diffusion of $FSiO_2$ increases, resulting in a more significant improvement in the tensile and dynamic material properties and a substantial reduction in the friction coefficient (25 percent) and specific wear

MOST WIEDZY Downloaded from mostwiedzy.pl

rate (Ws). The silica-filled surface of the rubber is relatively smooth, with few grooves and ridges, and the reinforcing fillers seem to have anti-wear properties. Due to the rubber surface's extremely high stiffness and rigidity, a small quantity of fumed silica could significantly decrease the coefficient of friction and specific wear rate of QMSi composites. The coefficient of friction and specific wear rate of QMSi composites are affected considerably by applied load and sliding velocity. As the applied load and sliding speed rise, all-composite materials' friction coefficient declines. The contact area also became temperature-independent during sliding, ruled primarily by the mechanical properties of the rubber and only marginally reliant on the sliding velocity. The friction and wear properties of silicone rubber with 3 phr fumed silica composite was the lowest of all the composites evaluated. Adding FSiO2 results in a positive rolling effect, improving the composite's tribological properties. A similar product is also observed with the dry abrasion results

It was noted that the QM nanocomposites exhibited improved mechanical, thermal, and tribological properties at the very low loading of fillers. However, it is concluded that such improvement in properties is only observed when fillers are uniformly dispersed and interact with QM chains. The improved thermal conductivity of silicone rubber nanocomposites could lead to its many promising industrial applications, e.g., circuit boards in power electronics, thermal greases, sealants, elastomeric thermal pads, and phase change materials.

Future Scope for research

Nowadays, polymer composite replaces metals from almost all areas, increasing their usage steadily. There is a remarkable improvement in tribological properties observed with nano-filler. A future study might focus on the tribological performance of polymer nanocomposites augmented with greener nanofillers, such as natural nanofibers and waste-derived wollastonite nanofibers, given the rising concern about environmental sustainability. The tribology of silicone rubber with natural and synthetic fibers is an area of future research. Moreover, silicone rubber with nanocellulose is also a promising area of study. Another good work is validating the tribological results with artificial intelligence or machine learning methods. For sealing applications, tribological properties under thermo-oxidative ageing are required. The tribological property of silicone rubber for the application as wire covers which enhance the fire safety of the building will be another area of importance.

MOST WIEDZY Downloaded from mostwiedzy.pl

Research achievements

List of publications

1. **Sarath, P.S**., Reghunath, R., Thomas, S., Haponiuk, J.T. and George, S.C., 2021. An investigation on the tribological and mechanical properties of silicone rubber/graphite composites. ***Journal of Composite Materials***, p.00219983211031634.
2. **Sarath, P.S**., Samson, S.V., Reghunath, R., Pandey, M.K., Haponiuk, J.T., Thomas, S. and George, S.C., 2020. Fabrication of exfoliated graphite reinforced silicone rubber composites-Mechanical, tribological and dielectric properties. ***Polymer Testing***, p.106601.
3. **Sarath, P.S**., Moni, G., George, J.J., Haponiuk, J.T., Thomas, S. and George, S.C., 2021. A study on the influence of reduced graphene oxide on the mechanical, dynamic mechanical and tribological properties of silicone rubber nanocomposites. **Journal of Composite Materials**, 55(15), pp.2011-2024
4. **Sarath, P.S**., Pahovnik, D., Utroša, P., CanOnder, O., Haponiuk, J.T., Thomas, S. and George, S.C., 2021. Study the characteristics of novel ionic liquid functionalized graphene oxide on the mechanical and thermal properties of silicone rubber nanocomposites. *Journal of Polymer Research*, *28*(11), pp.1-10.
5. **Sarath, P.S**, Prasad, V., Pahovnik, D. *et al.* study the effect of fumed silica on the mechanical, thermal and tribological properties of silicone rubber nanocomposites. ***Journal of Polymer Research,*** *Res* **29,** 53 (2022).
6. **Sarath, P.S**., T.Y.Mahesh, Haponiuk, J.T., Thomas, S. and George Tribological performance of ionic liquid modified graphene oxide/silicone rubber composite and the correlation of properties using machine learning. *Polymer Engineering & Science*, 10.1002/pen.25936
7. **P. S. Sarath**, S. Thomas, J. T. Haponiuk, S. C. George Fabrication, characterization and properties of silane functionalized graphene oxide/ silicone rubber nanocomposites**, J. Appl. Polym. Sci**. 2022, e52299.
8. **P. S. Sarath**, S. Thomas, J. T. Haponiuk, S. C. George Study the synergistic effect of fumed silica and reduced graphene oxide insertion on the thermal, mechanical,

MOST WIEDZY Downloaded from mostwiedzy.pl

tribological, and solvent transport properties of silicone rubber nanocomposites**, J. Appl. Polym. Sci**. 2022

9. **Sarath, P.S**., RintuJacob, T.J., Haponiuk, J.T., Thomas, S. and George, S.C., Effect of Graphite on The Pervaporation Performance of Silicone Rubber Membranes International **Journal of Membrane Science and Technology**, 2020.
10. George, E., Joy, J., vijayan P, P. **SarathP.S**, S., C. George, S. and Anas, S., Development, characterization, and tribological behavior of polymeric carbon nitride/acrylonitrile butadiene styrene nanocomposites. *Polymer Composites*.
11. Moni, G., Jose, T., Rajeevan, S., Mayeen, A., Rejimon, A., **Sarath, P.S**. and George, S.C., 2020. Influence of exfoliated graphite inclusion on the thermal, mechanical, dielectric and solvent transport characteristics of fluoroelastomer nanocomposites. Journal of Polymer Research, 27(3), pp.1-11.

Book Editing

1. **Book Editor** - Sarath, P.S., Reghunath, R, Haponiuk, Thomas, S. and George, S.C Trbology of polymers, polymer composites, and polymer nanocomposites – **Elsevier publication**

Book chapter Published

1. Sarath, P.S., Reghunath, R., Haponiuk, J.T., Thomas, S. and George, S.C., 2021. Tribology of Fiber Reinforced Polymer Composites: Effect of Fiber Length, Fiber Orientation, and Fiber Size. In Tribological Applications of Composite Materials (pp. 99-117). Springer, Singapore.
2. Sarath, P.S., Reghunath, R., Haponiuk, J.T., Thomas, S. and George, S.C., 2022. A Journey to the Tribological Behaviour of Polymeric Materials,Elsevier in Tribology of Polymers, Polymer Composites, and Polymer Nanocomposites.
3. Sarath, P.S., Reghunath, R., Haponiuk, J.T., Thomas, S. and George, S.C., 2022. Tribology of Graphene-based Polymeric Systems, Elsevier in Tribology of Polymers, Polymer Composites, and Polymer Nanocomposites.

MOST WIEDZY Downloaded from mostwiedzy.pl

Conference papers

1. Paper presented in the 7th INTERNATIONAL CAUCASIAN SYMPOSIUM ON POLYMERS AND ADVANCEDMATERIALS 2019 – KETCON 2019 – organised by Ivane Javakhishvili Tbilisi State University during 27-30 July, 2021.

2. Paper presented in the International Conference on Advanced Nanomaterials (ICAN-2021)– organised by Amal Jyothi College of Engineering, Mahatma Gandhi University, and Gdansk University of Technology, Poland during 14-16 December, 2021.

3. Paper presented in the "International Tribology Research Symposium ITRS-2020 on Impact of Tribology on Society online platform organised by SRM Institute of Science and Technology 5th – 7th November 2020.

4. Paper presented in the 'NANO MATERIALS & SMART MATERIALS' session of the Kerala State Technological Congress 2019 – KETCON 2019 – organized at Government Engineering College Thrissur from 15th to 17th February 2019.

Poster presentations

1. Poster presented in the national conference of recent material science and technology trends- A Study on the Mechanical, Tribological and Dielectric Properties of Silicone Rubber Exfoliated Graphite Nanocomposites, IIST December -2019.
2. Poster presented in the national conference of recent trends in material science and technology (NCMST)- Investigation of role of ionic liquid modified graphene oxide on the tribological properties of silicone rubber, IIST December -2020.

Funding

This studies were fully financed by the Defense Research and Development Organizations (DRDO, India) grant number ERIP/ER/1504758/M/01/1667.

MOST WIEDZY Downloaded from mostwiedzy.pl

ACKNOWLEDGEMENTS

First of all, I thank GOD for making everything possible by giving me the strength, wisdom, and courage to accomplish my dream. I am very thankful to my enthusiastic supervisor, Dr. Soney C George, for allowing me to work with him with immense support. Let me express my sincere gratitude to Prof. Sabu Thomas, who has been a truly dedicated mentor and supervisor. Similarly, I thank Prof. Józef Haponiuk wholeheartedly and my sincere appreciation for motivating and guiding me throughout my research.

Let me express my deepest gratitude to all my ACeNT (Amal Jyothi Centre for Nanoscience and Technology) and Department of Polymer Chemistry and Technology, National Institute of Chemistry, Slovenia friends and colleagues Dr. Thomasukutty Jose, Dr. Grace Moni, Dr. Maya M. G, Dr.David Pahovnik, Dr.Petra Utroša, Dr.Ozgun Can Onder, Anish Benny, Sreelakshmi, and Sreekanth for their timely help and advice.

I wish to express my sincere thanks and gratitude to all my respected teachers. They have taught me since my childhood and especially at UG, PG level at St: Dominic's college, Kanjirappally, and school of chemical sciences, M.G University. Most importantly, the deepest thanks from the bottom of my heart should be dedicated to my father, mother, Grandmother, Sister, and other relatives for their motivation to pursue my dream to undertake a research career and for their constant and personal support during this doctoral thesis work. I thank them for being there for me for all phases of several career steps during my education. Last but not least, I am profoundly and forever indebted to my loving son (Rithvik), wife (Akhila R Nair), and mother (Beena B Nair), who always made this entire endeavor worthwhile.

Once again, I acknowledge my deep gratitude to everybody important to the successful realization of this thesis and express my apology that I could not mention personally one by one. Thank you all for helping me one way or another in my struggle to complete a Ph.D. I surely remember you all for your constant support and care. Finally, I bow my head in front of my GOD with many thanks and admiration for the eternal love and grace.

Sarath P.S

MOST WIEDZY Downloaded from mostwiedzy.pl

References

[1] M. Marian and S. Tremmel, "Current trends and applications of machine learning in tribology—a review," *Lubricants*, vol. 9, no. 9, 2021, doi: 10.3390/LUBRICANTS9090086.

[2] P. Ghosh, K. Naskar, and N. C. Das, "Enhancement of tribological and thermo-mechanical properties of phenolic resin friction composites by improving interactions between elastomeric phase and matrix resin," *SN Appl. Sci.*, vol. 2, no. 11, pp. 1–13, 2020, doi: 10.1007/s42452-020-03728-5.

[3] B. J. Briscoe and S. K. Sinha, "Wear of polymers," *Proc. Inst. Mech. Eng. Part J J. Eng. Tribol.*, vol. 216, no. 6, pp. 401–413, 2002, doi: 10.1243/135065002762355325.

[4] T. Zeghloul, L. Dascalescu, K. Rouagdia, A. Fatihou, P. Renoux, and D. Souchet, "Sliding Conformal Contact Tribocharging of Polystyrene and Polyvinyl Chloride," *IEEE Trans. Ind. Appl.*, vol. 52, no. 2, pp. 1808–1813, 2016, doi: 10.1109/TIA.2015.2493065.

[5] N. Torbati-Fard, S. M. Hosseini, and M. Razzaghi-Kashani, "Effect of the silica-rubber interface on the mechanical, viscoelastic, and tribological behaviors of filled styrene-butadiene rubber vulcanizates," *Polym. J.*, vol. 52, no. 10, pp. 1223–1234, 2020, doi: 10.1038/s41428-020-0378-x.

[6] S. C. Shit and P. Shah, "A review on silicone rubber," *Natl. Acad. Sci. Lett.*, vol. 36, no. 4, pp. 355–365, 2013, doi: 10.1007/s40009-013-0150-2.

[7] A. K. Geim and K. S. Novoselov, "The rise of graphene," *Nanosci. Technol. A Collect. Rev. from Nat. Journals*, pp. 11–19, 2009, doi: 10.1142/9789814287005_0002.

[8] K. S. Novoselov *et al.*, "Electric field in atomically thin carbon films," *Science (80-.).*, vol. 306, no. 5696, pp. 666–669, 2004, doi: 10.1126/science.1102896.

[9] L. Gan, S. Shang, C. W. M. Yuen, S. X. Jiang, and N. M. Luo, "Facile preparation of graphene nanoribbon filled silicone rubber nanocomposite with improved thermal and mechanical properties," *Compos. Part B Eng.*, vol. 69, pp. 237–242, 2015, doi: 10.1016/j.compositesb.2014.10.019.

[10] Y. Song *et al.*, "Enhancing the thermal, electrical, and mechanical properties of silicone rubber by addition of graphene nanoplatelets," *Mater. Des.*, vol. 88, no. June, pp. 950–957, 2015, doi: 10.1016/j.matdes.2015.09.064.

[11] Z. Zheng, H. Yang, and X. F. Yao, "Wear-Resistant Graphene–Silicone Rubber Composites," *Tribol. Trans.*, vol. 63, no. 2, pp. 205–214, 2020, doi: 10.1080/10402004.2019.1670886.

[12] H. Xu *et al.*, "Influence of processing conditions on dispersion, electrical and mechanical properties of graphene-filled-silicone rubber composites," *Compos. Part A Appl. Sci. Manuf.*, vol. 91, pp. 53–64, 2016, doi: 10.1016/j.compositesa.2016.09.011.

[13] V. Kumar and D. J. Lee, "Studies of nanocomposites based on carbon nanomaterials and RTV silicone rubber," *J. Appl. Polym. Sci.*, vol. 134, no. 4, Jan. 2017, doi: 10.1002/app.44407.

MOST WIEDZY Downloaded from mostwiedzy.pl

[14] S. Park and R. S. Ruoff, “Chemical methods for the production of graphenes,” *Nat. Nanotechnol.*, vol. 4, no. 4, pp. 217–224, 2009, doi: 10.1038/nnano.2009.58.

[15] D. R. Dreyer, S. Park, C. W. Bielawski, and R. S. Ruoff, “The chemistry of graphene oxide,” *Chem. Soc. Rev.*, vol. 39, no. 1, pp. 228–240, 2010, doi: 10.1039/b917103g.

[16] T. Ge, M. Zhang, K. Tang, and H. Tang, “Diisocyanate-modified graphene oxide/hydroxyl-terminated silicone rubber composites for improved thermal conductivity,” *Mater. Chem. Phys.*, vol. 252, p. 123250, 2020, doi: 10.1016/j.matchemphys.2020.123250.

[17] Y. Bai, H. Cai, X. Qiu, X. Fang, and J. Zheng, “Effects of graphene reduction degree on thermal oxidative stability of reduced graphene oxide/silicone rubber nanocomposites,” *High Perform. Polym.*, vol. 27, no. 8, pp. 997–1006, 2015, doi: 10.1177/0954008315604205.

[18] H. Ren *et al.*, “Silane-functionalized graphene nanoplatelets for silicone rubber nanocomposites,” *J. Mater. Sci.*, vol. 57, no. 4, pp. 2683–2696, 2022, doi: 10.1007/s10853-021-06737-w.

[19] L. Gan, S. Shang, and S. X. Jiang, “Impact of vinyl concentration of a silicone rubber on the properties of the graphene oxide filled silicone rubber composites,” *Compos. Part B Eng.*, vol. 84, pp. 294–300, 2016, doi: 10.1016/j.compositesb.2015.08.073.

[20] N. M. Barkoula, B. Alcock, N. O. Cabrera, and T. Peijs, “Flame-Retardancy Properties of Intumescent Ammonium Poly(Phosphate) and Mineral Filler Magnesium Hydroxide in Combination with Graphene,” *Polym. Polym. Compos.*, vol. 16, no. 2, pp. 101–113, 2008, doi: 10.1002/pc.

[21] K. Vigneshwaran, N. Venkateshwaran, and S. P. Srinivasan, “Mechanical, thermal and vibration characteristics of Dosinia exoleta dispersed polymer composites,” *Int. J. Polym. Anal. Charact.*, vol. 23, no. 7, pp. 646–656, 2018, doi: 10.1080/1023666X.2018.1490563.

[22] M. Ravichandran, A. Naveen Sait, and V. Anandakrishnan, “Synthesis and forming characteristics of Al–TiO2 powder metallurgy composites during cold upsetting under plane stress state conditions,” *J. Sandw. Struct. Mater.*, vol. 17, no. 3, pp. 278–294, 2015, doi: 10.1177/1099636214565762.

[23] A. Ramesh, K. Ramu, M. A. Ali Baig, and E. D. Guptha, “Influence of fly ash nano filler on the tensile and flexural properties of novel hybrid epoxy nano-composites,” *Mater. Today Proc.*, vol. 27, no. xxxx, pp. 1252–1257, 2020, doi: 10.1016/j.matpr.2020.02.150.

[24] N. Nagaraj, S. Balasubramaniam, V. Venkataraman, R. Manickam, R. Nagarajan, and I. Sikiru Oluwarotimi, “Effect of cellulosic filler loading on mechanical and thermal properties of date palm seed/vinyl ester composites,” *Int. J. Biol. Macromol.*, vol. 147, pp. 53–66, 2020, doi: 10.1016/j.ijbiomac.2019.11.247.

[25] I. D. Ibrahim, T. Jamiru, R. E. Sadiku, W. K. Kupolati, S. C. Agwuncha, and G. Ekundayo, “The use of polypropylene in bamboo fibre composites and their mechanical properties - A review,” *J. Reinf. Plast. Compos.*, vol. 34, no. 16, pp. 1347–1356, 2015, doi: 10.1177/0731684415591302.

MOST WIEDZY Downloaded from mostwiedzy.pl

[26] S. Y. Nayak *et al.*, "Potential of Natural Fibers in Composites for Ballistic Applications–A Review," *J. Nat. Fibers*, vol. 00, no. 00, pp. 1–11, 2020, doi: 10.1080/15440478.2020.1787919.

[27] E. Sarikaya, H. Çallioğlu, and H. Demirel, "Production of epoxy composites reinforced by different natural fibers and their mechanical properties," *Compos. Part B Eng.*, vol. 167, pp. 461–466, 2019, doi: 10.1016/j.compositesb.2019.03.020.

[28] Sachinjith Krasno and Krishna Swathi, "A review on types of nanocomposites and their applications," *Int. J. Adv. Res. Ideas Innov. Technol.*, vol. 4, no. 6, pp. 235–236, 2018, [Online]. Available: www.IJARIIT.com.

[29] J. Abraham, T. Sharika, S. C. George, and S. Thomas, "Rheological Percolation in Thermoplastic Polymer Nanocomposites," *Rheol. Open access*, vol. 1, no. 1, pp. 1–15, 2017.

[30] J. González-Benito and D. Olmos, "Efficient dispersion of nanoparticles in thermoplastic polymers," *Plast. Res. Online*, no. January, pp. 2–4, 2010, doi: 10.2417/spepro.002566.

[31] "Enhancing the Mechanical Properties of an Epoxy Resin Using," pp. 1–27.

[32] M. Monti, M. Rallini, D. Puglia, L. Peponi, L. Torre, and J. M. Kenny, "Morphology and electrical properties of graphene-epoxy nanocomposites obtained by different solvent assisted processing methods," *Compos. Part A Appl. Sci. Manuf.*, vol. 46, no. 1, pp. 166–172, 2013, doi: 10.1016/j.compositesa.2012.11.005.

[33] P. Luo, M. Xu, S. Wang, and Y. Xu, "Structural, dynamic mechanical and dielectric properties of mesoporous silica/epoxy resin nanocomposites," *IEEE Trans. Dielectr. Electr. Insul.*, vol. 24, no. 3, pp. 1685–1697, 2017, doi: 10.1109/TDEI.2017.006151.

[34] D. Ratna, O. Becker, R. Krishnamurthy, G. P. Simon, and R. J. Varley, "Nanocomposites based on a combination of epoxy resin, hyperbranched epoxy and a layered silicate," *Polymer (Guildf).*, vol. 44, no. 24, pp. 7449–7457, 2003, doi: 10.1016/j.polymer.2003.08.035.

[35] V. Ojijo and S. S. Ray, *Processing Thermoset-Based Nanocomposites*. Springer International Publishing.

[36] D. Puglia and J. M. Kenny, *Structure-property relationships of thermoset nanocomposites*, 2nd ed. Elsevier Ltd., 2018.

[37] B. G. Soares, *Rubber nanocomposites with metal oxides as nanofillers*. Elsevier Ltd, 2017.

[38] S. T. Report, "Silicone Elastomers Market Size and Share Analysis by Type (HTV , RTV , LSR), Application (Electrical & Electronics , Automotive & Transportation , Industrial Machinery , Construction) – Global Industry Growth Forecast to 2030," no. June, pp. 1–6, 2022.

[39] Y. Xue, X. fei Li, D. hai Zhang, H. sheng Wang, Y. Chen, and Y. fa Chen, "Comparison of ATH and SiO2 fillers filled silicone rubber composites for HTV insulators," *Compos. Sci. Technol.*, vol. 155, pp. 137–143, 2018, doi: 10.1016/j.compscitech.2017.12.006.

MOST WIEDZY Downloaded from mostwiedzy.pl

[40] L. Xue, Y. Zhang, Y. Zuo, S. Diao, J. Zhang, and S. Feng, “Preparation and characterization of novel UV-curing silicone rubber via thiol-ene reaction,” *Mater. Lett.*, vol. 106, pp. 425–427, 2013, doi: 10.1016/j.matlet.2013.05.084.

[41] S. Diao, K. Jin, Z. Yang, H. Lu, S. Feng, and C. Zhang, “The effect of phenyl modified fumed silica on radiation resistance of silicone rubber,” *Mater. Chem. Phys.*, vol. 129, no. 1–2, pp. 202–208, Sep. 2011, doi: 10.1016/j.matchemphys.2011.03.077.

[42] C. Yoon *et al.*, “Highly luminescent and stable white light-emitting diodes created by direct incorporation of Cd-free quantum dots in silicone resins using the thiol group,” *J. Mater. Chem. C*, vol. 3, no. 26, pp. 6908–6915, 2015, doi: 10.1039/c5tc00660k.

[43] Y. Gan, X. Jiang, and J. Yin, “Thiol-ene photo-curable hybrid silicone resin for LED encapsulation: Enhancement of light extraction efficiency by facile self-keeping hemisphere coating,” *J. Mater. Chem. C*, vol. 2, no. 28, pp. 5533–5539, 2014, doi: 10.1039/c4tc00350k.

[44] H. Zhang *et al.*, “Graphene nanosheet/silicone composite with enhanced thermal conductivity and its application in heat dissipation of high-power light-emitting diodes,” *Curr. Appl. Phys.*, vol. 16, no. 12, pp. 1695–1702, 2016, doi: 10.1016/j.cap.2016.10.004.

[45] Q. Zhu, Z. Wang, H. Zeng, T. Yang, and X. Wang, “Effects of graphene on various properties and applications of silicone rubber and silicone resin,” *Compos. Part A Appl. Sci. Manuf.*, vol. 142, no. August 2020, p. 106240, 2021, doi: 10.1016/j.compositesa.2020.106240.

[46] L. Guo *et al.*, “A pinene-based silane crosslinker for improved mechanical strength/transparency of room-temperature vulcanizing silicone rubber,” *Mater. Chem. Phys.*, vol. 247, 2020, doi: 10.1016/j.matchemphys.2020.122868.

[47] Q. Zhao, Q. Liu, H. Xu, Y. Bei, and S. Feng, “Preparation and characterization of room temperature vulcanized silicone rubber using α-amine ketoximesilanes as auto-catalyzed cross-linkers,” *RSC Adv.*, vol. 6, no. 44, pp. 38447–38453, 2016, doi: 10.1039/c6ra04445j.

[48] L. Bokobza, “Elastomeric composites. I. Silicone composites,” *J. Appl. Polym. Sci.*, vol. 93, no. 5, pp. 2095–2104, Sep. 2004, doi: 10.1002/app.20684.

[49] P. Hron, “Hydrophilisation of silicone rubber for medical applications,” *Polym. Int.*, vol. 52, no. 9, pp. 1531–1539, 2003, doi: 10.1002/pi.1273.

[50] Z. Yang, H. Peng, W. Wang, and T. Liu, “Crystallization behavior of poly(ε-caprolactone)/layered double hydroxide nanocomposites,” *J. Appl. Polym. Sci.*, vol. 116, no. 5, pp. 2658–2667, 2010, doi: 10.1002/app.

[51] D. Li, “Mechanical & Tribological Properties of Carbon Fiber Composite,” *Nanovea*, p. 13, 2014.

[52] G. Raghavendra, “MECHANICAL AND TRIBOLOGICAL BEHAVIOR OF NANOFILLER REINFORCED POLYMER A THESIS SUBMITTED IN PARTIAL FULFILMENT OF MECHANICAL AND TRIBOLOGICAL BEHAVIOR OF NANOFILLER REINFORCED POLYMER A THESIS SUBMITTED IN PARTIAL FULFILMENT OF,” 2014.

MOST WIEDZY Downloaded from mostwiedzy.pl

[53] Y. Song *et al.*, "Enhancing the thermal, electrical, and mechanical properties of silicone rubber by addition of graphene nanoplatelets," *Mater. Des.*, vol. 88, pp. 950–957, 2015, doi: 10.1016/j.matdes.2015.09.064.

[54] G. Malucelli and F. Marino, "Abrasion Resistance of Polymer Nanocomposites – A Review," pp. 1–19, 2009.

[55] S. D. Ephraim, "Use of Nanotechnology in Reduction of Friction and Wear," vol. 1, no. 8, pp. 1–7, 2014.

[56] S. S. Pesetskii, S. P. Bogdanovich, and N. K. Myshkin, "Tribological Behavior of Nanocomposites Produced by the Dispersion of Nanofillers in Polymer Melts," vol. 28, no. 5, pp. 457–475, 2007, doi: 10.3103/S1068366607050091.

[57] Y. Xin, T. Li, D. Gong, F. Xu, and M. Wang, "Preparation and tribological properties of graphene oxide/nano-MoS2 hybrid as multidimensional assembly used in the polyimide nanocomposites," *RSC Adv.*, vol. 7, pp. 6323–6335, 2017, doi: 10.1039/C6RA27108A.

[58] S. X. X. W. Tangpong, "Review : Tribological behavior of polyethylene-based nanocomposites," pp. 578–597, 2013, doi: 10.1007/s10853-012-6844-x.

[59] D. D. L. Chung, "Review: Graphite," *J. Mater. Sci.*, vol. 37, no. 8, pp. 1475–1489, 2002, doi: 10.1023/A:1014915307738.

[60] D. D. L. Chung, "A review of exfoliated graphite," *J. Mater. Sci.*, vol. 51, no. 1, pp. 554–568, 2015, doi: 10.1007/s10853-015-9284-6.

[61] S. J. Rowley-Neale, E. P. Randviir, A. S. Abo Dena, and C. E. Banks, "An overview of recent applications of reduced graphene oxide as a basis of electroanalytical sensing platforms," *Appl. Mater. Today*, vol. 10, no. December, pp. 218–226, 2018, doi: 10.1016/j.apmt.2017.11.010.

[62] Y. Xu, Q. Gao, H. Liang, and K. Zheng, "Effects of functional graphene oxide on the properties of phenyl silicone rubber composites," *Polym. Test.*, vol. 54, pp. 168–175, 2016, doi: 10.1016/j.polymertesting.2016.07.013.

[63] G. Mittal, V. Dhand, K. Y. Rhee, S. J. Park, and W. R. Lee, "A review on carbon nanotubes and graphene as fillers in reinforced polymer nanocomposites," *J. Ind. Eng. Chem.*, vol. 21, pp. 11–25, 2015, doi: 10.1016/j.jiec.2014.03.022.

[64] Z. Lei, B. Chen, Y. M. Koo, and D. R. Macfarlane, "Introduction: Ionic Liquids," *Chem. Rev.*, vol. 117, no. 10, pp. 6633–6635, 2017, doi: 10.1021/acs.chemrev.7b00246.

[65] G. Moni, A. Mayeen, A. Mohan, J. J. George, S. Thomas, and S. C. George, "Ionic liquid functionalised reduced graphene oxide fluoroelastomer nanocomposites with enhanced mechanical, dielectric and viscoelastic properties," *Eur. Polym. J.*, vol. 109, pp. 277–287, 2018, doi: 10.1016/j.eurpolymj.2018.09.057.

[66] H. Yang *et al.*, "Covalent functionalization of chemically converted graphene sheets via silane and its reinforcement," *J. Mater. Chem.*, vol. 19, no. 26, pp. 4632–4638, 2009, doi: 10.1039/b901421g.

[67] C. J. Madadrang *et al.*, "Adsorption behavior of EDTA-graphene oxide for Pb (II)

MOST WIEDZY Downloaded from mostwiedzy.pl

removal," *ACS Appl. Mater. Interfaces*, vol. 4, no. 3, pp. 1186–1193, 2012, doi: 10.1021/am201645g.

[68] N. Rasana, K. Jayanarayanan, B. D. S. Deeraj, and K. Joseph, "The thermal degradation and dynamic mechanical properties modeling of MWCNT/glass fiber multiscale filler reinforced polypropylene composites," *Compos. Sci. Technol.*, vol. 169, no. October 2018, pp. 249–259, 2019, doi: 10.1016/j.compscitech.2018.11.027.

[69] W. H. Alhazmi, Y. Jazaa, S. Mousa, A. A. Abd-Elhady, and H. E. M. Sallam, "Tribological and mechanical properties of epoxy reinforced by hybrid nanoparticles," *Lat. Am. J. Solids Struct.*, vol. 18, no. 3, pp. 1–14, 2021, doi: 10.1590/1679-78256384.

[70] M. Jaafar, "Development of Hybrid Fillers/Polymer Nanocomposites for Electronic Applications," *Hybrid Nanomater.*, no. August, pp. 349–369, 2017, doi: 10.1002/9781119160380.ch7.

[71] J. X. Chan *et al.*, "Effect of nanofillers on tribological properties of polymer nanocomposites: A review on recent development," *Polymers (Basel).*, vol. 13, no. 17, pp. 1–47, 2021, doi: 10.3390/polym13172867.

[72] "interlocking Structure Formed by Multiscale Carbon Fiber−.pdf." .

[73] J. Yuan *et al.*, "Coupling hybrid of BN nanosheets and carbon nanotubes to enhance the mechanical and tribological properties of fabric composites," *Compos. Part A Appl. Sci. Manuf.*, vol. 123, no. May, pp. 132–140, 2019, doi: 10.1016/j.compositesa.2019.05.010.

[74] S. Nayak, R. K. Nayak, I. Panigrahi, and A. K. Sahoo, "Tribo-mechanical responses of glass fiber reinforced polymer hybrid nanocomposites," *Mater. Today Proc.*, vol. 18, pp. 4042–4047, 2019, doi: 10.1016/j.matpr.2019.07.347.

[75] M. H. Cho and S. Bahadur, "Study of the tribological synergistic effects in nano CuO-filled and fiber-reinforced polyphenylene sulfide composites," *Wear*, vol. 258, no. 5–6, pp. 835–845, 2005, doi: 10.1016/j.wear.2004.09.055.

[76] Z. Jiang, L. A. Gyurova, A. K. Schlarb, K. Friedrich, and Z. Zhang, "Study on friction and wear behavior of polyphenylene sulfide composites reinforced by short carbon fibers and sub-micro TiO2 particles," *Compos. Sci. Technol.*, vol. 68, no. 3–4, pp. 734–742, 2008, doi: 10.1016/j.compscitech.2007.09.022.

[77] I. Erukhimovich and M. O. de la Cruz, "Phase equilibria and charge fractionation in polydisperse polyelectrolyte solutions," vol. 48, no. December 2009, pp. 801–811, 2004, doi: 10.1002/polb.

[78] L. Liu *et al.*, "Enhanced tribological performance of PEEK/SCF/PTFE hybrid composites by graphene," *RSC Adv.*, vol. 7, no. 53, pp. 33450–33458, 2017, doi: 10.1039/c7ra04969b.

[79] O. J. Gbadeyan and K. Kanny, "Tribological Behaviors of Polymer-Based Hybrid Nanocomposite Brake Pad," *J. Tribol.*, vol. 140, no. 3, 2018, doi: 10.1115/1.4038679.

[80] Y. Liu, D. Shin, S. Xu, C. Kim, and D. Kim, "Jo ur na l P re of," *Carbon N. Y.*, 2020, doi: 10.1016/j.carbon.2020.11.007.

[81] M. Fox, "Lube-Tech Polymer Tribology Lube-Tech," *Eur. Lubr. Ind. Mag.*, vol. 135,

MOST WIEDZY Downloaded from mostwiedzy.pl

no. 106, pp. 32–37, 2016.

[82] A. Kurdi and L. Chang, “Recent advances in high performance polymers-Tribological aspects,” *Lubricants*, vol. 7, no. 1, pp. 1–31, 2018, doi: 10.3390/lubricants7010002.

[83] Q. Wang, Q. Xue, and W. Shen, “The friction and wear properties of nanometre SiO2 filled polyetheretherketone,” *Tribol. Int.*, vol. 30, no. 3, pp. 193–197, 1997, doi: 10.1016/S0301-679X(96)00042-4.

[84] W. Qihua, X. Qunji, S. Weichang, and Z. Junyan, “The friction and wear properties of nanometer ZrO2-filled polyetheretherketone,” *J. Appl. Polym. Sci.*, vol. 69, no. 1, pp. 135–141, 1998, doi: 10.1002/(sici)1097-4628(19980705)69:1<135::aid-app16>3.3.co;2-o.

[85] C. J. Schwartz and S. Bahadur, “Studies on the tribological behavior and transfer film – counterface bond strength for polyphenylene sulfide filled with nanoscale alumina particles,” pp. 261–273, 2000.

[86] F. Li, K. ao Hu, J. lin Li, and B. yuan Zhao, “The friction and wear characteristics of nanometer ZnO filled polytetrafluoroethylene,” *Wear*, vol. 249, no. 10–11, pp. 877–882, 2001, doi: 10.1016/S0043-1648(01)00816-X.

[87] M. Avella, M. E. Errico, and E. Martuscelli, “Novel PMMA/CaCO3 Nanocomposites Abrasion Resistant Prepared by an in Situ Polymerization Process,” *Nano Lett.*, vol. 1, no. 4, pp. 213–217, 2001, doi: 10.1021/nl015518v.

[88] W. G. Sawyer, K. D. Freudenberg, P. Bhimaraj, and L. S. Schadler, “A study on the friction and wear behavior of PTFE filled with alumina nanoparticles,” *Wear*, vol. 254, no. 5–6, pp. 573–580, 2003, doi: 10.1016/S0043-1648(03)00252-7.

[89] W. Qihua, X. Jinfen, S. Weichang, and L. Weimin, “An investigation of the friction and wear properties of nanometer Si3N4 filled PEEK,” *Wear*, vol. 196, no. 1–2, pp. 82–86, 1996.

[90] G. Shi, M. Q. Zhang, M. Z. Rong, B. Wetzel, and K. Friedrich, “Friction and wear of low nanometer Si3N4 filled epoxy composites,” *Wear*, vol. 254, no. 7–8, pp. 784–796, 2003, doi: 10.1016/S0043-1648(03)00190-X.

[91] B. Wetzel, F. Haupert, and M. Qiu, “Epoxy nanocomposites with high mechanical and tribological performance,” vol. 63, pp. 2055–2067, 2003, doi: 10.1016/S0266-3538(03)00115-5.

[92] S. Bahadur and C. Sunkara, “Effect of transfer film structure, composition and bonding on the tribological behavior of polyphenylene sulfide filled with nano particles of TiO2, ZnO, CuO and SiC,” *Wear*, vol. 258, no. 9, pp. 1411–1421, 2005, doi: 10.1016/j.wear.2004.08.009.

[93] P. S. Sarath, R. Reghunath, S. Thomas, J. T. Haponiuk, and S. C. George, “An investigation on the tribological and mechanical properties of silicone rubber/graphite composites,” *J. Compos. Mater.*, vol. 55, no. 26, pp. 3827–3838, 2021, doi: 10.1177/00219983211031634.

[94] Y. P. Wu *et al.*, “Rubber-pristine clay nanocomposites prepared by co-coagulating rubber latex and clay aqueous suspension,” *Compos. Sci. Technol.*, vol. 65, no. 7–8,

MOST WIEDZY Downloaded from mostwiedzy.pl

pp. 1195–1202, 2005, doi: 10.1016/j.compscitech.2004.11.016.

[95] W. Xing *et al.*, "Multifunctional properties of graphene/rubber nanocomposites fabricated by a modified latex compounding method," *Compos. Sci. Technol.*, vol. 99, pp. 67–74, 2014, doi: 10.1016/j.compscitech.2014.05.011.

[96] J. Yang *et al.*, "Improved mechanical and functional properties of elastomer/graphite nanocomposites prepared by latex compounding," *Acta Mater.*, vol. 55, no. 18, pp. 6372–6382, 2007, doi: 10.1016/j.actamat.2007.07.043.

[97] Torrtert, "Roth1943 Rubber Friction.Pdf." 1943.

[98] "schallamach1953.pdf." .

[99] P. Thavamani, D. Khastgir, and A. K. Bhowmick, "Microscopic studies on the mechanisms of wear of NR, SBR and HNBR vulcanizates under different conditions," *J. Mater. Sci.*, vol. 28, no. 23, pp. 6318–6322, 1993, doi: 10.1007/BF01352190.

[100] H. Wang, H. Zhang, J. Zhang, and Y. Zhao, "Improving tribological performance of fluoroether rubber composites by ionic liquid modified graphene," *Compos. Sci. Technol.*, vol. 170, no. May 2018, pp. 109–115, 2019, doi: 10.1016/j.compscitech.2018.11.041.

MOST WIEDZY Downloaded from mostwiedzy.pl